Self-Assembled Supramolecular Squares from Chiral [4,4']-Bipyridines and Mass Spectrometric Investigations of Oligothiophene-Based Catenates and Catenanes

Dissertation
zur Erlangung des Doktorgrades (Dr. rer. nat.)

der Mathematisch-Naturwissenschaftlichen Fakultät

der Rheinischen Friedrich-Wilhelms-Universität Bonn

vorgelegt von
Alexander Rang
aus
Bonn Bad-Godesberg

Bonn 2008

Angefertigt mit Genehmigung
der Mathematisch-Naturwissenschaftlichen Fakultät
der Rheinischen-Friedrich-Wilhelms-Universität Bonn

Erster Gutachter: Prof. Dr. Christoph A. Schalley (FU Berlin)
Zweiter Gutachter: Prof. Dr. Arne Lützen

Tag der mündlichen Prüfung: 09.02.2009
Diese Dissertation ist auf dem Hochschulschriftenserver der ULB Bonn unter
http://hss.ulb.uni-bonn.de/diss_online elektronisch publiziert.
Erscheinungsjahr: 2009

Für CALM

Das Mögliche unmöglich machen!
von Bertrand Russell (1872 – 1970; Literaturnobelpreisträger 1950)

Contents (Short)

Contents

Chapter 1

Introduction

1.1 The Lock and Key Principle – Induced Fit

Emil Fischer's postulate of the lock and key specificity of enzymes with respect to substrates[1] contains the two main tenets of the new research area. These are precisely what we nowadays – more than 100 years later – call supramolecular chemistry:[2] Molecular recognition and supramolecular function. In 1894, Fischer suggested that enzymes are very specific, since both the enzyme and the substrate possess specific complementary geometric shapes which fit exactly into each other. However, while this model explains enzyme specificity, it fails to answer several important questions, such as the stabilization of transition states.

Daniel Koshland hence proposed a modification to the lock and key model in 1958. In doing so, he claimed that the enzyme is reshaped,[3] when interacting with the substrate due to its rather flexible structure. Consequently, the substrate does not only bind to a rigid active site but rather to a flexible and thereby complex system. During the binding process of the substrate, the active site of the enzyme continues to change until the final shape and charge is reached.[4] In some cases, even the substrate molecule slightly changes its shape when it enters the active site.[5] Thus, Koshland's induced fit model has led to a paradigm shift, but still left many questions to be answered. Worth analyzing are thereby the hosts' and guests' structures prior and during the binding process, since detailed knowledge is needed to understand the principles of molecular recognition on its highest level.

1.2 Self-Assembly of Rigid and Flexible Systems

Biology is replete with examples of complex nanoscale structures[6] formed by self-assembly.[7] From the early 1990ies onward, there have been numerous attempts by chemists to transfer this strategy from biochemistry to supramolecular chemistry. In the beginning, the utilized components had, of course, a biological origin (e. g. cyclodextrins[9] or DNA[10]). For a detailed discussion see chapter 3.1. In his cutting-edge review[8] from 1991 about self-assembly in nanochemistry, George M. Whitesides suggested "that molecules designed for self-assembly should be as rigid as is consistent with achieving good intermolecular contact...". When rigid building blocks are used, the outcome of self-assembly reactions is more or less predictable. It is therefore not astonishing that many artificial examples are flat and rigid molecules. Self-assembly processes of rigid building blocks in small numbers are incredible examples of scientific results, but fail to convince completely when compared to natural systems.

However, when flexible building blocks are used, this predictability gets increasingly difficult. The same holds true, when the amount of different building blocks is increased, e. g. when racemic mixtures are used for the construction of larger assemblies with more than two subunits. The situation gets especially challenging, when conformational aspects are also involved. If multiple conformations of each subunit are comparable in energy and the activation barriers between them are small, the conformation of the final assembly is almost impossible to predict, if at all determined. Again, a deep knowledge of the structures of the involved subunits is indispensable.

1.3 State of the Art Instrumental Analytics

But which techniques can be used, to identify the exact 3D-structure of the subunits and the final assembly? In biology, biochemistry as well as chemistry, three sophisticated types of methodologies among others play a significant role. These are as follows:

- Mass spectrometry (MS), for instance, can be used to get at least a rough

idea of the amount of subunits in the final assembly (mostly Electro Spray Ionization[11](ESI)). For example, MS has helped to confirm the amount of subunits of the tobacco mosaic virus obtained by crystal structure analysis:[12] 2131 subunits with an overall weight of 40.5 MDa.[13] On the other hand, mass spectrometry is not the method of choice to analyze the **exact 3D-structure** of the final assembly.

- Solid-phase structures are usually obtained by X-ray crystallography. In the late 1950ies, scientists started to solve crystal structures of proteins.[14] Since then, over 40000 X-ray crystal structures of biological molecules have been determined. This technique, however, suffers from two crucial limitations: (i) perfectly ordered crystals of self-assembled systems are often hard to prepare, and (ii) the structures in solution might be different, if e. g. packing effects alter the structure in the crystal.

- Complex structures in solution[15] are usually obtained by nuclear magnetic resonance spectroscopy (NMR) with elaborate pulse sequences, like DOSY, ROESY, NOESY or EXSY. A detailed discussion of these techniques would certainly go beyond the scope of this thesis but can be found in standard text books listed in the references.[17] Structure determination by NMR is traditionally a time-consuming process. Furthermore, the superposition of several identical or almost similar building blocks hamper the signal assignment, which is quite common in self-assembly.

What follows from the above discussion is that only the combination of the mentioned methodologies might lead to a complete picture of the 3D-structure of the final assembly. For centuries, scientist have tried to fully understand the complex processes of natural systems. But despite of these efforts, the scientific community is still on the onset to solve this difficult research tasks. In further attempts, the aim must be to mimic the complexity of natural processes by simpler artificial systems[18] (supramolecular function).

1.4 Interdependent Stimulation

Undoubtedly, chemical research would be impossible without new materials or new analytical enhancements. New materials and molecules can be found either accidentally, which generally raises new analytical questions, or target-oriented, which generally raises as many questions. In both cases, each new answer to each question facilitate more elaborate questions to be asked.

On the other hand, several examples can be found, in which the invention of new analytical methodologies has paved the way for new areas of research. In 1985, Michael Karas and Franz Hillenkamp have developed the matrix assisted laser desorption/ionization (MALDI[19]). In the same year, Koichi Tanaka applied this ionization method to large bio molecules like proteins. Together with HPLC-MS, which couples the power of High-Performance Liquid Chromatography with Mass Spectrometry,[20] these ionization techniques have revolutionized whole research disciplines. Since then, mass spectrometry has become a major tool in chemistry, biology and medical science, enabling related disciplines like proteomics, just to name one. In conclusion, synthetical and analytical chemistry are interdependently stimulating each other.

The present thesis can be seen as a further relevant, but still evanescent, building block to a solution of this difficult task by combining fundamental and applied research as well as synthesis of new materials and analytical structure elucidation.

Chapter 2

Aim of this Study

Due to this interdependent stimulation between synthesis and analytical structure elucidation, the aim of this study diverge into several different tasks along the research path from fundamental towards applied research. The following list of questions gives first insight, whereas detailed introductions and descriptions can be found prior to each chapter of this thesis, respectively.

1. **A Supramolecular Construction Kit of Functionalized Self-Assembled Metallo Supramolecular Squares**

   A supramolecular construction kit of **S**elf-**A**ssembled **M**etallo Supramolecular **S**quares (SAMS) should be made available for several applications within the Collaborative Research Center (SFB 624) "Template - From the Design of Chemical Templates towards Reaction Control", such as Electro Chemical Scanning Tunneling Microscopy (EC-STM; Group of Prof. Dr. K. Wandelt in Bonn) or Quartz Micro Balances (QMB; Group of Prof. Dr. J. Bargon in Bonn). SAMS consist of three different building blocks: cationic metal precursors, anions and neutral organic ligands. From two different metal precursors with two different anions, respectively, and two organic ligands already $2^3 = 8$ compounds are obtained, with to some extent different properties (see Figure 2.1). This construction kit makes tailor-made compounds with desired properties possible - naturally within certain limits. When a screening technique for the desired purpose is available, the obtained compounds might be further optimized: Which components can be modified to

obtain such a construction kit of functionalized self-assembled supramolecular squares?

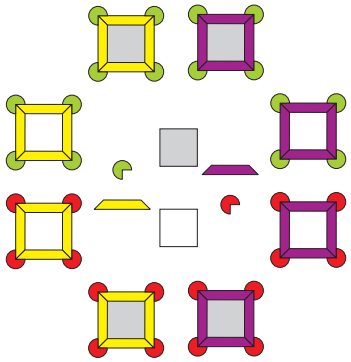

Figure 2.1: A supramolecular construction kit: Two different metal complexes (green and red) with two different anions, respectively (gray and white) and two different ligands (yellow and purple) give eight ($2^3 = 8$) different compounds.

2. **Self-Assembled Defect Free Dendrimers**

   Self-assembly is an ideal approach to construct large to giant architectures via the "bottom up approach"[21] without the effort necessary to generate such large structures through total synthesis. A major disadvantage of divergent[22] dendrimer synthesis is the growing amount of defects observed at higher generations of dendrimers. To apply self-assembly to dendrimer synthesis has proven to be a way to overcome this problem in a convergent fashion.[23] Hence, this thesis should answer the question, if [4,4']-bipyridines, functionalized with *Fréchet* dendrons (see Figure 2.2) of higher generation, self assembly into dendrimers with molecular masses of more than 15000 Da?

3. **Chiral Self-Assembled Supramolecular Squares**

   Functionality should be introduced into the organic ligands by several functional groups. In numerous research areas chirality plays an unambiguous role, e. g. diastereomeric host guest complexes have different physical properties. Hence, chiral components should be used as well. In a first approach, chiral amino acid residues are used to obtain organic ligands with point chirality. As the overall chiral induction of the final assemblies might be larger,

Figure 2.2: Self-assembly strategy to synthesize defect free dendrimers with nanometer-sized cavities at their cores. Dendrons are attached covalently to a bipyridine ligand, which in combination with the appropriate metal corner complexes undergoes self-assembly of metallo-supramolecular squares.

when axially chiral [4,4']-bipyridine systems are used, an approach to this new class of compounds (see Scheme 2.1) needs to be found. How can chiral [4,4']-bipyridines be made available?

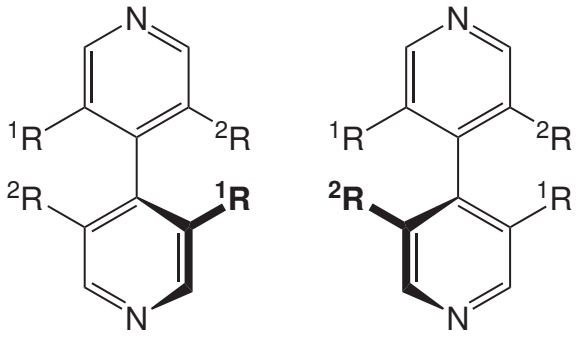

Scheme 2.1: A dissymmetrical axially chiral [4,4']-bipyridine (^{1}R$\neq$ ^{2}R).

4. Isomeric Structures in Self-Assembly

As already discussed in the introduction, multiple conformations of the final assemblies might co-exist in solution. 560 isomers are in principle possible (see chapter 8.7), when substituted [4,4']-bipyridine systems are used in self-assembly reactions (Compare two of them in Scheme 2.2). Steric or electronic effects might of course reduce this amount drastically. Which of these isomers are formed in solution and in the solid phase? Is it possible to alter the outcome? Are they inter converting into each other?

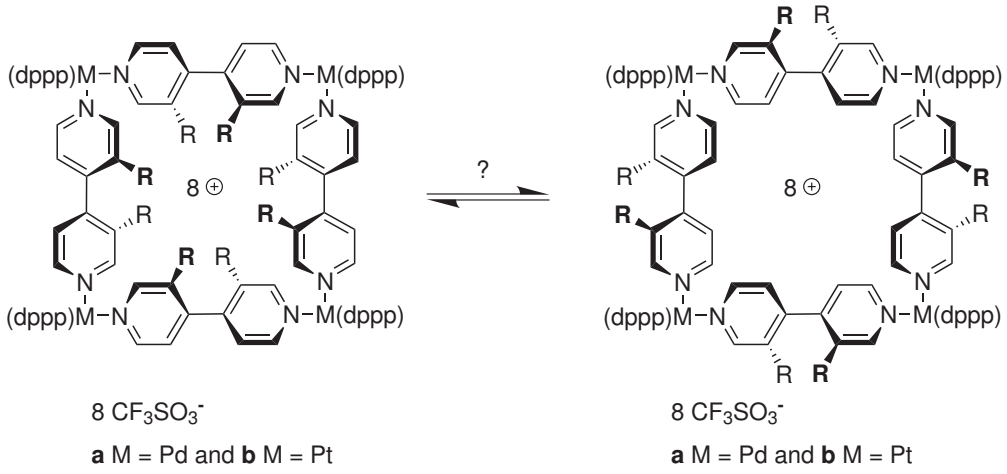

Scheme 2.2: Two isomers of self-assembled supramolecular squares (left: All residues are pointing inside the cavity; right: All residues are pointing away from the cavity).

5. **Unidirectional Self-Assembled Supramolecular Squares**

   In supramolecular chemistry unidirectionality plays a crucial role (see chapter 5.5). Can unidirectional self-assembled supramolecular squares be designed from simple building blocks?

6. **Mass Spectrometric Investigations of *Fujita*-Squares**

   Mass spectrometry might reveal the exact amount of subunits of the final assemblies. Unfortunately, mass spectrometric investigations of *Fujita*-assemblies have proven to be more difficult than those devoted to *Stang*-assemblies. Hence, a method for reproducible ionization needs to be found.

7. **ESI-FTICR Mass Spectrometric Investigation of Oligothiophene-Based Macrocycles, Catenates and Catenanes**

   Several different - to some extent complementary - methodologies have been developed to examine supramolecular systems in the condensed phase, in solution as well as in the gas phase. In September 2003, the Kekulé-Institute for Organic Chemistry and Biochemistry received a Bruker APEX IV Fourier-Transform Ion-Cyclotron-Resonance (FT-ICR) Mass Spectrometer, which was installed at the University of Bonn for the above mentioned

SFB 624 of the Deutsche Forschungsgemeinschaft. With this instrument, oligothiophene-based macrocycles, catenates and catenanes of the research group of Prof. Dr. P. Bäuerle (Institute for New Materials of the University of Ulm) should be investigated in the gas phase, to obtain valuable structural information of this new class of organic electronic materials with defined structures.

Chapter 3

Theoretical Part

A general introduction into the compounds used in this thesis should be given in the theoretical part. As one class of compounds is obtained in self-assembly reactions, a more detailed overview into the fundamentals of self-assembly should be given at first.

3.1 Introduction into Self-Assembly

Self-assembly[8] is a fundamental principle which generates structural organization by non-covalent interactions,[24] without guidance or management from an outside source. It is defined as a reversible process in which pre-existing, disordered components, which may be the same or different, form larger structures by interaction with each other. A simple, long known example is the formation of a micelle by tenside molecules in solution. Classical, covalent synthesis is so successful in these days that it can make most target molecules. However, self-assembly has the potential to provide the basis for a new form of super molecular synthesis,[25] which allows the chemists to generate aggregates with structural complexity comparable to that of biological macromolecules. Synthesis of structures of this complexity will require new strategies that rely heavily on non-covalent synthesis. Self-assembly is, in some sense, the core of non-covalent, molecular synthesis.

Self-assembly can be classified as either static or dynamic. In static self-assembly, the system is in equilibrium, whereas in dynamic self-assembly, the

system requires the continuous conversion of energy. In general, chemistry has focused almost exclusively on equilibrium systems.

The success of self-assembly in a molecular system is determined by at least five characteristics of the system:[25]

- **Components:** As the self-assembly process organizes without guidance or management from an outside source, the involved components must be programmed prior to the actual process. The complementarity in shape and electrostatic potential surface among the self-assembling components is crucial. When the building blocks fit nicely, rigidity is appropriate. When small errors in binding geometries need to be corrected, flexibility is desired at least to some extent.

- **Interactions:** The interactions in self-assembly are generally weak, comparable to thermal energies, and non-covalent (van der Waals and Coulomb forces, hydrophobic interactions, hydrogen bonds, or coordination bonds). A balance of attractive and repulsive interactions is required.

- **Reversibility (or Adjustability):** The association must be reversible or must allow the components to adjust their positions within an aggregate to suppress undesired side products. Therefore, the strength of the bonds between the components must be comparable to the forces tending to disrupt them. For example, processes in which interaction between molecules leads to irreversible binding generate glasses, not crystals.

- **Environment:** The interaction of the components with their environment can strongly influence the outcome of the process. A competitive environment may well destroy the assemblies, for example, if strong electro-donating solvent molecules can replace ligands with lower donating ability.

- **Mobility:** The self-assembly of molecules normally is carried out in solution to allow the required motion of the components.

As the whole scope of self-assemblies is to large to be summarized, the complementary results from two groups, *Fujita et al.* and *Stang et al.*, are presented in more detail on the next pages.

3.2 Water Soluble Assemblies by Fujita

3.2.1 Self-Assembled Supramolecular Squares

In 1990, *Fujita et al.* reported a water soluble, cyclic, tetranuclear Pd complex, $[(en)Pd(NO_3)_2([4,4']\text{-bipyridine})]_4$, wherein the square-planar Pd atoms are bridged by [4,4']-bipyridine.[26] In water, $(en)Pd(NO_3)_2$ **[c]** and [4,4']-bipyridine are mixed in a 1:1 ratio and the solution is stirred for 10 minutes at room temperature. Upon addition of ethanol, a pale yellow powder immediately precipitates. The structure of this complex is estimated to be a macrocyclic tetramer by the following facts:

- The elemental analysis of the solid agreed with the empirical formula.
- All pyridines of the complex are completely equivalent in the ^{1}H NMR spectrum; only one set of signals is observed indicating high symmetry.
- Right bond angles ($\sphericalangle$ ($N_{py.}$-Pd-$N_{py.}$) = 90°) rule out the formation of other cyclic oligomers, which must have significant ring strain, as [4,4']-bipyridine is to stiff to be bound.

Since then, other proofs for this structure have been found:

- Coldspray Ionization Mass Spectrometry[27] showed peaks for $[(en)Pd([4,4']\text{-bipyridine})]_4^{8+}(NO_3{}^-)_x$, with $x = 5-7$ usually carrying a number of solvent molecules.
- A solid-phase structure could be obtained by X-ray crystal structure analysis.[28]

With this simple technique, mixing, stirring, and precipitating, this water soluble, cyclic, highly charged, tetranuclear Pd complex is available in high yields by self-assembly.

When the metal complex is slightly modified, Pd is exchanged by analogous Pt, the self-assembly conditions change drastically. After mixing equimolar amounts of $(en)Pt(NO_3)_2$ **[d]** and [4,4']-bipyridine in D_2O, the self-assembly was monitored by ^{1}H NMR.[29] Initially, an intractable mixture was formed, which may be

composed of oligomers. Not until four weeks at 100°C, the spectra converged to one set of signals. Precipitation yields $[(en)Pt(NO_3)_2([4,4']\text{-bipyridine})]_4$. The results of the above mentioned methods (elemental analysis, ^1H NMR, Coldspray Ionization Mass Spectrometry, etc.) agreed likewise in the Pt case.

Unfortunately, *Fujita et al.* do not discuss, why these two metal precursors, $(en)Pd(NO_3)_2$ **[c]** and $(en)Pt(NO_3)_2$ **[d]**, differ that drastically in self-assembly.

3.2.2 Larger Assemblies

Almost all of the following larger assemblies are prepared from $(en)Pd(NO_3)_2$ **[c]** with two binding sites or $Pd(NO_3)_2$ with four. The corresponding Pt complexes are used rather rarely. It is almost impossible to summarize the work of *Fujita et al.* in the last decade. All sorts of assemblies are reported: e. g. catenanes,[30–32] a hexahedron,[33] an open octahedron,[34,35] a cuboctahedron,[36] a cube,[37] boxes,[38] prisms,[39] and nanotubes.[40] Guest inclusion inside these assemblies contains:

- anionic guest, like various sodium carboxylates,[29]
- neutral guests, like boranes,[42] adamantane,[42] porphyrins,[43] coronene,[44] siloxanes and silanol oligomers,[45]
- and even cationic guest, like tetrabutylammonium.[46]

However, anions play in important role in the later case, as all supramolecular assemblies introduced by this group are positively charged.

3.2.3 Chemistry Inside Containers

Fujita and coworker demonstrated that general rules for chemistry in solution are not always valid inside these containers (micro environment): e. g. pH-switchable through-space interactions of organic radicals,[47] unusual peptide folding,[48] stereo selective photodimerization of olefins,[49] formation of defined water cluster,[50] and stable dimers of cis-azobenzene[51] are observed. Three further topics of special interest for this study are discussed in more detail.

3.2.4 Structural Switching

Structural switching between two different assemblies is controlled by e. g. guest inclusion: In the case of a flexible tridentate ligand and (en)Pd(NO_3)$_2$ [**c**], a polymeric mixture is obtained.[52,53] The desired M_3L_2 complex assembles only in the presence of specific guest molecules (here: sodium 4-methoxyphenylacetate) in high yields. The authors titled this communication "A Prototype for 'Induced-Fit' Molecular Recognition".

In the case of a triangular tetradentate ligand and (en)Pd(NO_3)$_2$ [**c**], a M_8L_4 composition is formed (see Scheme 3.1).[54] Two structures are in equilibrium: an open cone (tetragonal pyramidal) and a closed tetrahedron structure. Adding of large guest molecules such as dibenzoyl induces quantitative assembly of the open cone structure, whereas small tetrahedral guests give the closed tetrahedron structure. Therefore, both assemblies constitute a dynamic receptor library[55] from which each receptor is selected by its optimal guest.

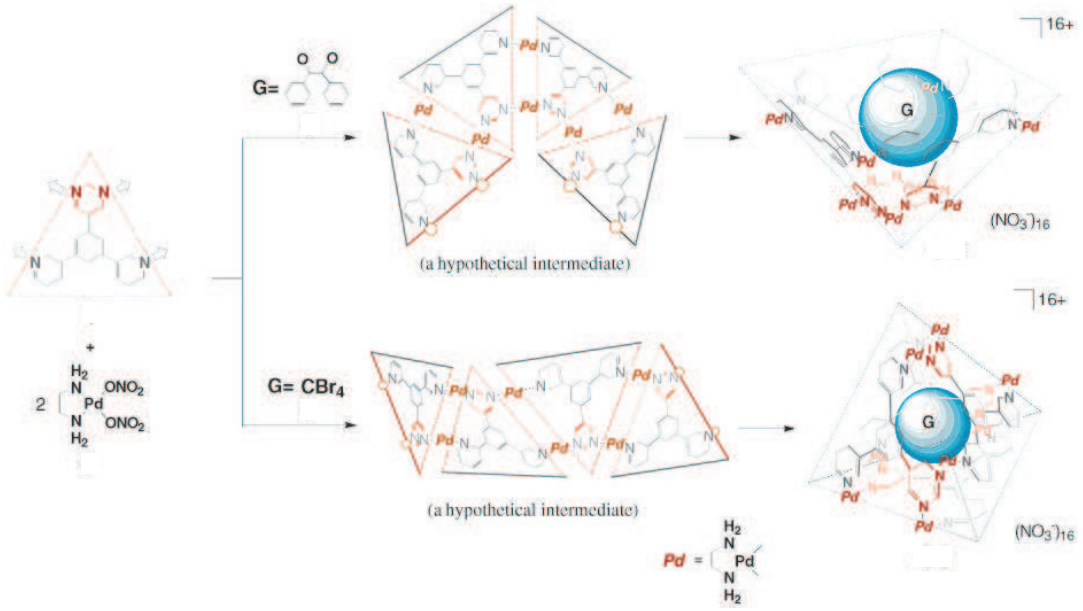

Scheme 3.1: Four triangular tetradentate ligands and eight metal centers self assemble into an open cone (tetragonal pyramidal, top) or a closed tetrahedron structure (bottom).

Recently, *Fujita et al.* showed that the choice of solvent can also change the outcome of self-assembly. A 1:1 mixture of Pd(NO_3)$_2$ and a bidentate ligand can

self-assemble into two box-shaped structures:[56] M_4L_8 and M_3L_6 (see Scheme 3.2). The authors demonstrated that the ratio of these two assemblies is almost completely controlled by changing solvents: In dimethylsulfoxide the M_4L_8 complex is formed exclusively, while in acetonitrile the M_3L_6 is the only product. Adding acetonitrile to an dimethylsulfoxide solution of the M_4L_8 complex leads to an equilibrium, which is depending on to the concentration of acetonitrile. When the acetonitrile is removed (*in vacuo*), the M_4L_8 complex is reverted back.

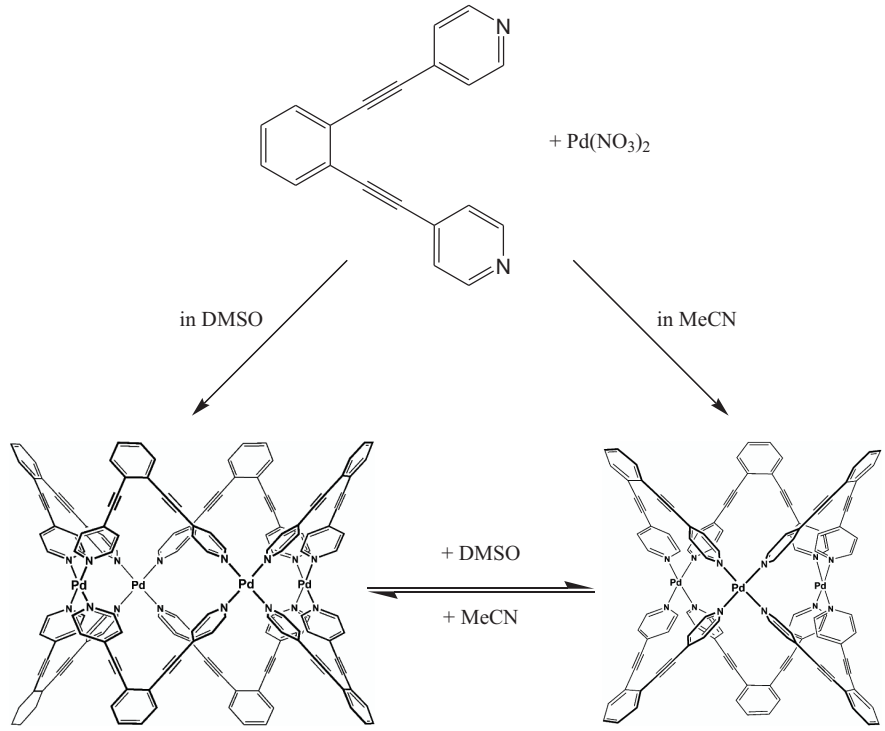

Scheme 3.2: The solvato-controlled assembly of M_4L_8 and M_3L_6 structures and their interconversion.

3.2.5 "Kinetic Self-Assembly"

In 2004, *Fujita et al.* reported an example of what the authors call "Kinetic Self-Assembly":[57] Two different macrocycles precursors, i. e. two U-shaped bidentate ligands, are mixed with (en)$Pd(NO_3)_2$ **[c]**. The two ligands only differ in exocyclic bulky alkoxy side chains. In the beginning, selective cross-catenation (AB) is observed by ^{1}H NMR and mass spectrometry as the only of three expected products

(A_2:AB:B_2), because the homo-catenation of the macrocycle with the bulky side chains is kinetically unfavorable (steric demand of the side chains).

If the mixture is allowed to stand at room temperature for one week, the three expected products, two different homo-catenanes and one hetero-catenane, are obtained in statistical ratio: 1:2:1 = A_2:AB:B_2.

One might consider this "kinetic self-assembly" not to be in line with what chemists consider in general with "kinetic control" (e.g. reversible Diels-Alder-reactions or the deprotonation of ketones at the α-position). In the covalent case, two different product distributions can be obtained in the end, individually (of course by two different routes). One of these products is NOT the thermodynamic product. Hence, the product distribution might alter over time depending on the system's temperature. Whereas in the self-assembly case, only one product is obtained in the beginning, which is transferred over time into THE thermodynamic product (or product distribution). One can consider this "Kinetic Self-Assembly" to be a slow reaction, which is following the basic laws of thermodynamics. Nevertheless, this example shows nicely that self-assembly is controlled by quite a lot of circumstances.

3.2.6 Theoretical Considerations

Recently, *Fyles et al.* developed a method to predict the outcome in a multi-component equilibrium self-assembly process[58] and applied it to the formation of self-assembled supramolecular squares of the Fujita type. The method is based on an additive free energy approach that derives the cumulative formation constants of all possible 56 species at equilibrium. Estimates for the required values of the pair-wise interactions are derived from potentiometric titrations. The method calculates the equilibrium speciation as a function of reactant concentrations and pH and produces a map of the range of compositions: quite expected, the square tetranuclear Pd complex is the most dominant at pH=7, when equimolar amounts of ligand and metal complex are used. The authors predict that even at μM concentrations this finding holds true. From these finding, *Fyles et al.* were able to form a highly conducting ion channel[59] by self-assembled supramolecular squares of the Fujita type.[60]

As all materials, introduced in the last chapter, are self-assembled in water, and only a few are soluble in organic media unlike highly polar solvents (dimethylsulfoxide and dimethylformamide), a large amount of puzzle pieces would be missing without *Stang's* contribution to self-assembly (3.3).

3.3 Organo-Soluble Assemblies by *Stang*

3.3.1 Self-Assembled Supramolecular Squares

Four years later than *Fujita et al.*, *Stang* and coworker introduced self-assembled supramolecular squares,[61] which are highly soluble in organic solvents such as dichloromethane, chloroform, nitromethane, ethanol, methanol, and acetone, but insoluble in diethylether, hexane, pentane, benzene, toluene, acetonitrile, and water. The bidentate blocking ligand as well as the counter anion are exchanged, to achieve this different solubility: NO_3^- is replaced by OTf^- and (en) by 1,3-bis(diphenylphosphino)-propane (dppp). Reaction of the resulting metal complexes (dppp)M$(OTf)_2$ with M = Pd(II) **[a]** or Pt(II) **[b]** with equimolar amounts of [4,4']-bipyridine, in dichloromethane at room temperature results in the formation of molecular squares in a matter of minutes. If desired, the squares can be precipitated with diethylether in excellent yields. Both compounds are air-stable, robust, microcrystalline solids and are characterized by elemental analyses and multinuclear NMR techniques:

- The elemental analyses are consistent with the 1:1 (complex:ligand) compositions.
- The ^{31}P NMR and ^{19}F NMR spectra display sharp singlets as expected for the highly symmetrical compounds. The ^{31}P NMR signals are shifted about several ppm, relative to the precursor metal(II) triflates. Most importantly, the coordinated ligands [4,4']-bipyridine display only two signals in the ^{1}H NMR spectra. Integration of the proton signals is consistent with the requirements.

Like in the case of *Fujitas* squares, right bond angles ($\sphericalangle$ ($N_{py.}$-M-$N_{py.}$) = 90°) rule out the formation of other cyclic oligomers which must have significant ring

strain. Since then, other proofs for this tetrameric structure have been found:

- FAB-Mass Spectrometry[62] showed peaks for $[(\text{dppp})\text{M}([4,4']\text{-bipyridine})]_4(\text{OTf})_7^+$, with M = Pd and Pt.
- ESI-FTICR-Mass Spectrometry[63,64] showed peaks for $[(\text{dppp})\text{M}([4,4']\text{-bipyridine})]_4(\text{OTf})_x^{(8-x)+}$ with $x = 1 - 6$. Furthermore, this methodology gave inside into the fragmentation path ways in the gas phase and the square-triangle equilibrium in solution, when [4,4']-bipyridine is exchanged by more flexible ligands (see 3.3.4).
- A solid-phase structure could be obtained by X-ray crystal structure analyses for $[(\text{dppp})\text{Pt}([4,4']\text{-bipyridine})(\text{OTf})_2]_4$,[61] whereas a triangular structure[65] is found in the case of $[(\text{dppp})\text{Pt}((\text{E})\text{-1,2-di(pyridin-4-yl)ethene})(\text{OTf})_2]_3$.
- EC-STM examinations on Cu(100)[66] showed the tetrameric structure nicely (see 6.1).

To assess the solution stability of these self-assembled supramolecular squares, the ^{1}H NMR spectra of $[(\text{dppp})\text{Pt}(2,7\text{-diazapyrene})(\text{OTf})_2]_4$ in CD_3NO_2 is examined between the temperatures of -20 and +90 °C. No change in the ^{1}H NMR spectra is observed in this 110 °C temperature range.[61]

The dramatic differences between Pd and Pt (see 3.2.1) are not observed by *Stang*. Unfortunately, it is not discussed, why these two metals differ that drastically in self-assembly reaction of $(\text{en})\text{M}(\text{NO}_3)_2$ and $(\text{dppp})\text{M}(\text{OTf})_2$.

Again, with this simple technique, mixing, stirring and precipitating, this readily soluble, cyclic, highly charged, tetranuclear Pd and Pt complexes are available in high yields by self-assembly.

3.3.2 Smaller and Larger Assemblies

The variety of assemblies introduced by *Stang et al.* is quite comparable, but equally elegant to the list of *Fujita et al.*: A small triangle (pyrazine as ligand),[67] larger triangles,[68] rectangles,[69,70] cycles,[71] a trigonal bipyramid,[72] tetrahedra,[73] dodecahedra,[74] cuboctahedra,[75] a dimeric rhomboid,[76] and other cages.[77] Unlike

Fujita et al., *Stang* and coworker have developed quite a large variety of different metal complexes as building blocks, to achieve this impressive list of assemblies.

3.3.3 Transport Experiments

Simple "passive transport" experiments demonstrate that some macrocycles are capable of transporting sodium tosylates from one aqueous phase into another through chloroform.[78]

3.3.4 Structural Switching

In 2002, *Schalley et al.*[63] explored the equilibrium between self-assembled supramolecular squares and triangles from (dppp)M(OTf)$_2$ with M = Pd(II) **[a]** or Pt(II) **[b]** and organic ligands (E)-1,2-di(pyridin-4-yl)ethene **1** and (E)-1,2-di(pyridin-4-yl)diazene **2** by ^{1}H NMR and ^{31}P NMR as well as mass spectrometry. As both organic ligands are more flexible than [4,4']-bipyridine, triangle formation is not excluded anymore. Of course, they do not bear a geometry that is in line with the requirements of the cis-coordinated metal centers. Thus, they suffer from some ring strain. On the other hand they are entropically favored due to the larger number of triangles formed from the same number of building blocks. In most cases, this fine balance between entropy and enthalpy determines which species are formed and where the equilibrium lies.

In the ^{31}P NMR spectra (see Figure 3.1 c), two sets of signals (assigned to squares and triangles) are observed for [(dppp)Pt(**1**)(OTf)$_2$]$_x$ (x=3 or 4), which change in their relative ratios from about 5:1 (square:triangle) in [D$_7$]-dimethylformamide to about 2:1 in [D$_7$]-dimethylformamide:[D$_6$]-acetone = 30:70. Thus, the smaller macrocycle is suppressed, when acetone is added. This finding is quite comparable with the results from *Fujita et al.* (see 3.2.4), where a M$_4$L$_8$ complex is more dominant in dimethylsulfoxide and the M$_3$L$_6$ complexes in acetonitrile. Furthermore, the square-triangle-equilibrium shows temperature dependence in ^{1}H NMR and ^{31}P NMR experiments: The square concentration decreases in intensity with increasing temperature. This behavior is expected, as the entropy contribution to the free energy becomes more important at higher temperatures

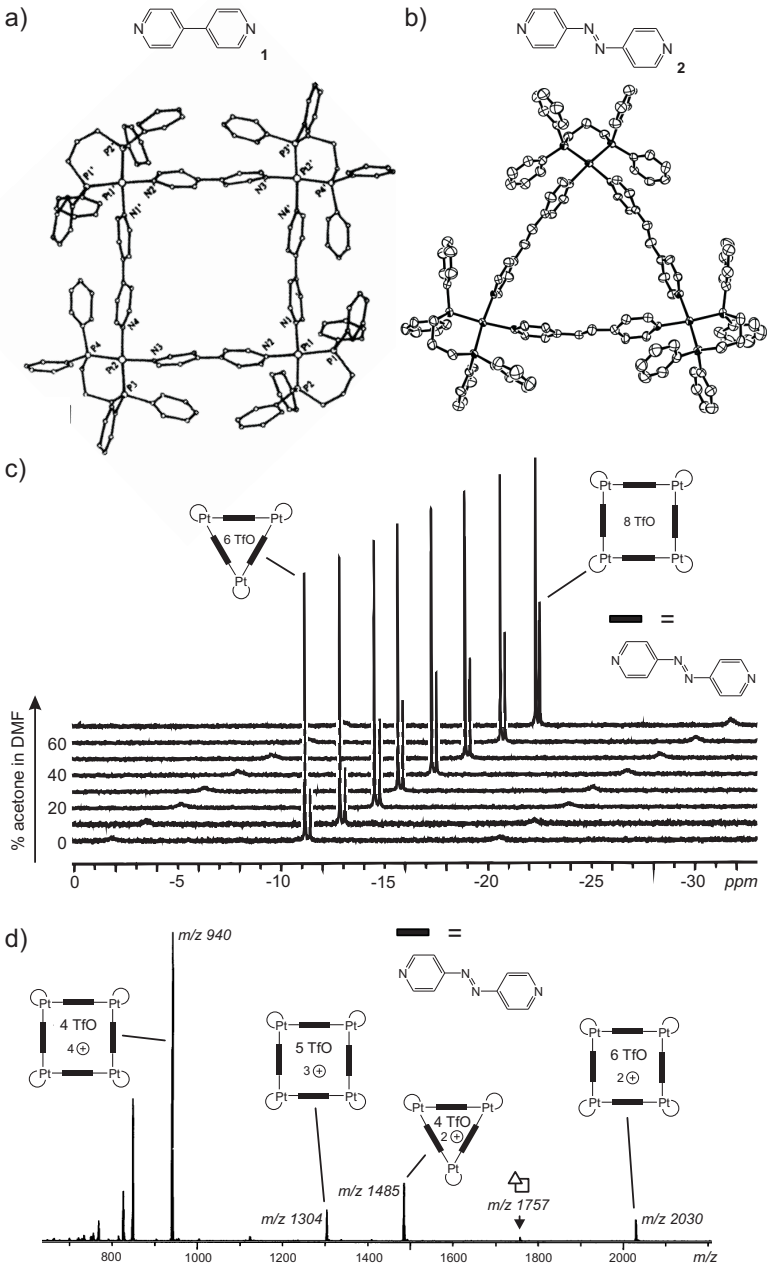

Figure 3.1: Crystal structures of a) $[(dppp)Pt(OTf)_2([4,4']\text{-bipyridine})]_4$[61] and b) $[(dppp)Pt(OTf)_2(\mathbf{2})]_3$; c) square-triangle equilibrium between $[(dppp)Pt(OTf)_2(\mathbf{2})]_4$ and $[(dppp)Pt(OTf)_2(\mathbf{2})]_3$ observed by ^{31}P NMR; d) MS spectra of the above mentioned equilibrium.

and thus more and more disfavors the squares.

One year later, *Stang et al.* showed a concentration- and temperature dependent equilibrium between a dimeric rhomboid and a trimeric hexagon following Le Châtelier's principle.[76] The study of the equilibrium by ^{1}H NMR allowed the quantitative determination of the thermodynamic equilibrium constants, where such variables as ionic strength and activity coefficients have also been considered.

3.3.5 Summary

In the last two sub chapters an enormous number of different assemblies has been introduced, both soluble in water and organic media. Complementary methods have been applied to characterize the resulting compounds or equilibria as well as the chemistry inside these special micro-environments. Furthermore, it has been shown that self-assembly (and structural switching) can be controlled by quite a lot of circumstances: On one hand, there are the expected factors like programming (flexibility vs. rigidity), the molar ratio of the subunits, temperature, concentration, pH-value, or guest inclusion. On the other hand, rather unexpected criteria have been found to govern the outcome of self-assembly like solvent and time ("kinetic self-assembly").

3.4 Chirality in Self-Assembly

3.4.1 Chiral Assemblies from Achiral Building Blocks

Quite a lot of examples exist, where achiral building blocks assemble into chiral assemblies. For example, an assembly process of two achiral molecules leads to a chiral supermolecule, when the symmetry planes of the molecular components are perpendicular to each other in the assembly,[79] like in the case of dimeric capsules by *Rebek et al.*[80,81] The problem with such approaches is that the resulting complexes are obtained in racemic mixtures. However, self-resolution[82] occurs in some cases; self-resolution is the spontaneous selection of components with the same chirality from a racemic mixture that leads to the formation of homochiral

assemblies. This is a characteristic phenomenon in the solid state (e. g. crystallization) or on surfaces, but it still is a rare event in solution. Usually, one can not predict with nowadays methods the outcome of these separations. As this approach is not the subject of this thesis, these assemblies are not discussed in more detail.

3.4.2 Chiral Assemblies from Chiral Building Blocks

For functional supramolecules[18] it is important to control the stereoselectivity in the self-assembly process. The general method to control supramolecular chirality is the introduction of chiral building blocks (asymmetric induction). In principle, all types of chirality may be included in particles, which self-assemble: Point chirality, axial chirality, helical chirality, planar chirality, or topological chirality. Two different approaches might be followed. Several examples can be found, in which chiral side groups (point chirality, chiral pool) are peripherally attached:

- helically chiral metal helicates, formed by organic ligands with chiral side groups attached,[83]
- a chiral pyramidal polyhedron, assembled by chiral [2,2']bipyridine-derivatives and Pr(III)-ions,[84]
- chiral hydrogen-bonded oligo(p-phenylenes), which aggregate in chiral stacks,[85] or
- chiral calix[4]arenes, which only assemble into one out of two possible diastereoisomeric assemblies.[86]

However, when chiral ligands are introduced in metal helicates[87] three forms of chirality must be distinguished. At first, the chirality given by the optically active carbon (R/S), secondly, the coordination environment around the metal centers (D/L), and thirdly the overall sense of the helix(P/M).[88]

Fewer examples can be found, where chiral subunits self-assemble, without the help of chiral side groups:

- cyclic octapeptides, with alternating point chirality which self-assemble into nanotubes[89] (chiral pool),
- self recognition of ligands[90] in a Cu(I)-complex, with (R,R)-1,2-diamino-cyclo-hexane (dach, commercially available) as central building block, or
- chiral subunits (the chirality is due to the curved geometry and a lack of symmetry, separation of enantiomers), which produce cyclic, tetrameric capsules.[81]

Both approaches have their advantages and disadvantages: When inherent chiral subunits need to be synthesized, the obtained racemic mixtures must be separated into enantiomers, or enantioselective syntheses must be used. The use of peripherally attached chiral molecules from the chiral pool is certainly easier, but somehow less elegant. From the point of view of atom efficiency[91] (introduced by *Trost*), chiral self-assembly without the help of peripherally attached, chiral side groups uses a smaller number of atoms and is thus more efficient.

3.4.3 Examples from *Fujita et al.*

As the square planar metal complexes used by *Fujita et al.* are achiral, the chirality must be introduced by (i) chiral, bidentate, blocking ligands attached to the metal complex or (ii) chiral organic ligand subunits. In 2002, *Fujita et al.* reported an example of the first type.[92] When (R,R)-1,2-diaminocyclo-hexane (dach) is used as bidentate blocking ligand for $Pd(NO_3)_2$, (dach)$Pd(NO_3)_2$ is obtained as chiral building block for self-assembly. Several U-shaped, achiral, bidentate ligands are "ring-closed" by reaction with (dach)$Pd(NO_3)_2$. The macrocycles themselves are CD silent, whereas the resulting catenanes are CD active. Obviously, chirality induction of the assemblies is achieved by the use of chiral building blocks.

3.4.4 Examples introduced by *Stang et al.*

Again like *Fujita et al.*, chiral assemblies are designed with chiral metal complexes, which were obtained from (R)-BINAP,[93,94] as well as (R)-DIOP and (S)-DIOP[95] as chiral, bidentate, blocking ligands. In the first case, *Stang et al.* monitored the

rotation of one ligand between two metal complexes by ^{1}H NMR to obtain rotational barriers. In the latter case, circular dichroism studies are used to observe neutral guest inclusion. As these systems are not comparable with the systems introduced in this thesis, the results are not discussed herein.

3.4.5 Summary

In the introduced chiral assemblies by *Fujita et al.* and self-assembled supramolecular squares by *Stang et al.*, only chiral metal subunits, obtained by chiral, bidentate, blocking ligands, are used. However, chiral ligands, a main focus of this thesis, remain by and large unexplored.

3.5 Catenanes and Rotaxanes

Besides self-assembled supramolecular squares, a second class of supramolecular compounds plays an ancillary role in this thesis: Catenanes and rotaxanes.

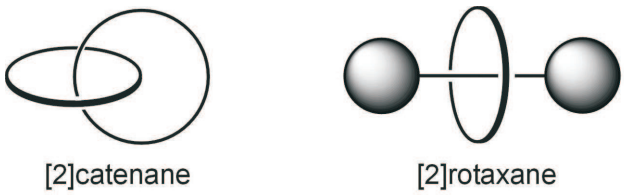

Figure 3.2: A [2]-catenane and a [2]-rotaxane.[96]

This sub chapter should give a very brief introduction into these fascinating compounds. Catenanes[97] (from the Latin word "catena" for "chain") are two entangled macrocycles mechanically interlocked[98] with each other. Rotaxanes[99] are likewise mechanically-interlocked compounds consisting of a "dumbbell shaped molecule" which is threaded through a macrocycle. The name is derived from the Latin word for wheel (rota) and axle (axis). Catenanes can not be separated without breaking a covalent bond, although they are not bound to each other by such a bond. The two components of rotaxanes are kinetically trapped since the ends of the dumbbell (called stoppers) are usually larger than the internal diam-

eter of the macrocycle. Among other facts, the size[100] of the stoppers and the macrocycle defines the timescale of disassociation ("unthreading") of the components. These complex molecules cannot be obtained in adequate yields without templated[101] synthesis. Also, catenanes feature some challenging properties as polymers,[102] switches,[103] or potentially as molecular machines,[104] in which they are able to circumrotate.[105] Last but not least, catenanes and rotaxanes can be topological chiral.[106]

Chapter 4

Methodological Overview

Whereas in the last chapter the access towards the substances used in the thesis was introduced, this chapter deals with the methods used to analyze the obtained substances and materials. Several different - to some extent complementary - methodologies have been developed to examine supramolecular systems in the condensed phase, in solution and in the gas phase. For example:

- in the condensed phase: Crystallography, Scanning Tunneling Microscopy (STM) and other proximal probes, Infrared spectroscopy (IR, also in solution and the gas phase)
- in solution: Ultraviolet visible spectroscopy (UV/VIS), nuclear magnetic resonance spectroscopy (NMR, including 1D and 2D techniques, also in the solid state), isothermal titration calorimetry (ITC), circular dichroism spectroscopy (CD)
- in the gas phase: Mass Spectrometry (MS).

Each of these methods has been developed continuously over the last decades. Thus, a complete introduction into each method is impossible in the scope of this thesis. The issues of each research area related to this work are highlighted thoroughly: At first, fundamental techniques like NMR and MS are discussed. In the following sub chapter, the Scanning Tunneling Microscopy (STM) and the advanced Electrochemical STM (EC-STM) are described briefly. The research

path towards applied sensor techniques, like Quartz Micro Balances(QMB), is followed in the last sub chapter.

4.1 NMR in Supramolecular Chemistry

Nuclear magnetic resonance (NMR) spectroscopy exploits the magnetic properties of certain nuclei like ^{1}H, ^{13}C, ^{15}N, ^{19}F, or ^{31}P. The most important applications for organic chemist are ^{1}H NMR and ^{13}C NMR spectroscopy in solution. This holds true for supramolecular chemists as well. Nevertheless, some important aspects for supramolecular chemistry needs to be addressed.

The ratio of different building blocks can be assigned with simple ^{1}H NMR or ^{13}C NMR experiments under certain circumstances (e. g. when signal overlapping is not observed). If the symmetry of a large assembly is low, signal integration might be difficult due to signal overlapping. Moreover, the ratio of building blocks alone is not sufficient when the absolute amount of building blocks is under question. For example, a 1:2-complex and a 2:4-complex of A and B might have analogous ^{1}H NMR spectra. If both complexes are present in equilibrium the situation gets challenging. Again, the ratio of these two complexes might be obtained by signal integration, but the assignment which set of signals corresponds to which complex is somewhat speculative.

Complexes that are not satisfactorily represented in 1D NMR spectra might be further elucidate by 2D experiments. Several elaborate pulse sequences have been developed. One the one hand, the second dimension might be time, to evaluate the kinetic of self-assembly reactions, or temperature, to get first insight into thermodynamic aspects. On the other hand, magnetization transfer might be used to correlate nuclei. Depending on the experiment, this transfer can be achieved through bonds (HH-COSY, HH-TOCSY, HMQC, or HMBC) or space (ROESY or NOESY). Furthermore, DOSY experiments[107] (**D**iffusion **O**rdered **S**pectroscop**y**) might be used to measure the diffusion coefficients of different complexes by NMR. This tool has become a valuable tool to examine self-assembly reactions. Last but not least in this incomplete list, EXSY[16] (**Ex**change **S**pectroscop**y**) experiments offer a simple way to obtain information about dynamic processes in complexes.

Again, a detailed discussion of these techniques is omitted but can be found in standard text books listed in the references.[17]

4.2 MS in Supramolecular Chemistry

Mass spectrometry is an analytical technique that identifies the mass-to-charge ratio of charged particles. Usually, a mass spectrometer has three essential parts:

- **Ion Source**: In the ion source, the analyte is converted into ions and transferred into the gas phase. Typical ionization techniques are Electron Ionization (EI), Chemical Ionization (CI), Fast Atom Bombardment (FAB), Electrospray Ionization (ESI), and Matrix Assisted Laser Desorption Ionization (MALDI).
- **Mass Analyzer**: A mass analyzer sorts the ions by their masses in electric and magnetic fields. Sector field, time-of-flight (TOF), quadrupole, ion traps, and ion cyclotron resonance (ICR) mass analyzers might be used.
- **Detector**: In or at the detector the somehow "sorted" ions or fragments of ions are detected and counted. Usually, electron multipliers are used to "count" single ions.

The building blocks in self assembly are usually hold together by weak interaction. Hence, ionization is rather difficult and can only be achieved by soft ionization conditions. Nondestructive transfer into the gas phase is usually achieved by ESI. As most substances in the experimental part of this work were indeed transferred into the gas phase by ESI, and sorted and detected inside an FT-ICR, these techniques will be discussed in more detail in the following chapters.

4.2.1 Electrospray Ionization (ESI)

In electrospray ionization,[11] first introduced by Dole in 1966[111] and further developed by Fenn,[112] a liquid, containing the analyte, is pushed through a very thin capillary in a very strong electric field. As charges repel, the liquid pushes itself out of the capillary and forms a mist or an aerosol of small droplets about

10 μm across. This jet of aerosol droplets is produced by a process involving the formation of a Taylor cone[113] and a jet from the tip of this cone. A neutral carrier gas, such as nitrogen, is used to help nebulize the liquid and to help evaporate the neutral solvent in the small droplets. From here on, two different mechanisms of ionization are discussed: Coulomb fission and Ion Evaporation. As the small droplets evaporate, the charged analyte molecules are forced closer together. The proximity of the molecules becomes unstable as the equally charged molecules come closer together. The droplets once again explode when the repulsion of the charges is higher than the surface tension.[114] This process repeats itself until the analyte is free of solvent and is a lone ion (Coulomb fission). Alternatively, it is assumed that the increased charge density, resulting from solvent evaporation causes Coulombic repulsion to overcome the liquid's surface tension resulting in a release of ions from droplet surfaces (Ion Evaporation). Which of those two pathways is the major one is still under discussion.

Nevertheless noteworthy is that the use of the word "ionization" in "electrospray ionization" is misleading, due to that many of the ions observed are preformed in solution before the electrospray process or created by simple changes in concentrations (or in some cases pH-value) as the aerosolized droplets shrink. It is argued that electrospray is simply an interface for transferring ions from the solution phase to the gas phase.

Electrospray ionization is also ideal for studying non-covalent complexes (see below). The electrospray process is sometimes capable of transferring non-covalent complexes into the gas phase without disrupting the non-covalent interaction. If ESI is not "soft enough", cold-spray ionization (CSI),[115] a variant of ESI operating at low temperature (ca -80 to 10 °C), may be used with good results.

In 2003, Prof. Dr. John B. Fenn was awarded the Nobel Price for Chemistry for his contribution on the field of ESI applied to BIO-molecules.

4.2.2 Basic Principle of Fourier Transform Ion Cyclotron Resonance Mass Spectrometry (FT-ICR-MS)

In 1974, Fourier-transform ion-cyclotron-resonance mass spectrometry was introduced by Comisarow and Marshall.[108] First, the basic physical principles of FT-

ICR-MS are briefly presented. After that, the instrument, the techniques and the experiments used in this thesis are discussed in more detail. An ion of charge z moving with velocity v in a static magnetic field B is subjected to a force F that is proportional to the magnitude of the charge and the speed of the particle[109] (Lorentz force, see 4.1):

$$F = zv \times B \tag{4.1}$$

The magnitude and direction of the force depend on the direction of the velocity as described using the vector cross product. An important characteristic of the magnetic force on a moving charged particle is that the force is always perpendicular to the velocity of the particle. The magnetic force does no work on the particle, so this force does not affect the kinetic energy of the particle. While the direction of the force changes, its magnitude remains constant. In the special case where the velocity of a charged particle is perpendicular to a uniform magnetic field the particle moves in a circular orbit. If we apply Newton's second law to the particle (eq. 4.2):

$$zv \times B = \frac{mv^2}{r} \quad \Leftrightarrow \quad \frac{v}{r} = \frac{zB}{m} \tag{4.2}$$

where m is the mass of the ion and $\frac{v}{r}$ represents the cyclotron frequency ("cyclotron" equation), the experimentally measured ion cyclotron frequency can thus be converted to the mass-to-charge ratio of an ion. The frequency of the cyclotron gyration of an ion is inversely proportional to its mass-to-charge ratio $\frac{m}{z}$ and directly proportional to the strength of the applied magnetic field. A remarkable feature of eq. 4.2 is that all ions of a given mass-to-charge ratio, $\frac{m}{z}$, have the same ICR frequency, independent of their velocity. This property makes ICR especially useful for mass spectrometry, because translational energy "focusing" is not essential for the precise determination of $\frac{m}{z}$.[110]

In an FT-ICR mass spectrometer, ions are trapped in a cell which is positioned inside a strong magnetic field and composed of three distinct sets of plates: trapping, transmitter and receiving plates. The ions are trapped in the cell by electric potentials applied to the trapping plates that are perpendicular to the magnetic field.

As r is limited by the instrument's size, the maximum $\frac{m}{z}$ value of an ion that can be trapped is a function of the magnetic field strength. The greater the field strength, the higher the $\frac{m}{z}$ value of the ion can be. In order to obtain the desired magnetic field strength, it is necessary to use a super-conducting magnet (nowadays up to 14.5 Tesla, 2004).

Although ions in a static magnetic field move in cyclotron orbits, they will not generate any signal if placed between a pair of receiving plates, due to randomly oriented and thus incoherent motion. In order to obtain a signal, a packet of ions of a given mass-to-charge ratio needs to be converted into coherent motion by applying an oscillating electrical field such as provided by a AC signal generator (transmitter plates). If the frequency of the applied field is the same as the cyclotron frequency of the ions, the ions absorb energy thus increasing their velocity (and the orbital radius) but keeping a constant cyclotron frequency.

When the radio-frequency current is turned off, each packet of ions of a specific $\frac{m}{z}$ induces an image current that is detected by a pair of electrodes in the analyzer cell (receiving plates). The amplitude of the detected current is proportional to the number of ions in the analyzer cell while its frequency is the same as the cyclotron frequency of the ions. A small AC voltage is generated across a resistor and this signal is amplified and detected. The ions are therefore detected without ever colliding with the electrodes. This non-destructive detection scheme is unique to ICR and allows for improved sensitivity and versatility compared to more traditional approaches that utilize destructive detection methods.

The decay over time of the image current resulting after applying a short radio-frequency sweep that excites all ions simultaneously, is transformed from the time domain into a frequency domain signal by a Fourier transformation. Because the cyclotron frequency $\frac{v}{r}$ is related to $\frac{m}{z}$ by equation (4.2) a spectrum as a function of $\frac{m}{z}$ can be obtained. Cyclotron frequencies can be measured with very high precision leading to high accuracy mass measurements and ultra-high resolving power.

4.2.3 Tandem Mass Spectrometry

Tandem mass spectrometry[116] (MSMS or MS^n) is inter alia used to gain structural information about a complex compound by fragmenting specific ions inside the mass spectrometer and identifying the resulting fragment ions. This information can then be pieced together to generate structural information regarding the intact molecule. Primary ("precursor") ions are energetically activated and then dissociated followed by mass analysis of the resulting secondary ("product") ions.

A tandem mass spectrometer in many cases is a mass spectrometer that has more than one analyzer, in practice usually two. The two analyzers are separated by a collision cell into which an inert gas (e.g. argon, xenon) is admitted to collide with the selected sample ions. As an alternative, ions may be trapped for sometime in a confined space using a a magnetic field (see 4.2.2). Thus a second analyzer is obsolete in this case.

Inside a FT-ICR instrument, dissociation is commonly achieved by collisions of ions with neutrals, collision-induced dissociation[117] (CID), electron capture dissociation[118] (ECD), ultraviolet photodissociation (UVPD),[119] multiphoton infrared photodissociation (IRMPD),[120] or blackbody infrared dissociation (BIRD)[121] which makes the experimental setup much easier.

Mainly CID and IRMPD were used for fragmentation in this work. For CID of ions, the most popular method is sustained off-resonance irradiation (SORI),[122] because it is the simplest to implement and tune. Photodissociation has also proved effective. Typically, IR (10.6μm) laser photons are used for "slow heating," and fragments similar to those obtained by CID are produced. One advantage of IRMPD is that gas pulses are not necessary, so that high-resolution FT-ICR detection can occur quickly after dissociation, as no pump down is required.

For large ions, two fundamental limits severely constrain fragmentation in tandem mass spectrometry.[123] First, the center-of-mass collision energy - the absolute upper limit of energy transfer in a collision process - decreases with increasing mass of the projectile ion for fixed ion kinetic energy and mass of the neutral molecule. Secondly, the dramatic increase in density of states with increasing internal degrees of freedom of the ion decreases the rate of dissociation by many orders of magnitude at a given internal energy. Consequently, most practical MS/MS

experiments with complex ions involve multiple-collision activation (MCA-CID).

4.2.4 The Bruker Apollo IV FT-ICR-MS

In September 2003, the "Kekulé-Institut for Organic Chemistry" received a Bruker APEX IV Fourier-Transform Ion-Cyclotron-Resonance (FT-ICR) Mass Spectrometer which was installed at the University of Bonn for the Collaborative Research Initiative 624 of the German Science Foundation.

Analyte solutions were introduced into the ion source with a syringe pump (Cole-Palmers Instruments, Series 74900) at flow rates of around 3–4 μl/min. The instrument is equipped with an Apollo ESI ion source(off-axis 70° spray needle). Ion transfer into the first of three differential pumping stages in the ion source was performed through a glass capillary with 0.5 mm internal diameter and nickel coatings at both ends. Ionization parameters, some with a significant effect on signal intensities, were adjusted as follows: capillary voltage: –4.1 to –4.4 kV; end-plate voltage: –2.8 to –3.5 kV; cap-exit voltage: +200 to +300 V; skimmer voltages: +8 to +12 V. The flow of the drying and nebulizer gases were kept in a medium range (ca. 700 mbar). The ions were accumulated in the instrument's hexapole for 0.5–1 s, introduced into the FT-ICR cell (inside a 7 Tesla super conducting magnet), which was operated at pressures below 10^{-10} mbar, and detected by a standard excitation and detection sequence. For each measurement 16–256 scans were averaged to improve the signal-to-noise ratio. For MSMS experiments, the complete isotope patterns of the ion of interest were isolated by applying correlated sweeps followed by shots to remove the higher isotopes. After isolation, argon was introduced into the ICR cell as the collision gas through a pulsed valve at a pressure of around 10^{-8} mbar. The ions were accelerated by a standard excitation protocol and detected after a 2 s pumping delay. For IRMPD a CO_2 IR laser at a wavelength of 10.6 μm and a power of maximum 25W was used. A detailed description can also be found in the references.[124]

4.2.5 Examples for Structural Information by Tandem MS

Although most tandem mass spectrometry experiments nowadays are performed for peptide and oligonucleotide sequencing, there are several examples were MS^n is used to produce structural information[125] of complex supramolecules. One example should be discussed in more detail. Compounds from the research groups of *Prof. Vögtle* and *Prof. Schalley* like macrocycles and non-covalent complexes like catenanes and rotaxanes were investigated in the gas phase to obtain structural information.[126,127] Among others, five different compounds **6** - **10** (see following three figures) were investigated by ESI tandem mass spectrometry. They were sprayed from methanol (30μm solutions). MSMS spectra were recorded as described before. On collision with argon protonated tetralactam macrocycle **6** looses one water molecule. Several other fragmentations occur and appear in the spectra with much lower intensities. All these fragments are assigned to two subsequent bond cleavages within the macrocycle and loss of the neutral fragment (six categories, see Fig. 4.1) and there is evidence that the first step is cleavage of the protonated amide bond. Three out of the four other compounds under study have the tetralactam macrocycle as building block, the fifth is a octalactam macrocycle with the same subunits (see Fig. 4.2 and 4.3).

The following two compounds, catenane **7** and octalactam macrocycle **8**, have the same elemental composition, which leads to the same mass and the same isotopic pattern, but they differ in topology resulting in different properties. Whereas ordinary MS fails to distinguish between these two isobaric species, MS^n is able to: The MS^n-spectra from **7** and **8** differ from each other in two significant respects. While the protonated octalactam macrocycle **8** predominantly loses a water molecule like the tetralactam macrocycle **6**, the protonated catenane **7** yields only a very minor signal for such a reaction. Instead, a stronger signal is observed at half the mass which corresponds to tetralactam macrocycle **6** or rather its open-chain analogue. This fragment can easily be explained by a ring cleavage reaction within one of the two macrocycles, which is then followed by deslipping of the neutral macrocycle finally leaving the complex.

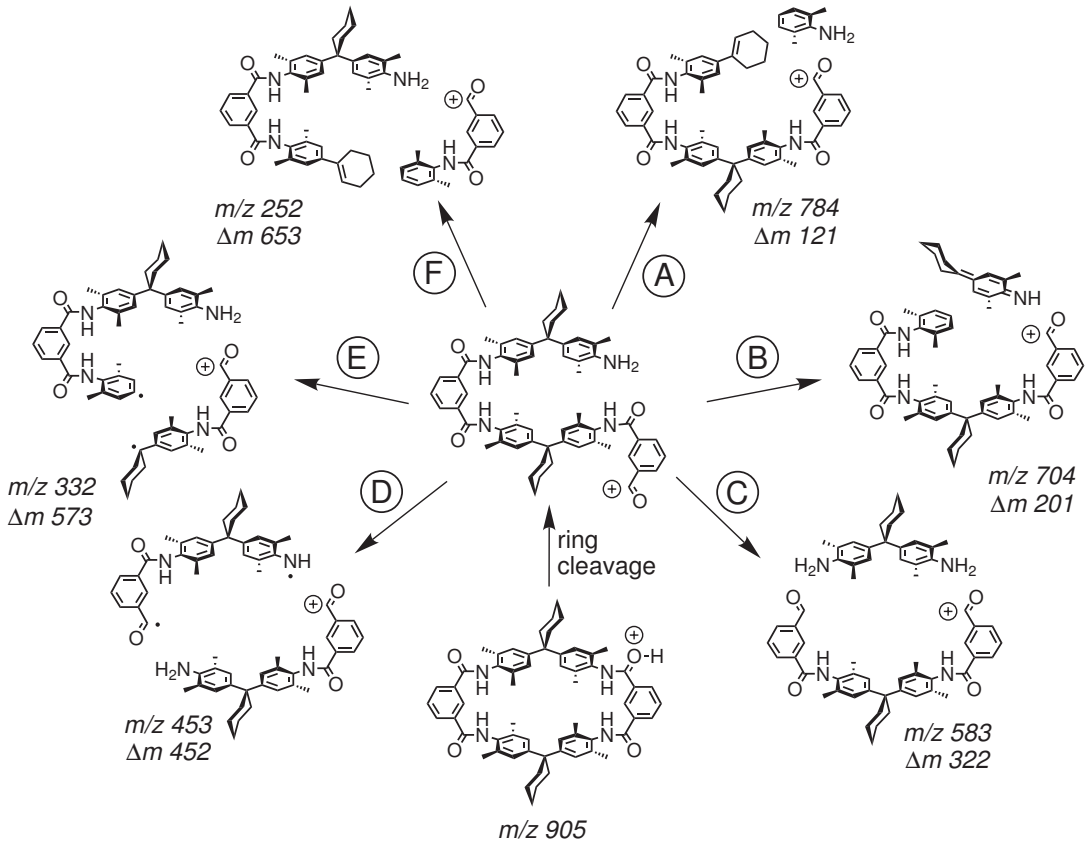

Figure 4.1: Fragmentation of the protonated tetralactam macrocycle.

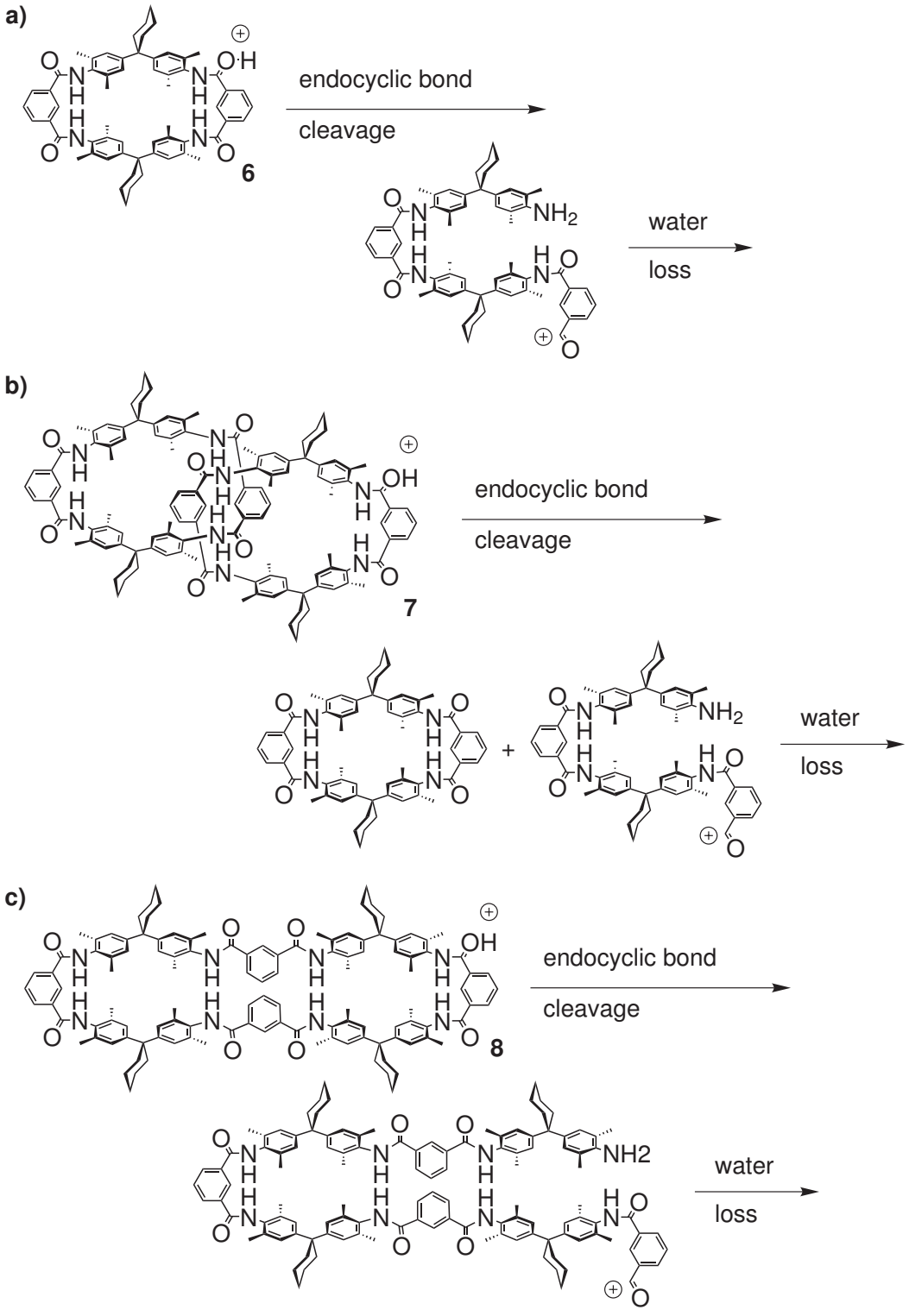

Figure 4.2: Fragmentation of the protonated compounds **6** - **8**.

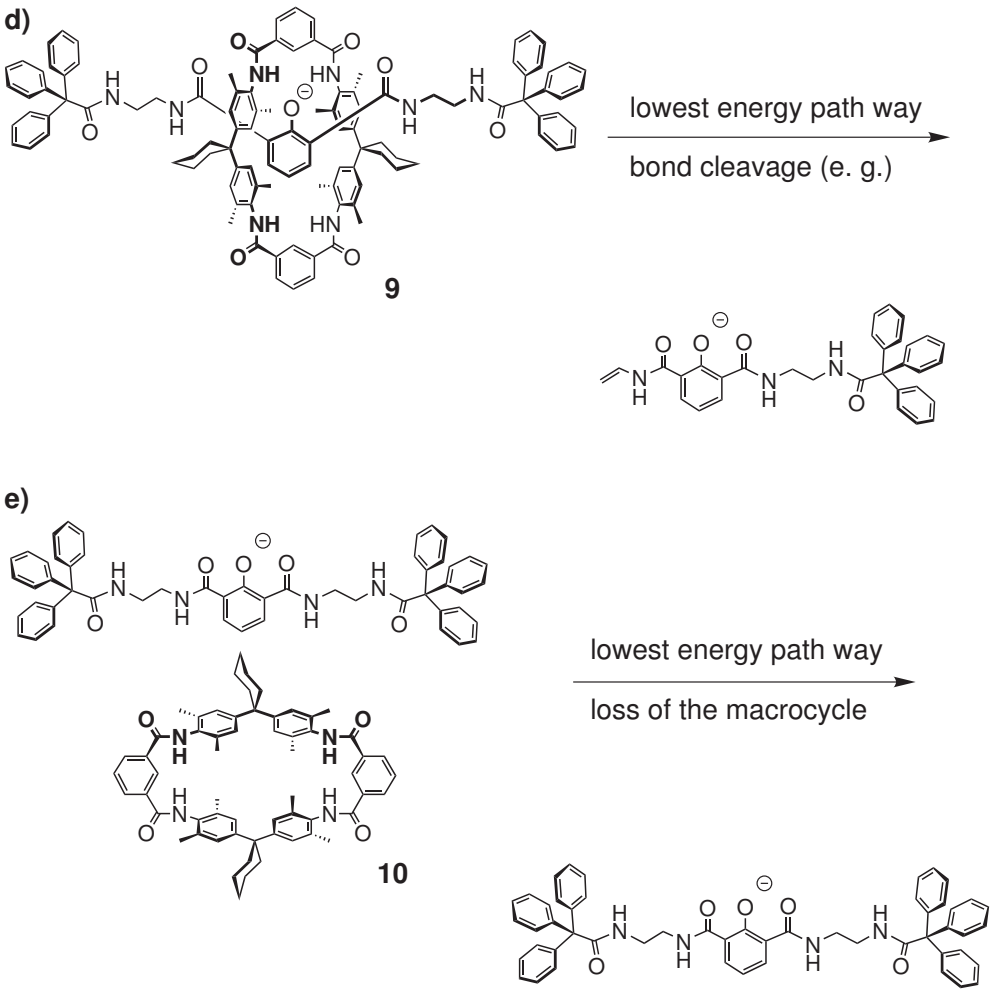

Figure 4.3: Fragmentation of the deprotonated supramolecular compounds **9** and **10**.

The next two compounds have again both the same elemental composition, and can be distinguished by MS^n, as well: When deprotonated rotaxane **9** is isolated and collided with argon, only fragments of the axle are observed as products, but not the intact axle alone. The typical decomposition products of the tetralactam macrocycle **6** are not observed. This indicates that the decay of the axle is less energy demanding than that of the macrocycle. In marked contrast, complex **10**, in which the axle is weakly bound to the wheel, shows the intact axle as major product of dissociation. Of course, for a non-covalently bound complex in which the two components are held together by weak interactions, one would not

expect energy-demanding bond rupture to compete, and thus this result is not unexpected.

The most important conclusion from these experiments is that mass spectrometry, carefully used, may provide more than just an exact mass. Beyond its 'normal' use for mass analysis, it gives structural information, even for such large molecules as catenanes and rotaxanes **6** - **9**. Of course, control experiments with isomeric structures should be done whenever possible.

Only noted in passing is that ion mobility mass spectrometry[128] (IMS/MS, a technique where ions are first separated by drift time through some neutral gas under an applied electrical potential gradient) might also been used to gather structure information.

4.2.6 Reactivity in the Gas Phase

In summary, mass spectrometry is used to characterize various analytes and gather valuable structure information. Maybe even more important, mass spectrometry reveals the intrinsic properties of chemical compounds. Interactions with other molecules like solvent molecules do not take place, as the ion is highly diluted in the gas phase. Hence, comparison with data obtained from solution may reveal the effects of solvation.

In this context, several fascinating results were obtained by mass spectrometric investigations including metal organic chemistry[129] in the gas phase or homogeneous catalysis,[130] just to name two. In 1997, *Armentrout et al.* developed CRUNCH,[131] a combined MS and computational chemistry approach to obtain binding constant for small complexes from gas phase experiments. Recently, *Chen et al.* described an advanced methodology[132] for larger complexes. Last but not least, H/D-exchange experiments[133] might be used to distinguish between isobaric isomers.

4.3 Scanning Tunneling Microscopy (STM)

4.3.1 Introduction into STM

Traditionally, diffraction-based probes have played the major role in structural analysis, and have provided most of our basic knowledge about the atomic arrangement of materials. For example, the diffraction of beams of a wavelength that is comparable to the spacing between atoms in a crystal indicates the spacing between the atoms. Thus, X-ray diffraction is the primary tool for analyzing the long-range, atomic ordering of solids. Diffraction measurements however reveal only the internal atomic arrangements of a material. A separate class of tools is desired, when the surface atoms of a material in real space are under study, rather than its three-dimensional bulk structure. The Scanning Tunneling Microscopy (STM) was the first of several "proximal probes" (STM, Atomic Force Microscopy (AFM), Electrostatic Force Microscopy (EFM), etc.) that in the past decades have revolutionized the ability to explore solid surfaces on the size-scale of atoms.

The Scanning Tunneling Microscopy (developed in the 1980ies[134,135]) provides a "picture" of a surface by sensing corrugations in the electron density that arise from the positions of surface atoms. A finely sharpened metal wire (or "tip") is first positioned within a few nanometers of the sample by a piezoelectric transducer, a ceramic positioning device that expands or contracts in response to a change in applied voltage. This arrangement enables the STM to control the motion of the tip with subnanometer precision in all directions in space. At this small separation electrons "tunnel" through the gap, the region of vacuum, gas or liquid between the tip and the sample. If a small voltage (bias) is applied between tip and sample, then a net current of electrons (the "tunneling current"[136]) flows through the gap in the direction of the bias. Now, the tip is rastered across a small region of the sample. As the tip scans across the surface, corrugations in the electron density at the surface of the sample cause corresponding variations in the tunneling current. By detecting the very fine changes in tunneling current as the tip is swept across the surface, a map of the corrugations (i. e. a topographic map) in electron density at the surface can be derived.[137]

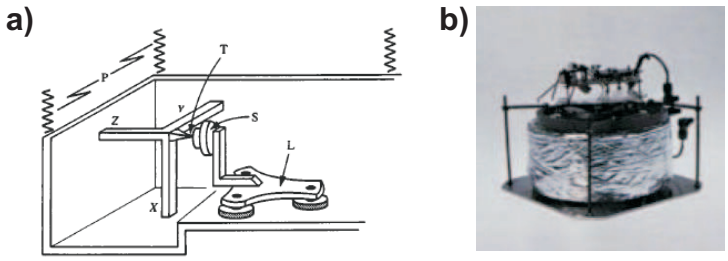

Figure 4.4: a) Schematic representation of a STM: The tip T of the microscope is scanned over the surface of a sample S with a piezoelectric tripod (X,Y,Z). The rough positioner L brings the sample within reach of the tripod. A vibration filter system P protects the instrument from external vibrations; b) Photograph of the prototype (both taken from[138]).

Two different modes can be applied: in the constant current mode, the tip is moved along a fixed trajectory in the x direction, and the tunneling current is monitored. A feedback loop is then used to move the tip towards or away from the sample in order to maintain a constant current. At the end of a single scan, the tip is displaced a single step in the y-direction, and the scan repeated.

In the constant height approach, the tip-sample distance is fixed during the scan, and the variation in tunneling current is plotted as a function of lateral position. Thus, only the electronics have to respond, rather than the piezoelectric crystal. As a result, the imaging speed can be increased drastically. The constant height method can however only be used to image very flat areas of the sample.

In 1986, Gerd Binnig and Heinrich Rohrer of IBM's Zürich Research Center were awarded the Nobel Prize in Physics for developing the STM. For recent reviews see reference.[140]

4.3.2 Electro Chemical STM (EC-STM)

Basically, an Electro Chemical Scanning Tunneling Microscopy (EC-STM) consists of the components of a general STM and additionally the components used in Cyclic Voltammetry (CV).[141] This allows two important modifications: a) The tunneling process occurs at the solid/liquid interface[142] (mostly an aqueous electrolyte) and b) electric currents in the CV can directly be correlated with the physico-chemistry on top of the sample surface (electrode surface). All STM

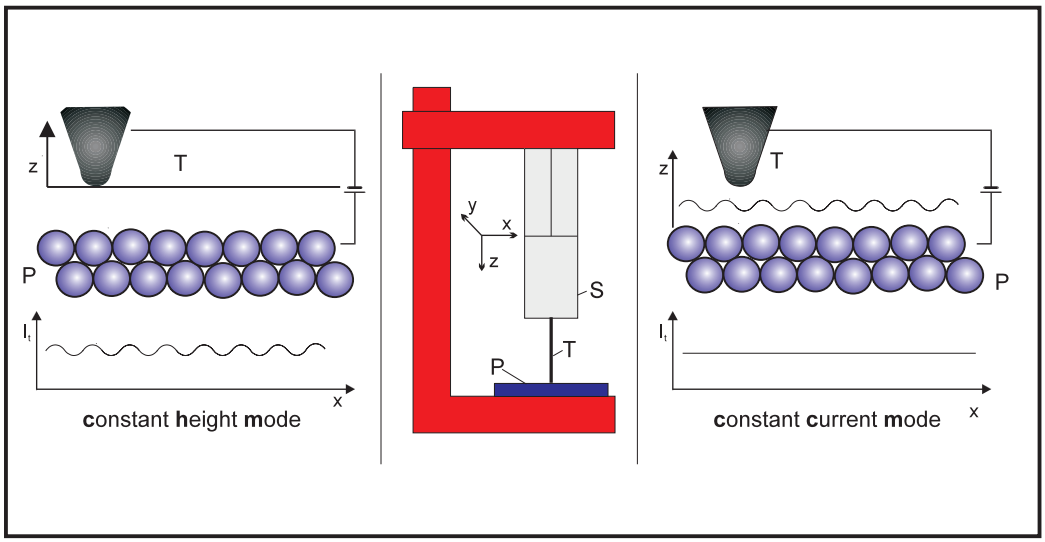

Figure 4.5: left) Constant Height Mode and right) Constant Current Mode; abbreviations see Figure 4.4 (taken from[139]).

measurements presented in the experimental chapter have been carried out by Dr. Caroline Zörlein using a home-built EC-STM that has been described in detail in reference[143] (Fig. 4.6 b).

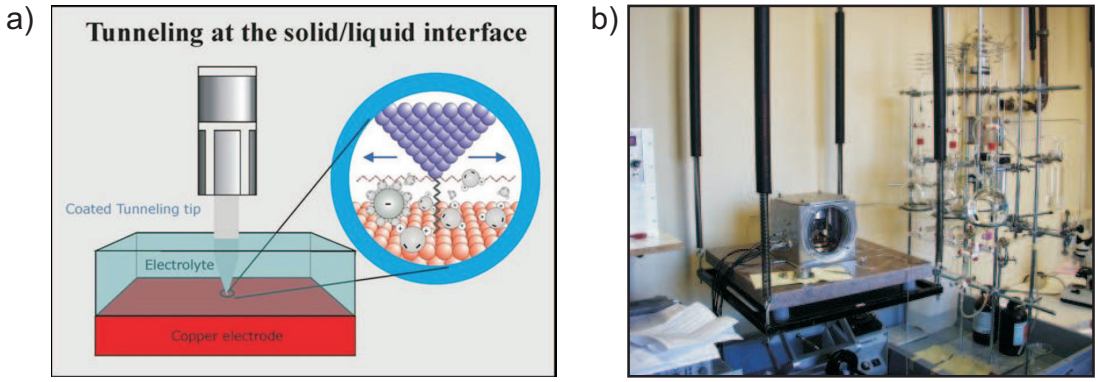

Figure 4.6: a) Schematic representation of an EC-STM b) Photograph of the EC-STM of the Institute for Physical and Theoretical Chemistry of the University Bonn (Working group of Prof. Wandelt).

The potentials between (a) the working electrode (the sample) and (b) the tip have to be controlled independently against a reference electrode. In this case, the

tunneling bias voltage is the difference between these two potentials. A counter electrode is used in order to follow the current by the reaction on the electrode surface. By using these four electrodes, the electrochemical reaction is controlled precisely by an external voltage, and the solid-liquid interface can be observed by the means of STM. For two early reviews about electrochemical applications of *in situ* STM see.[144] For non-aqueous electrolytes see.[145]

4.4 Quartz Micro Balances (QMB)

4.4.1 Quartz Micro Balances as Chemical Sensors

Nowadays, the most frequently used bulk acoustic wave sensors (BAW) is the Quartz Micro Balance (QMB). The basic principle of QMBs as chemical sensors is the Piezo electric effect.[146] When an alternating voltage with defined frequency is impressed across a quartz crystal (7 to 14 mm diameter), the crystal starts to oscillate. If one adsorbs a special chemical substance (a "sensor-active layer"[147]), the resonance frequency is reduced proportional to the mass of the substance[148] (Sauerbrey relation).

A gaseous analyte can now be bound in or at the sensor-active layer. The mass increase causes again a decrease in its resonance frequency. Thus, the quartz can be regarded as a high-precision balance. To develop a sensor from this type of scale is easy. The interactions between layer (host) and analyte (guest) have to be selective. The layer should have cavities, which have to match the sterical and electronic demands of the guest molecules.[149] These interactions have to be reversible in order to be able to release the sensor or to monitor an analyte online in real time. The bound guest molecules have to be set free as soon as the concentration of the guest in the gaseous phase is decreased. After flushing with inert gas the quartz oscillates in its normal frequency again. If differently coated quartz are combined in an array, a "'chemical nose" is obtained (see Fig. 4.7).

Each single modified quartz reacts individually onto different analytes, a rather complex, but unambiguous pattern is generated. The pattern recognition takes place inside an ordinary computer, which makes the recognition of quite complex analyte mixtures possible in real time. The technical effort is small (and with this

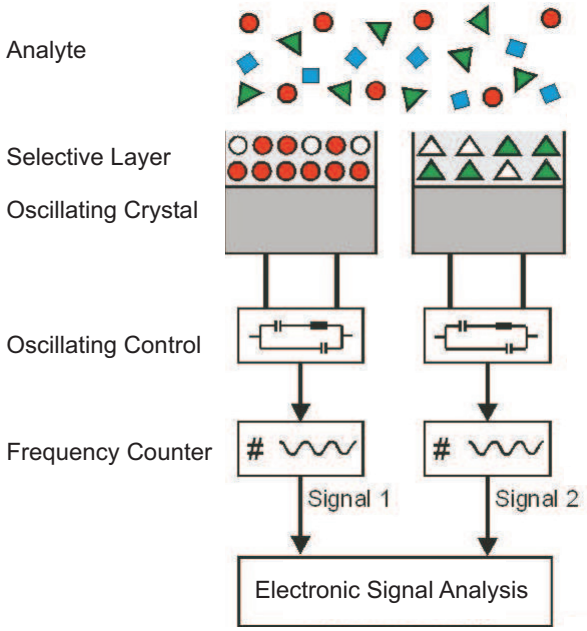

Figure 4.7: Principle of combined QMBs[150]).

the price) compared to established methods for example GCMS.[151] The size of the hole array is typically smaller than a cigarette packet.

More and more technical applications are possible for the usage of QMBs: Already in 1964, *King* showed a first application for this phenomena.[152] Recent results related to practice are the concentration determination of ammonia in pig stables[153] or SO_2 in the gas phase.[154] But also complex food flavors (*Emmentaler* cheese) can be analyzed:[155] 2-Heptanone is the key substance for the determination of the degree of ripeness in the flavor of this cheese and can be detected by QMBs.

Two points have to be discussed in the following sections in more detail: The Sauerbrey relation and the sensor-active layers.

4.4.2 Sauerbrey Relation

In 1952, *Sauerbrey* reported that upon absorption of any kind of compound on an oscillating quartz its reduction of frequency is following a certain relation:

$$\Delta f \sim (f_0)^2 \Delta m \tag{4.3}$$

with Δf being the frequency difference, f_0 being the ground frequency, and Δm the mass difference if Δf is smaller than 2 % of f_0. Two aspects are of major importance: a) a quartz with higher f_0 is more sensitive. As f_0 is anti-proportional to the quartz' thickness, there is a technical limit for applications (right now up to 200 MHz). b) The proportionality between frequency shift and mass makes light analytes hard to trace. However, lightweights like ethene (28 g/mol) can be detected (see 6.2).

4.4.3 Sensor-Active Layers

But a real sensor not only has to measure accurately, selectivity for special analytes is also needed. As the quartz itself is not that selective, it has to be coated with a sensor-active layer. This layer can be from whatever composition which is needed. In the case of the *Emmentaler* cheese QMBs, tetralactam macrocycles of the group of Prof. *Vögtle* were used.[155] But also cyclodextrines[156] or cyclophanes[157] can be coated on top of a quartz plate.

If large and reproducible sensor responses are needed, not only the chemical structure of the sensor-active layer on top of the quartz but also the coating technique is of major importance: Spin Coating[158] and Electrospray coating[159] are the most frequently used methods.

Chapter 5

Results and Discussion

The presentation of the results are divided into two chapters: At first, the synthesis of the organic ligands based on [4,4']-bipyridine and metal precursors is presented, which is of course the basis for the self-assembly reactions, the main theme of this thesis. In the following chapter, Results of Collaborative Projects, applications of the obtained compounds are discussed.

5.1 Syntheses and Properties of the Organic Ligands for Self-Assembly

5.1.1 Programming of the Building Blocks

When self-assembly is used to design complex molecular architectures, the programming of the involved particles, here metal complexes and organic ligands, is of major importance.[160] Modification of the ligand is chosen, to obtain a modular approach with minimal synthetic steps. Hence, the ligands are modified and the metal precursors (Stang and Fujita types) are used unchanged. Three different positions of the organic ligands (bi(s)-pyridines) might be modified:

1. The ortho positions of the pyridine ring should not be substituted at all, not to hinder the assembly formation due to steric repulsion.

2. The substitution of the meta position seem rather promising.

3. Elongation of the bipyridine system, leads to the discussed triangle-square-equilibrium (see 3.3.4). Thus, rigid [4,4']-bipyridines are needed, without any spacer between the two pyridine rings.

To avoid complicated product mixtures (see Scheme 5.1 b), the ligands must be C_2 symmetrical. In supramolecular chemistry, general approaches for the attachment of functional groups are amide, sulfonamide or ester bond formations. Thus, substitution of both meta positions of [4,4']-bipyridine with sulfonic acid, carboxylic acid, amine or hydroxy functionalities, respectively, seems to be a straightforward procedure. When these requirements are followed, the ligands are dissymmetrical[162] and axially chiral. The latter point should be discussed in more detail: 3,3'-Di-substituted [4,4']-bipyridines do not possess an S_n-axis and are thus chiral. However, the rotation around the central biaryl-bond should be fast on the human timescale with only two substituents:[161] racemic mixtures are the consequence. With all four positions (3,3',5 and 5') substituted, the rotation should occur much more slowly. Atropisomers are hence obtained (see 5.1.4.3). In this case, the separation into enantiomers is desired.

5.1.2 [4,4']-Bipyridine as Starting Material

Influenced by the electronegative nitrogen atom, the aromatic ring of pyridine is electron poor compared to benzene. This restrains the electrophilic substitution, which is typical for aromatic systems (see Scheme 5.2). Otherwise, nucleophilic substitution at the ortho position is possible in good yields. An early review from 1958 about the introduction of substituents in the pyridine ring can be found in the references.[165] Polarity reversal (Umpolung) is achieved by oxidation of the nitrogen atom leading to pyridine-N-Oxide, which is now attacked by electrophiles at the para position easily (see Scheme 5.2 c). In conclusion, the introduction of substituents into pyridine's meta position seems difficult.

Since the direct twofold nitration and sulphonation of [4,4']-bipyridine turned out not to be realizable, the desired target compounds can be synthesized by homo coupling of precursor pyridines with functional groups at the meta position. These functional groups are then inter converted subsequently. Following this approach, different precursor pyridines are discussed in the following sub chapters.

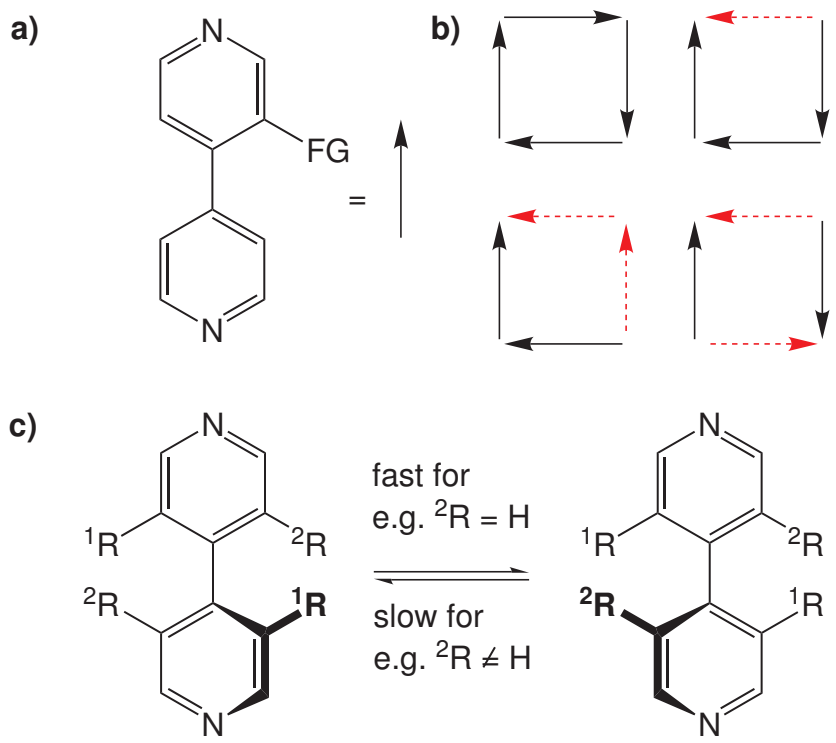

Scheme 5.1: a) If the ligand is not dissymmetrical, product mixtures b) are obtained. Red, dotted arrows are rotated by 180°. c) With two small substituents the rotation around the bipyridyl bond should be fast, whereas with four substituents atropisomers might be obtained.

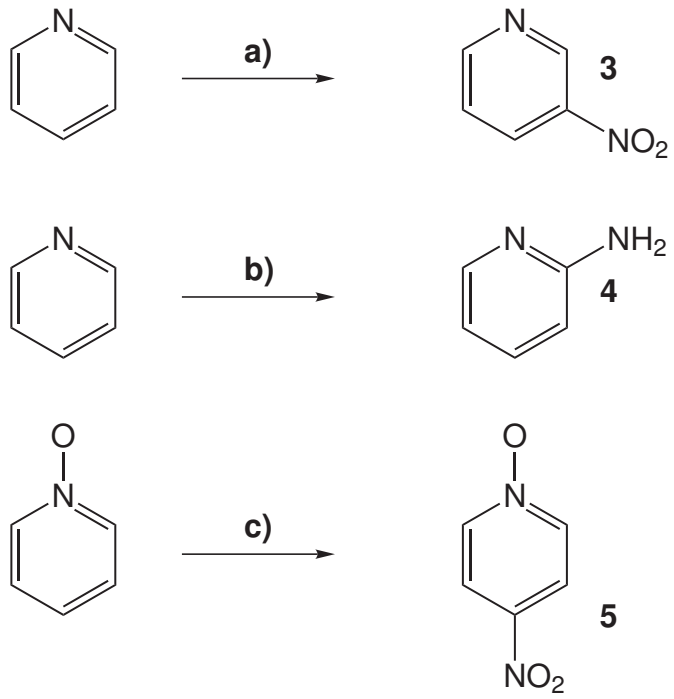

Scheme 5.2: a) Electrophilic Substitution: $NaNO_3$, H_2SO_4 (Oleum), 300°C, 5 %;[163] b) Tschitschibabin Reaction: 1. $NaNH_2$, liquid NH_3 2. H_3O^+, 70 %;[164] c) Electrophilic Substitution of Pyridine-N-oxide: HNO_3, H_2SO_4 78 %[166] .

5.1.3 [4,4']-Bipyridinyl-3,3'-diamine *

3-Nitro-pyridin-4-ol **15** can be converted to 4-chloro-3-nitro-pyridine **16** with phosphorylchloride and phosphorpentachloride. Homo coupling with copper(0) (Ullmann coupling) leads to 3,3'-dinitro-[4,4']-bipyridine **17**,[169] which can be reduced with tin dichloride dihydrate. [4,4']-Bipyridinyl-3,3'-diamine **18** is thus obtained in 32% yield over three steps (see Scheme 5.3). With this compound in hands, diurea and diamide compounds are easily available.[171]

5.1.4 Homo Coupling of Alkyl Pyridines

A wide variety of chemical transformations[172] for the benzylic methyl group can be found in the literature, among others: oxidation, halogenation or deprotonation. Hence, 3,3'-dimethyl-[4,4']-bipyridine **20** is chosen to be an ideal start-

*In cooperation with Torsten Weilandt (Diploma Thesis 2004).[171]

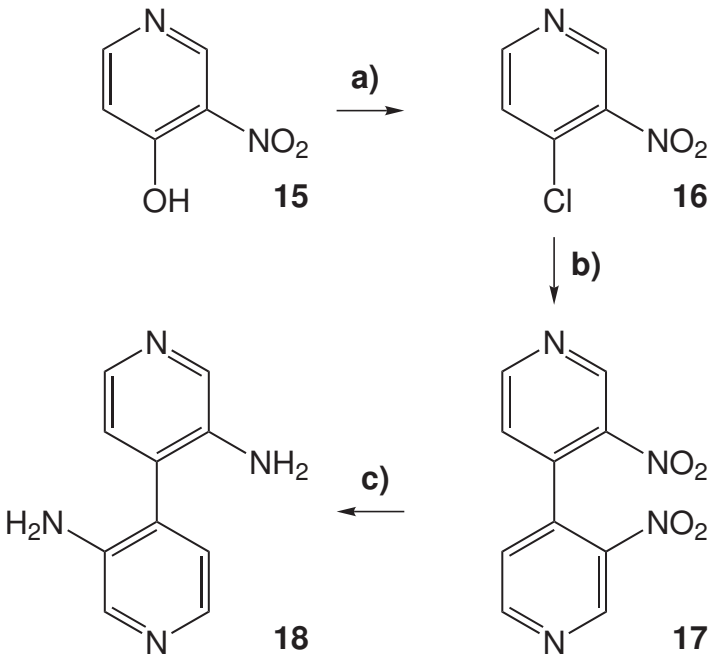

Scheme 5.3: a) PCl_5, $POCl_3$, 135°C, 5 hours, 88%; b) Cu, DMF, 100°C, 15 hours, 48%; c) $SnCl_2(H_2O)_2$, HCl, 100°C, 1 hour, 77%.

ing material for ligand syntheses. Commercially available 3-methyl pyridine **19** can be converted into 3,3'-dimethyl-[4,4']-bipyridine **20** by reductive coupling (chlorotrimethylsilane, sodium) followed by oxidation (potassium permanganate), a reaction sequence introduced by *Rebek et al.*[170] (see Scheme 5.4). Three further alkyl substituted pyridines are converted into the corresponding 4,4'-bipyridines by a slightly modified approach, to achieve higher yields: The alkyl-pyridines are solved in diethylether instead of tetrahydrofuran to elongate reaction time up to 24 hours (tetrahydrofuran is polymerizing under the given reaction conditions) and sodium powder is used instead of grounded sodium. While 3,3'-diethyl-[4,4']-bipyridine **22** and 2,6,2',6'-tetramethyl-[4,4']-bipyridine **27** are target molecules, 3,3'-dimethyl-[4,4']-bipyridine **20** and 3,5,3',5'-tetramethyl-[4,4']-bipyridine **24** are valuable starting materials for further transformations (see 5.1.4.2 and 5.1.4.3). Please note that 3,5,3',5'-tetramethyl-[4,4']-bipyridine **24** is only obtained in 47%. However, 3,5-dimethyl-4-trimethylsilanyl-pyridine **25** (ca. 15%, see 5.1.4.4) and unreacted 3,5-dimethyl pyridine **23** (ca. 25%) can be recycled.

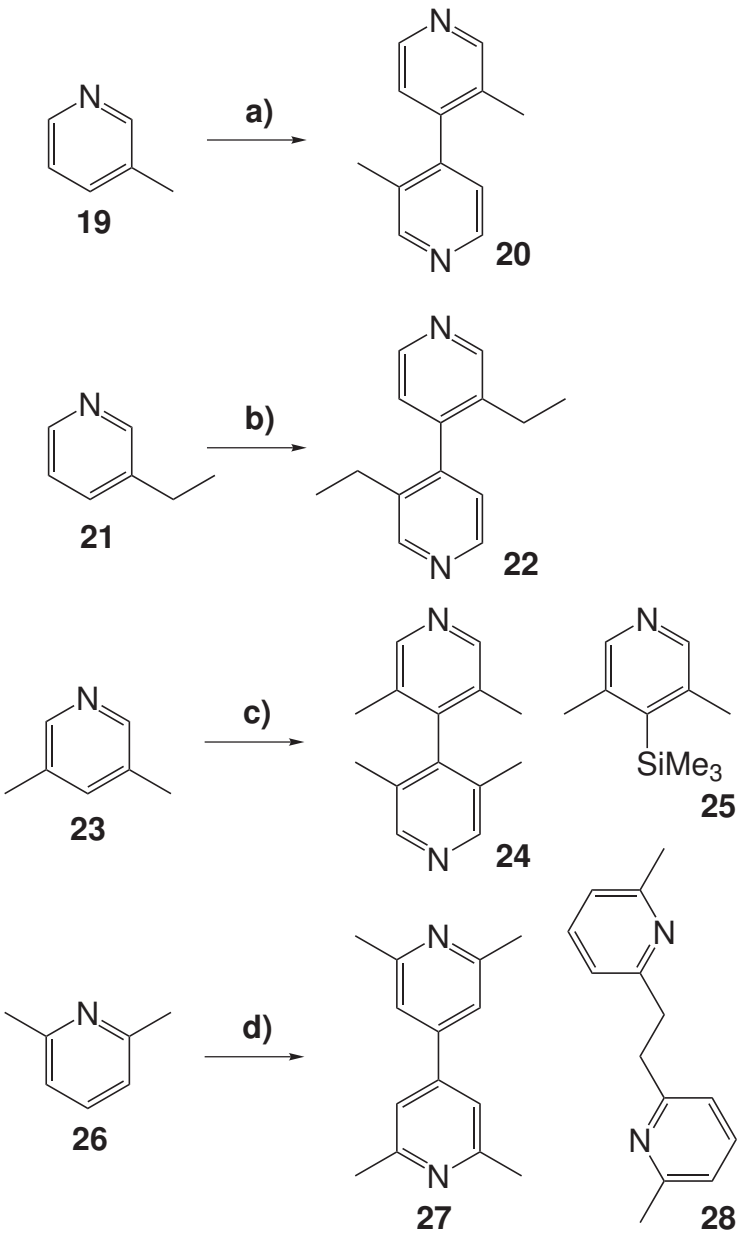

Scheme 5.4: Conversion of four alkyl-pyridines into the corresponding 4,4'-bipyridines: a) to c) 1) $SiMe_3Cl$, Na, Et_2O, 24 hours at 0°C to RT 2) $KMnO_4$, H_2O, RT, 1 hour, a) 48 % yield, b) 19 % yield, c) 47 % yield, d) 1) Na, Et_2O, 24 hours at 0°C to RT 2) $KMnO_4$, H_2O, RT, 1 hour, 7 % yield; Among the desired products the following byproducts are isolated and characterized: 3,5-dimethyl-4-trimethylsilanyl-pyridine **25** and 2,2'-ethane-1,2-diylbis(6-methylpyridine) **28**.

5.1.4.1 Racemization Barrier of 3,3'-Diethyl-[4,4']-bipyridine

Figure 5.1 shows the variable temperature ^{1}H NMR spectra obtained for **22** in two different solvents ([D_2]-tetrachloroethane and [D_6]-dimethylsulfoxide). In both cases, the two diastereotopic protons at each methylene group are clearly separated at lower temperature and coalesce at the same coalescence temperature of T_c= 363 K. The behavior is very similar in both solvents and from the peak distances, the coupling constants, and the coalescence temperature, two very similar racemization barriers are obtained, which amount to

- $\Delta G^{\ddagger} = 76.9\,\mathrm{kJ\,mol^{-1}}$ in $C_2D_2Cl_4$ (estimated from $\Delta\nu = 59.11$ Hz, $J_{AB} = 7.43$ Hz, $T_c = 363$ K at 500 MHz) and
- $\Delta G^{\ddagger} = 77.1\,\mathrm{kJ\,mol^{-1}}$ in [D_6]-DMSO (estimated from $\Delta\nu = 79.42$ Hz, $J_{AB} = 7.40$ Hz, $T_c = 368$ K at 500 MHz).

Irrespective of the exact values of these barriers, the racemization is assumed to be slow on the NMR time scale at room temperature.

5.1.4.2 3,3'-Dimethyl-[4,4']-bipyridine as Starting Material

5.1.4.2.1 Deprotonation of the CH_3-Groups Deprotonation of the methyl groups of 2-methyl pyridine ($pK_a = 34.0$)[173] and 4-methyl-pyridine ($pK_a = 32.2$)[173] is achieved with lithium diisopropylamide (pK_a of the corresponding acid = 35.7). The base must be sterical demanding, to avoid nucleophilic attack at the ortho positions of the pyridine ring. As the acidity of 3-methyl pyridine **19** is considerably lower ($pK_a = 37.7$),[173] a stronger base is needed. And indeed deprotonation is possible with lithium-2,2,6,6-tetramethyl-piperidine,[174] which is generated *in situ* by deprotonation of 2,2,6,6-tetramethyl-piperidine with *n*-butyllithium in tetrahydrofuran at 0°C in 30 minutes: 3-Methyl pyridine **19** is added at -78°C and stirring is continued, while the temperature is raised to 0°C. Deuterated water is added, and the degree of deuteration is determined by GCMS analysis. After optimization (1.1 eq. base, 0.5 hour reaction time), complete deprotonation is achieved. With these preliminary results in mind, 3,3'-dimethyl-[4,4']-bipyridine **20** can be deprotonated at both methyl groups with 2.3 eq.

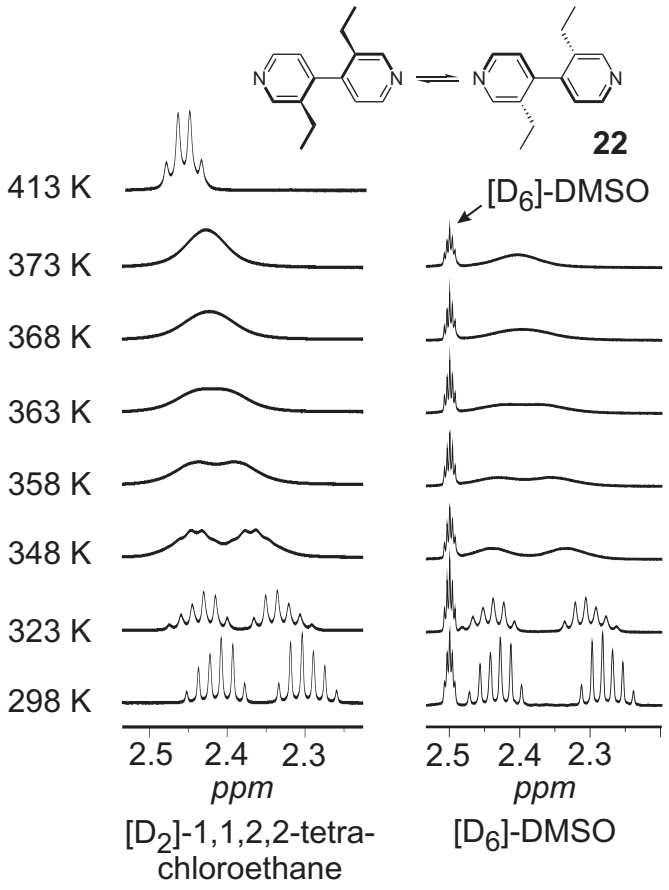

Figure 5.1: Variable-temperature ^{1}H NMR spectra of **22** in [D_2]-tetrachloroethane (left) and [D_6]-dimethylsulfoxide (right).

of lithium-2,2,6,6-tetramethyl-piperidine as base within 1 hour at 0°C. It was planned to attack the dianion with two equivalents of iodide, to obtain 3,3'-bis(iodomethyl)-[4,4']-bipyridine **29**. Unexpectedly, 5,6-dihydro-[3,8]phenanthroline **30** is isolated in high yields (see Scheme 5.5 a). Obviously, the dianion is oxidized twofold by iodide, and the third ring is closed. Unfortunately, aromatization to [3,8]-phenanthroline **31** is neither achieved by oxidation with 2,3,5,6-tetrachloro-[1,4]benzoquinone (Chloranil) nor by 4,5-dichloro-3,6-dioxo-cyclohexa-1,4-diene-1,2-dicarbonitrile (DDQ) (see Scheme 5.5 b) and c).

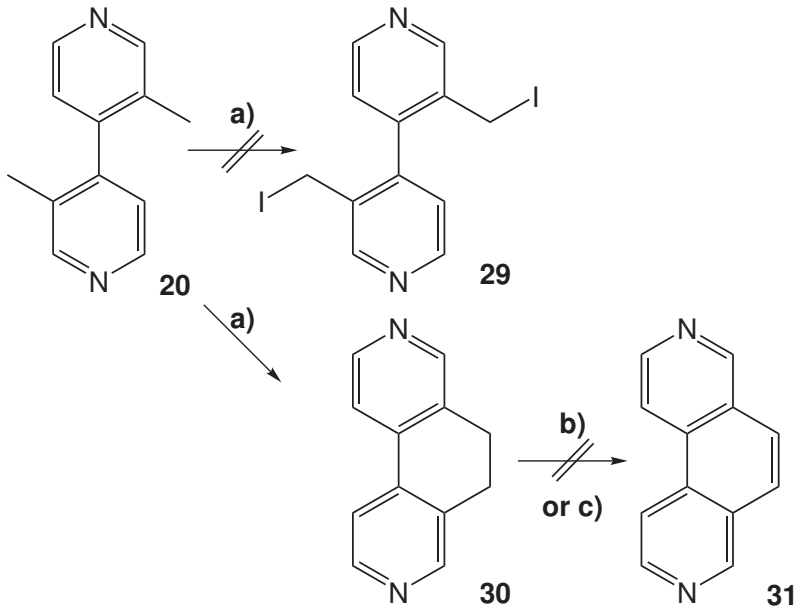

Scheme 5.5: a) 1) 2.3 eq. lithium-2,2,6,6-tetramethyl-piperidine, THF, -78°C to 0°C, 1 h 2) 2.3 eq. I_2 -78°C to RT, 85%; b) 2,3,5,6-tetrachloro-[1,4]benzoquinone (Chloranil), toluene, 110°C, 7 days; c) 4,5-dichloro-3,6-dioxo-cyclohexa-1,4-diene-1,2-dicarbonitrile (DDQ), toluene, 110°C, 7 days.

5.1.4.2.2 Achiral and Chiral Diamides 3,3'-Dimethyl-[4,4']-bipyridine **20** is oxidized into [4,4']-bipyridinyl-3,3'-dicarboxylic acid **36**[170] with potassium permanganate in 73% yield. After conversion into [4,4']-bipyridinyl-3,3'-dicarbonyl dichloride dihydrochloride[175] with thionyl chloride, several diamide compounds are accessible: [4,4']-Bipyridinyl-3,3'-dicarbonyl dichloride dihydrochloride, 2.5 eq. of the amine of choice and triethylamine are suspended in tetrahydrofuran and the

resulting suspensions are stirred at room temperature over night. In the case of [4,4']-Bipyridinyl-3,3'-dicarboxamide **37**, gaseous ammonia is used as amine and base. The resulting diamides are purified by flash column chromatography.

In addition to simple amine compounds, methoxy protected alanine is used as a chiral amine compound. With two chiral residues attached to the bipyridine system and the axially chirality of the central bipyridyl bond, two diastereomers are formed: While the chirality of the (S)-alanine moieties is fixed, the bipyridine backbone can still interconvert between two axially chiral forms yielding the (*S*,*S*,*aS*)- and (*S*,*S*,*aR*)-diastereomers. Like discussed before, 3,3'- and/or 5,5'-substituents attached to the [4,4']-bipyridine-backbone hinder the rotation around the biaryl bond and thus have a large effect of the racemization rates.[161] Analogously, incorporation of an additional chiral information, e.g. the (*S*)-alanine esters in **41** leads to interconverting diastereomers. Not unexpectedly, the signals for the amino acid residues are sharp in the ^{13}C NMR spectrum of **41** in [D_1]-chloroform while the signals for the bipyridine backbone are broad. Broadened signals are also observed in the room-temperature ^{1}H NMR spectrum (see Figure 5.2). Low-temperature measurements (^{1}H) reveal the coexistence of two species in an almost temperature independent 3:1 ratio. The activation barrier of their mutual interconversion can be estimated to amount to ca. $\Delta G^{\ddagger} = 60$ kJ mol^{-1}. In [D_6]-acetone, sharp signals are found in the room temperature ^{1}H NMR spectrum as well as the ^{13}C NMR spectrum. Thus, the interconversion of the two isomers is faster in acetone than in chloroform. Low-temperature measurements show again two sets of signals, now in a 3:2 ratio. Together with the crystal structure analysis (see 8.6), these results point to the existence of an intramolecular hydrogen bond in chloroform which needs to be broken during the interconversion of diastereomers. Acetone weakens this hydrogen bond and thus, the interconversion is faster. For the corresponding biphenyls, see citation.[176] Due to packing effects, only one diastereomer is however found in the solid-phase structure (see chapter 8.6).

5.1.4.2.3 An Unsymmetrical Amide In one batch, the oxidation of 3,3'-dimethyl-[4,4']-bipyridine **20** to [4,4']-bipyridinyl-3,3'-dicarboxylic acid **36** was

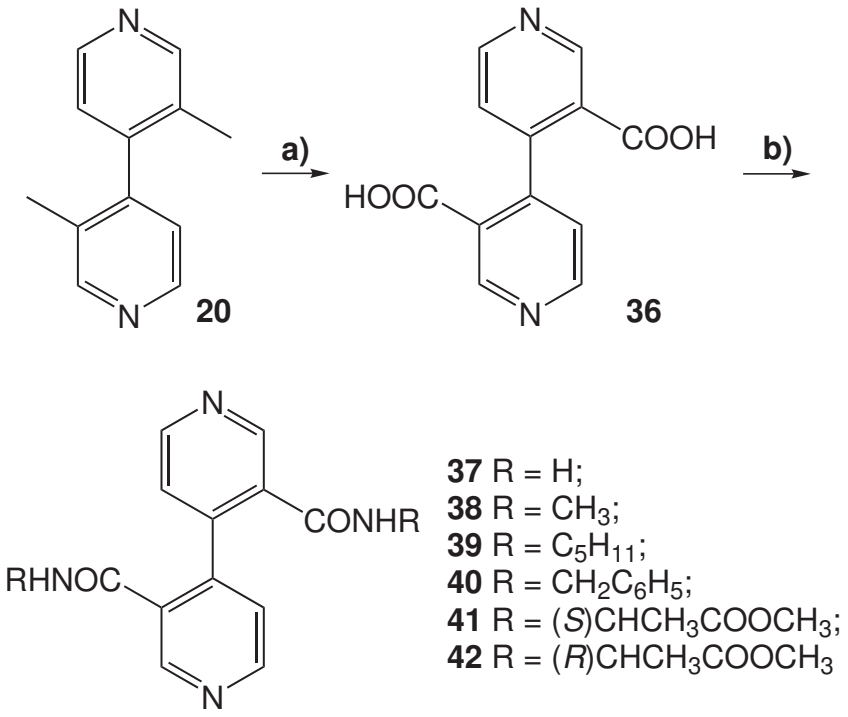

Scheme 5.6: a) $KMnO_4$, H_2O, 95°C, 8 hours, 73%; b) 1) $SOCl_2$, 76°C, 5 hours, quant.; 2) amine of choice, Et_3N, THF, RT, variable reaction times (typically over night).

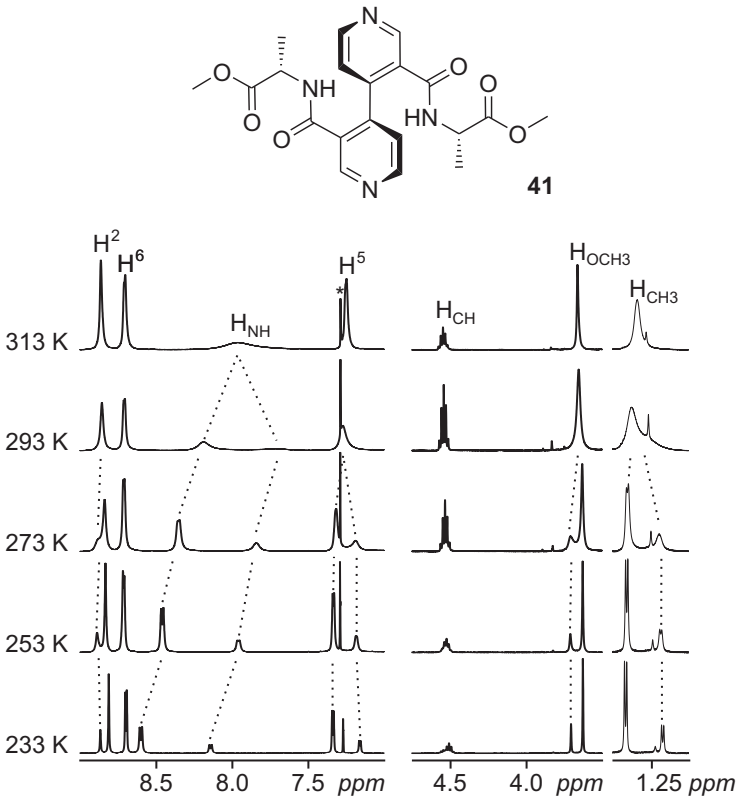

Figure 5.2: Variable-temperature ^{1}H NMR spectra of (*S*,*S*)-2-[3'-(1-methoxycarbonyl-ethyl-carbamoyl)-[4,4']-bipyridinyl-[4]-3-carbonyl]-amino-propionic acid methyl ester **41** in [D_1]-chloroform (*).

incomplete. As the separation of (3'-methyl-[4,4']-bipyridinyl-3-yl)-acetic acid and [4,4']-bipyridinyl-3,3'-dicarboxylic acid **36** is almost impossible, the following reactions are carried out without purification. 3'-Methyl-[4,4']-bipyridinyl-3-carboxylic acid methyl ester **43** and 3'-methyl-[4,4']-bipyridinyl-3-carboxylic acid-methylamide **44** are isolated. As both compounds are not dissymmetrical, they play an important role in chapter 5.3.

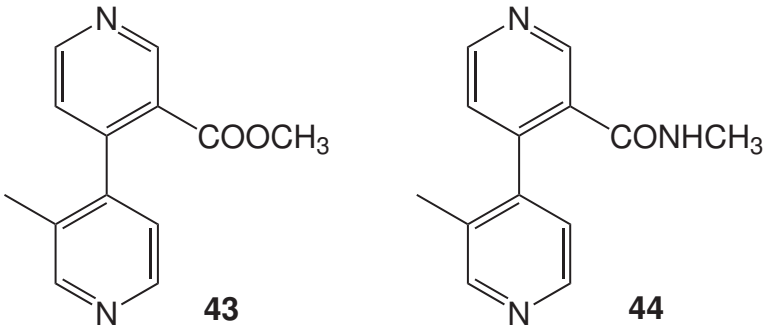

Scheme 5.7: Isolated mono carbonyl compounds.

5.1.4.2.4 Dendron Decorated [4,4']-Bipyridines In cooperation with Dr. T. H. Baytekin dendron decorated [4,4']-bipyridines are designed and synthesized (see Scheme 5.8). Dendron amines are synthesized using Fréchet's procedures for the preparation of benzyl bromide dendrons,[177] followed by Gabriel reaction.[178] The amide bonds are formed with the same procedure mentioned above (see Scheme 5.6).

5.1.4.3 3,5,3',5'-Tetramethyl-[4,4']-bipyridine as Starting Material

One of the two possible rings of 3,5,3',5'-tetramethyl-[4,4']-bipyridine **24** can be closed by the same reaction sequence like for 3,3'-dimethyl-[4,4']-bipyridine **20** (deprotonation, oxidation with iodide). However, the yield of 1,10-dimethyl-5,6-dihydro-[3,8]phenanthroline **49** is significant lower (20%) compared to **31** (85%). The second ring can not be closed at all. Neither a higher amount of base nor longer reaction times, increase these yields. In both cases, the distances of the resulting two negative charges after twofold deprotonation are much smaller than

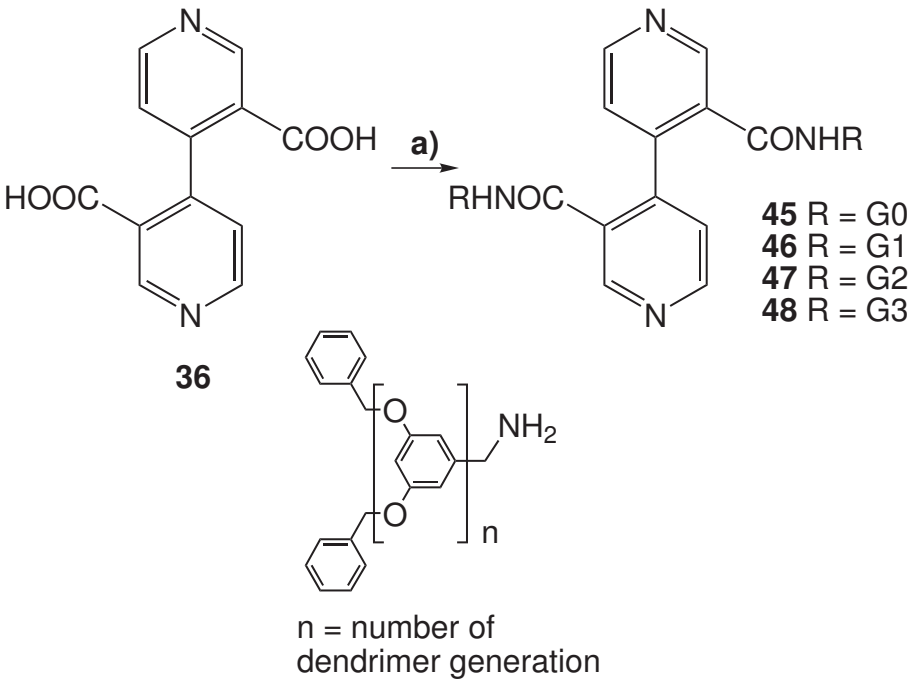

Scheme 5.8: a) 1) $SOCl_2$, 76°C, 5 hours, quant.; 2) amine, Et_3N, THF, RT, variable reaction times.

in the case of 3,3'-dimethyl-[4,4']-bipyridine **20**. This means that the intermediates should be higher in energy. In this case, two reaction parameters can be altered: choice of base and temperature. As no stronger and sterical demanding base is found in the literature, the reaction temperature is increased to 20°C; not unexpectedly, 3,3',5,5'-tetramethyl-2-(2",2",6",6"-tetramethylpiperidin-1-yl)-[4,4']-bipyridine **51** is obtained as side product (see Scheme 5.9 c) with constant yield of the desired product **49**. This means that at higher temperatures not only the desired reaction gets faster, but also a second type of reaction, the nucleophilic attack at the pyridine's ortho position, comes into play. In conclusion, the yield for **49** could not be increased.

5.1.4.3.1 Axial Chiral Diamides Without Spacer 4,4'-Bipyridine is an extraordinarily versatile key intermediate: It is a precursor to the herbicide paraquat,[180] a useful building block in liquid crystals[181] as well as in supramolecular chemistry.[182] In marked contrast to the large number of known atropisomeric

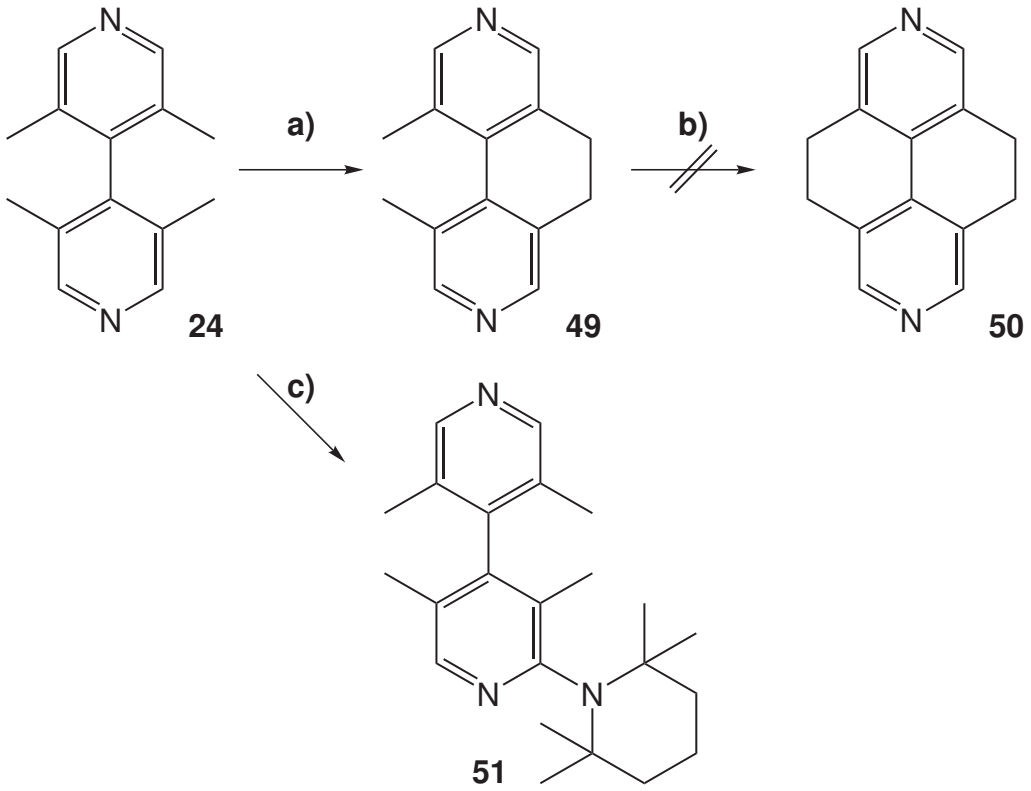

Scheme 5.9: a) 1) 2.3 eq. lithium-2,2,6,6-tetramethyl-piperidine, THF, -78°C to 0°C, and 1 h at 0°C, 2) 2.3 eq. I_2, -78°C to RT, 20%; b) like a); c) side product when reaction temperature is increased to 20°C.

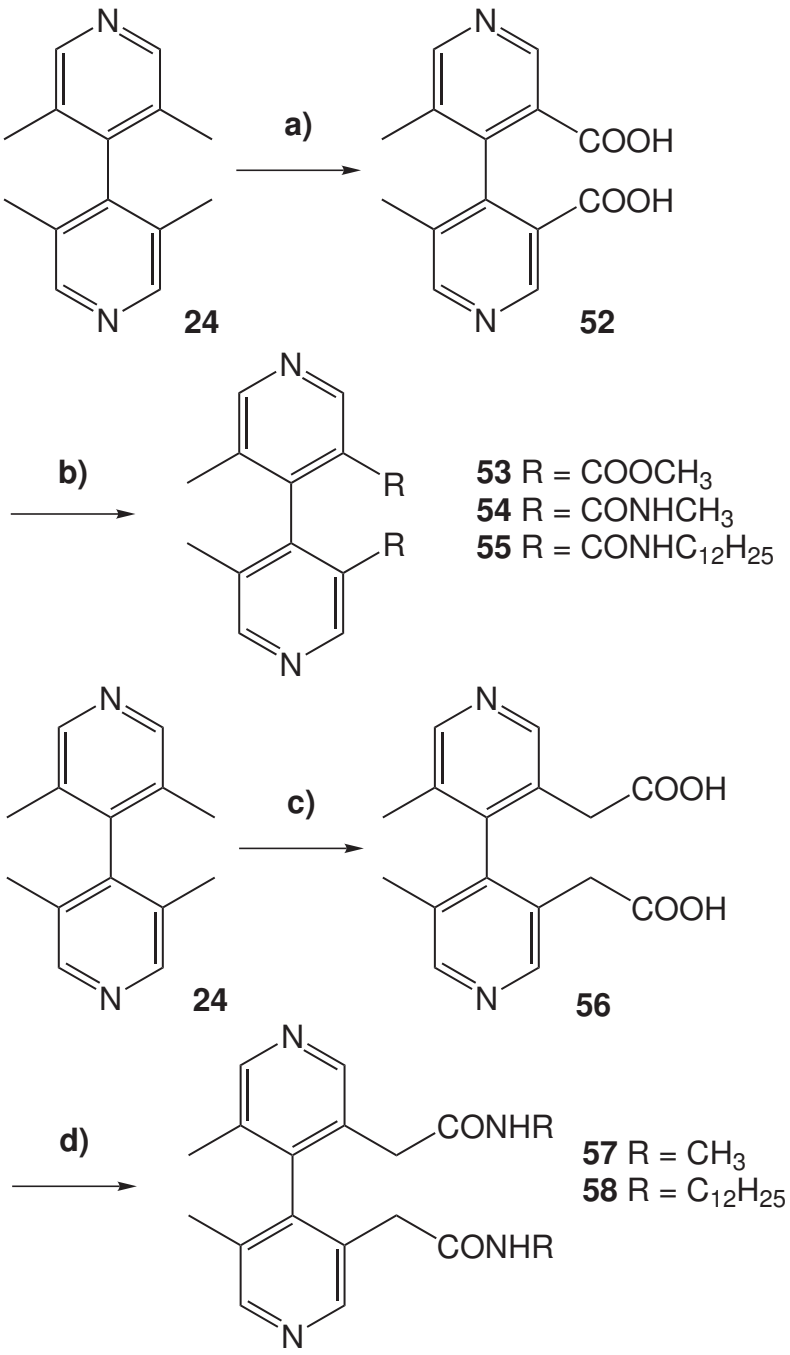

Scheme 5.10: a) $KMnO_4$, H_2O, 95°C, 8 hours, not isolated; b) 1) $SOCl_2$, 76°C, 10 hours, quant.; 2) amine or alcohol, Et_3N, THF, RT, variable reaction times; c) 1) 2.3 eq. lithium-2,2,6,6-tetramethyl-piperidine THF, -78°C to 0°C, 1 h; 2) CO_2, 0°C, 45%; d) benzotriazole-1-yl-oxy-tris-pyrrolidino-phosphonium hexafluorophosphate (PYBOP),[179] amine, Hünig's base, DCM, RT, variable reaction times (typically over night).

biphenyls, surprisingly no axially chiral 4,4'-bipyridines are available in the literature except for a few biquinoline compounds,[183] although chirality plays a crucial role in these fields.

With 3,5,3',5'-tetramethyl-[4,4']-bipyridine **24** in hands, two routes toward atropisomeric [4,4']-bipyridines can be followed. On one hand, oxidation of two out of the four methyl groups (not at the same pyridine ring) leads to an axially chiral diacid. Unfortunately, the oxidation of benzylic positions is typically not a selective procedure. Thus, it is not surprising that one monoacid, two diacids, one triacid and one tetraacid is obtained, when 3,5,3',5'-tetramethyl-[4,4']-bipyridine **24** is oxidized with potassium permanganate. As the resulting product mixture is hard to separate, the following steps are carried out, without separation. The acid groups of the mixture are converted into the acid chlorides by thionyl chloride. Reaction with

- methanol gives a mixture of esters. While the compounds with different amounts of ester groups, can be obtained individually by column chromatography, the two diesters can not be separated from each other by ordinary column chromatography.

- amines (methylamine and dodecylamine) give mixtures of amides. In both cases all formed compounds are separated from each other by column chromatography. Unlike the two diesters, the two diamides are separable, respectively.

In conclusion, this route permits a whole variety of different compounds with a lot of column chromatography.

5.1.4.3.2 Axial Chiral Diamides With CH_2-Spacers On the other hand, deprotonation of two methyl groups – as seen before – and quenching of the resulting dianion with CO_2 leads to an axially chiral diacid (2,2'-(5,5'-dimethyl-[4,4']-bipyridine-3,3'-diyl)diacetic acid **56**) with CH_2-spacers between pyridine ring and carboxylic acid functionality. The only byproduct is 2-(3',5,5'-trimethyl-[4,4']-bipyridin-3-yl)acetic acid, the corresponding mono acid, which can be removed by column chromatography. As the resulting acid groups can not be converted into

the acid chlorides by thionyl chloride, another standard amide coupling strategy (PYBOP[179]/Hünig's base) is chosen. Again, two different chiral diamides from methylamine and dodecylamine are prepared. In conclusion, the second route is more expensive (lithium compounds, dry and oxygen free solvents, PYBOP), but give the desired axially chiral diamides with CH_2-spacers with less column chromatography.

5.1.4.3.3 Chiral HPLC Chromatography on a home-made immobilized Chiracel OD stationary phase[184] affords enantiomer separation of racemic **54**, **55** and **58** with $> 92\%$ ee. CD spectroscopy of the resulting pairs of enantiomers showed the appropriate mirror inverted CD spectra. Tetrasubstituted bipyridyl compounds **54** and **55** are reasonably stable against racemization. After 70 hours in methanol at 50°C, only a minor decay of the CD signal of (*aR*)- or (*aS*)-**55** is observed. Bipyridine **58** racemizes somewhat more easily: After 26 hours at 50°C, racemization is observed in detectable amounts. We suggest the higher barrier for racemization of **54** and **55** to be caused by the flexibility-reducing conjugation of the amide carbonyl groups to the pyridyl rings.

In conclusion, an effective two-step synthesis for axially chiral 4,4'-bipyridines was developed, which provides easy access to a long neglected class of chiral building blocks not only highly useful for supramolecular chemistry. As shown by a combination of CD-spectroscopy and HPLC traces, a separation of the enantiomers is possible with the appropriate chiral stationary phase. Two different classes of these bipyridine have been prepared: One offers rigidity due to carbonyl group conjugation with the pyridine π-system, the other is more flexible due to the CH_2-spacer between the carbonyl and the pyridine ring. The enantiomers obtained in more than 92% ee were quite stable in solution at room temperature.

5.1.4.4 4-Iodo-3,5-dimethyl-pyridine

One byproduct of the reductive coupling of 3,5-dimethyl pyridine **23** to 3,5,3',5'-tetramethyl-[4,4']-bipyridine **24** is 3,5-dimethyl-4-trimethylsilanyl-pyridine **25**. The TMS-group can be converted into iodide with iodmonochloride in high yields. 4-Iodo-3,5-dimethyl-pyridine **59** can be isolated, but the free base is unstable even

in the solid-phase and at low temperatures. Within two days in the freezer the white crystals decompose. 4-Iodo-3,5-dimethyl-pyridine **59** should either be stored as the HI-salt or used without delay. As iodide containing hetero cycles can be used in standard palladium catalyst cross coupling reactions, to form unsymmetrical [4,4']-bipyridines or larger ligands, 4-iodo-3,5-dimethyl-pyridine **59** might be a valuable building block for further studies.

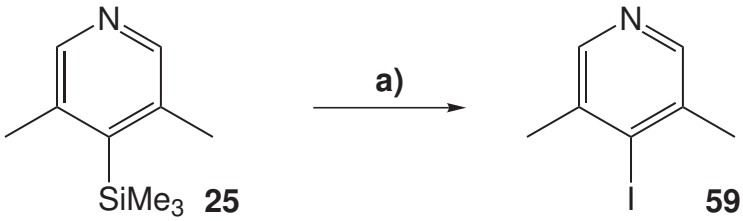

Scheme 5.11: a) ICl, 0°C to room temperature, 79%.

5.1.5 2,6-Dimethyl-[4,4']-bipyridine

For unidirectional molecular squares (see 5.5.1) 2,6-dimethyl-[4,4']-bipyridine **81** is needed. Two routes can be followed: Literature known Hantzsch reaction starting from isonicotinaldehyde **78** (see 5.12 a) followed by oxidation b) and decarboxylation c) yields the target molecule in three steps in 10%.[185]

A modern route is presented in the next paragraph. 2,6-Dimethyl-pyridin-N-oxide **82** can be converted into 4-chloro-2,6-dimethyl-pyridine **83** in 53% yield with phosphorylchloride, after protonation with hydrochloric acid.[186] The resulting byproduct 2-chloromethyl-6-methyl-pyridine can be either removed by distillation or synthetically (refluxing in triethylamine). Suzuki coupling with 4-pyridinyl boronic acid in the presence of a catalytic amount of bis(tri-*tert*-butylphosphine)palladium(0) (Buchwald-type) yields the target molecule in 19%. As 4-Chloropyridines give lower yields in cross coupling reactions than the corresponding bromo-compounds,[187] the same reaction sequence is carried out towards 4-bromo-2,6-dimethyl-pyridine **86**. However, when 2,6-dimethyl-pyridin-N-oxide hydrobromide is reacted with phosphorylbromid, three monobrominated compounds are detected in the GCMS spectrum (see Figure 5.3): 4-Bromo-2,6-dimethyl-pyridine

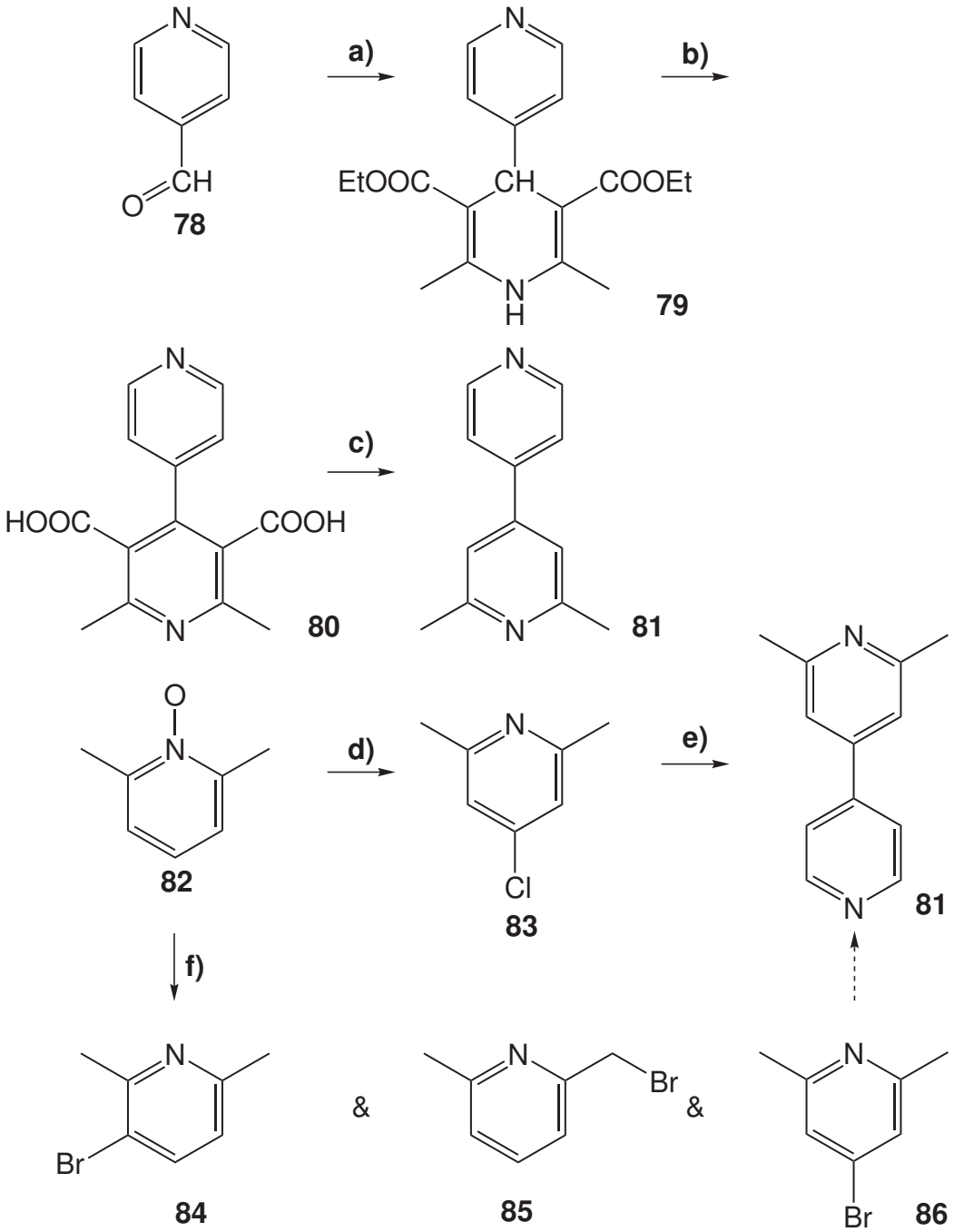

Scheme 5.12: a) CH_3COCH_2COOEt, NH_3, EtOH, 80°C, 8 hours, 47%; b) 1) H_2SO_4, HNO_3, H_2O, 40°C, 1 hour; 2) KOH, EtOH, 78°C, 1 hour, 40%; c) CaO, 500°C, 1 hour, 53%; d) 1) HCl, RT, 30 min, 2) $POCl_3$, 0°C to 105°C, 12 hours, 53%; e) 4-pyridinyl boronic acid, $CsCO_3$, bis(tri-*tert*-butylphosphine)palladium(0), 1,4-dioxane, 80°C, 4 hours, 19%; f) 1) HBr, RT, 30 min, quant. 2) $POBr_3$, 100°C, 1 hour, three isomers.

86, 3-bromo-2,6-dimethylpyridine **84** and 2-(bromomethyl)-6-methylpyridine **85**. The later can be removed from the product mixture by reaction with sodium hydroxide. The remaining two regioisomers can neither be separated by column chromatography nor distillation.

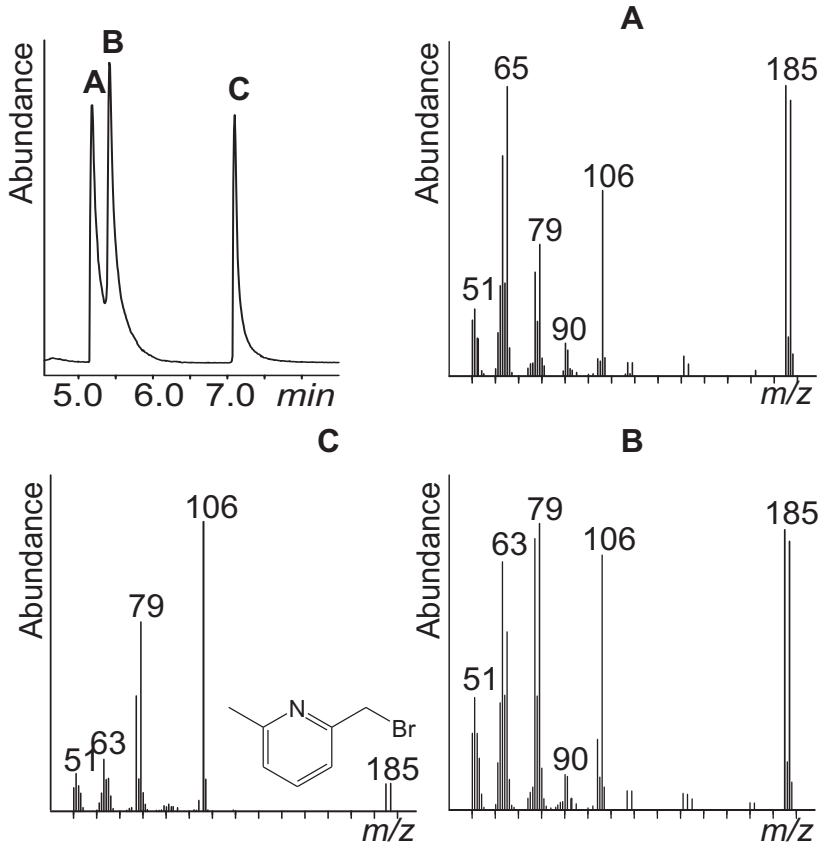

Figure 5.3: Three isomers (30%:46%:24%) are formed, when 2,6-dimethyl-pyridin-N-oxide hydrobromide is reacted with phosphorylbromid.

A possible mechanism for the conversion of 2,6-dimethyl-pyridin-N-oxide hydrobromide into 4-bromo-2,6-dimethyl-pyridine **86** is shown in Scheme 5.13. For this reason, 2,6-dimethyl-pyridin-N-oxide hydrobromide is heated in $[D_6]$-dimethylsulfoxide as well as $[D_2]$-tetrachloroethane at 140°C for 7 days. Several ^{1}H NMR spectra are recorded, but unfortunately, a conversion into 4-bromo-2,6-dimethyl-pyridine **86** does not take place.

As only small quantities of 2,6-dimethyl-[4,4']-bipyridine **81** are needed, no further optimization is performed. Hence, 2,6-dimethyl-pyridin-N-oxide **82** can

be converted into 2,6-dimethyl-[4,4']-bipyridine **81** over 4-chloro-2,6-dimethyl-pyridine **83** in two steps in 10% yield.

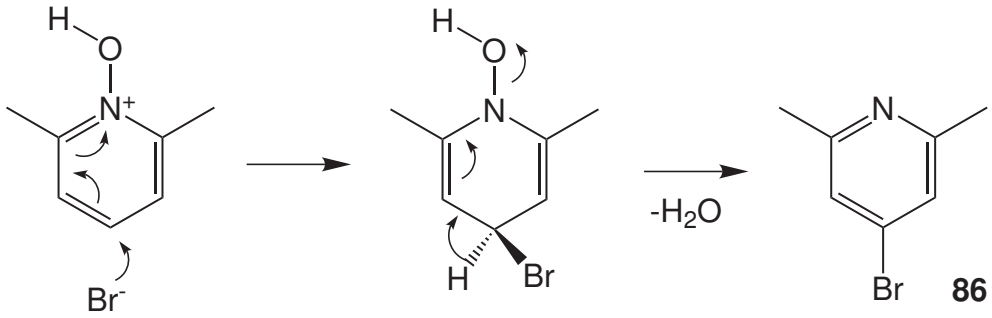

Scheme 5.13: A possible mechanism for the conversion of 2,6-dimethyl-pyridin-N-oxide hydrobromide into 4-bromo-2,6-dimethyl-pyridine **86**.

5.2 Synthesis of Self-Assembled Supramolecular Squares (SAMS)

The second building blocks for self-assembled supramolecular squares, the metal complexes, were synthesized according to well-known literature procedures: (dppp)Pd(OTf)$_2$ [**a**],[61] (dppp)Pt(OTf)$_2$ [**b**][188] (with dppp = 1,3-propandiylbis-(diphenylphosphan)), (en)Pd(NO$_3$)$_2$ [**c**],[26,189] and (en)Pt(NO$_3$)$_2$ [**d**][29,190] (with en = ethylenediamine).

As now both building blocks for self-assembled supramolecular squares are introduced, i. e. the organic ligands as well as the metal complexes, the self-assembly reactions can be discussed:

5.2.1 Stang Squares

For square formation, equimolar amounts of metal precursor and organic ligand are mixed in organic solvents like: dichloromethane, acetone or methanol. If the solubility of the organic ligand is poor in these solvents, dimethylsulfoxide or dimethylformamide might be used as well. Usually, the mixtures are stirred for at least one hour, to avoid kinetically driven processes. Precipitation with

e. g. diethylether yields the desired solids in high yields (typically > 90%). As both metal precursors react readily with chloride anions, the organic ligands are washed thoroughly with water prior to the self-assembly reactions, not to hamper assembly formation. For mass spectrometric measurements, acetone solutions (400 μm concentration) produce best results. For CD measurements, methanol solutions of variable concentrations are used.

5.2.2 Fujita Squares

Unfortunately, the syntheses of Fujita squares are more difficult to prepare. The first synthesis of Fujita squares[26] is described as follows: An ethanol solution of [4,4']-bipyridine **11** is added at room temperature to a methanol-water (1:l) solution of (en)Pd(NO_3)$_2$ **[c]**, and the solution is stirred for 10 min at that temperature. Upon addition of more ethanol, a pale yellow powder immediately precipitated.

In this thesis, a slightly modified procedure is used: Both components are mixed in an equimolar ratio in D_2O. The mixture is heated to 40°C until the kinetically formed oligomers (broad signals in the ^{1}H NMR spectra) merge into the desired macrocycle (sharp signals). If desired, precipitation is possible with ethanol. For the platinum species, it may take up to four weeks, until the equilibrium is reached.[29] Two equivalents of nitric acid accelerate the reaction (seven days).[29]

5.3 Functionalized SAMS

The syntheses and characterization of self-assembled supramolecular squares from [4,4']-bipyridine derivatives are presented in the following chapter. These are characterized by means of mass spectrometry (ESI-FTICR), NMR spectroscopy (^{1}H NMR, ^{31}P NMR, as well as some 2D NMR techniques) and in one case by crystal structure analysis. In order to facilitate a full understanding of these results, a few remarks on the squares' geometries are given beforehand. Steric repulsion and hydrogen bonds will play an important role for squares from 3,5,3',5'-tetramethyl-[4,4']-bipyridine **24** derivatives.

5.3.1 Symmetry Considerations – 560 Isomers

When the pyridine rings of unsubstituted bipyridines are coordinated to metal corners of the Stang type, they tend to adopt an orientation almost perpendicular to the plane through the four metal corners. Each pyridine ring is solvated on the outside of the square by one phenyl ring attached to the dppp ligand. This arrangement is not only found in molecular modeling calculations,[192] but also in the crystal structures of unsubstituted squares.[61,193] However, when the 3,3' positions of the bipyridine ligands are substituted, the torsional angle around the aryl-aryl bond increases and both pyridines must make a compromise.

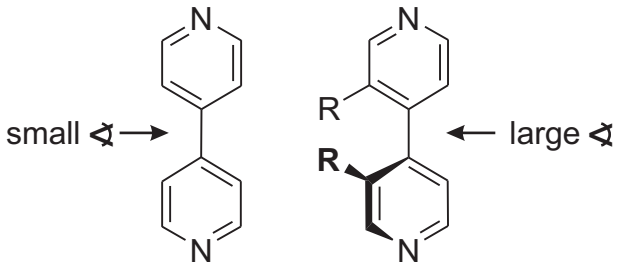

Scheme 5.14: The dihedral angles of diaryl systems depend on the substitution patterns.

In order to accommodate both their needs, they are positioned in an orientation tilted against their preferred position. In principle, this leads to two kinds of isomerism: (i) The absolute configuration of each of the four ligands can either be aR or aS (aR/aS isomerism). (ii) Independently, each of the eight substituents can either point inwards if room permits, i. e. towards the cavity, or point outwards, away from the cavity (In/Out-isomerism). The combination of these two types of isomers lead to a multitude of different isomeric structures.

In chapter 8.7 a complete derivation can be found, how many isomers can´be generated. In principle, 560 isomers can co-exist in equilibrium. Furthermore, they are conformers, which can interconvert into each other due to the supramolecular nature of the system. Three different processes (or a combination of these) contribute to the interconversion:

1. A **stereoisomerization** around the central aryl-aryl bond, which interconverts (*aR*)-[4,4']-bipyridines into (*aS*)-[4,4']-bipyridines,

2. **rotation of one complete ligand** around the metal-metal-axis in steps of 90°, which would e. g. change the In/Out position of the substituents, and

3. **dissociation** after breaking of two M-N-bonds and recombination to form another isomer.

The latter point should be explained in more detail: Dissociation of two metal-ligand-bonds yields two fragments which can react (a) with each other into another [4:4:8]-complex upon stereoisomerization or rotation of one complete ligand (see above) or (b) with other fragments present in solution. As it seems almost impossible to clearly distinguish between these two marginal cases, no further differentiation is made in the following chapters.

Two challenges can be outlined from these findings: (i) Mixtures are expected to be formed on the one hand. On the other hand, if steric and electronic interactions sum up, individual isomers might be preferred in some cases. Is it possible to find factors which allow the precise prediction of the outcome of self-assembly? (ii) Can experiments be designed to distinguish between the three types of interconversion?

In the following paragraphs, the outcome of several self-assemblies is discussed in order to answer these questions.

5.3.2 SAMS from [4,4']-bipyridine Derivatives Disubstituted at the 3 and 3' Positions

5.3.2.1 Small Substituents

Scheme 5.15 shows the organic ligands used in self-assembly reactions to yield small self-assembled supramolecular squares. These are characterized by means of mass spectrometry (ESI-FTICR) and NMR spectroscopy (^{1}H, ^{13}C, ^{19}F, and ^{31}P NMR). Unfortunately, all attempts to grow single crystals for crystal structure analysis failed.

Results from Mass Spectrometry † It has been shown previously that self-assembled supramolecular squares can be detected by ESI mass spectrometry

†In cooperation with Dr. Marianne Engeser and published in reference.[64]

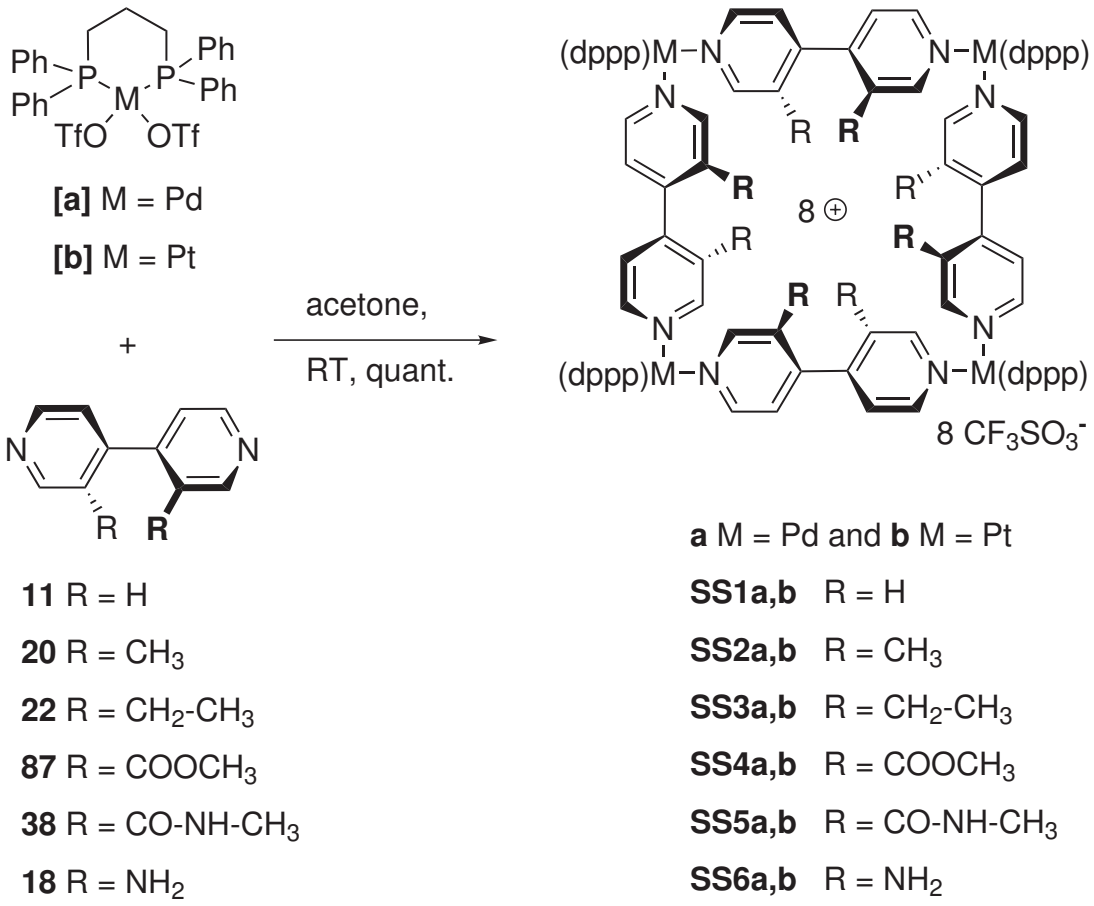

Scheme 5.15: Self-assembly reactions of organic ligands **11**, **20**, **22**, **87**, **38**, and **18** and metal precursors [**a**] and [**b**] yielding **S**mall **S**quares **SS1a,b** to **SS6a,b**. All palladium squares in this and the following chapters are labeled **a**, whereas platinum squares are labeled **b**.

under very soft ionization conditions[63] if acetone is used as solvent.

Although intact square ions are observed, the spectra are in many cases still dominated by mono and dinuclear complexes. These fragments may originate from two sources: either they are already present in solution or they are formed during the ESI process. Careful adjustment of the ionization parameters, in particular lowering the hexapole accumulation times (< 0.2 sec), increases the abundance of intact ions. Almost fragment-free spectra are however obtained only when solutions with rather high concentrations of squares (in the 400 μm range) are used. This behavior can be explained when one considers that self-assembled species exist in solution within an optimal concentration regime which is limited at the lower end by the so-called lowest self-assembly concentration.[194] To the upper end, polymer formation limits the concentration range. Consequently, relatively high concentrations compared to the ones typically used (ca. 50 μm) for ESI are needed for an efficient ionization of the squares under study here. The corresponding ESI mass spectra mostly consist of a series of differently charged self-assembled squares (see Figure 5.4). The almost exclusive observation of 4:4 complexes is a strong

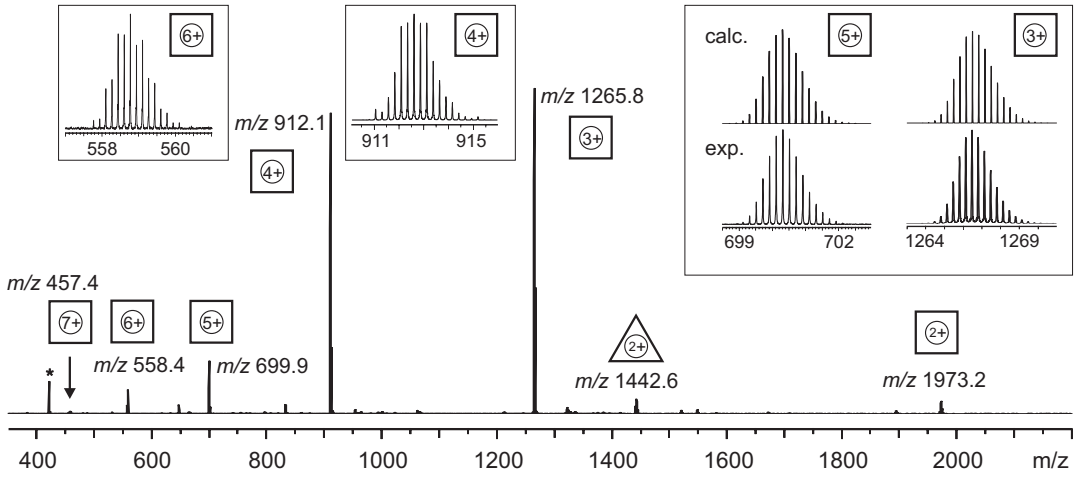

Figure 5.4: Mass spectra of **SS1b**. Peaks for [4:4:8-x]$^{x+}$ with x = 2 to 7 can be found (this notation represents the composition as [metal:ligand:OTf]$^{n+}$).

indication that the squares present in solution are transferred into the gas phase as intact macrocycles. The series of signals is caused by stripping off triflate counter ions from the squares. In the case of **SS1a,b**, the observed signals range from

the loss of two triflates giving rise to $[4:4:6]^{2+}$ (this notation represents the composition as [metal:ligand:OTf]$^{n+}$) up to the sevenfold charged $[4:4:1]^{7+}$ square.[64] While the experimental isotope patterns for the odd charge states closely match those calculated on the basis of natural abundances, the even charged ions are in some cases superimposed by a minor amount of smaller fragments at the same $\frac{m}{z}$ value: For example, a doubly charged square $[4:4:6]^{2+}$ might be superimposed by a $[2:2:3]^{+}$ fragment. The actual charge distribution observed strongly depends on ionization conditions, i. e. drying and nebulizing gas flows. In general, the platinum squares show less fragmentation compared to their palladium analogues due to the more stable metal-nitrogen bonds. In addition, the tendency to fragment decreases with increasing size of the organic ligands. This stability of the ions can be attributed to the increasing number of degrees of freedom, which permit to store more internal energy before fragmentation is induced.

The spray-solvent (in most cases: acetone) should be distilled before use to remove anions such as chloride or formiate, acetate and propionate. If necessary, the NMR-solutions ([D_6]-dimethylsulfoxide, [D_7]-dimethylformamide) might be diluted by acetone (to 400 μm) and sprayed.

Figure 5.5 shows exemplary mass spectra of **SS5a,b**. Each spectrum is dominated by the $[4:4:6]^{2+}$ square. The experimental isotope patterns for the +2 charge states closely match those calculated on the basis of natural abundances (see insets), as – in this case – no smaller fragments at the same $\frac{m}{z}$-value are present. In table 5.1, the measured signals for the +2 and +3 charge state for **SS1a,b** to **SS6a,b** are summarized.

Results from NMR NMR spectra for **SS1a,b** to **SS6a,b** (see Scheme 5.15) are recorded in different solvents ([D_2]-dichloromethane, [D_6]-acetone, [D_6]-dimethylsulfoxide, and [D_7]-dimethylformamide) with variable concentrations (10 to 0.3 mm) and at variable temperatures (223 to 373 K). Figure 5.6 shows the ^{1}H and ^{31}P NMR of **SS2b** in acetone at room temperature. In the ^{1}H NMR spectrum more than one set of broad signals is observed. Although a complete assignment of the signals observed in the ^{1}H NMR spectrum is impossible, the downfield shift of the aliphatic protons of the dppp-subunit relative to the same signals in the

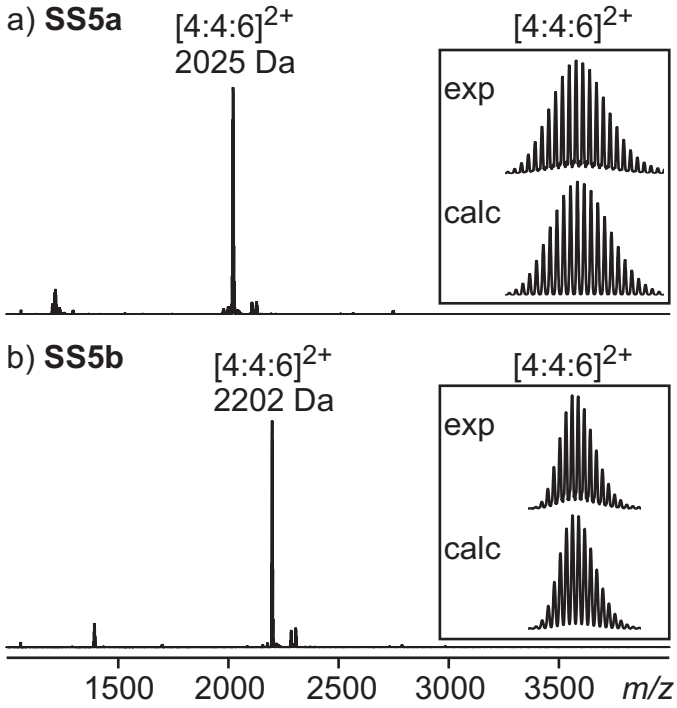

Figure 5.5: Exemplary mass spectra of a) **SS5a** and b) **SS5b**.

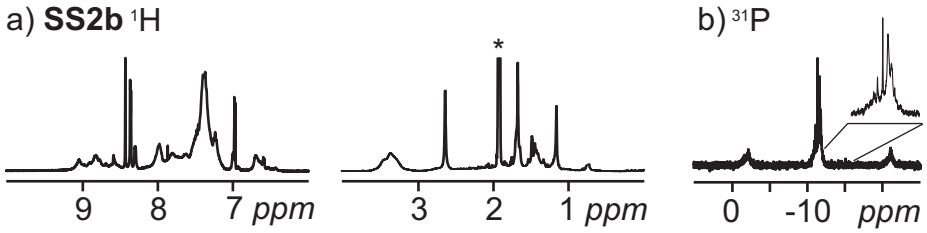

Figure 5.6: a) and b) Partial ^{1}H and ^{31}P NMR of **SS2b** in [D_6]-acetone (*) at room temperature.

Compound	Formula	chemical Composition	m/z
SS1a	$[4{:}4{:}6]^{2+}$	$C_{154}H_{136}P_8Pd_4N_8F_{18}S_6O_{18}$	1797
	$[4{:}4{:}5]^{3+}$	$C_{153}H_{136}P_8Pd_4N_8F_{15}S_5O_{15}$	1148
SS1b	$[4{:}4{:}6]^{2+}$	$C_{154}H_{136}P_8Pt_4N_8F_{18}S_6O_{18}$	1974
	$[4{:}4{:}5]^{3+}$	$C_{153}H_{136}P_8Pt_4N_8F_{15}S_5O_{15}$	1266
SS2a	$[4{:}4{:}6]^{2+}$	$C_{162}H_{152}P_8Pd_4N_8F_{18}S_6O_{18}$	1853
	$[4{:}4{:}5]^{3+}$	$C_{161}H_{152}P_8Pd_4N_8F_{15}S_5O_{15}$	1185
SS2b	$[4{:}4{:}6]^{2+}$	$C_{162}H_{152}P_8Pt_4N_8F_{18}S_6O_{18}$	2030
	$[4{:}4{:}5]^{3+}$	$C_{161}H_{152}P_8Pt_4N_8F_{15}S_5O_{15}$	1303
SS3a	$[4{:}4{:}6]^{2+}$	$C_{170}H_{168}P_8Pd_4N_8F_{18}S_6O_{18}$	1909
	$[4{:}4{:}5]^{3+}$	$C_{169}H_{168}P_8Pd_4N_8F_{15}S_5O_{15}$	1223
SS3b	$[4{:}4{:}6]^{2+}$	$C_{170}H_{168}P_8Pt_4N_8F_{18}S_6O_{18}$	2086
	$[4{:}4{:}5]^{3+}$	$C_{169}H_{168}P_8Pt_4N_8F_{15}S_5O_{15}$	1341
SS4a	$[4{:}4{:}6]^{2+}$	$C_{170}H_{152}P_8Pd_4N_8O_{34}F_{18}S_6$	2029
	$[4{:}4{:}5]^{3+}$	$C_{169}H_{152}P_8Pd_4N_8O_{31}F_{15}S_5$	1303
SS4b	$[4{:}4{:}6]^{2+}$	$C_{170}H_{152}P_8Pt_4N_8O_{34}F_{18}S_6$	2206
	$[4{:}4{:}5]^{3+}$	$C_{169}H_{152}P_8Pt_4N_8O_{31}F_{15}S_5$	1421
SS5a	$[4{:}4{:}6]^{2+}$	$C_{170}H_{160}P_8Pd_4N_{16}O_{26}F_{18}S_6$	2025
	$[4{:}4{:}5]^{3+}$	$C_{169}H_{160}P_8Pd_4N_{16}O_{23}F_{15}S_5$	1300
SS5b	$[4{:}4{:}6]^{2+}$	$C_{170}H_{160}P_8Pt_4N_{16}O_{26}F_{18}S_6$	2202
	$[4{:}4{:}5]^{3+}$	$C_{169}H_{160}P_8Pt_4N_{16}O_{23}F_{15}S_5$	1418
SS6a	$[4{:}4{:}6]^{2+}$	$C_{154}H_{144}P_8Pd_4N_{16}F_{18}S_6O_{18}$	1857
	$[4{:}4{:}5]^{3+}$	$C_{153}H_{144}P_8Pd_4N_{16}F_{15}S_5O_{15}$	1188
SS6b	$[4{:}4{:}6]^{2+}$	$C_{154}H_{144}P_8Pt_4N_{16}F_{18}S_6O_{18}$	2034
	$[4{:}4{:}5]^{3+}$	$C_{153}H_{144}P_8Pt_4N_{16}F_{15}S_5O_{15}$	1306

Table 5.1: Mass spectrometric results for compounds **SS1a,b** to **SS6a,b**, sprayed from acetone (400 μm solutions).

metal precursor, is clearly visible, as expected for pyridine coordination. Further proof for metal-ligand-coordination comes from the ^{31}P NMR spectrum. Multiple sets of overlapping signals are observed at the ppm regime (-11 ppm) and with the $^{1}J_{Pt195,P}$-coupling (3060 Hz) expected from the data known for **SS1b** (-13 ppm, 3041 Hz)[61]). These findings differ considerably from the free metal precursor: -7 ppm with a $^{1}J_{Pt195,P}$-coupling of 3650 Hz (same solvent and temperature). Hence, coordination of the organic ligands to the metal precursors is unquestionable.

When the NMR solvent is changed to [D_6]-dimethylsulfoxide, the situation gets less complicated: Figure 5.7 shows the ^{1}H and ^{31}P NMR of **SS4a,b** in [D_6]-dimethylsulfoxide at room temperature. While the ^{1}H NMR spectrum for palladium species **SS4a** shows only one set of broad signals, the spectrum of the corresponding platinum species **SS4b** is still complex (more than one broad set of signals). Obviously, the interconversion processes are faster in [D_6]-dimethylsulfoxide than in [D_6]-acetone. Indeed, the signals sharpen when the temperature is increased[‡] for the palladium species **SS4a** and the platinum species **SS4b**. Nevertheless, the signals in the ^{1}H NMR spectra of **SS4b** at 373 K are still as broad as the signals observed for **SS4a** at room temperature ($\Delta T = 65$ K).

As mass spectra for compounds **SS1a,b** to **SS6a,b** show the almost exclusive presence of [4:4]-complexes (see above), the multitude of signals in the NMR spectra is assigned to mixtures of interconverting square isomers as discussed in 8.7. Hence, two important aspects can be deduced from the temperature dependent NMR spectra: (i) The solvent and the temperature of choice have drastic effect onto the kinetics of interconversion between the possible isomers. (ii) Platinum species seem to interconvert more slowly than palladium species (for a more detailed discussion see 5.3.2.3).

To answer the question, which of the three types of interconversion causes the coalescence in the NMR spectra, ^{1}H and ^{31}P NMR spectra of octaethyl square **SS3a,b** are recorded in [D_6]-dimethylsulfoxide at variable temperatures. In line with **SS4a**, one broad signal is observed in the ^{31}P NMR spectra of **SS3a**, which sharpens with increasing temperature (see Figure 5.8 b). Quite unexpectedly, the ^{1}H NMR spectra of **SS3a,b** show broad and overlapping sets of signals at

[‡]Valuable discussions with Torsten Weilandt are acknowledged.

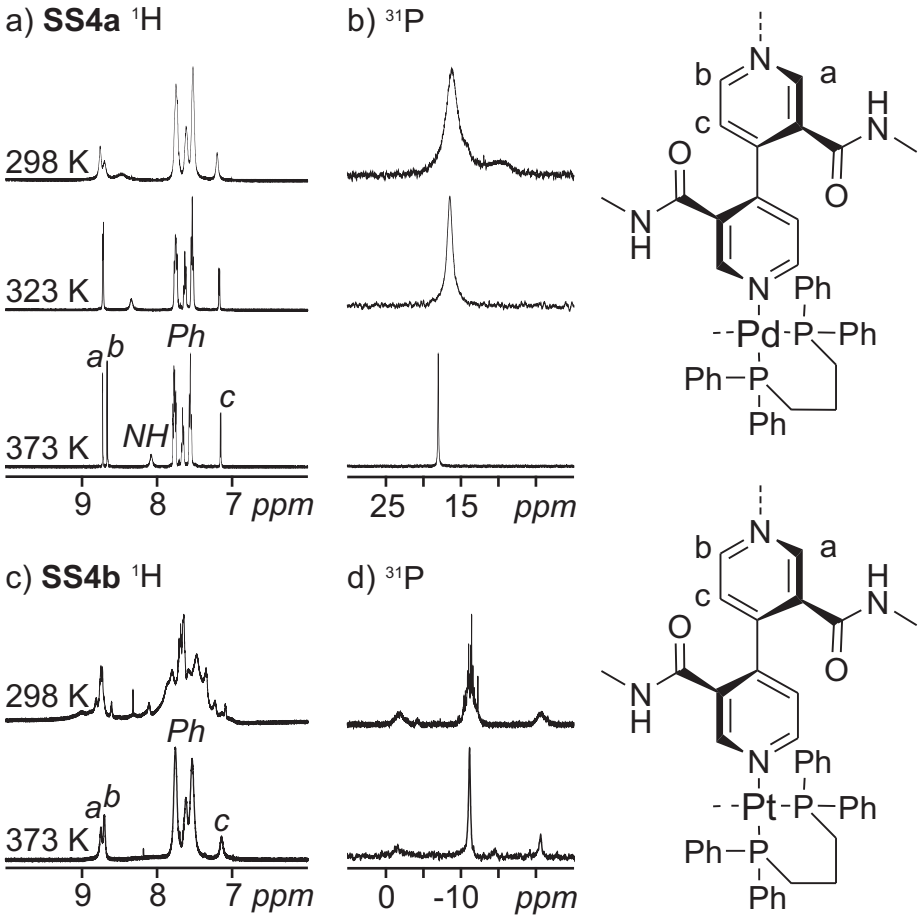

Figure 5.7: a) and b) Partial ^{1}H and ^{31}P NMR of **SS4a** in [D_6]-dimethylsulfoxide at variable temperatures; c) and d) Partial ^{1}H and ^{31}P NMR of **SS4b** in [D_6]-dimethylsulfoxide at variable temperatures.

room temperature (see Figure 5.8). The two signals of pyridine's *ortho*-hydrogen atoms overlap at 8.5 ppm as well as the central CH_2-group of the dppp-subunit with the diastereotopic protons of the CH_2-CH_3-group at 2.0 ppm over a wide temperature regime, respectively. The latter point is especially disappointing, as therefore the exact coalescence temperature of a ligand stereoisomerization can not be obtained. However, for **SS3a**, sharp signals are already observed at 323 K, which is 40 K lower than the coalescence temperature obtained for the free ligand **22** (see 5.1.4.1). Three explanations might be considered for this finding:

1. If the barrier for stereoisomerization might be smaller in **SS3a** than in the free ligand **22**, T_C might be smaller, too. This might be explained by the hypothesis that the $\pi - \pi^*$-stacking of the dppp's phenyl group with the pyridine backbone of the ligand might stabilize the transition state of stereoisomerization.

2. A complete dissociation of the squares into their building blocks occurs, before the T_C of the stereoisomerization is reached.

3. Two or more metal-nitrogen bonds are broken and the resulting fragments rebuild other square-isomers, again before T_C of the stereoisomerization is reached.

A reduced barrier of stereoisomerization (1.) should however be observed for palladium as well as for platinum species, which is not the case: The spectra for **SS3b** stay broad over the whole accessible temperature range. Hence, possibility (1.) might be ruled out. Furthermore, the signals of the ligand component within the supramolecular aggregates are shifted when compared to the free ligand **22** in the same solvent at the same temperature and concentration regime. These shifts are a strong indication that squares are still present in solution in considerable amount. Therefore, (2.) can be excluded as well. As a conclusion, the third explanation becomes more reasonable: Metal-nitrogen bonds are continuously broken and rebound at higher temperatures causing averaged signals in the NMR spectra. Another evidence for this explanation comes from the NMR results of self-assembled supramolecular squares from unsymmetrical ligands (see next sub chapter).

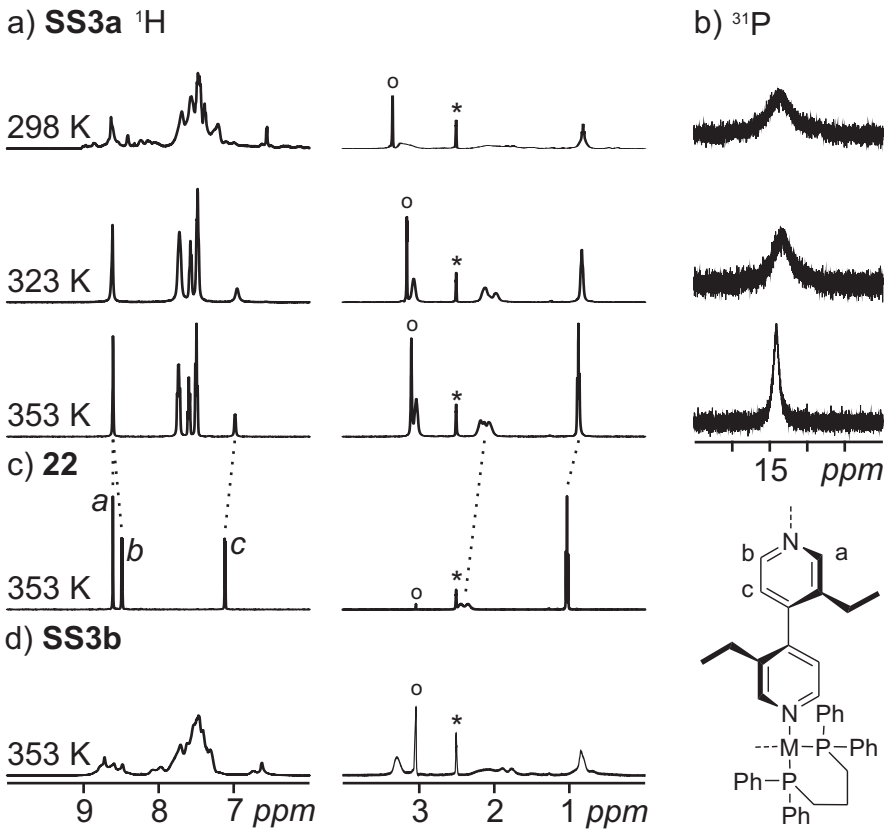

Figure 5.8: All spectra recorded in [D_6]-dimethylsulfoxide (*) (residual water is marked with circles) with comparable concentrations: a) and b) partial ^{1}H and ^{31}P NMR of **SS3a** at variable temperatures; c) partial ^{1}H NMR of the free ligand **22** at 353 K; d) partial ^{1}H NMR of **SS3b** at 353 K.

5.3.2.2 Self-Assembled Supramolecular Squares from Unsymmetrical [4,4']-Bipyridines

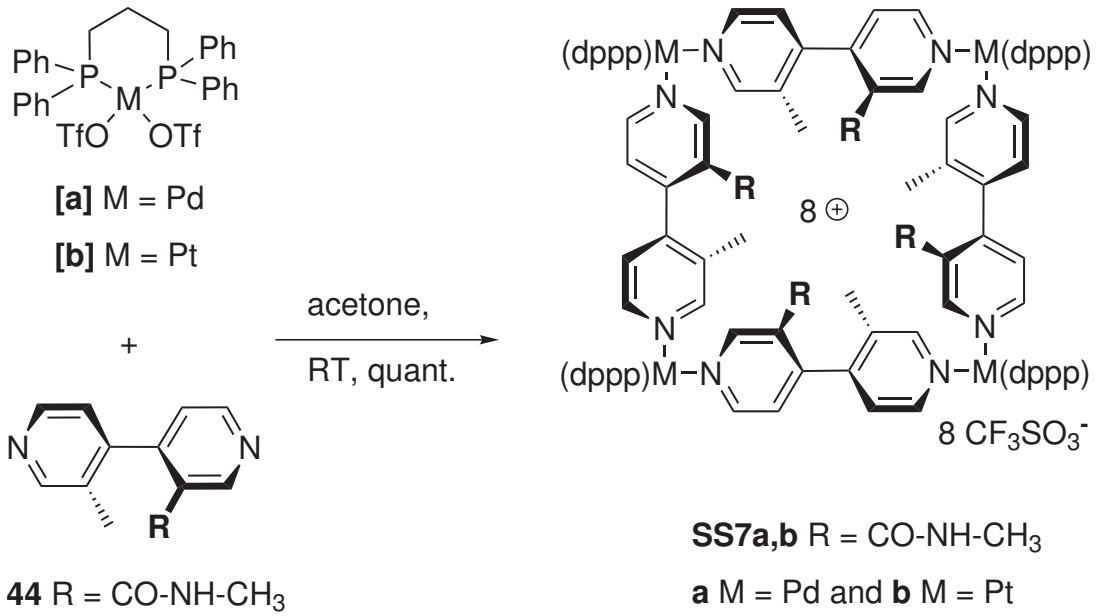

Scheme 5.16: Synthesis of **SS7a,b** (only one out of four isomers drawn, see below).

When unsymmetrical ligands, such as **44**, are used in self-assembly reactions for square formation (see Scheme 5.16), the ligand can be oriented either M-N-N'-M or M-N'-N-M. Four constitutional isomers (see Figure 5.9 f) might be formed, each with its own set of conformers. Two or more metal-nitrogen-bonds must be broken for isomerization of the constitutional isomers.

At 323 K, the ^{1}H NMR spectrum of **SS7a** shows one set of sharp signals (see Figure 5.9 a). This finding indicates that isomerization of the constitutional isomers is fast on the NMR time scale at 323 K. Thus, the dissociative mechanism should play a crucial role in the isomerization of conformers, too. In conclusion, some indication is found which of the three processes contribute to the interconversion. Unfortunately, no evidence is found which isomers exist in solution in considerable amount.

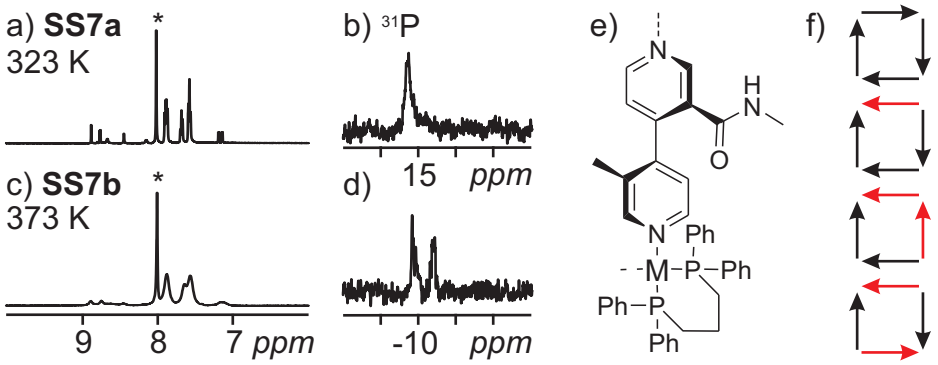

Figure 5.9: All spectra recorded in [D_7]-dimethylformamide (*) with comparable concentrations: a) and b) partial ^{1}H and ^{31}P NMR of **SS7a** at 323 K; c) and d) partial ^{1}H and ^{31}P NMR of **SS7b** at 373 K; f) **44** can be oriented either M-N-N'-M or M-N'-N-M in **SS7a,b**. Thus, four constitutional isomers exit, each with its own set of conformers.

5.3.2.3 Large Substituents – Self-Assembled Dendrimers[§]

Dendron[197] amines are synthesized according to Chapter 5.1.4.2.4. Self-assembly yields the corresponding metallo-supramolecular squares **DSG0a,b** to **DSG3a,b** in high yields (see Scheme 5.17): Equimolar amounts of (dppp)M$(OTf)_2$ with M = Pd(II) [**a**] or Pt(II) [**b**] and the desired bipyridine are mixed in dichloromethane and the resulting mixtures are stirred for 2 hours. It turned out that filtering the solution once and reducing the volume of the filtrate to 50% is advantageous in order to remove some insoluble remainders and adjust the concentration for the following precipitation of the product. Slow addition of diethyl ether to the reaction mixture then resulted in a white precipitate with a yield of 85% to 95%. The only exceptions from this procedure are the G3-substituted squares **DSG3a,b**, which are well soluble in diethyl ether and even in such nonpolar solvents like hexane due to the large lipophilic dendrons. Consequently, metal corners and bipyridine ligands are mixed and used without workup in the case of G3.

ESI mass spectra show again the +2 and +3 charge states of the squares formed through stripping away counterions as the most prominent peaks in the spectra (Figure 5.10). For instance, the mass spectrum of **DSG2a** shows the doubly charged ions $[4{:}4{:}6]^{2+}$ at $\frac{m}{z} = 4877$ and that of the Pt analogue **DSG2b**

[§]In cooperation with Dr. Tarik H. Baytekin and Dr. Marianne Engeser and published.[195,196]

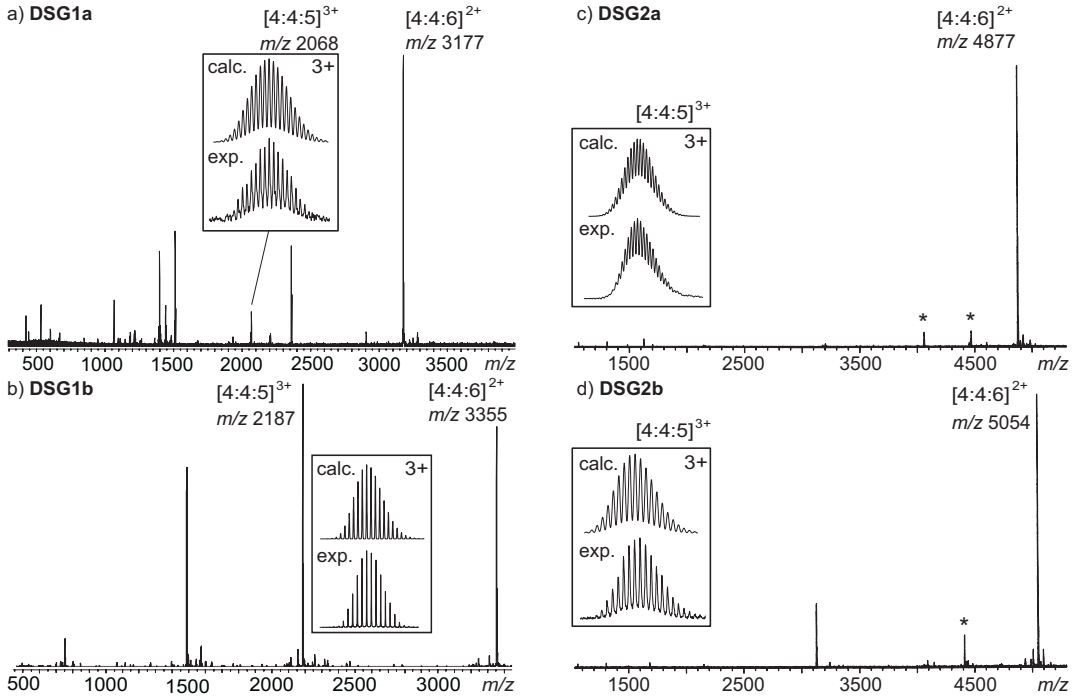

Figure 5.10: ESI-FTICR mass spectra of 200 μm acetone solutions of a) **DSG1a**, b) **DSG1b**, c) **DSG2a**, and d) **DSG2b** (asterisks indicate small contributions from defects originating from dendron synthesis). Insets: The isotope patterns of the +3 charge states have been generated independently in a second measurement and agree with those calculated, since they cannot be superimposed by fragments.

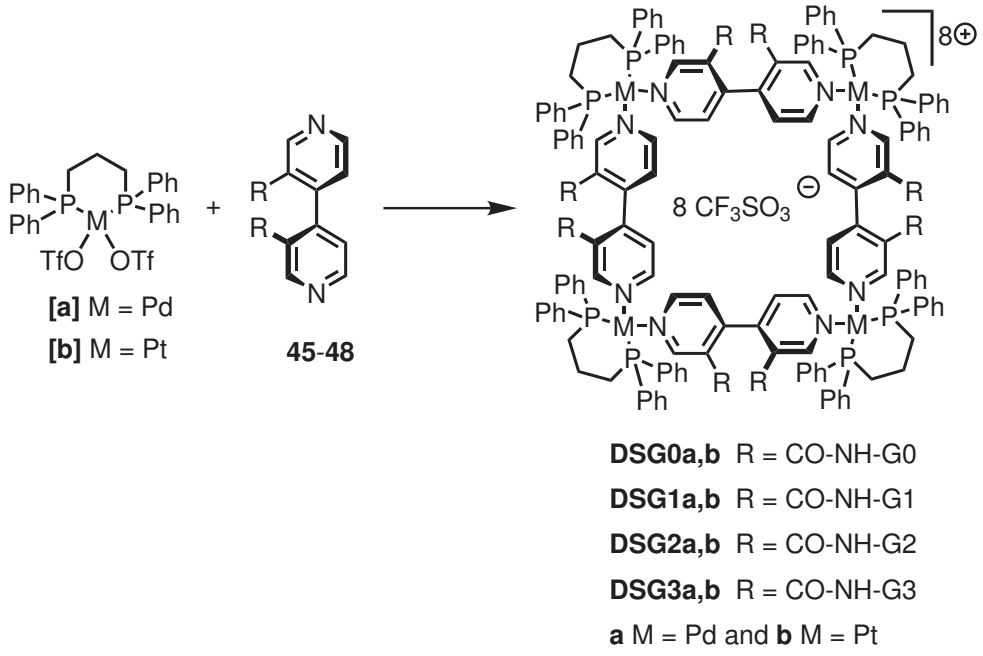

Scheme 5.17: Synthesis of self-assembled **D**endrimer **S**quares **DSG0a,b** to **DSG3a,b**.

exhibits a signal for $[4{:}4{:}6]^{2+}$ at $\frac{m}{z} = 5054$. The +2 charge states are superimposed by minor contributions of $[2{:}2{:}3]^{+}$ fragments. By tuning the ionization conditions, the +3 charge states can be generated without any contributions of other ions and the isotope patterns obtained now are in excellent agreement with those calculated (insets in Figure 5.10). A superposition with fragments is not possible due to the odd number of charges. The tendency to generate higher charge states as well as the trend to fragment decrease with increasing dendron generation. While the mass spectra of first generation dendritic squares exhibit some fragments, the spectra obtained for the second generation compounds are almost fragment free. As discussed before (see Chapter 4.2.3), this increased stability of the ions can be attributed to the increasing number of degrees of freedom, which permit to store more internal energy before fragmentation is induced. The G0 squares **DSG0a,b** behave similarly and are thus not shown here. The mass spectrometric experiments provide a clear picture of the species present in solution for all squares with dendrons up to the second generation. No signals for other polygons or larger open-chain oligomers are observed. Despite of the size of the dendrons, the self-

assembly of squares proceeds therefore easily in solution. The +2 charge states of the largest compounds under study, i.e. G3 dendrimers **DSG3a,b**, are outside the available $\frac{m}{z}$ range of the FT-ICR instrument. All attempts to generate higher charge states for the G3 squares **DSG3a,b** failed so far so that a mass spectrometric characterization is unfortunately not available yet. Nevertheless, the G3 dendritic squares show a behavior in the NMR as well as the AFM experiments strictly analogous to that observed for the smaller dendrimers (see below). We therefore conclude that the G3 dendron-decorated bipyridines yield squares as well.

In order to test ligand-exchange reactions, two squares with different bipyridine ligands are mixed. For the mixture of G0 and G1 Pd(II) squares **DSG0a** and **DSG1a**, a full equilibration is reached after less than ca. 30 s, after which the first ESI-MS spectrum could be obtained (Figure 5.11 a). The distribution of $G0_4$:$G0_3G1_1$:$G0_2G1_2$:$G0_1G1_3$:$G1_4$ squares is close to the statistically expected 1:4:6:4:1 ratio. In marked contrast, ligand exchange is much slower for the corresponding G0 and G1 Pt square mixture **DSG0b** and**DSG1b** (Figure 5.11 b). Only after ca. 2 days, the equilibrium is reached and no further intensity change is observed. From these experiments, we can conclude a rather drastic difference in the ligand-exchange kinetics to exist depending on the metal corner.[198] Palladium squares exchange ligands remarkably faster than their Platinum analogues. These finding are in excellent agreement with the NMR results for unsymmetrical ligands (Chapter 5.3.2.2).

Figure 5.12 compares a series of ^{1}H NMR spectra obtained for the G1-G3-substituted Pd assemblies at room temperature and G1 Pt squares at high temperature (373 K). The ^{1}H NMR spectra of dendritic Pd squares exhibit quite sharp signals at room temperature (Figures 5.12a-c). With the above remarks in mind (^{1}H and ^{31}P NMR of **SS4a,b** in Figure 5.7), it is not surprisingly to find only one set of easily assignable signals for all Pd squares. Evidence for coordination of the pyridine nitrogen atoms to the metal centers comes from the small, but typical downfield shifts (Δ = 0.2 ppm) of the H-2 and H-6 pyridine protons. In contrast, the H-5 protons are shifted to higher field by ca. 0.1 ppm due to the shielding effects of the dppp phenyl rings of the corners. The ^{31}P NMR signals

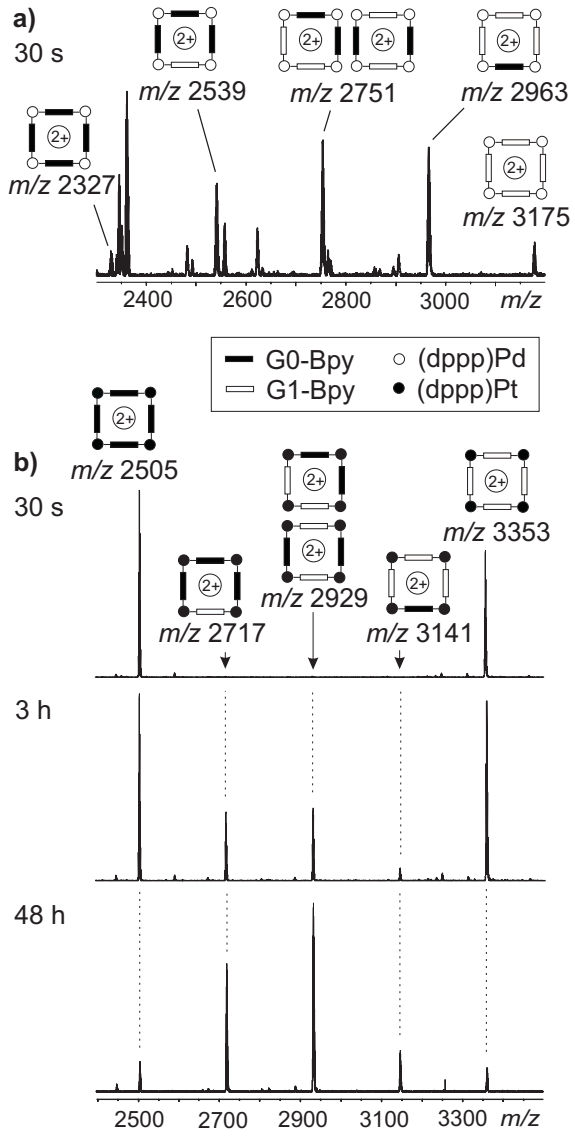

Figure 5.11: a) Partial ESI-FTICR mass spectrum of a mixture of **DSG0a** and**DSG1a** in acetone (each 200 μm) measured directly after mixing (corresponding to a ca. 30 second delay). b) Partial ESIFTICR mass spectra of a mixture of **DSG0b** and**DSG1b** in acetone (each 200 μm) kept at room temperature and measured after 30 seconds, 3 hours, and 48 hours after mixing.

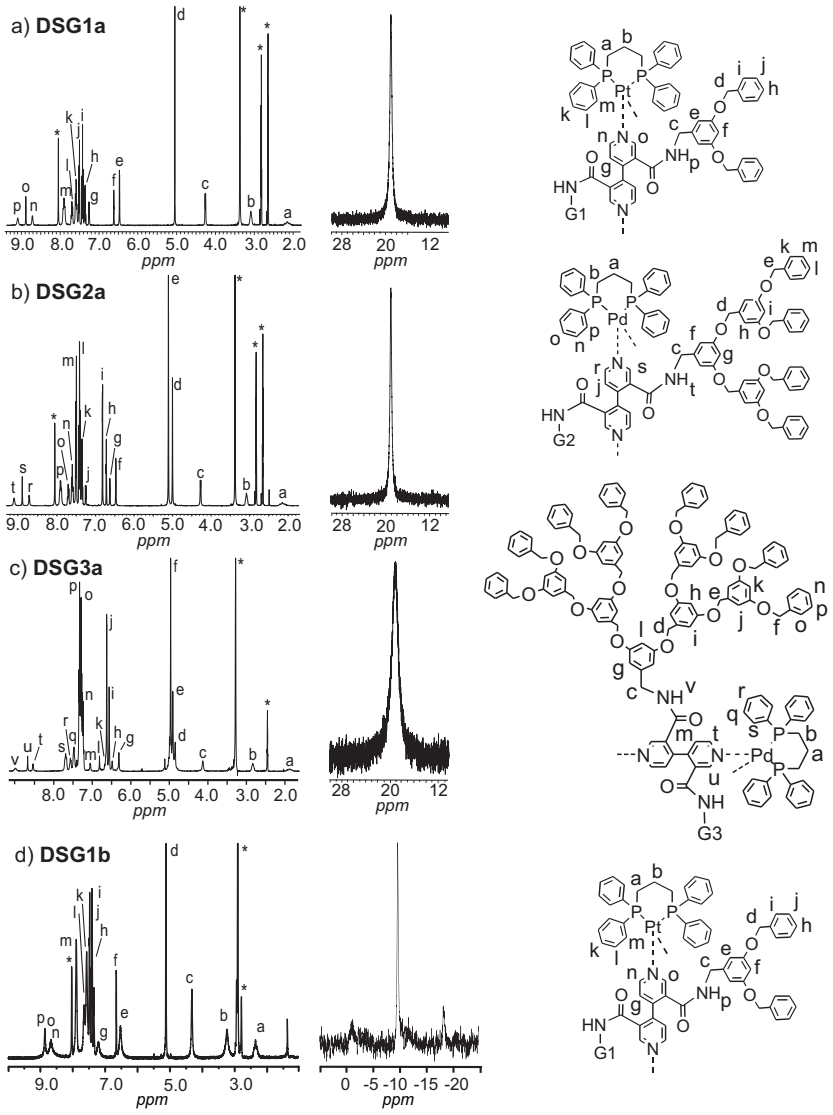

Figure 5.12: a) - c) Room temperature ^{1}H NMR (left) and ^{31}P NMR spectra (center) of G1 to G3 substituted Pd squares **DSG1a**, **DSG2a** and **DSG3a**. For all three compounds, the ^{1}H NMR spectra show one set of signals which can be assigned as shown in the drawings on the right. Asterisks indicate solvent signals and residual water ([D_7]-dimethylformamide for **DSG1a** and **DSG2a**, [D_6]-dimethylsulfoxide for **DSG3a**). d) ^{1}H and ^{31}P NMR spectra of **DSG1b** in [D_6]-dimethylsulfoxide at 373 K.

appear at around 19 ppm for all Pd squares. Chemical shift differences of ca. 1 ppm as compared to the free triflate salt of the Pd corners are in line with pyridine coordination, too. The ^{31}P NMR signals are somewhat broadened, presumably indicating that several out of the many possible conformers discussed above equilibrate with each other slow enough to cause some peak broadening. In contrast to the Pd squares, all Pt analogues give rise to rather complex ^{1}H and ^{31}P NMR spectra at room temperature as expected from the above discussion. At 298 K, signals are broad and many sets of signals strongly overlap. At high temperature (373 K), however, the spectra become similarly simple as compared to the Pd analogues (Figure 5.12 d). Pyridine coordination is again confirmed by similar shifts as discussed above. Furthermore, the $^{1}J_{Pt195,P}$ coupling constant is highly indicative of coordination, because it is much lower for the squares (3150 – 3250 Hz) than that for the (dppp)Pt(OTf)$_2$ **[b]** precursor (3647 Hz) in [D$_7$]-dimethylformamide. The highly complex room temperature ^{1}H NMR spectra for the Pt squares indicate slow dynamic processes indeed to occur. In order to understand the marked difference between the Pd and Pt squares in more detail, variable temperature ^{1}H NMR experiments are conducted with both.

Figure 5.13 shows the two series recorded for **DSG1a** and **DSG1b**. Clearly, similarities can be seen between spectra of **DSG1a** and those obtained for **DSG1b** at much higher temperature. For example, the 373 K ^{1}H NMR spectrum of **DSG1b** resembles in its appearance the 293 K spectrum of **DSG1a**. An exact determination of coalescence temperatures is of course not possible due to the strong overlap of signals at lower temperature. Consequently, the determination of interconversion barriers is not straightforward. But the temperature difference caused by the metal change is drastic and clearly visible: The isomer interconversion for the Pt complexes is approximately as fast as that of the Pd complexes at room temperature when the temperature is raised by ca. 60 - 80 K. Consequently, the spectra of Pd squares are already in the fast exchange regime at room temperature, while the Pt squares still interconvert slowly on the NMR timescale. This temperature dependent behavior is very similar to the one already discussed above for **SS3a,b** and **SS4a,b**. With respect to the three isomerization mechanism discussed above, only one conclusion can be drawn from these

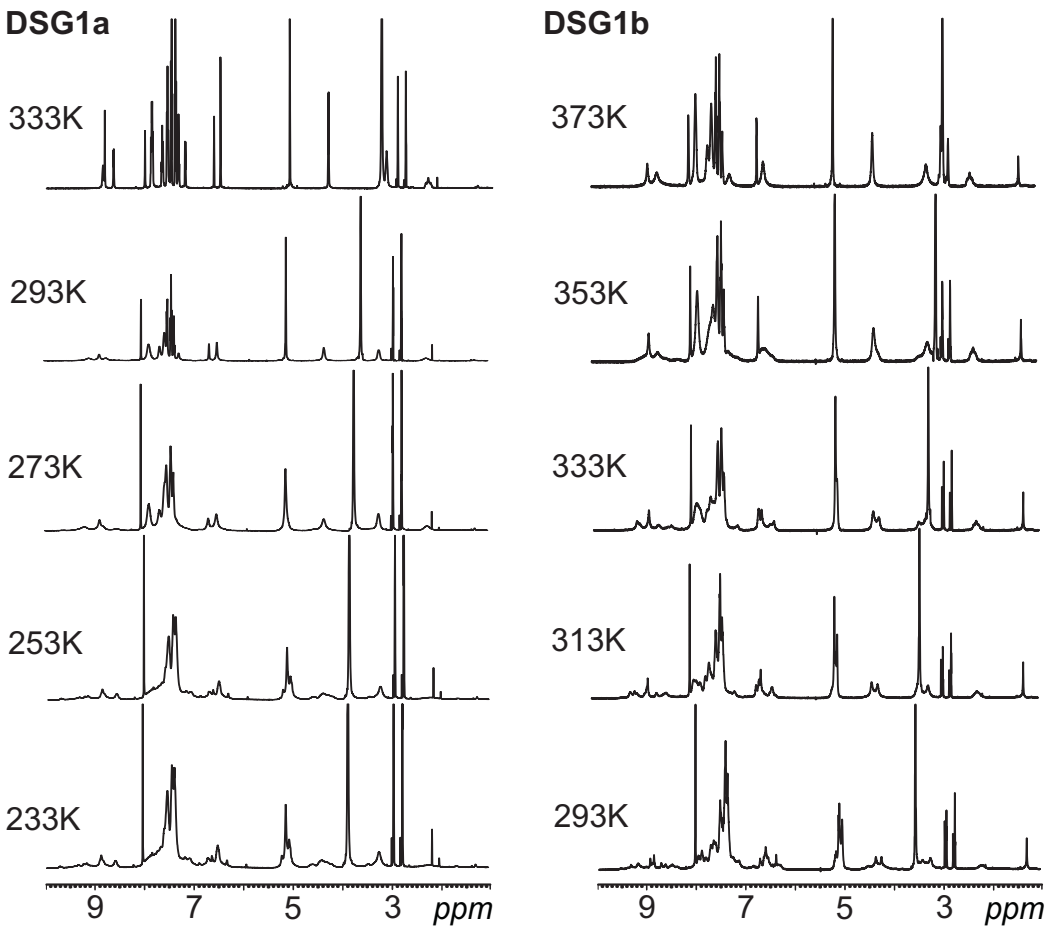

Figure 5.13: Variable-temperature ^{1}H NMR spectra of **DSG1a** (left) and its Pt(II) analogue **DSG1b** (right). Please note that the temperature is 40 to 60 K higher in the Pt spectra.

results: Interconversion through the combination of ligand rotation around the metal-metal-axis with stereoisomerization of the ligands cannot explain the large difference in exchange rates. On the contrary, if these processes alone accounted for the observed conformer interconversion, no significant difference would be expected. Ligand exchanges[199] thus contribute here at least significantly. These conclusions are in excellent agreement with the ^{1}H NMR results of **SS4a,b** in [D_6]-dimethylsulfoxide and the mass spectrometric ligand-exchange experiments discussed above. Thus, even though a more detailed or even quantitative analysis is not straightforward, some qualitative conclusions can be drawn on the dynamic behavior of the dendritic squares under study.

Visualization of films of these dendrimers using atomic force microscopy (AFM) provides information on their molecular dimensions. After deposition of a square monolayer on the surface, a slow reorganization within this layer is observed which leads to the formation of "tower-like" aggregates and multi-layer formation. The interplay of interactions between the dendrimers and the surface and interactions between different dendrimers are invoked to rationalize the observations. For a more detailed analysis of the AFM results please see ref.[195]

In conclusion, a reasonably short synthesis for self-assembling dendrimers[23] that bear a nanometer-sized cavity at their cores is described. The synthetic strategy includes a first step in which Fréchet-dendrons are attached to bipyridine ligands covalently, followed by a self-assembly step generating metallo-supramolecular squares. Careful analysis by NMR and MS revealed that square formation and isomer interconversion is not prevented by the size of the dendrons. Valuable facts (differences between Pd and Pt, isomer interconversion) could be deduced from these achiral substituents, whereas the introduction of chirality is the major topic of the following chapters.

5.3.2.4 Self-Assembled Supramolecular Squares from Amino Acid Decorated Ligands¶

Both, homochiral assembly[201] formation from racemic building blocks (self-recognition) and heterochiral assembly formation (self-discrimination)[202] are quite rare.

¶The results of this chapter are submitted for publication.[200]

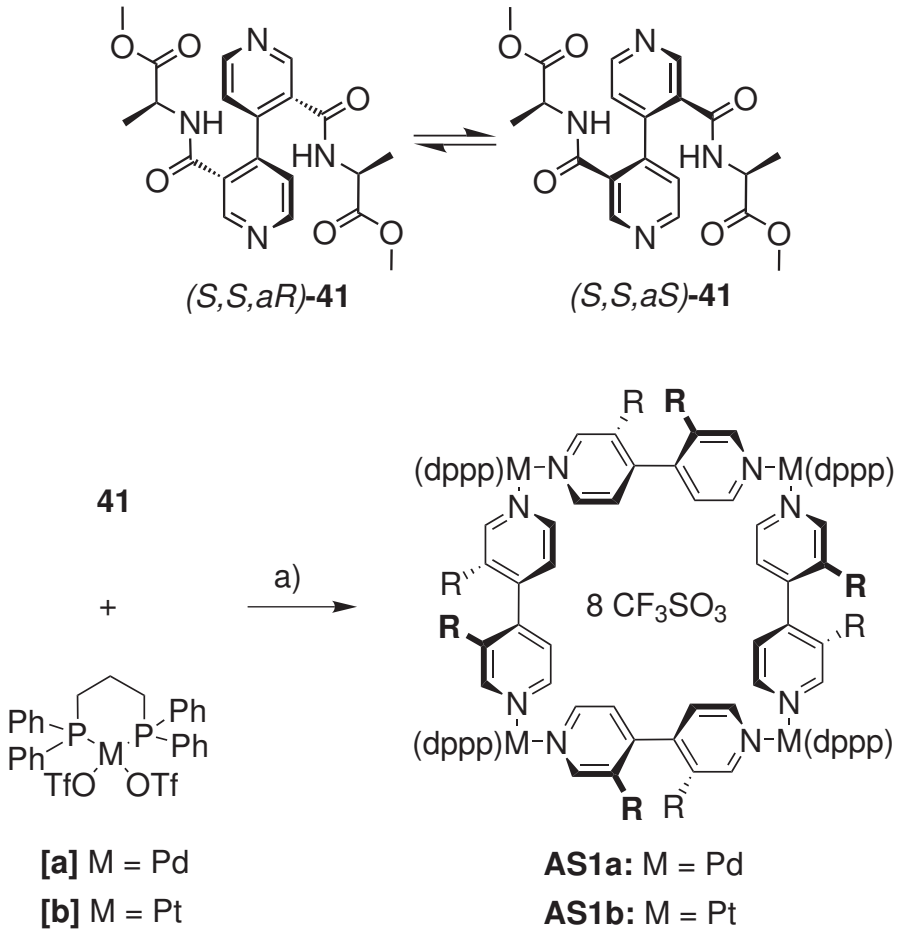

Scheme 5.18: Synthesis of self-assembled supramolecular squares **AS1a,b** (**A**mino acid **S**quares) from amino acid decorated ligand **41**. a) acetone, 1 h, RT, quant.

Even more complex situations arise when diastereomers can interconvert quickly even after assembly formation.9 In the following chapter, heterochiral self-assembled supramolecular squares from amino acid decorated ligand **41** are presented (see Scheme 5.18. For other chiral squares see references.[203]

The synthesis of **41** is described in Chapter 5.1.4.2.2). Ligand **41** forms chiral assemblies when mixed with equimolar amounts of metal precursors [**a**] and [**b**], respectively. Except for a small, coordination-indicating shift of the 215 nm band, the CD spectra for chiral assemblies **AS1a,b** (see Figure 5.14) resemble that of **41**.

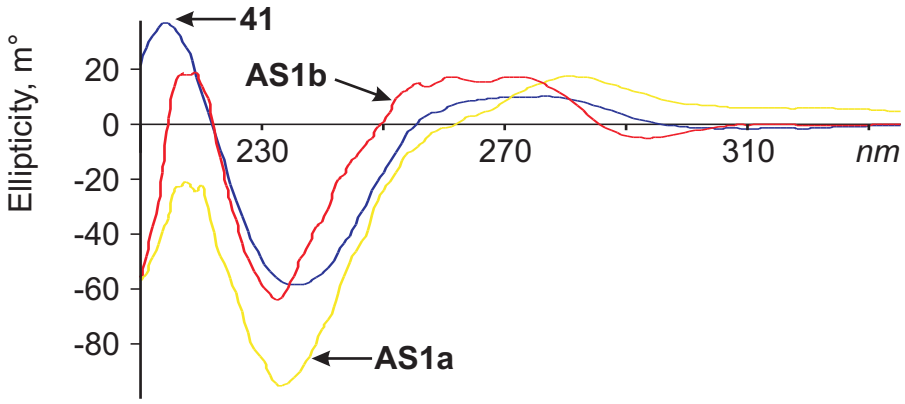

Figure 5.14: CD spectra of **41** and **AS1a,b** (all: methanol, 500μm of **41** and 125μm for **AS1a,b**.

In the ESI mass spectra of **AS1a,b**, doubly and triply charged squares are observed similar to the squares discussed so far (see Figure 5.15) together with the typical fragments (see Chapter 4.2.3). Elemental compositions of the resulting assemblies are confirmed by exact mass and high-resolution isotope patterns. Consequently, other assemblies than squares can be ruled out.

As discussed in paragraph 8.7, 560 possible isomers might in principle coexist in solution. Consequently, one may expect to obtain rather complex NMR spectra. Surprisingly, this is not the case (Figure 5.16). In the rather simple ^{1}H NMR spectra of **AS1a,b** in [D_6]-acetone, the symmetry of the ligand component within the supramolecular aggregates is reduced as compared to the free ligand **41** as indicated by two sets of signals that appear in a 1:1 ratio. Two doublets in

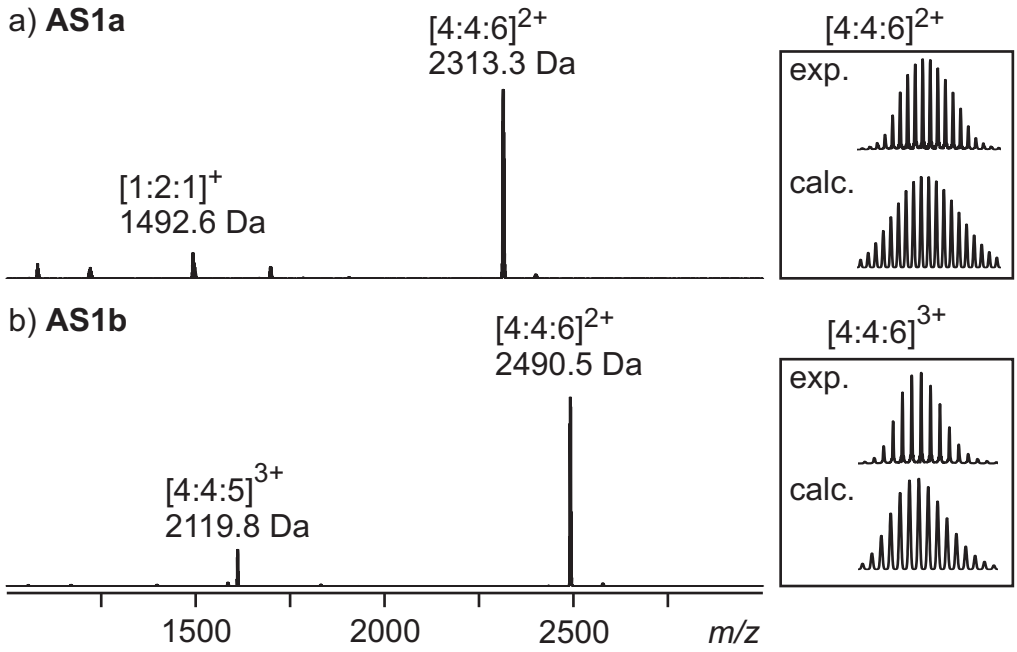

Figure 5.15: FTICR-MS spectra of a) **AS1a** and b) **AS1b** (both: acetone, 400 μm, labels represent the composition as [metal:ligand:OTf]$^{n+}$); insets: experimental and calculated isotope patterns. Note that for **AS1a** the signals for $[4{:}4{:}6]^{2+}$ overlap with minor signals for $[2{:}2{:}3]^{+}$ ($< 5\%$ intensity).

the ^{31}P NMR spectra of **AS1a,b** ($^{2}J_{PP}$ = 30.5 Hz (**AS1a**) and $^{2}J_{PP}$ = 29.8 Hz (**AS1b**), again in a 1:1 ratio) confirm the symmetry reduction. The coupling indicates that both P atoms at each corner are different from each other. From this finding, the symmetry of the resulting assemblies can be obtained, since only three scenarios would be in accordance with these observations: (i) The first one would be the formation of an almost exact 1:1:1:1 mixture of four different, D_4-symmetric isomers which at the same time coincidentally correctly mimic the roof effect observed in the ^{31}P NMR spectra. This, however, is very unlikely compared to the other alternatives which would be (ii) D_2 or (iii) C_4 symmetrical isomers that also agree with the obtained NMR results. Thus, it is indicated that only one isomer is formed exclusively.

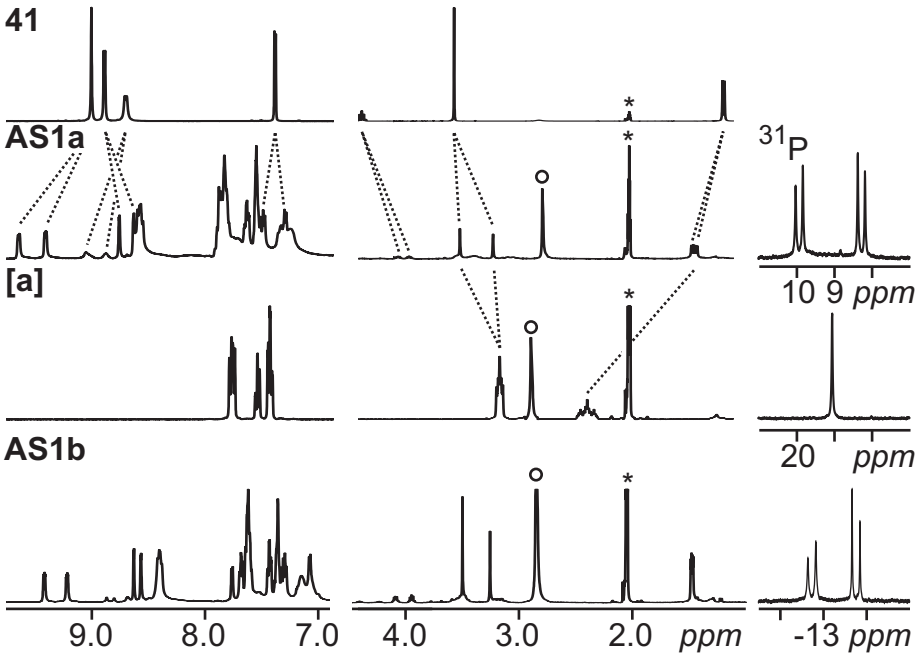

Figure 5.16: Room-temperature ^{1}H NMR (left) and ^{31}P NMR spectra (right) of **41**, **AS1a**, (dppp)Pd(OTf)$_2$ **[a]**, and **AS1b** in [D_6]-acetone (*); circles: residual water.

Symmetry considerations for all possible isomers allows to identify eight candidate structures which meet the criteria obtained from the NMR experiments (see Figure 5.17): The two C_4 symmetrical isomers (**I** and **II**) bear one amide group pointing inwards and one pointing outwards on each ligand. The absolute

configuration of all ligands is (*S*,*S*,*aR*) for **I** and (*S*,*S*,*aS*) for **II**. In the six D_2-symmetric isomers, the situation is a bit more complex. In isomers **III** (all amides out) and **IV** (all amides in), two ligands are (*S*,*S*,*aR*)-configured, the other two (*S*,*S*,*aS*). In the remaining four isomers, the amide groups of two opposite ligands are pointing inside and the other two outwards: **V** (aR in, aS out), **VI** (aS in, aR out), **VII** (all aR) and **VIII** (all aS). The symmetry considerations depicted in Figure 5.17 lead to the following conclusion: For C_4-symmetrical structures **I** and **II**, each ligand contributes to both sets of signals in the NMR spectra, since its two pyridine rings are not equivalent. For all D_2-symmetric structures, both pyridine rings in each ligand are equivalent, but the structure contains two pairs of ligands, each one of which causes one set of signals in the ^{1}H NMR.

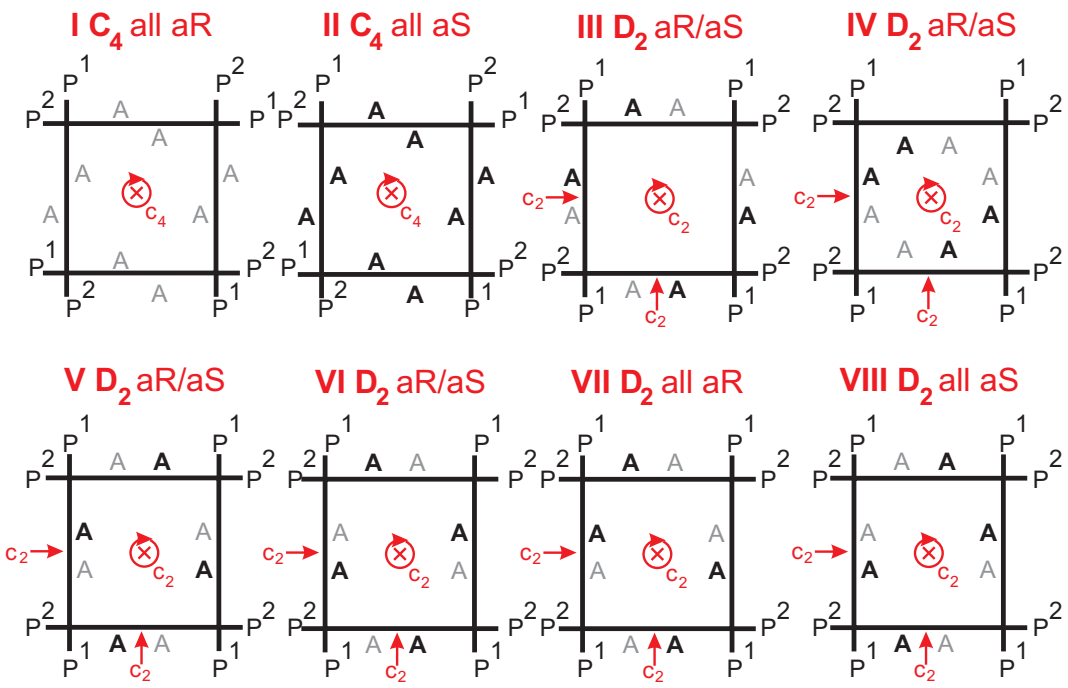

Figure 5.17: Eight candidate structures that meet the NMR-derived symmetry criteria (black A: amides above; grey A : amides below square plane; symmetry elements and resulting symmetry groups labeled in red). Note that **III** and **IV** do not possess mirror planes due to the chiral amino acid residues A.

2D-NMR experiments (HH-COSY, HMQC, HMBC) of **AS1a,b** are performed to assign all ^{1}H and ^{13}C nuclei of the ligand component (see Figure 5.18 top)

and to narrow down the number of possible isomers. In the HMBC spectrum (Figure 5.18 bottom) each signal is assigned to one set (A or B). Only A/A and B/B cross signals are found. Cross signals between "A-protons" and "B-carbons" or vice versa are not observed. In particular, cross signals exist for the ^{3}J couplings between H^5_B and C^4_B as well as H^5_A and C^4_A. These can only appear in D_2-symmetrical isomers **III** to **VIII** because both pyridine rings of each ligand belong to the same set of signals. In C_4-symmetrical structures **I** and **II**, couplings between H^5_B and C^4_A as well as H^5_A and C^4_B should instead be observed. Therefore isomers **I** and **II** can be clearly ruled out.

A discrimination between the remaining candidates is not possible by NMR experiments alone. Therefore, single crystals of **AS1b** are grown from saturated acetone solutions kept at 50°C over three days. The crystal structure of **3b** shown in Figure 5.19 clearly demonstrates the assembly to be a square with all amide groups pointing away from the cavity. The absolute configuration of two opposite ligands is (*S*,*S*,*aR*), while the two remaining ligands are (*S*,*S*,*aS*)-configured. As the solid-phase structure agrees well with the symmetry and coupling conditions found in the NMR spectra, it can be safely concluded that this is the isomer found in solution, too.

More profound insight into the reasons for this remarkable selectivity in the self-assembly reactions of **AS1a,b** comes from the solid-state structure: Crystal structures of simpler squares of the Stang type[61,193] show a) two of the four phenyl rings of each dppp to be π-stacked with one pyridine ring and b) the remaining two dppp phenyl rings to self-solvate each other either above or below the square's plane. As clearly visible in Figure 5.19, the amino acid substituents avoid steric congestion with these phenyl groups that are in the axial position of the diphosphametallacyclohexane rings. Consequently, the dppp ligands dictate an up-down-down-up-up-down-down-up arrangement of the amino acid substituents. At the same time, they all point away from the cavity, most likely in order to maximize stacking with the equatorial phenyl groups. Both arguments together unambiguously lead to the structure found in the crystal.

In conclusion, the remarkably diastereoselective self-assembly of self-assembled supramolecular squares incorporating four bipyridine ligands carrying two

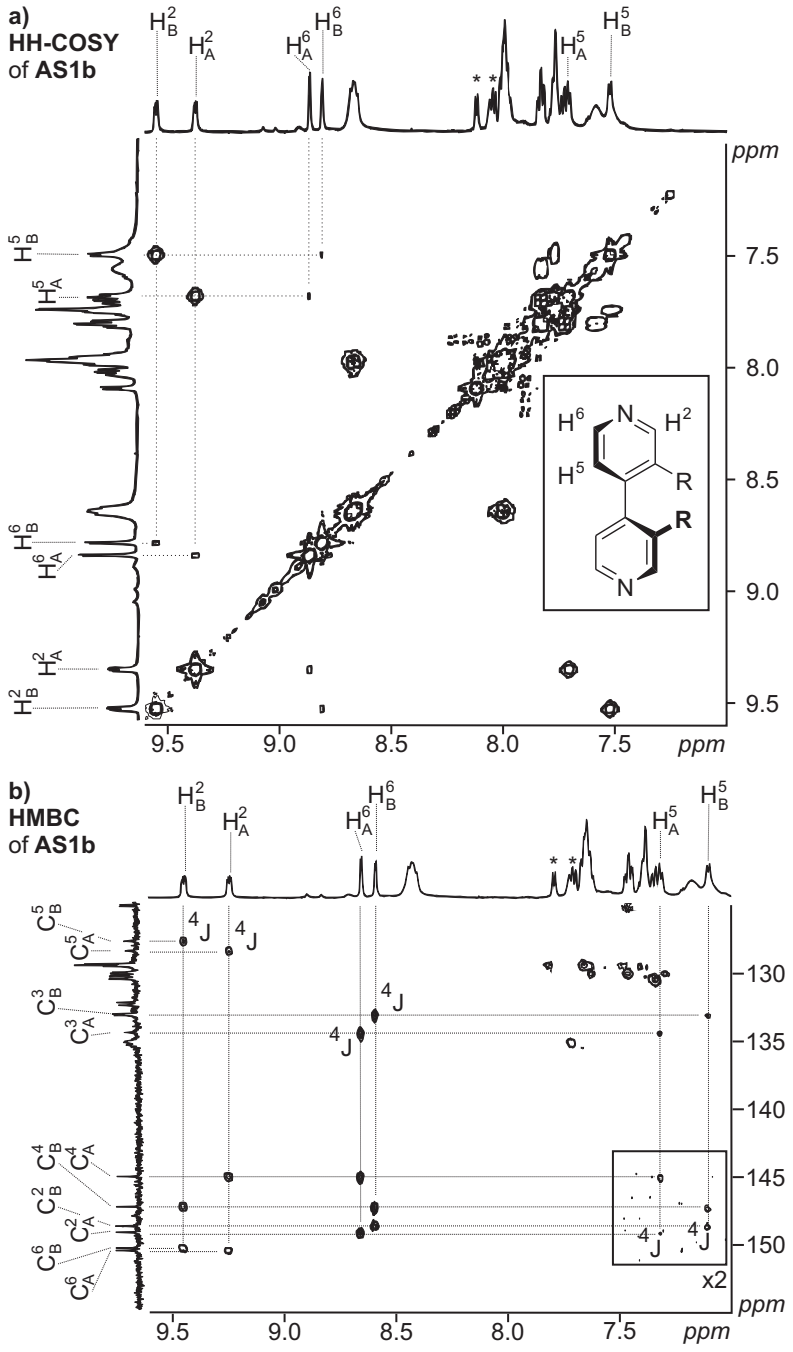

Figure 5.18: Top: The HH-COSY spectrum (aromatic region) of **AS1b** in [D_6]-acetone allows the assignment of the two sets of peaks (A or B). Bottom: The room-temperature HMBC spectrum (aromatic region) of **AS1b** in [D_6]-acetone shows cross peaks resulting from ^{3}J and ^{4}J ^{1}H-^{13}C couplings. Cross peaks for ^{4}J couplings are labeled, ^{3}J couplings are unlabeled. Lines are drawn for cross peaks belonging to bipyridine signals. * indicate ligands amide signals.

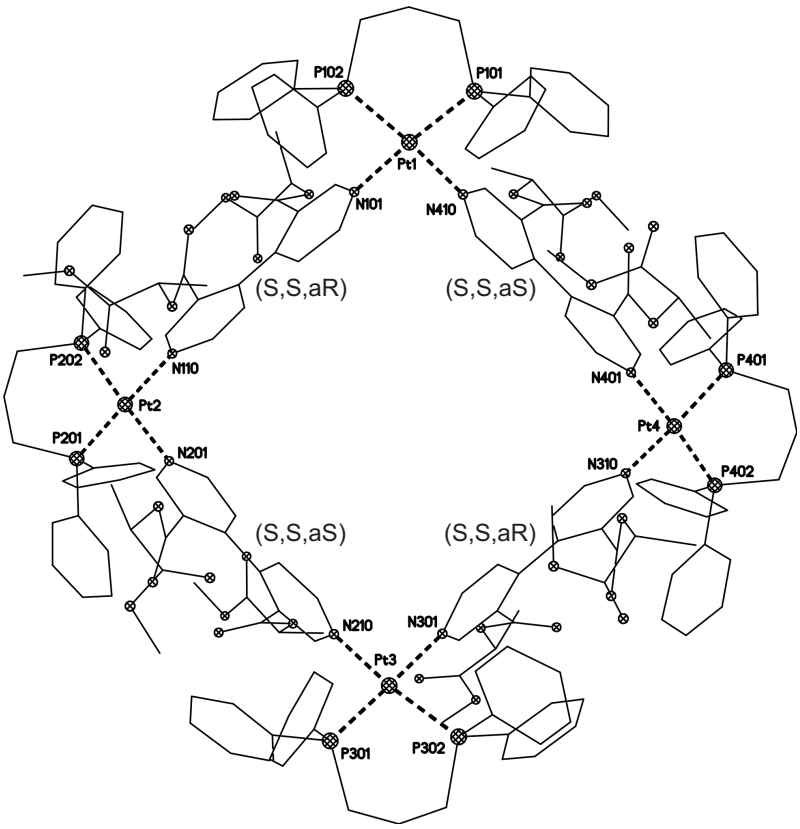

Figure 5.19: Solid-phase structure of **AS1b** derived from X-ray crystal structure analysis. It is clearly visible that all amino acid residues are pointing away from the square's cavity. The absolute configuration of two opposite ligands is (*S*,*S*,*aR*), while the two remaining ligands are (*S*,*S*,*aS*)-configured. Hydrogen atoms, anions and solvent molecules (acetone) are omitted for clarity.

alanine substituents each is described. NMR experiments and crystal structure agree that only one isomeric structure is formed, in which all amino acid residues point away from the cavity and pair wise opposite bipyridine ligands have the same chirality. Although the chiral information introduced with the alanines favors one configuration of the axially chiral biaryl backbone, the ratio of both diastereomers is strictly 1:1 in the squares. Consequently, the diastereoselectivity is not governed by the alanyl moieties alone any more but largely influenced by the steric and stereoelectronic effects from the dppp ligand which ultimatively lead to the exclusive formation of heterochiral assemblies.

Two important aspects can be derived from the findings with **AS1a,b**: (i) [D_6]-acetone is the solvent of choice for NMR measurements, if the precise outcome of self-assembly reactions should be analyzed. (ii) A first idea can be obtained from **AS1a,b** if the outcome of self-assembly regarding mixture formation (560) can be controlled by the size and the properties of the substituents.

5.3.3 Self-Assembled Supramolecular Squares from 3,5,3',5'-Tetramethyl-[4,4']-bipyridine Derivatives

5.3.3.1 Chiral Self-Assembled Supramolecular Squares from Axial Chiral Ligands[‖]

3,3'-disubstituted [4,4']-bipyridines can not be separated into enantiomers due to their fast interconversion on the human timescale at room temperature. 3,5,3',5'-tetrasubstituted [4,4']-bipyridines, however, might be obtained enantiomerically pure (or enriched). A convenient two-step synthesis for axially chiral [4,4']-bipyridines starts from commercial lutidine which is converted on multigram scale into **24**. Modification of two methyl groups (one of each pyridine ring) yields axially chiral bis-amides ***rac*-55** and ***rac*-58**, which can be separated into enantiomers by column chromatography (see 5.1.4.3.3).

Both types of ligands form chiral assemblies[205] when pure enantiomers of **55** or **58** are mixed with equimolar amounts of (dppp)M$(OTf)_2$ with M = Pd(II) [**a**]

[‖]The results of this sub chapter are obtained in cooperation with Dr. Marianne Engeser, M. Nieger and N.M. Maier and are published.[204]

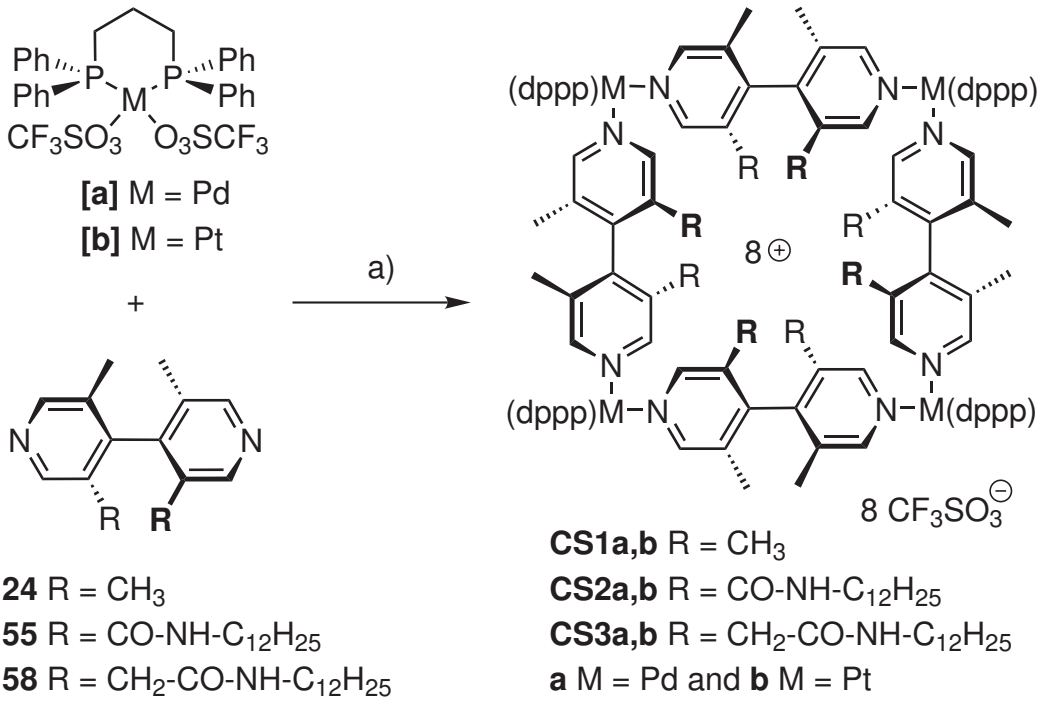

Scheme 5.19: a) acetone, 1 h, RT, quant. Square formation through self-assembly of (dppp)M(OTf)$_2$ with M = Pd(II) [**a**] or Pt(II) [**b**] and **24** as well as axially chiral 4,4'-bipyridines **55**, and **58** (only one enantiomer shown).

or Pt(II) [**b**] (Scheme 5.19).[61]

Not unexpectedly, the differences between the CD spectra (Figure 5.20) of Pd (blue lines) and Pt compounds (red lines) are small because the chiral information in the ligands' bipyridyl backbone is not changed significantly by the self-assembly process.

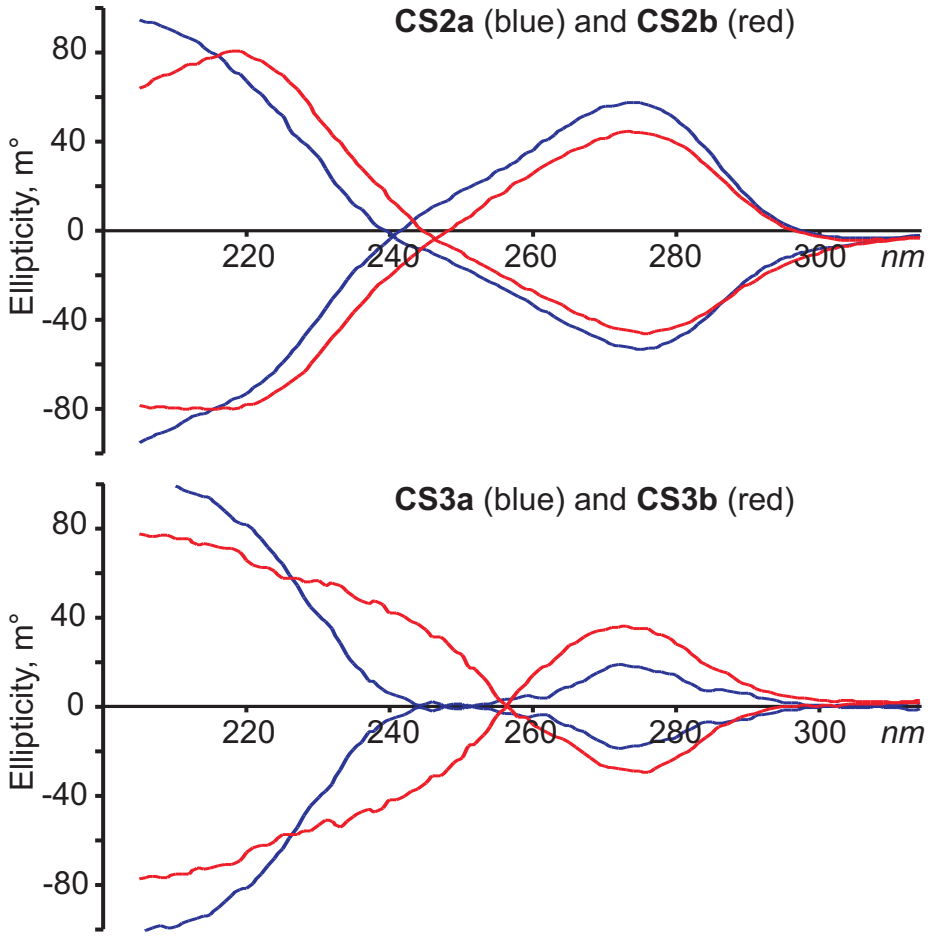

Figure 5.20: CD-spectra of **CS2a,b** (top, 1 mm, methanol, 60 μm) and **CS3a,b** (bottom, 10 mm, methanol, 60 μm).

Again, electrospray mass spectrometry of **CS1a,b** - **CS3a,b** clearly rules out the formation of assemblies other than squares: Doubly (for **CS2a,b**) and triply (for **CS1a,b** and **CS3a,b**) positively charged complexes are formed by losses of triflate counterions (Figure 5.21). Elemental compositions of the resulting assemblies are confirmed by exact masses and high-resolution isotope patterns. For

both, the Pd as well as the Pt compounds some typically observed fragmentation (see Chapter 4.2.3) occurs.

For an understanding of the NMR spectra of **CS1a,b - CS3a,b**, it is helpful to consider the following points:

- a) In contrast to 4,4'-bipyridine, its tetrasubstituted derivatives have much larger torsional angles around the aryl-aryl bond. For example, this angle is 83° and 86° in the two independent molecules in the unit cell of the solid state structure of **24** (see Chapter 8.6 and Figure 5.22, left).

- b) Upon coordination to the metal corners, the pyridine rings usually[61] prefer an orientation perpendicular to the square's M-M-M-M plane and are stacked with neighboring dppp phenyl groups. This arrangement is not feasible here: If one pyridine were perpendicular, the other one needed to be co-planar with the square plane. Molecular modeling[192] thus suggests the pyridines to compromise in a tilted conformation with an angle of ca. 40°-50° relative to the square plane (Figure 5.22, right).

- c) The bipyridines can thus adopt four different conformations by rotation around the metal-metal axis in ca. 90° steps.

- d) Based on the results from Chapter 5.3.2.3 the neighboring dppp phenyl groups make the rotation of bipyridines around the M-M axis slow on the NMR time scale.

Taking these considerations into account, the self-assembly of **CS1a,b** can potentially give rise to six conformers **I** – **VI** (Scheme 5.20). The latter five conformations can be obtained from **I** by rotating one ligand (**II**, shown red in Scheme 5.20), two adjacent ligands (**III**), two opposing ligands (**IV**), three (**V**), and all four ligands (**VI**) by 90° around the M-M axis. Three aspects should be noted:

- a) Rotation of one ligand around 180° yields the same conformer due to the ligand symmetry.

- b) **I** and **VI** as well as **II** and **V** are pairs of enantiomers.

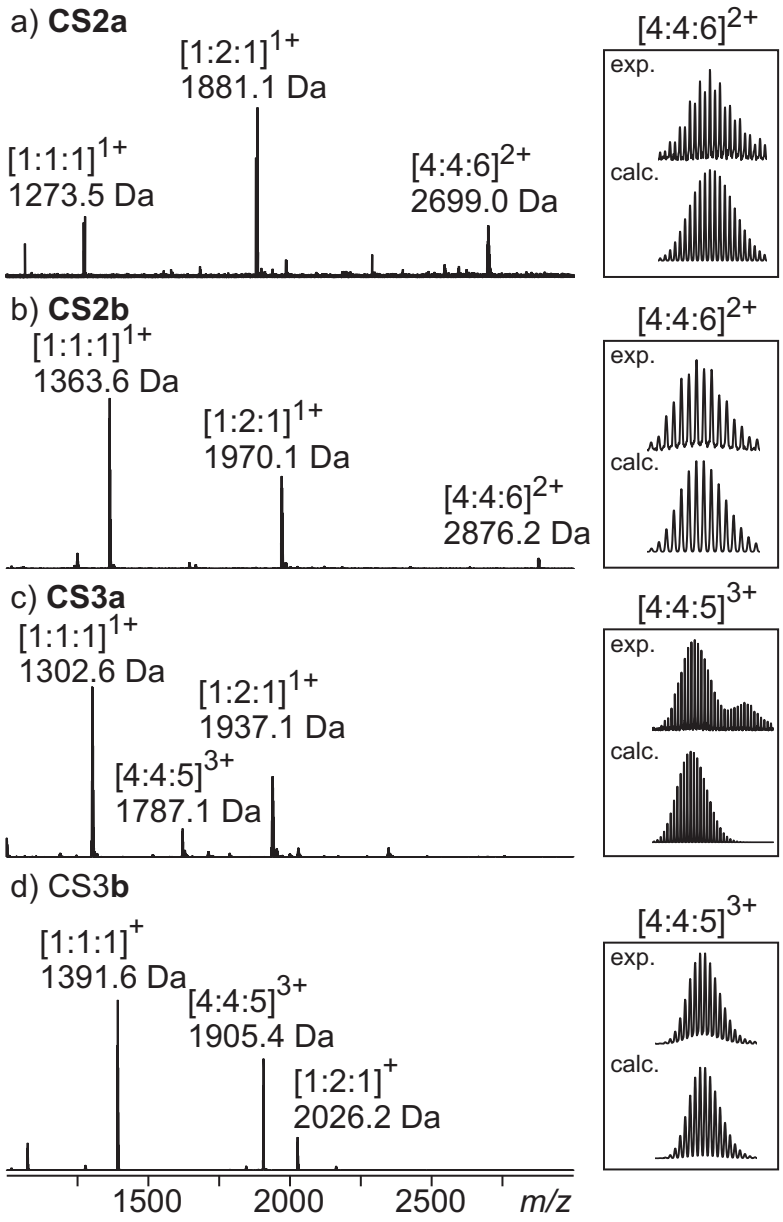

Figure 5.21: ESI-FTICR-MS spectra of **CS2a,b** and **CS3a,b** (all: acetone, 400 μm, labels represent the composition as [metal:ligand:OTf]$^{n+}$); insets: experimental and calculated isotope patterns. For **CS2a,b** the [4:4:6]$^{2+}$ ion overlaps with fragment signals ([2:2:3]$^{+}$; $<$ 10% intensity).

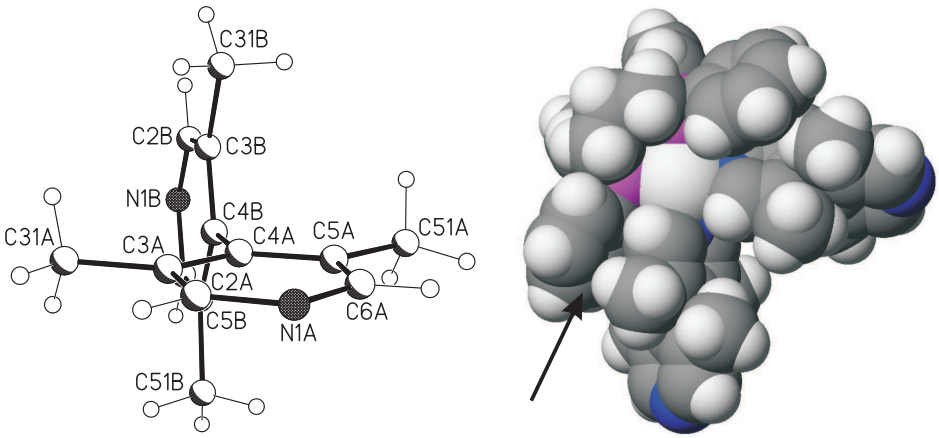

Figure 5.22: Left: X-ray single crystal structure of **24** (one of the two independent molecules). The C3-C4-C4'-C3' dihedral angle is 83° and 86°, respectively. Right: MM2 geometry-optimized structure of (dppp)Pd(**24**)$_2^{2+}$.[192] The coordinated pyridine rings adopt a tilted geometry. Arrow: The dppp phenyl ring hinders bipyridine rotation.

- c) In conformers **II** - **V**, the pyridine rings marked with double arrows in Scheme 5.20 are tilted towards each other. This generates steric repulsion between two *ortho*-hydrogen atoms of adjacent pyridines (Scheme 5.21, inset right).

In **I** and **VI**, no such repulsion occurs because one of the two adjacent pyridines at each corner is tilted outwards, the second one inwards (Scheme 5.21, inset left). These two enantiomeric conformations should thus be energetically favored and are expected to be the major, if not exclusive, products of the self-assembly process.

Indeed, exactly two signals for the *ortho*-hydrogen atoms and two signals for the methyl groups are observed in the ^{1}H NMR spectrum of **CS1a,b** in [D$_6$]-acetone (Figure 5.23a). The *ortho*-hydrogens and methyl groups pointing towards the cavity feel the anisotropy of the second pyridine ring coordinated to the same corner. They are therefore shifted upfield with respect to those pointing away from the cavity ($\Delta\sigma = 0.4$ ppm for the *ortho*-hydrogen atoms and $\Delta\sigma = 0.3$ ppm for the CH_3 groups). All phosphorus nuclei are symmetry-equivalent and thus only one sharp signal is seen in the ^{31}P NMR spectrum. In [D$_7$]-dimethylformamide, broadened signals are observed in the ^{1}H and ^{31}P NMR spectra at room

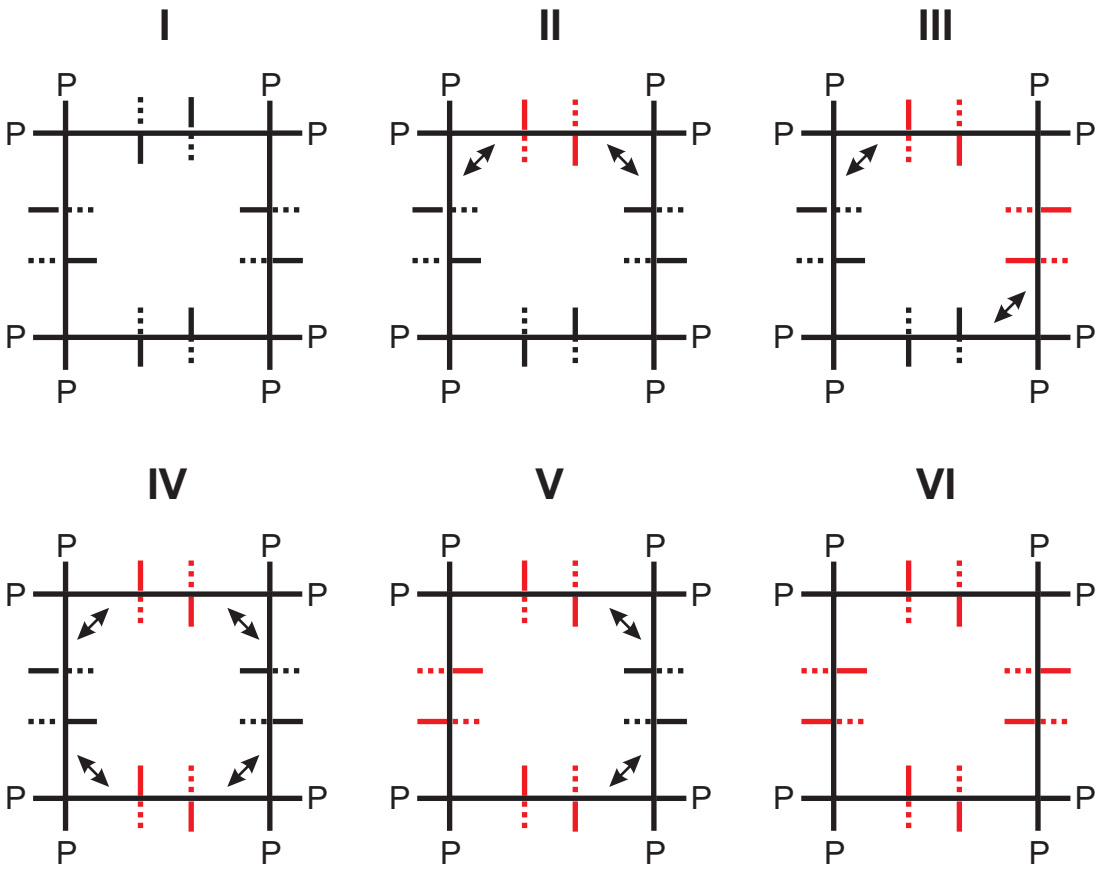

Scheme 5.20: Self-assembly of (dppp)M(OTf)$_2$ with M = Pd(II) **[a]** or Pt(II) **[b]** and **24** can result in the formation of six conformers **I** to **VI**. The ligands' methyl groups are either above (thick) or below (dotted) the plane through the four metal atoms. Red ligands are turned by 90° around the M-M axis. Black arrows indicate steric repulsion between the *ortho*-hydrogen atoms of pyridine rings (also, see inset in the next Scheme).

temperature (Figure 5.23b). Below a coalescence temperature of 308 K at 500 MHz, the ligands' signals split into a pattern analogous to that observed in [D_6]-acetone. This behavior is indicative of an interconversion of conformations **I** and **VI** which shows some solvent-dependence and is faster in dimethylformamide than in acetone. In agreement with previous data (see 5.3.2.3), these results confirm both the operation of slow exchange processes and the importance of avoiding the pyridine *ortho*-hydrogen repulsion.

Symmetry considerations for **CS2a,b** and **CS3a,b** are more complex, but can be based on the same considerations (Scheme 5.21). Self-assembly reaction of (dppp)M$(OTf)_2$ with one pure enantiomer of **55** or **58** may result in the formation of up to ten conformers, already excluding those which suffer from steric repulsion between pyridine *ortho*-hydrogen atoms. In conformation **I**, all eight amide groups are pointing towards the cavity. Ligand rotations by 180° yields five additional conformers, **II** – **VI**, in analogy to those discussed for **CS1a,b** (Scheme 5.20). Conformer **VII** is obtained from **I** by rotation of all ligands by 90°. From **VII**, conformations **VIII** - **X** can again be generated by 180° rotations of the appropriate ligands. Any process which involves a 90° ligand rotation of less than all four ligands would unavoidably lead to steric repulsion of pyridine *ortho*-hydrogen atoms. Based on the NMR results obtained for **CS1a,b**, they are expected not to be formed in the assembly process and thus are not listed here. Furthermore, the resulting symmetry elements for **I** - **X** are analyzed in Scheme 5.21.

Table 5.3.3.1 provides the expected number of NMR signals and the expected ^{31}P NMR multiplicities. Mixtures of these ten slowly interconverting conformers would certainly result in complex and hard-to-interpret NMR spectra. However, this is interestingly not the case. In the ^{31}P NMR spectrum of **CS2a** in [D_6]-acetone, four doublets are observed in an exact 1:1:1:1 integration ratio, two sharp, two somewhat broadened (Figure 5.21c, right). From this result, we can draw three important conclusions:

- a) Exchange processes are still slow on the NMR time scale under the conditions applied here; otherwise, only one singlet would be observed.
- b) Mixtures of conformers unlikely result in an exact 1:1:1:1 ratio of doublets.

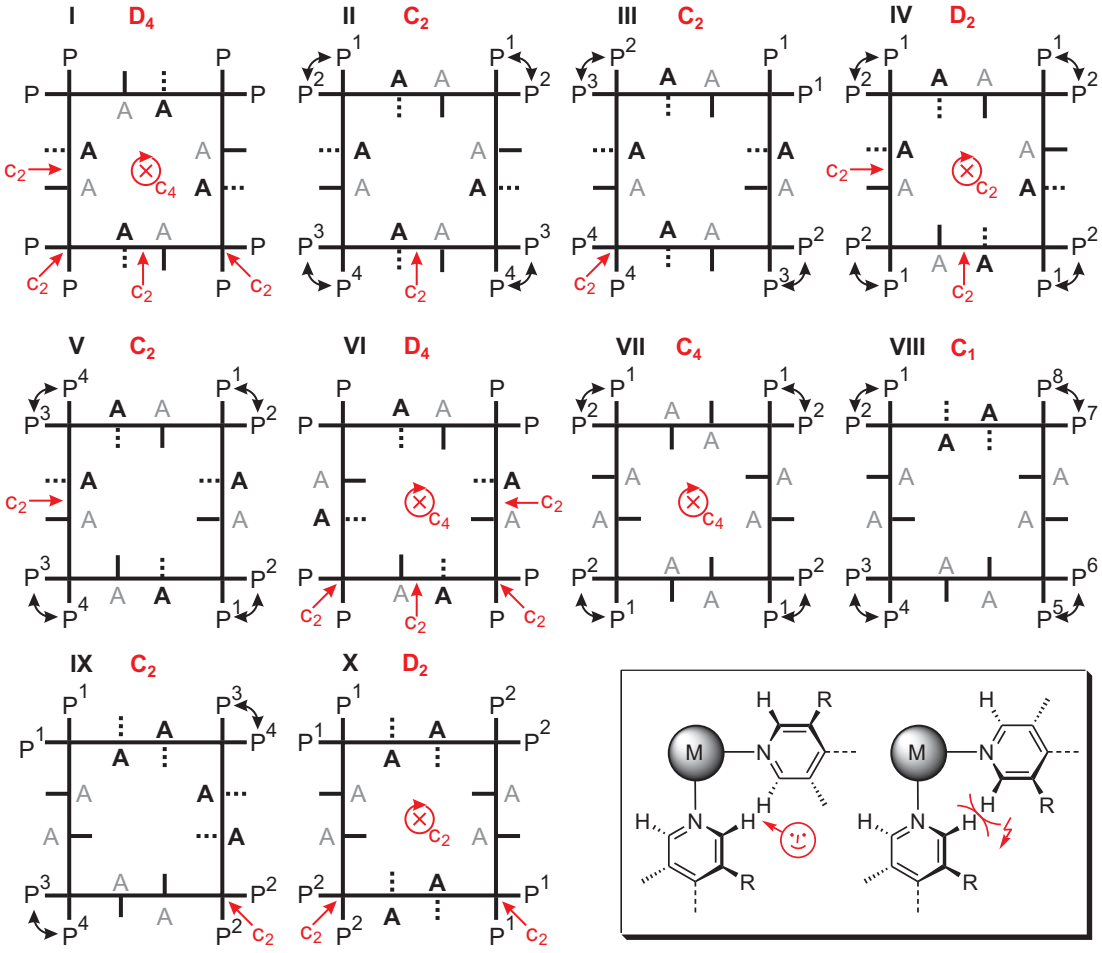

Scheme 5.21: Self-assembly of (dppp)M(OTf)$_2$ with M = Pd(II) **[a]** or Pt(II) **[b]** and enantiomerically pure, axially chiral [4,4']-bipyridines can result in the formation of ten conformers **I** to **X**. Ligand amides are either above (black A) or below (grey A) the square plane; methyl groups are indicated by solid (above) and dashed lines (below the plane). P atoms which are chemically non-equivalent are labeled with indices. Curved arrows indicate NMR coupling between non-equivalent P atoms. Inset: Steric repulsion between pyridine ortho-hydrogen atoms (right) can be avoided (left).

Isomer	symmetry	Set of signals ^{1}H NMR^{a}	Signals ^{31}P NMR^{b}
I	D_4	1	1s
II	C_2	4	4d
III	C_2	4	2d,1s
IV	D_2	2	2d
V	C_2	4	4d
VI	D_4	1	1s
VII	C_4	2	2d
VIII	C_1	8	8d
IX	C_2	4	2d,1s
X	D_2	2	2s

Table 5.2: Symmetry considerations for conformers **I** - **X** and the resulting symmetry reductions in their ^{1}H and ^{31}P NMR spectra. ^{a} some of these signals may overlap; ^{b} s = singlet, d = doublet; coupling due to chemically non-equivalent 31P atoms.

Thus, only one conformer is formed exclusively. Similar behavior is found for other chiral assemblies.[93,94,206]

- c) Only conformers **II** and **V** agree with the coupling pattern observed in the ^{31}P NMR spectrum.

In the corresponding ^{1}H NMR spectrum, the reduction to a C_2 symmetry can be seen as well. Four signals are found for one of the two non-equivalent pyridine *ortho*-hydrogen atoms (arrows in Figure 5.23 c). Similarly, four methyl signals are seen (not shown). The same situation is observed for the Pt analogue **CS2b**: The patterns are very similar and only differ from the NMR results obtained for **CS2a** in that minor peak shifts occur and two doublets coincide in the ^{31}P NMR spectrum (Figure 5.23 d). The P-Pt coupling constants agree well with earlier results[61] and confirm assembly formation: $^{1}J_{Pt195,P} = 3050$ Hz (**CS1b** and **CS2b**), compared to $^{1}J(^{195}Pt,P) = 3600$ Hz for the precursor complex (dppp)Pt(OTf)$_2$ **[b]**. Without crystal structure analysis, it is impossible to safely deduct from the obtained spectroscopic data alone, which of the two remaining conformers, i.e. **II**

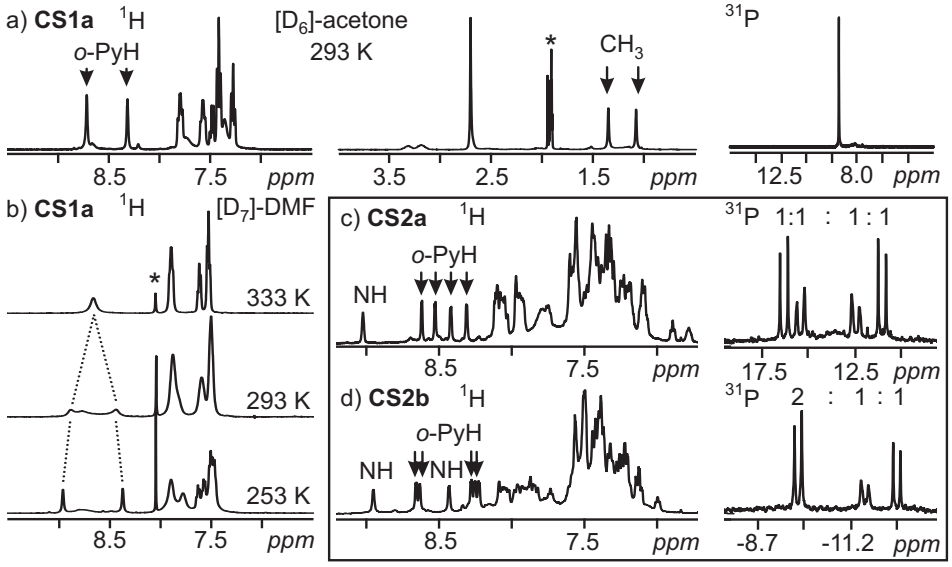

Figure 5.23: a) ^{1}H and ^{31}P NMR spectra of **CS1a** in [D_6]-acetone at room temperature; b) Aromatic region of variable temperature ^{1}H NMR spectra of **CS1a** in [D_7]-dimethylformamide. c) and d) Partial ^{1}H NMR and ^{31}P NMR spectra of **CS2a** and **CS1b** in [D_6]-acetone at room temperature. Asterisks indicate solvent signals.

or **V**, is preferred. Therefore, a tentative assignment is omitted. Nevertheless, two important aspects can be derived from these findings: (i) [D_6]-acetone is again the solvent of choice for NMR measurements, if the precise outcome of self-assembly reactions should be analyzed, as the obtained assemblies are kinetically more stable than in [D_6]-dimethylsulfoxide or [D_7]-dimethylformamide. (ii) The amount of formed isomers is reduced drastically upon increased steric repulsion.

5.3.3.2 SAMS from Axial Chiral Ligands in Racemic Mixtures

When axially chiral ligand **55** is used in a racemic mixture in self-assembly reactions (see Scheme 5.22), the amount of expected isomers increases drastically. Again, 560 isomers are possible as discussed in Chapter 8.7. In marked contrast to the racemic mixtures of Chapter 5.3.2.1, these conformers can only interconvert by ligand rotation around the metal-metal axis. Alternatively, two M-N-bonds can be broken and the resulting fragments can undergo further reactions.

Electrospray mass spectra of **RS1a,b** perfectly mimic the spectra obtained

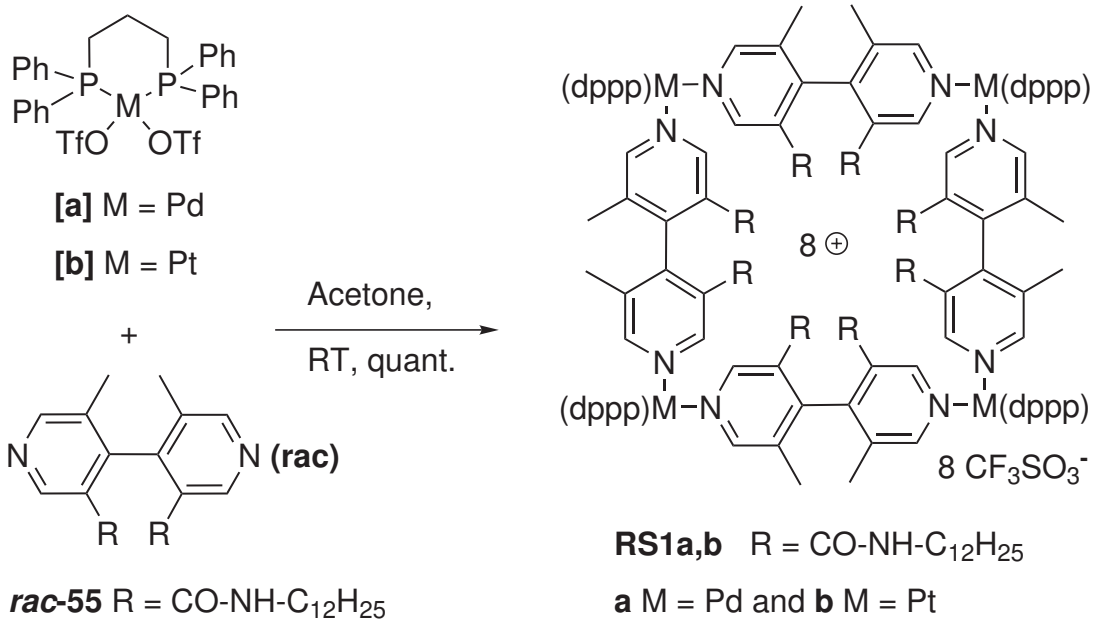

Scheme 5.22: Self-assembly reaction of ***rac*-55** into **RS1a,b** (**R**acemic **S**quares).

for their enantiopure analogues. The formation of assemblies other than squares is clearly ruled out: Doubly positively charged complexes are formed by losses of triflate counterions (Figure 5.24).

Superposition of the ^{31}P NMR spectra of **CS2a,b** and **RS1a** reveals that the major product of **CS2a,b** (Isomer **II** or **IV**) is not formed in the racemic case. Instead, three sets of peaks can be found in the ^{31}P NMR of **RS1a** (see Figure 5.25):

1. seven doublets with similar intensities and coupling constants (one doublet is presumably superimposed by other peaks, blue),
2. four doublets (two sharp and two broad, red), and
3. two doublets and one singulet in a 1:2:1 ratio (green).

Before possible isomers are deduced, the following aspects should be taken into account:

- Steric repulsion of the *ortho*-hydrogen atoms of adjacent pyridine rings is avoided (see Chapter 5.3.3.1).

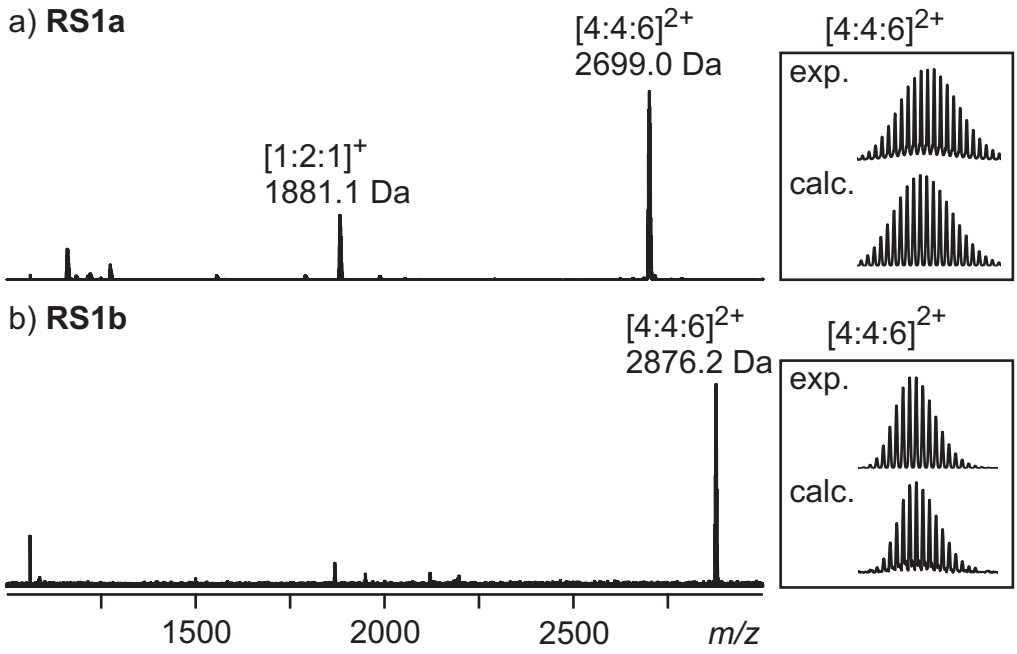

Figure 5.24: FTICR-MS spectra of a) **RS1a** and b) **RS1b** (both: acetone, 400 μm, labels represent the composition as [metal:ligand:OTf]$^{n+}$); insets: experimental and calculated isotope patterns.

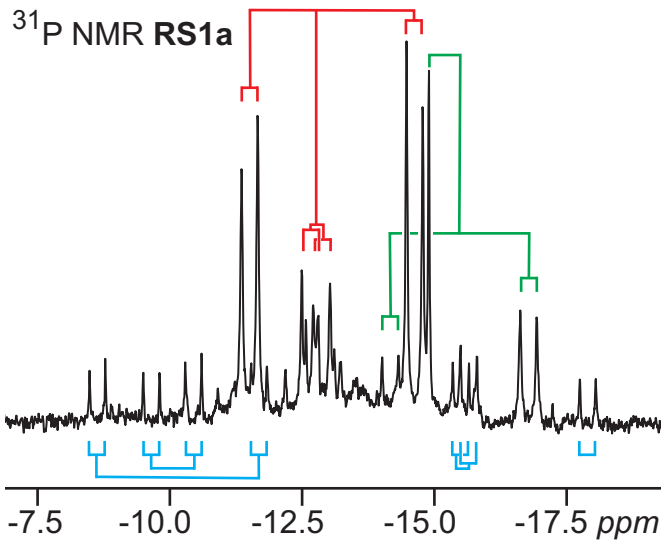

Figure 5.25: ^{31}P NMR spectra of **RS1a** in [D_6]-acetone at room temperature. The three sets of signals are marked in blue, red and green.

- Hydrogen bond formation might adjust the amide groups to point inside the cavity to maximize bonding interactions. The results from Chapter 5.3.2.4, however, proof that the amide groups might point outside as well due to steric repulsion.

- Assemblies which incorporate two (*aR*)-**55** and two (*aS*)-**55** should be entropically favored, as (aR)-X and (aS)-X are present in a 1:1 ratio (racemic mixture).

As unfortunately not enough isomers can be ruled out, the obtained sets of signals are not assigned to their corresponding isomers. Nevertheless, several important conclusions can be drawn:

- The outcome of self-assembly with racemic ligands is different and more complex as in the case of enantiopure axially chiral ligands.

- Mixture formation occurs due to the larger amount of building blocks.

- Obviously, the entropy term in self-assembly reactions is quite important when racemic mixtures are used.

- However, less isomers are formed than in the self-assembly reactions from achiral bipyridines discussed in Chapter 5.3.2.1. This finding might be explained by steric repulsions.

As the obtained NMR spectra are complex, alternative spectroscopic or spectrometric methods should be applied. For example, squares built from mass-labeled enantiomers could be mixed in equimolar amounts. Time resolved mass spectra might give deeper insight into the kinetic stability of the obtained assemblies. A more detailed picture is given in the outlook in Chapter 7.2.

5.3.3.3 Self-Assembled Supramolecular Squares from C_{2v} Ligands

On the first glance, the situation seems even more complex when [4,4']-bipyridine ligands with two different pyridines are used in self-assembly reactions. However, only four isomers are expected when equimolar amounts of organic ligand **US1**,

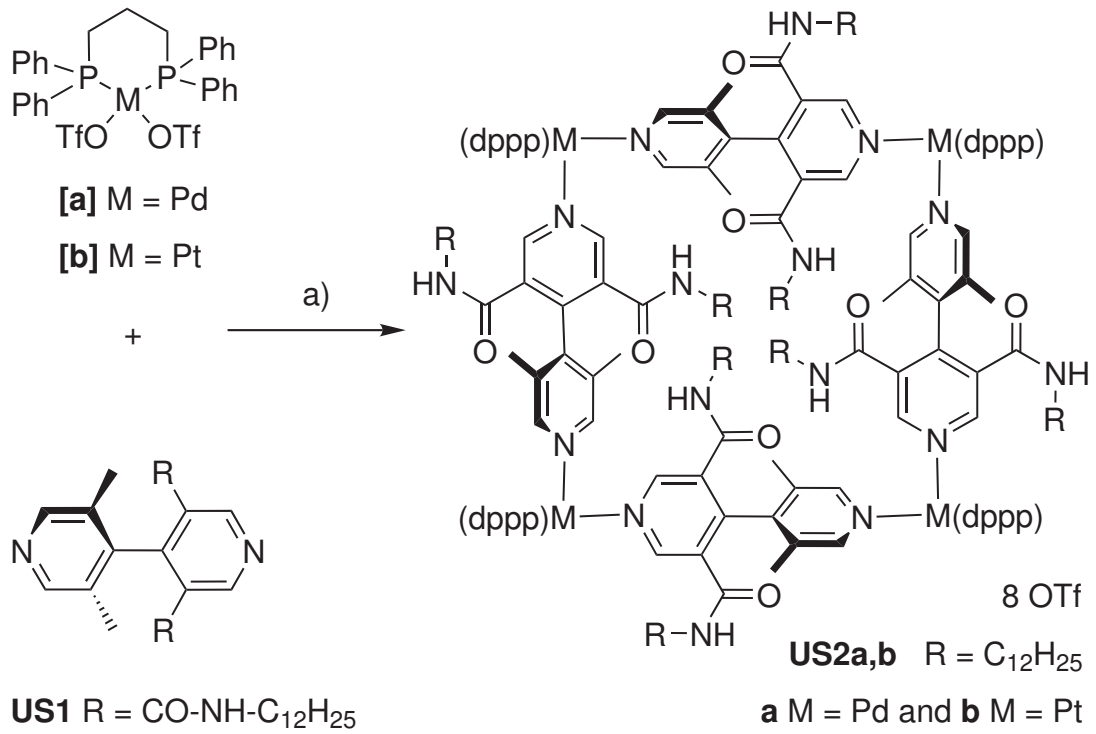

Scheme 5.23: a) acetone, 1 h, RT, quant. Self-assembly of (dppp)M(OTf)$_2$ (M= Pd [**a**] or Pt [**b**]) and **US1** yields unidirectional squares **US2** (**U**nidirectional **S**quares, only one out of four isomers is shown).

a byproduct from the synthesis of **55**, and metal precursors (dppp)M(OTf)$_2$ with M = Pd(II) [**a**] or Pt(II) [**b**] are mixed, respectively. The amount of possible isomers is reduced that drastically because of the mirror plane of **US1**. Thus, **US1** is inherent achiral. Starting from isomer (**I**) (see Scheme 5.26 a), isomer (**II**) is obtained by rotating one ligand around 180°. Please note that hereby two metal nitrogen bonds need to be broken and reestablished. Two adjacent ligands are turned in isomer (**III**), and two opposite ligands in isomer (**IV**). When three out of four ligands are turned around, isomer (**II**) is obtained again. Analogously, isomer (**I**) is reobtained when all four ligands are turned around. From a statistical point of view, the expected ratio should be 1:4:2:1 for **I**:**II**:**III**:**IV**. And indeed, the situation in the ^{1}H NMR spectra of **US2b** (see Figure 5.26 b) is complex. In the ^{31}P NMR spectra, a mixture of two components can be found (see Figure 5.26 c):

- A main component with two doublets ($^2J_{PP}$ = 32.0 Hz) in 73% intensity and
- a by-product with four doublets ($^2J_{PP}$ = 31.3 Hz) in a 2:4:1:1 ratio with 27% intensity (marked with arrows).

Isomer	symmetry	Set of signals ^{1}H NMR^a	Signals ^{31}P NMR^b
I	C_4	1	2d
II	C_1	4	8d
III	D_2	1	2s
IV	C_2	2	2s,2d

Table 5.3: Symmetry considerations for conformers **I** - **IV** of **US2a,b** and the resulting symmetry reductions in their ^{1}H and ^{31}P NMR spectra. ^{a} some of these signals may overlap; ^{b} s = singlet, d = doublet; coupling due to chemically non-equivalent ^{31}P atoms.

Like in the paragraphs before, symmetry considerations (see Figure 5.26) can be applied to assign which isomers contributes to which set of signals. In Table 5.3, the expected signals (^{1}H and ^{31}P NMR) for isomers (**I**) to (**IV**) are listed. As

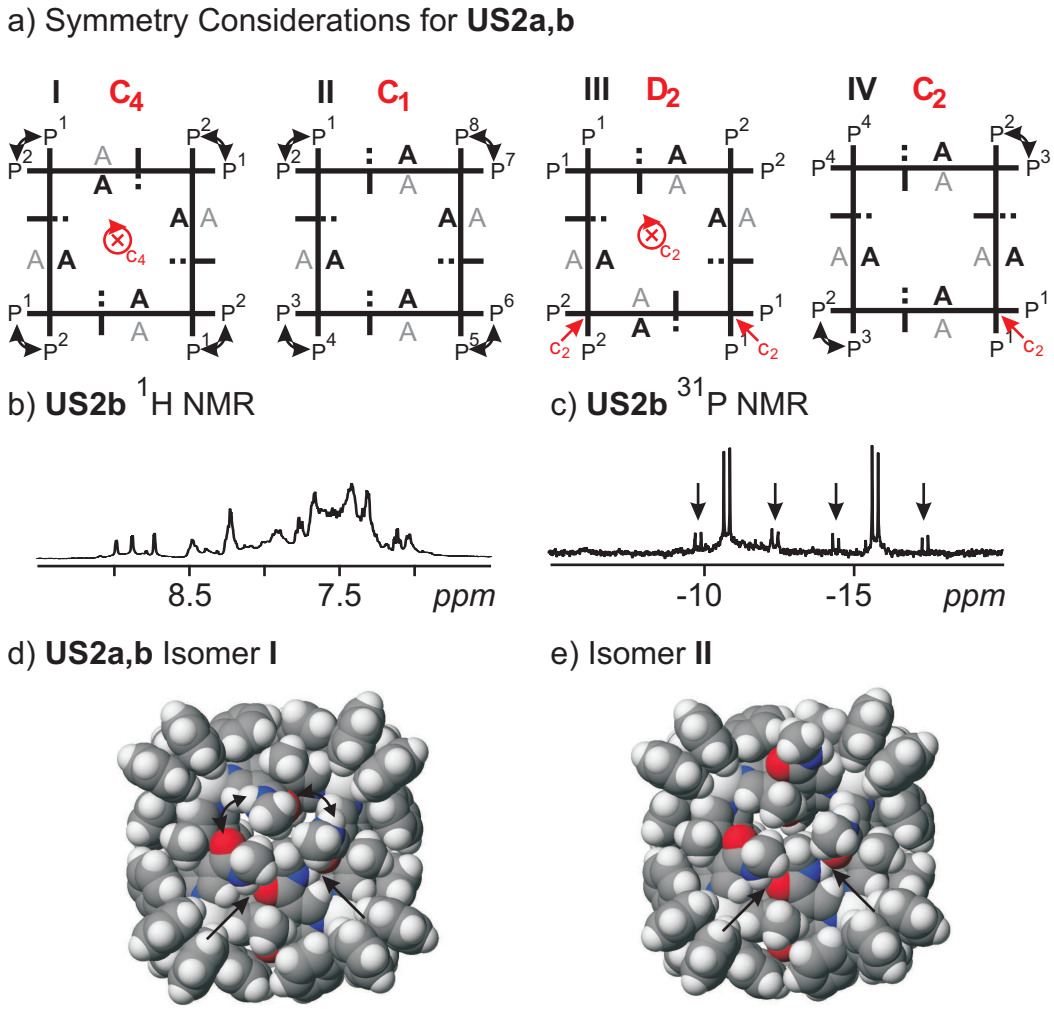

Figure 5.26: a) Symmetry considerations for **US2a,b**: four isomers are expected; b) and c) ^{1}H and ^{31}P NMR of **US2b**, [D_6]-acetone; d) molecular modeling of isomer **I** (Arrows indicate hydrogen bonds. Curved arrows indicate that the distance is too large for hydrogen bonds) and e) molecular modeling of isomer **II**. Arrows indicate hydrogen bonds.

only one structure with two doublets exists, isomer (**I**) is the major product of self-assembly and isomer (**II**) seems to be the byproduct because four doublets in a 2:4:1:1 ratio only agree with the eight independent phosphorous atoms, from which some coincide. This finding is rather unexpected when the statistical distribution is taken into account.

Without crystal structure analysis, it is impossible to understand the driving force for this selectivity. However, one structure-based argument derived from simple molecular modeling calculations may be helpful for a tentative assignment: The space filling model of the MM2 minimized structure[192] of **US2a** (isomer **I**) is depicted in Figure 5.26 d). As expected, four amide groups are pointing away from the square's cavity and four are pointing inside. These four amide groups are all on the same side of the plane of the four metal atoms (above this plane in Figure 5.26 d). Two hydrogen bonds between these four amide groups are indicated by black arrows (N-O-distances = 0.29 and 0.28 nm). Two further H-bonds seem possible, but the N-O-distances are quite long (0.44 and 0.43 nm, indicated by curved arrows). Of course, there might be another local minimum on the challenging hyper surface, in which three amide bonds are possible. Steric interactions which might destabilize this isomer are not found, although these interaction are difficult to predict. If one ligand (i. e. the top ligand, see Figure 5.26 d) is turned around, the two involved amide groups change sides: The amide group above the square's plane is now pointing away from the cavity, while the amide group which is pointing inside is now below the plane, apart from the remaining three In-amide groups. Certainly, only two hydrogen bonds are possible in this isomer (again indicated by black arrows). This finding is clearly visible in the space filling model of the MM2 minimized structure[192] of isomer (**II**). Please note that the fourth amide group can not point into the square's cavity, due to same steric repulsion of the *ortho*-hydrogen as seen in Chapter 5.3.3.1. From these molecular modeling results, two tentative conclusions can be drawn: (i) hydrogen bonding yields in isomer (**I**) and isomer (**II**) the most stable isomers, (ii) with a small preference ($< 5\,\mathrm{kJ\,mol^{-1}}$, MM2) for isomer (**I**).

As these findings are in line with the results obtained from ^{31}P NMR, they might explain the unexpected selectivity far away from the statistical distribution.

In conclusion, the amount of possible isomers is reduced to only four when inherent achiral **US1** is used in self-assembly reactions. The large dihedral angle of the two pyridine halves causes larger sterical repulsion of the organic ligands in the supramolecular assembly. Thus, only one isomer is the major product in **US2a,b**.

In this chapter, the fascinating self-assembly of different [4,4']-bipyridines is reported. In cases of racemic mixtures of ligands, the outcome of self-assembly reactions is still hard to predict and usually mixtures are obtained. However, several examples are shown in which non-covalent interactions, which are commonly regarded as weak, govern the reaction outcome. Thus, single products are obtained, even though statistical mixtures might have been expected. As a final point, it should be addressed that the careful choice of solvent plays an important role in the NMR-analysis of assemblies when isomerization processes are fast on the NMR time scale and only averaged signals are observed.

5.4 Mass Spectrometric Investigations of Self-Assembled Metallo Supramolecular Squares of the Fujita Type**

The following two sub chapters, preliminary results of ongoing research projects are described. As these results might be of special interest for future mass spectrometric investigations, they are presented although unfinished.

5.4.1 Simple mass spectra

Previously, all attempts to observe mass spectra of intact squares of the *Fujita* type $[(en)Pd(L)(NO_3)_2]_4$ with L = [4,4']-bipyridine **11** failed. Different solvents like water, methanol, acetonitrile and nitromethane as well as various mixtures of these were tried, but only smaller aggregates or fragments were detected. High concentrations – up to 400μm, above the critical concentration (see 5.3.2.1) which lead to success in the case of Stang's squares did not change the outcome. Only

**Many thanks to Dr. Marianne Engeser for helpful discussions.

after anion exchange (PF_6^- instead of NO_3^-), larger complexes were observed by *Sakamoto* and *Yamaguchi*.[27] Therefore, [(en)Pd(**11**)$(NO_3)_2]_4$ was dissolved in water and eight equivalents of NH_4PF_6 were added. The white precipitate is filtered off, and dried roughly. Indeed, only two peaks were observed in the MS spectrum of [(en)Pd(**11**)$(PF_6)_2]_4$, when sprayed from nitromethane solutions (1500μm): $[1:2:1]^+$ at 623.1 Da and $[4:4:5]^{3+}$ at 671.7 Da, the latter being the base-peak (this notation represent the composition as $[\text{metal:ligand:}PF_6]^{n+}$, see Figure 5.27). Please note that no further changes were applied, i. e. no cooling of the solution, the drying or the nebulizing gas like in Cold-Spray-Ionization[115] (CSI).

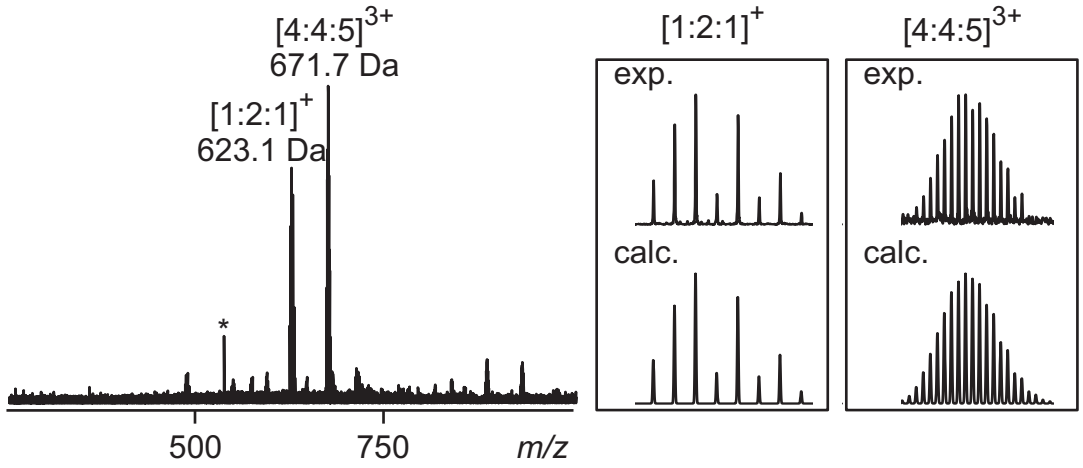

Figure 5.27: The ESI-FTICR spectrum of [(en)Pd(**11**)$(PF_6)_2]_4$; * = electronic noise; Insets: experimental and calculated isotope patterns on the basis of natural isotope abundances.

For platinum analogue [(en)Pt(**11**)$(PF_6)_2]_4$, the case is somewhat more difficult. Under the same preparation and spraying conditions, several peaks for

- 4:4-complexes: $[4:4:1\text{-}4H]^{3+}$ at 595.1 Da and $[4:4:3\text{-}2H]^{3+}$ at 692.8 Da,
- a 3:3 complex: $[3:3:1\text{-}3H]^{2+}$ at 687.6 Da (rather a gas phase fragment than present in solution),
- fragments $[2:2:0\text{-}2H]^{2+}$ at 410.1 Da and $[2:3:0\text{-}2H]^{2+}$ at 488.1 Da and
- even higher aggregates $[6:6:4\text{-}4H]^{4+}$ at 833.8 Da

were observed (see Figure 5.28). In marked contrast to $[(en)Pd(\mathbf{11})(PF_6)_2]_4$, the loss of neutral HPF_6 is observed upon ionization in the spraying process. The same phenomena was observed in the case of chiral self-assembling rhombs[206] of the composition $[(en)PdL(NO_3)]_2$, here loss of neutral HNO_3. Assuming that the proton of HPF_6 is one of the N-H protons of ethylenediamine, the negative charge is at least partially balanced by one of the positive charges of the platinum complex (see Scheme 5.24). The reduction of the charge might however weaken the Pt-N_{Py}-bonds: Thus, more fragments are observed. This finding is rather unexpected because in the case of squares of the Stang type, the platinum squares were more stable than the analogue palladium squares. It is noted in passing that incomplete square formation before ESI can be ruled out. In the ^{1}H NMR spectrum ([D_3]-nitromethane), one sharp set of signals is observed exclusively as expected for this highly symmetrical compound.

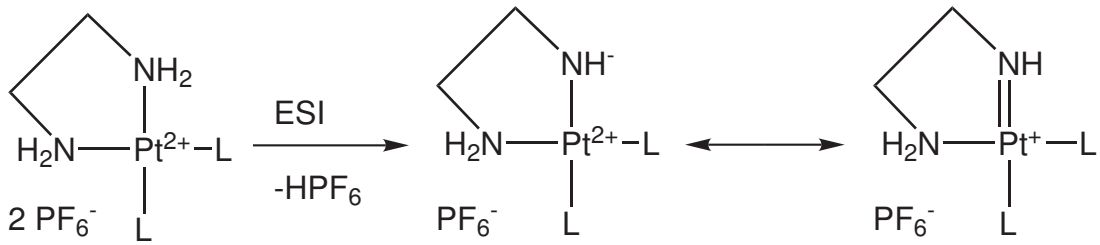

Scheme 5.24: Loss of HPF_6 in the ESI-process.

5.4.2 MS-MS-spectra obtained by IRMPD

Both peaks of the MS-spectrum of $[(en)Pd(\mathbf{11})(PF_6)_2]_4$, the mononuclear complex $[1:2:1]^+$ and the square $[4:4:5]^{3+}$, were subjected to IRMPD-MSMS measurements:

- After irradiation, the mononuclear complex $[1:2:1]^+$ looses (i) neutral HPF_6 yielding a $[1:2:0\text{-}H]^+$ complex and (ii) neutral PF_5 as well as one ligand yielding a $[1:1:0+F]^+$ complex (see Figure 5.29 a - c). The latter case needs to be discussed in more detail. As a neutral ligand loss itself is not observed (arrow in Figure 5.29 b and c), one can conclude that after loss of one neutral PF_5 the remaining F^- is directly replacing one of the two neutral ligands

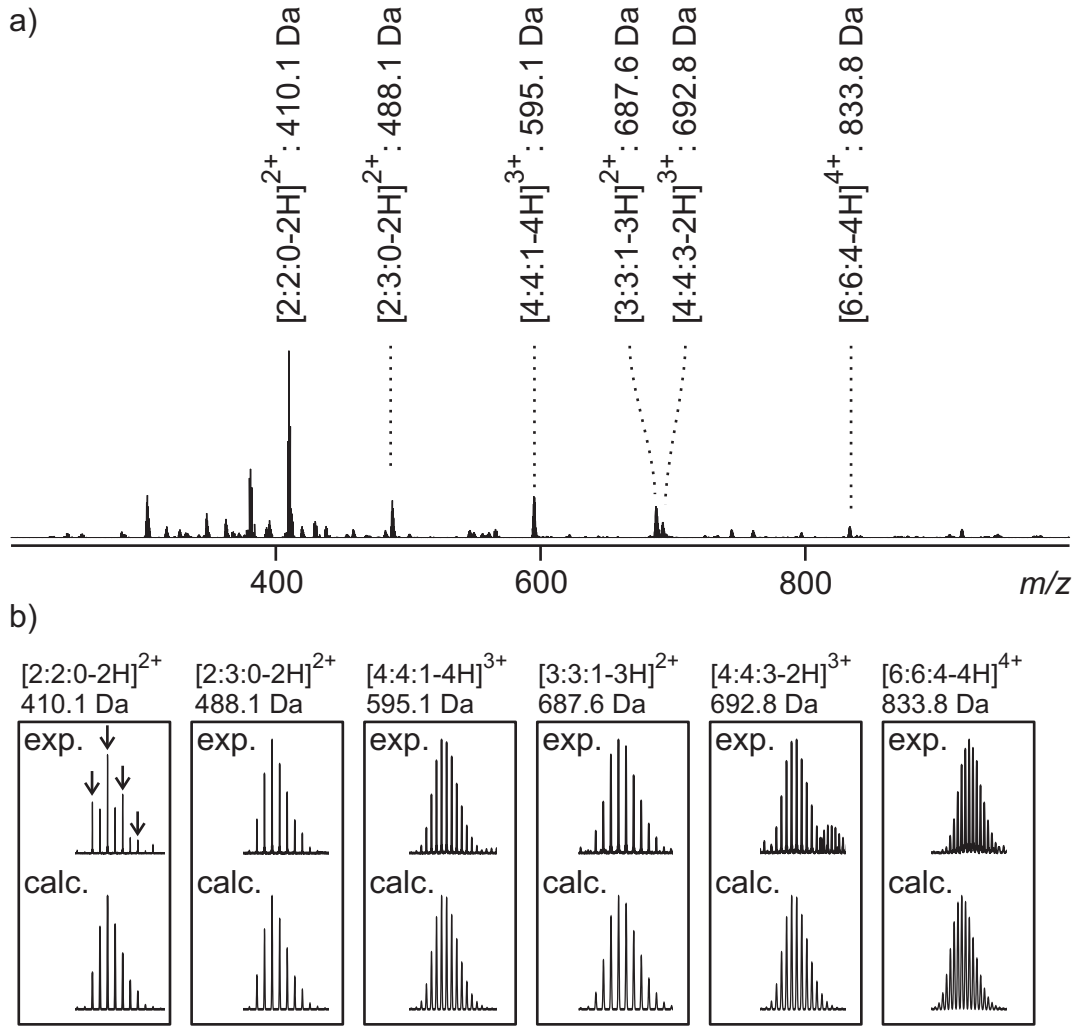

Figure 5.28: a) ESI-FTICR spectrum of [(en)Pt([4,4']-bipyridine)$(PF_6)_2]_4$; b) isotope patterns of the cited peaks (experimental and calculated); note that in the case of $[2{:}2{:}0\text{-}2H]^{2+}$ there is a significant contribution of $[1{:}1{:}0\text{-}H]^{+}$ at the same m/z value (arrows).

from one of the four binding positions of the metal, because of its higher binding energy. For a loss of ethylenediamine (chelate ligand) two bonds need to be broken. Thus, loss of one **11** (only one side bound) should be the lowest energy pathway.

- In the case of the triply charged square ($[4{:}4{:}5]^{3+}$), the twofold loss of neutral PF_5 is observed after 0.25 sec irradiation time. If the irradiation time is elongated to 0.5 sec, the formerly [4:4]-complex fragments into smaller pieces: $[1{:}2{:}1]^+$ and $[1{:}1{:}0{+}F]^+$ (see Figure 5.29 d - f). Taking the results from $[1{:}2{:}1]^+$ into account, the twofold loss of neutral PF_5 – before the square fragments into smaller pieces – is rather unexpected. One would expect that the square breaks apart, as soon as two M-N_{Py}-bonds are broken by coordination by fluoride. In marked contrast to the situation in the mononuclear complex $[1{:}2{:}1]^+$, both nitrogen atoms of each **11** are bound to metal centers, albeit not in a chelate fashion. Thus, F^- might cleave one of the two M-N_{en}-bonds instead, as both types of ligands are not expelled. Further fragments are not observed in the MS MS spectra. This is however even more astonishing as a trinuclear $[3{:}2{:}4]^{2+}$ -2 PF_5 complex or its fragments should be generated.

In conclusion, these preliminary results are a first indication that mass spectrometric measurements can indeed be performed with larger *Fujita*-type complexes without the need of CSI.[115] First MS MS-experiments show that their fragmentation reactions are certainly different and thereby more interesting than the well understood MS and MSMS-spectra of *Stang*-squares.

In marked contrast, the outcome of self-assembly reactions is still hard to predict, as the following results for unidirectional squares indicate.

5.5 Unidirectional Self-Assembled Supramolecular Squares

In supramolecular chemistry, unidirectionality plays a crucial role: Unidirectional motion[207] is an indispensable requirement in molecular motors.[104] Catenanes from

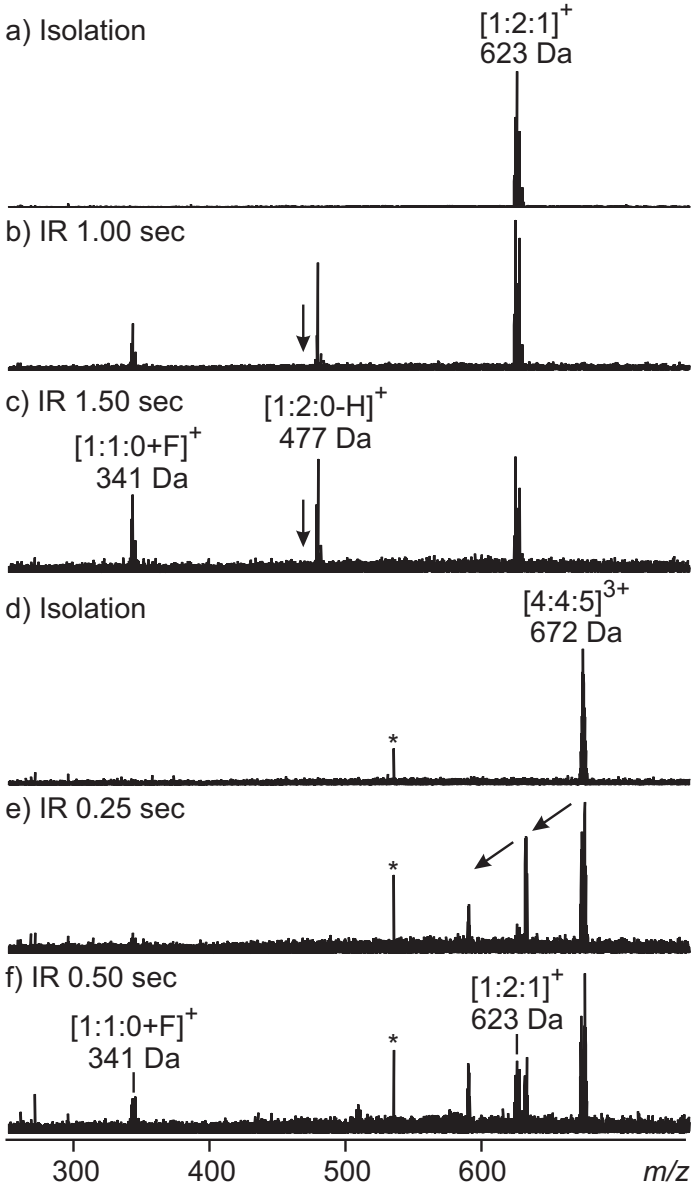

Figure 5.29: a) - c): MS MS-Experiments (IRMPD) of the mononuclear complex $[1:2:1]^+$: a) Mass selection of 623 Da (whole isotope pattern); b) 1.00 sec irradiation; c) 1.50 sec irradiation: two new peaks arise which were assigned to $[1:1:0+F]^+$ at 341 Da and $[1:2:0\text{-}H]^+$ at 477 Da; arrows indicate the m/z value of $[1:1:1]^+$, which is not present in detectable amounts; d) - f) MS MS-Experiments (IRMPD) of $[4:4:5]^{3+}$: d) Mass selection of 671.7 Da; * = electronic noise; e) 0.25 sec irradiation: arrows indicate loss of neutral PF_5; f) 0.50 sec irradiation: two new peaks arise, which were assigned to $[1:1:0+F]^+$ at 341.0 Da and $[1:2:1]^+$ at 623.1 Da.

unidirectional macrocycles[208] are topological chiral. Unidirectional guest inclusion is widely observed.[209] In self-assembly, unidirectionality might reduce the number of possible structures when mixtures are formed.[210]

When [4,4']-bipyridine **11** is exchanged by 2,6-dimethyl-[4,4']-bipyridine **81** in self-assembled supramolecular squares, several isomers are possible in principle, because of the reduced symmetry (see Fig. 5.30a-c). Due to the sterical demand of the two methyl groups, it should be energetically favorable when two ligands bind to one metal subunit with different sides of the ligand, i. e. one pyridine and one lutidine side. When this assumption is followed in a 4:4 complex at each metal subunit, only one out of this isomers is favored: an unidirectional square is formed (see Fig. 5.30c top left isomer). Noteworthy, this unidirectional square itself is of course achiral.

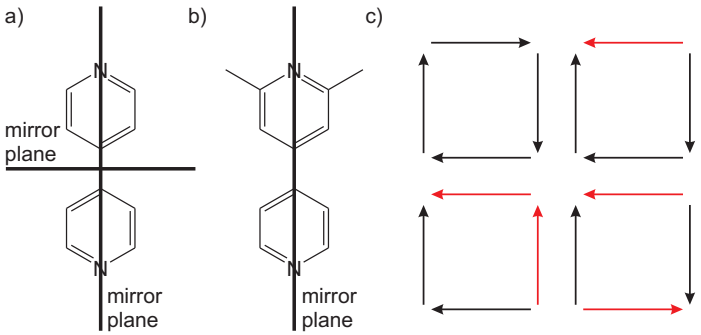

Figure 5.30: a) [4,4']-bipyridine **11**; b) 2,6-dimethyl-[4,4']-bipyridine **81**; c) possible self-assembled supramolecular squares isomers formed from 2,6-dimethyl-[4,4']-bipyridine **81**.

5.5.1 Unidirectional Stang Squares?

First evidence that only one lutidine side can bind to one metal subunit is obtained from mass spectrometry: When dpppPt$(py)_2(OTf)_2$ is sprayed from acetone (c = 400μm), two major peaks at 834 Da and 913 Da can be found in the (+)ESI-MS-spectra. The first one can be assigned to dpppPt$(py)_1(OTf)^+$, while the later corresponds to dpppPt$(py)_2(OTf)^+$.

When dpppPt$(py)_2(OTf)_2$ or dpppPt$(OTf)_2$ are sprayed from pyridine (same concentrations), these findings remain unchanged. Not unexpected, two pyri-

dine nitrogen atoms can bind to the metal subunit. In marked contrast, in the MS spectra of dpppPt(OTf)$_2$ sprayed from 2,6-lutidine only one peak for dpppPt(Lut)$_1$(OTf)$^+$ is found at 862 Da. These findings might be a first indication that only one 2,6-lutidine ring can bind to one metal precursor.

When equimolar amounts of 2,6-dimethyl-[4,4']-bipyridine **81** and (dppp)Pt(OTf)$_2$ **[b]** are mixed in [D$_6$]-dimethylsulfoxide three sets of signals can be found in the ^{31}P NMR spectrum (see Figure 5.31 and Table 5.4).

Chemical Shift [ppm]	Splitting	Coupling $^1J_{PtP}$ [Hz]	Intensity	Remark
-8.50	singlet	3680	16 %	free **[b]**
-9.13 & -10.12	doublets (31 Hz)	ca. 3050	34 %	
-11.28	singlet	3040	50 %	

Table 5.4: Set of signals found in the ^{31}P NMR spectrum of an equimolar mixture of 2,6-dimethyl-[4,4']-bipyridine **81** and (dppp)Pt(OTf)$_2$ **[b]**.

With these findings in hand, the outcome of the self-assembly reaction can be described as follows: All ligands bind with their pyridine binding site to platinum complexes. As the binding constant for the second ligand is higher than the binding constant for the first ligand,[211] 1:2 = **[b]**:**81** complexes are formed exclusively. Two thirds of unreacted **[b]** (2/3*50 % ≈ 34 %) bind to one of the two lutidine binding sites of the 1:2-complexes, whereas one third (2/3*50 % ≈ 16 %) remains unbound. Three complexes are the result: [1:0:2] (16%), [1:2:2] (14%) and [2:2:4] (34%). Please note that the latter two contribute both to the singlet at -11.28 ppm with a coupling constant of 3040 Hz.

As expected, the ^{1}H NMR spectrum of this mixture is rather complex. Fortunately, the signals of the ortho-pyridine protons of **81** can be identified. Two sets of signals at 8.98 and 8.83 ppm with a 69:31 ratio can be found. This ratio is in good agreement with the results obtained from the ^{31}P NMR spectrum.

From these finding, one can conclude that the 2,6-dimethylpyridine side of **81** can indeed bind to **[b]**. The binding energy of the lutidine binding site of **81** is – as expected – lower than the pyridine side. Molecular squares are however not formed. The NMR sample is heated to 100°C for three days, but after cooling

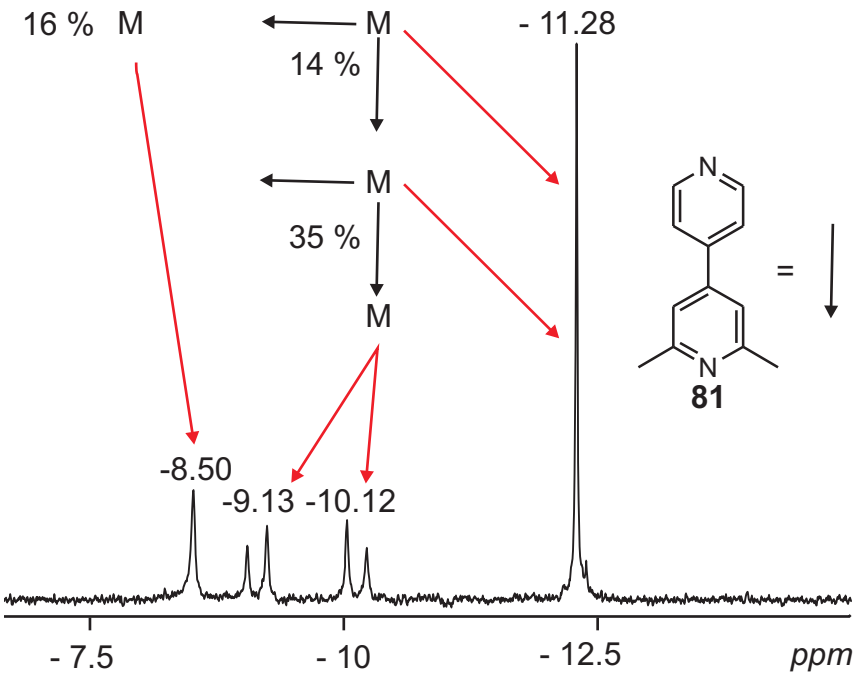

Figure 5.31: Partial ^{31}P NMR spectrum of an equimolar mixture of 2,6-dimethyl-[4,4']-bipyridine **81** and (dppp)Pt(OTf)$_2$ **[b]** in [D$_6$]-dimethylsulfoxide.

to room temperature the ^{31}P NMR spectra remains unchanged. Thus, square formation is not hindered kinetically, but thermodynamically.

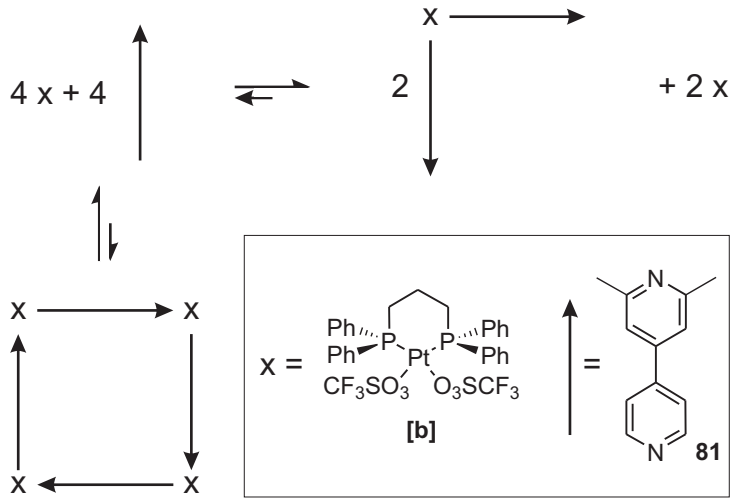

Figure 5.32: Schematic representation of a section of the complex equilibrium between **81** and (dppp)Pt(OTf)$_2$ [**b**].

In Scheme 5.32, two possible outcomes of the self-assembly reaction are shown: the unidirectional square and the equimolar mixture of [**b**] and [2:2:4]. Rather unexpectedly, the free metal complex [**b**] seems to be too stable to push the equilibrium to the formation of unidirectional squares. Two modifications might destabilize the free metal complex: a different solvent or different bidentate blocking ligands. Unfortunately, [**b**] is not soluble in many apolar solvents at all.

Alternatively, steric repulsion between the methyl groups of **81** and the dppp-blocking ligand may also reduce the M-N-binding constant. Metal precursors [**c**] and [**d**] might thus be better metal precursors.

5.5.2 Unidirectional Fujita Squares

When equimolar amounts of 2,6-dimethyl-[4,4']-bipyridine **81** and [**c**] are mixed in D_2O (see Scheme 5.25), a rather complex ^{1}H NMR spectrum is observed. When the sample is heated for three days at 90°C, three signals arise: an AA'XX' pattern and a singlet (see Figure 5.26 a). The AA'XX' pattern, with an downfield shift of 0.3 ppm and 0.5 ppm compared to free **81** (in D_2O, same concentration,

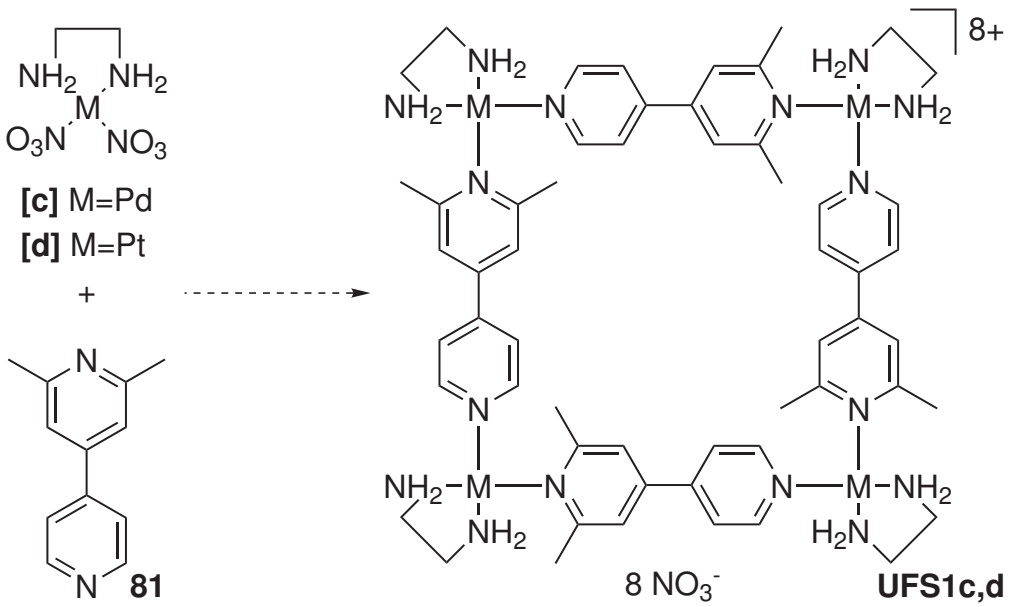

Scheme 5.25: Self-assembly reaction between equimolar amounts of **81** and metal complexes (en)Pd(NO_3)$_2$ [**c**] or (en)Pt(NO_3)$_2$ [**d**] might lead to the formation of unidirectional squares **UFS1c,d** (**U**nidirectional **F**ujita **S**quares).

see Figure 5.26 b), can be assigned to the pyridine side of **81**, and the singlet, with an downfield shift of 0.7 ppm compared to the meta protons of **81**. No further changes in the spectra are observed when heating is continued. Thus, a thermodynamic minimum (either local or global) seems to be reached, which seems not to unidirectional squares exclusively. To increase the metal-nitrogen binding constant, palladium might be exchanged by platinum.

In case of the platinum metal precursor (en)Pt(NO_3)$_2$ [**d**], the synthesis is less straightforward. Based on earlier results from *Fujita et al.*,[29] the equilibrium between different species might be reached only after weeks at 100°C. Adding of a catalytic amount of nitric acid reduces this time span to one week, in some cases. As it turned out that both methods failed to produce unidirectional Fujita squares, an alternative route based on the results from *Ferrer et al.*,[212] is used: Equimolar amounts of **81** and (en)Pt(NO_3)$_2$ [**d**] are mixed in dichloromethane and the suspension (the metal precursor (en)Pt(NO_3)$_2$ [**d**] is not soluble in dichloromethane) is stirred. The metal precursor's crystal size, shape and color changes over a period of two days. After removal of the solvent, which does not

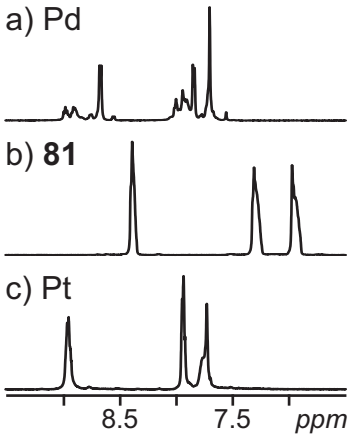

Scheme 5.26: Partial ^{1}H NMR spectra of a) an equimolar mixture of **81** and (en)Pd$(NO_3)_2$ [**c**], b) **81**, and c) an equimolar mixture of **81** and (en)Pt$(NO_3)_2$ [**d**] (all in D_2O at room temperature with the same concentration of **81**.

contain significant amounts of **81** anymore, the ^{1}H NMR spectrum in D_2O shows only one set of signals (see Figure 5.26 c). Again, strong downfield shifts (0.6 - 0.8 ppm) are observed for the three aromatic signals of the organic precursor. These high shift differences might be the result of binding of both the ligand's binding sites to the metal complex, and thus, the unidirectional square **UFSc,d** might have been formed. Unfortunately, no single crystals for crystal structure analysis could be grown so far and no [4:4]-complexes could be observed by mass spectrometric investigations. Hence, further proof for unidirectional squares based on these building blocks must be found.

Chapter 6

Results and Discussion of Collaborative Projects

As already discussed previously, the aim of this study diverge into several different tasks along the research path from fundamental towards applied research. Whereas the results described in the last chapter are more of fundamental interest, this chapter covers the results of collaborative projects within the SFB 624 and with the working group of Prof. Dr. P. Bäuerle. New materials are obtained and characterized thoroughly. In the first two sub chapters self-assembled supramolecular squares are deposited on surfaces and used as sensor active layers for the detection of ethene, whereas in the last sub chapter oligo- and polythiophenes, organic semiconductors, are analyzed in the gas phase.

6.1 Second-Order Template Effects Observed by EC–STM*

6.1.1 Introduction and Motivation

Within the last three decades supramolecular chemistry has become an inherent part of modern chemistry[236,237] having significant impact also on other branches of science and nano-technology, in particular on those which are mainly dealing with the design, the fabrication and characterization of molecular architectures with dimensions on the nanometer scale. One challenging task for supramolecular chemists is certainly to provide artificial model systems allowing them to study the working principle of nano-sized devices, machines and actuators[104,238] or to gain deeper insights into the mechanism of fundamental (bio)chemical processes such as the molecular recognition via highly specific host-guest interactions.

Following the so-called "bottom-up" approach, rather than the "top-down" approach, most supramolecular structures are self-assembled from simple molecular building blocks via non–covalent and weak forces. Such a self-assembly results in molecular superstructures which reveal a higher complexity than the individual molecular building blocks following Lehn's definition of supramolecular chemistry as the "chemistry beyond the molecule".[239] Related to the increase in structural complexity also new functionalities are often introduced into these artificial systems of higher order. It appears obvious that experimental control of e.g. orientation upon the self-assembly process is strongly required in order to keep the size, the electronic and geometric structure and finally the functionality of these supramolecular architectures under control. A quite new approach to steer the ordering process of supramolecular architectures is the use of well defined surfaces of single crystals acting as electronic and geometric templates due to the presence of specific adsorbate-substrate interactions. These are modulated according to the symmetry and periodicity of the substrate surface. While in solution and in the 3D solid-state only the specific and directional intermolecular interactions determine

*The results of this section were obtained in collaboration with Dr. Caroline Zörlein and Dr. Peter Broekmann in the working group of Prof. Dr. K. Wandelt as well as Leo Merz in the working group of Prof. B. A. Hermann and are published.[66,235]

the formation of supramolecular architectures we find on surfaces, by contrast, a complex interplay between the inter-adsorbate (intermolecular template effect) and the adsorbate-substrate interactions (surface template effect) controlling the 2D phase behavior at surfaces. Thus, it is not astonishing that structure motifs and intermolecular spacings of supramolecular ensembles are observed at surfaces which are known neither from the solution phase nor from the 3D solid-state.[240]

Besides the surface mediated template effects it is also the unique possibility of applying structure sensitive tools such as the scanning probe techniques which makes a combination of supramolecular chemistry and surface science approach to a promising and challenging task. In particular Scanning Tunneling Microscopy (STM) provides direct access to structural information of supramolecular architectures. Nowadays scanning probe techniques can be used for surface characterization in various environments, not only in UHV (Ultrahigh Vacuum) or under ambient conditions but also at solid/liquid interfaces, particularly in an electrochemical environment.[241]

The formation process mentioned before is controlled by a hierarchical sequence of template effects starting with the initial adsorption of an anion layer on-top of a metal electrode surface. A strong interaction of this anion layer with the metal substrate leads to a highly ordered adsorbate layer that frequently adopts the symmetry of the underlying substrate (first order template effect, see Fig 6.1).

For a recent review on the phenomenon of "specific anion adsorption" see ref.[241] In the following step cationic complexes are locked onto the anion layer mainly by enhanced electrostatic interactions. Hydrophobic solvent effects may also support this process. The supramolecular architectures on-top of the anion layer should reveal molecular host-cavities, which are preferentially oriented towards the solution phase. For that purpose we use the specific interaction between the anion layer and the supramolecular cavitands forcing them into the desired adsorption geometry (second order template effect). This particular orientation of the cavitands (i.e. flat and parallel to the surface) is required since our final goal is the direct observation of the specific inclusion of guest molecules[242] into the host cavitands (third order template effect) by use of the STM.

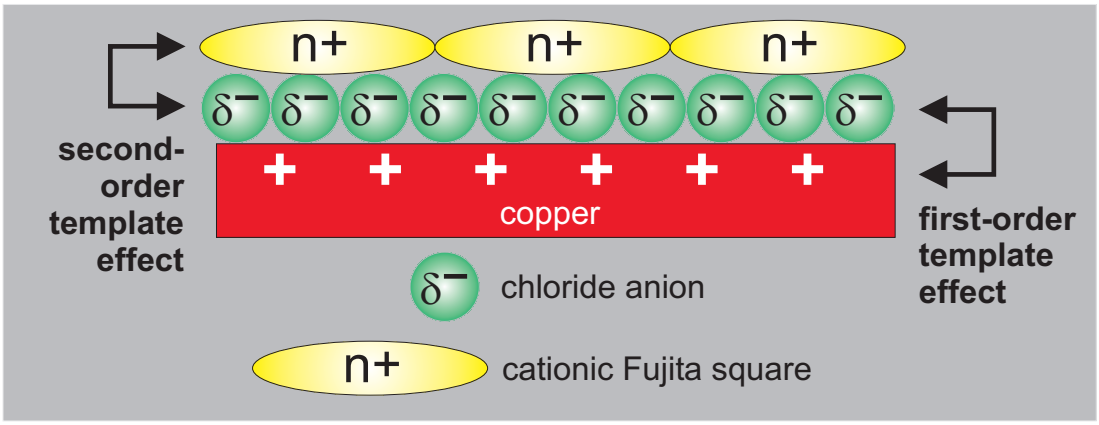

Figure 6.1: Schematic drawing representing the sequence of template effects used for the hierarchical assembly of supramolecular architectures at the electrode surface.[66]

6.1.2 Experimental Section

To observe structure motifs of supramolecular ensembles (here macro-cycles) at surfaces by ECSTM (see chapter 6.1), the building blocks need to be prepared, at first. In this case, the EC-STM solvent of choice is water. Therefore, the desired building blocks need to be water-soluble and available in at least mg quantities. Two different approaches were chosen to obtain the desired macro-cycles: On the first hand, covalent molecular rectangles were prepared, which were first introduced by *Stoddart et al.*:

- cyclobis(paraquat-p-phenylene)tetra(hexafluorophosphate),[243]
- N,N'-1,4-phenylene-bis(methylene)bis-4,4'-bipyridinium-bis-(hexafluorophosphate),[244] and
- cyclobis(paraquat-p-biphenylene)tetra(hexafluorophosphate).[245]

All three were synthesized by irreversible bond formations, i.e. S_N type reactions from bisbenzylbromides and [4,4']-bipyridines under high dilution conditions to form the desired compounds and undesired polymeric waste (see Scheme 6.1).

Purification is achieved either by recrystallization or by column chromatography, which however is rather difficult, because of the polycationic nature of the desired compounds. In the last steps the tetra(hexa-fluorophosphate) salts

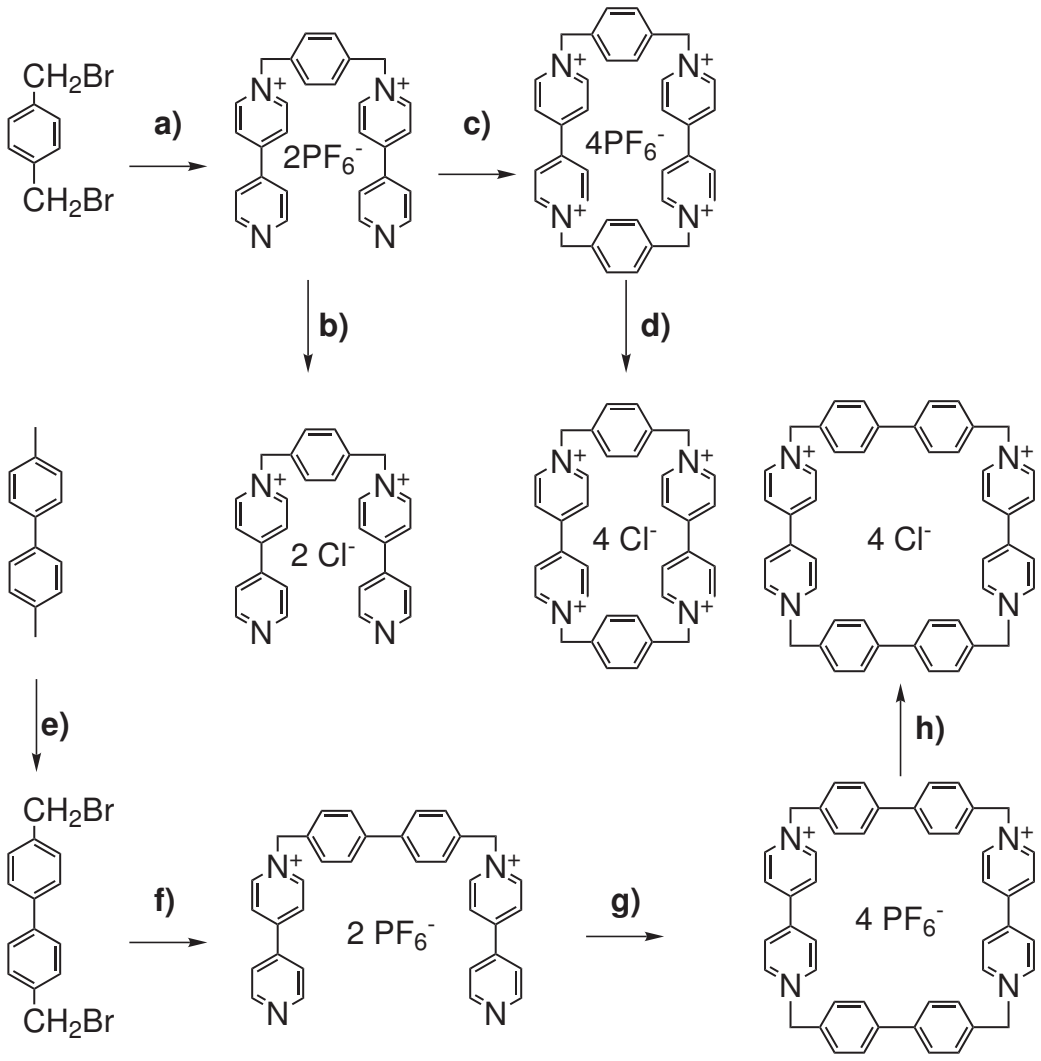

Scheme 6.1: a) 1) [4,4']-bipyridine **11**, acetonitrile, 82°C, 18 hours, 2) NH_4PF_6, H_2O, 68%; b) $NBut_4Cl$, acetonitrile, quant.; c) 1) 1,4-bis-bromomethyl-benzene, acetonitrile, 82°C, 18 hours, 2) NH_4PF_6, H_2O, 12%; d) like b); e) N-bromosuccinimide, N,N-azobisisobutyronitrile, DCM, $h\nu$, 2 hours, 47%; f) [4,4']-bipyridine **11**, acetonitrile, 82°C, 18 hours, 2) NH_4PF_6, H_2O, 42%; g) 1) 4,4'-bis-bromomethyl-biphenyl, acetonitrile, 82°C, 18 hours, 2) NH_4PF_6, H_2O, 26 %; h) like b).

were converted into the water-soluble tetra-chloride salts: Cyclobis(paraquat-p-phenylene)tetrachloride, N,N'-1,4-phenylene-bis(methylen)bis-4,4'-bipyridinium-bis-chlorideand cyclobis(paraquat-p-biphenylene)tetrachloride.[246]

Prior to each STM experiment the copper substrate needs to be treated by an electrochemical etching procedure in order to remove the native oxide layer that is ineluctably formed in air. For this purpose, the Cu(100) sample (MaTeck company, Jülich, Germany) is immersed into 50 % orthophosphoric acid. For the copper dissolution reaction an anodic potential of $\approx$ 2 V is routinely applied between the copper sample and a platinum foil for about 20 to 40 s. Subsequently, the surface is rinsed with degassed supporting electrolyte (10 mM HCl/5 mM KCl) which removes not only the phosphate from the copper surface but also protects the surface against re-oxidation due to the formation of a specifically adsorbed chloride layer. Under these conditions the sample is mounted into the electrochemical cell of the EC-STM system and brought under potential control. The tunneling tips used in our experiments were electrochemically etched from 0.25 mm tungsten wire in 2 M KOH solution and subsequently isolated by passing the tip through a drop of nail polish. For all solutions high purity water is used. The electrolyte solution had to be purged with oxygen-free argon several hours before use. All potentials given in this chapter refer to an internal Ag/AgCl reference electrode.

6.1.3 First Order Template Effect – c(2x2)–Chloride Adlayer on Copper (100)

Therefore, STM and CV (Cyclic Voltammetry) measurements were first performed in pure supporting electrolyte (10 mM HCl or 10 mM HCl/5 mM KCl). The template structure displays representative STM images of the morphology and atomic structure of the chloride pre-covered Cu(100) electrode surface (Fig. 6.2).

Chloride anions specifically adsorb on the Cu(100) electrode surface under formation of a well ordered c(2 $\times$ 2)-Cl phase[241,247] adopting the fourfold rotational symmetry of the copper substrate (first order template effect) with individual chloride particles residing in substrate fourfold hollow sites (Fig. 6.2) (coverage V= 0.5 ML, the V value is defined as the chloride to copper ratio, at V=0.5

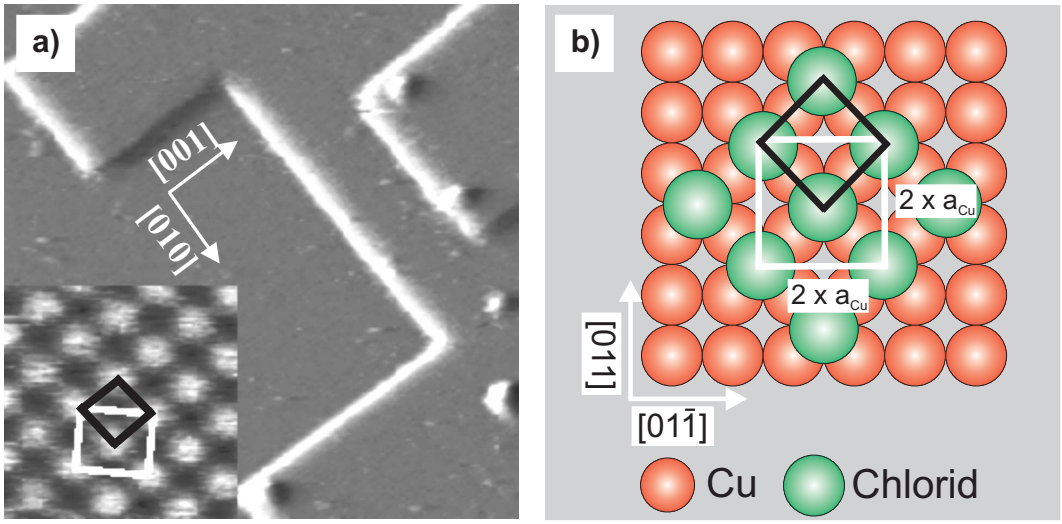

Figure 6.2: Representative STM images of the chloride modified Cu(100) electrode surface: a) morphology of the Cu(100) electrode surface in the presence of specifically adsorbed chloride: 69 nm × 69 nm, I_t = 1 nA, U_b = 25mV, E = -300 mV vs. Ag/AgCl, the in–set displays an atomically resolved STM image of the $c(2 \times 2)$–Cl adlayer; b) hard–sphere model of the $c(2 \times 2)$–Cl structure.[235]

the maximum coverage of the surface with chlorides is reached.). This adlayer is stable in the potential range between -250 mV and about -680 mV. For a surface template effect not only a strong adsorbate-substrate interaction is required but also a strong modulation of these interactions according to the lattice symmetry and dimensions of the substrate. It is well known that strongly adsorbing anions not only acquire a typical atomic surface structure but also have a strong influence on the surface morphology (Fig. 6.2). Substrate steps are preferentially aligned parallel to the main symmetry axes of the chloride layer, which are rotated by 45° with respect to the substrate main symmetry axes. In particular, chloride layers are ideal substrates and templates for the adsorption of cationic species, since the chloride retains practically its full charge upon adsorption,[248] while the heavier homologues bromide and iodide exhibit an increased partial charge transfer to the metal.

6.1.4 Synthesis of the Adsorbates

Before discussing the second-order template effect, the water soluble adsorbates have to be introduced, which can be divided into two groups: Fujita's metallo supramolecular squares and triangles and *Stoddart's* Cyclobis(paraquat-p-phenylene), an electron poor cyclophane. The first class self-assembles under thermodynamic control from two different, easily available building blocks.[26, 29, 249] These complexes consist of four Pt(II) centers located at the corners of the molecular square. The Pt(II) centers are bridged by [4,4']-bipyridine ligands and further stabilized by chelating ethylene-diamine molecules resulting in a square planar fourfold coordination of each Pt(II) center (counter anions: 8 NO_3^-). What makes this type of supramolecular square interesting is the fact that it features a molecular cavity with nanometer dimensions (Fig. 6.3) and – quite important for EC-STM experiments – its solubility in aqueous electrolytes.
Cyclobis(paraquat-p-phenylene) is synthesized by irreversible bond formations, i.e. S_N type reactions from bisbenzylbromides and [4,4']-bipyridines under high dilution conditions to form the desired macrocycle and undesired open chain analogues. Cyclobis(paraquat-p-phenylene) can be purified by column chromatography, which however is rather difficult, because of its polycationic nature. Its size (1.32 × 1.18 nm) is comparable with the Fujita ensembles, it is highly charged (+4) and water soluble.

6.1.5 Second-Order Template Effect – Fujita Squares on Top of the Chloride Adlayer

A first approach towards the formation of cavitand structures at electrode surfaces is the adsorption of supramolecular entities from the solution phase. In order to demonstrate this we use fourfold symmetric metallo-supramolecular complexes of the Fujita type .

After exchanging the pure supporting electrolyte by a solution also containing the Fujita-squares, copper steps can be observed on a mesoscopic length scale which are oriented parallel to substrate directions (Fig. 6.4 a) which is clearly indicative for the presence of the c(2 × 2) chloride layer. Molecularly resolved

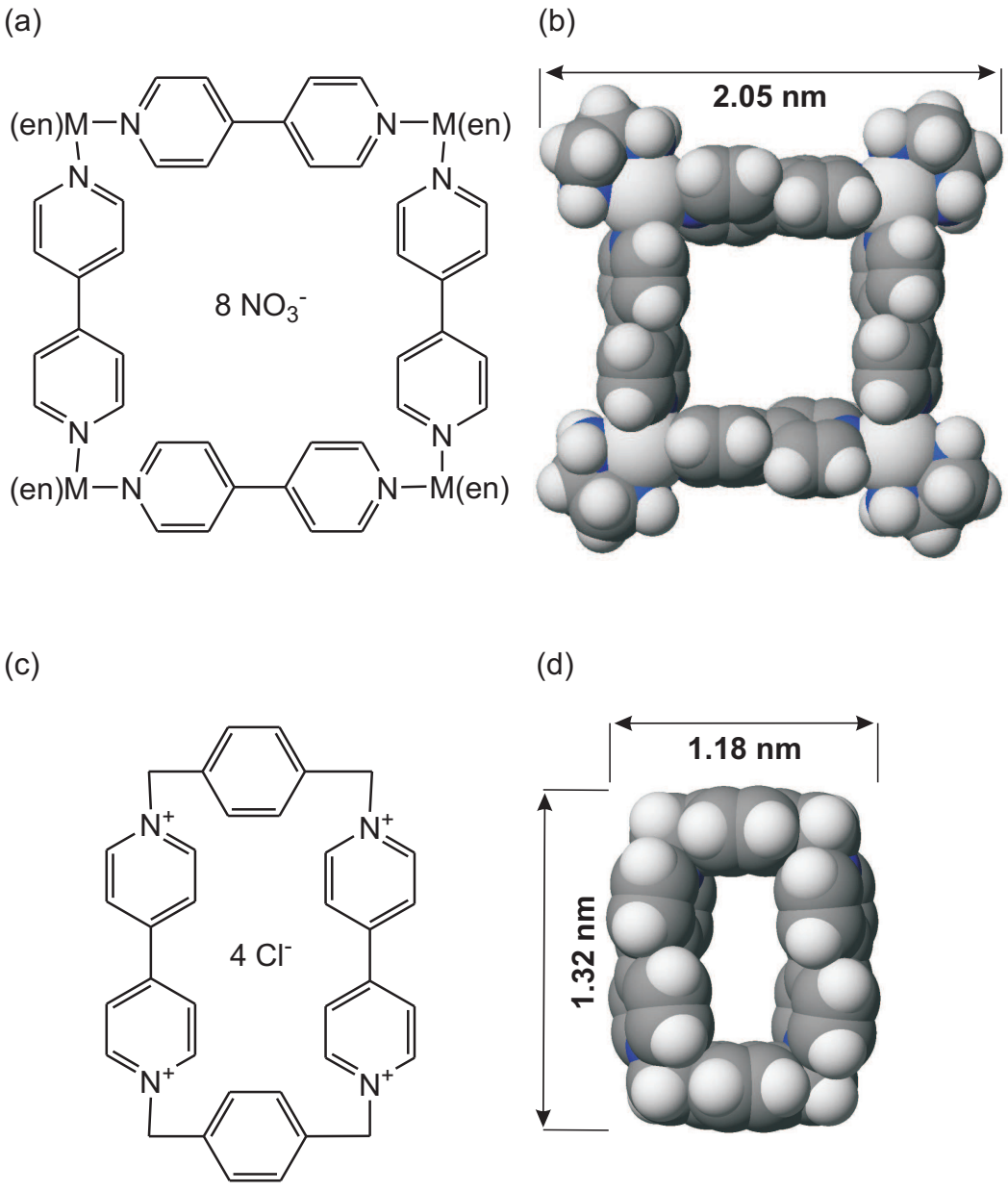

Figure 6.3: (a) Schematic representation of the Fujita–squares; (c) schematic representation of the Cyclobis(paraquat-p-phenylene); (b) and (d) MM2–minimized space–filling models.[192]

STM images indeed exhibit Fujita-squares lying flatly on the electrode surface (Fig. 6.4 b-d) as desired. Clearly visible are the pronounced cavities of the supramolecular entities imaged as dark depressions surrounded by square-shaped brighter rims. The presence of flat lying squares on-top of the chloride lattice can be seen as a direct prove for enhanced adsorbate-substrate interactions via electrostatics.

The lateral order of the Fujita-squares on Cu(100)-c(2 $\times$ 2)-Cl is apparently quite poor (Fig. 6.4 b). One reason for that is the presence of co-adsorbed chain-like oligomers which are disturbing the lateral order of the squares. By contrast, surface areas with higher density of molecular squares and a lower concentration of oligomers do reveal a locally confined 2D order (Fig. 6.4 c-d).

Two different packing motifs can be distinguished, one exhibiting a fourfold symmetry ($|\overrightarrow{a}| = |\overrightarrow{b}|, \gamma = 90°$) adopting the symmetry of the c(2 $\times$ 2)-Cl lattice underneath (Fig. 6.5 c) and another one (Fig. 6.5 b) revealing a distorted (quasi)hexagonal arrangement of squares ($|\overrightarrow{a}| < |\overrightarrow{b}|, \gamma < 90°$) as displayed in Fig. 6.4 d. This leads to a commensurate superstructure (5x5)-1 square structure regarding the chloride adlayer (Fig. 6.6).

The "Nearest Neighbor Distance" of = 1.9 nm $\pm$ 0.05 nm in both cases compares well with the calculated van-der-Waals diameter of the Fujita-square.[192] The value of 2.05 nm given in Fig. 6.3 b) is inclusive of the van-der-Waals radius of the peripheral hydrogen atoms. The lower observed value of 1.90 nm seems reasonable, when one takes into account that the peripheries of two adjacent squares may well interdigitate thus maximizing the van-der-Waals contacts.

The Pt-Pt distance of 1.14 nm determined by molecular modeling agrees well with the values of 1.11 nm reported in a recent X-ray crystal structure analysis of the Fujita-square.[28] The lateral ordering is apparently dominated by short-range van-der-Waals interactions.

Applying more drastic tunneling conditions leads to a locally confined removal of the organic layer by the tunneling tip. This procedure allows a precise determination of the molecular orientation with respect to the chloride lattice underneath. For the sake of simplicity we have superimposed the chloride lattice to the STM image in Fig. 6.4 e) (white lattice). From that it becomes evident that the Fujita-

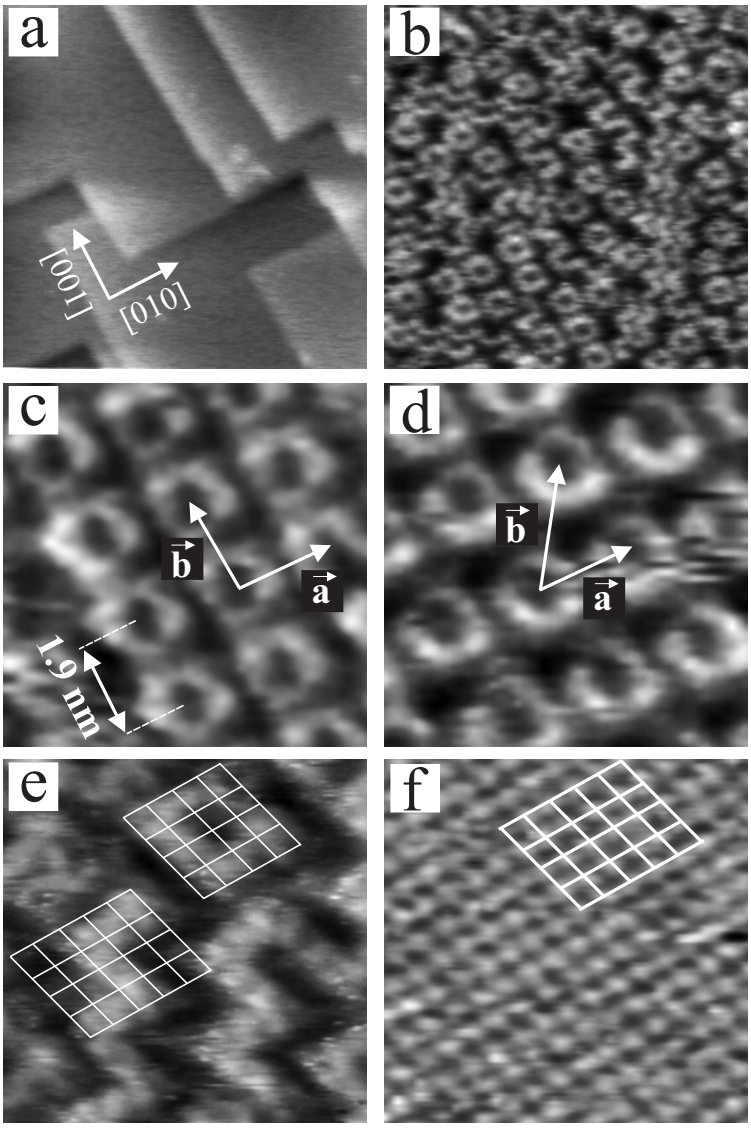

Figure 6.4: (a) Morphology of the chloride pre-covered Cu(100) electrode in the presence of the Fujita–squares: 56 nm × 56 nm, I_t = 0.6 nA, U_b = 278 mV, E =–500mV vs. Ag/AgCl; (b) coexistence of Fujita–squares and chain–like oligomers: 20.5 nm × 20.5 nm, I_t = 0.7 nA, U_b = 280 mV, E =–550 mV vs. Ag/AgCl; (c) four–fold symmetric arrangement of Fujita–squares: 6 nm × 6 nm, I_t = 0.7 nA, U_b = 280 mV, E =–550mV vs. Ag/AgCl; (d) quasi–hexagonal arrangement of Fujita–squares: 6 nm × 6 nm, I_t = 0.7 nA, U_b = 280mV, E =–550mV vs. Ag/AgCl; (e) 4 nm × 4 nm, I_t = 0.7 nA, U_b = 280mV, E =–550mV vs. Ag/AgCl; (f) $c(2\times2)$–Cl phase imaged after tip–induced removal of the Fujita–squares: 4 nm × 4 nm, I_t = 0.7 nA, U_b = 280mV, E =–550mV vs. Ag/AgCl.[235]

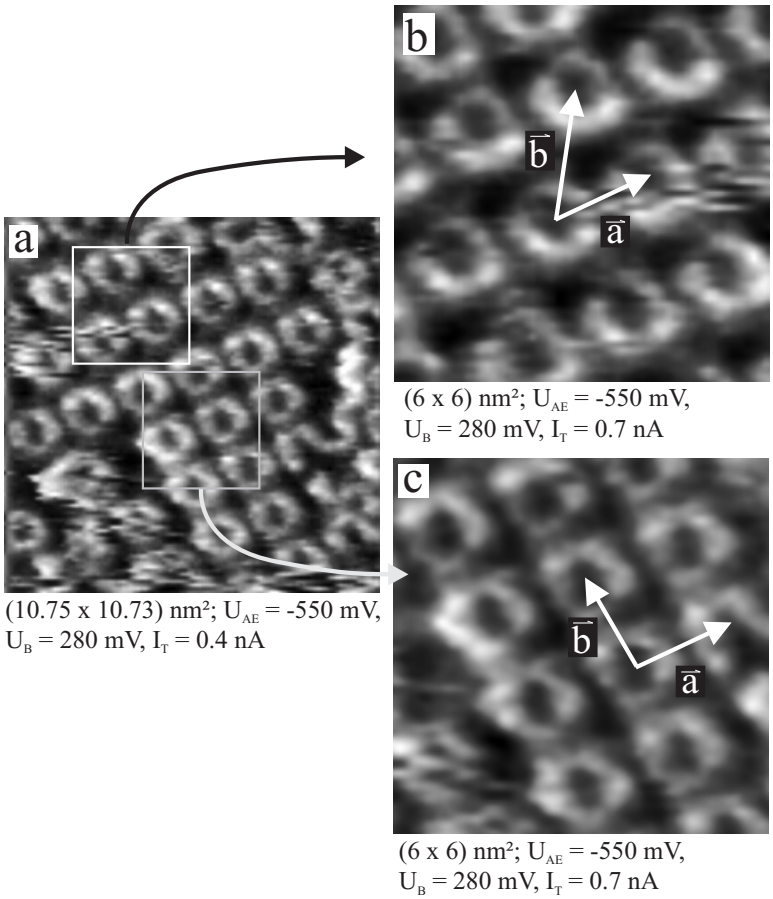

Figure 6.5: Two different packing Motifs.[139]

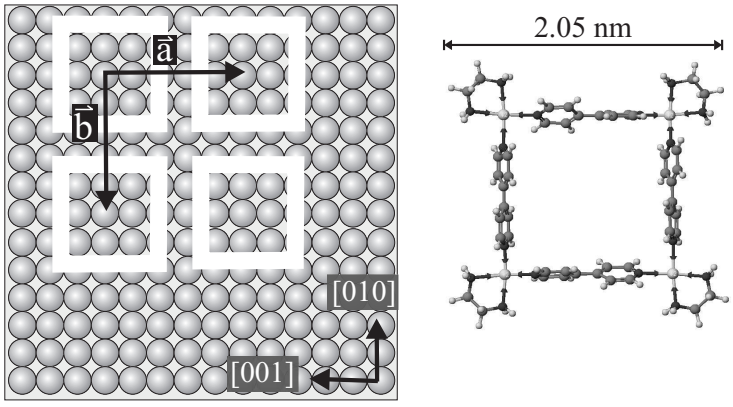

Figure 6.6: Model of the Fujita Squares on top of Cu (100).[139]

squares with their Pt-Pt connecting axes are oriented parallel to the close packed chloride rows. The same is valid even for the zig-zag chains of the oligomers in the same figure.

^{1}H-NMR experiments under similar experimental conditions (in 0.1 M DCl/ D_2O solutions) confirmed that some of the squares opened and new signals for oligomers were found. The overall length of these oligomers can of course not be determined by simple NMR-techniques. The degradation does not take place instantaneously, but proceeds on a time scale of about 30 min. In this sense the observed co-adsorption of squares and oligomers of variable chain lengths at the electrode surface simply reflects the existence of these various supramolecular species in the solution phase. It should be stressed that the beginning decomposition of the Fujita-squares is not a surface effect.

This becomes evident when the contact time between the chloride containing solution and the Fujita-squares is minimized. If the Fujita-squares are added to the electrolyte solution just before the STM experiment large and well ordered domains of the supramolecular squares are obtained (Fig.6.7 a) which remain stable at least on the time scale of our STM experiments.

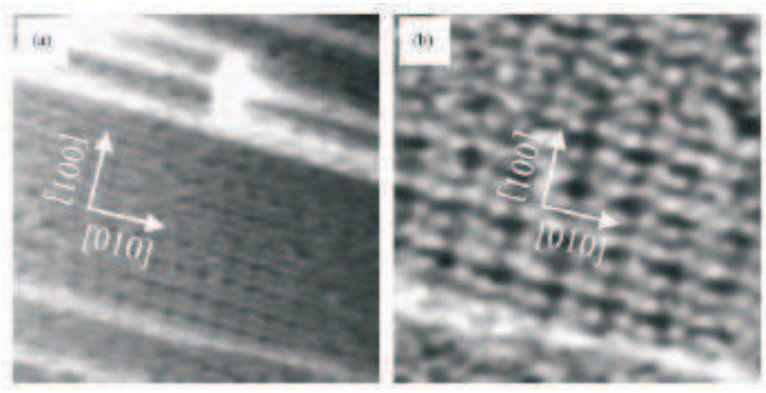

Figure 6.7: Long–range order of Fujita–squares after optimized preparation techniques: 35.6 nm × 35.6 nm, I_t = 0.7 nA, U_b =–110mV, E =–480mV vs. Ag/AgCl; (b) 13.3 nm × 13.3 nm, I_t = 0.7 nA, U_b =–110mV, E =–480mV vs. Ag/AgCl.[235]

Quite interestingly, the imaging properties of the Fujita-squares seem to depend on the absolute value and the polarity of the bias voltage. With a bias voltage of -110 mV and a tunneling current of 0.7 nA at a working potential of

-480 mV the squares are imaged as square-shaped entities with four pronounced STM spots at their corners (Fig.6.7 b). Please note that in our STM set-up a negative bias means that the electrons tunnel from the tip into the surface. Hence, it appears most likely that by using negative bias voltages (e.g. -100 mV) the Pt(II) centers at the corner sites of the Fujita-squares are predominantly imaged in the STM experiment while at positive bias (+280 mV) the MOs of the molecular ligands are preferentially visualized (figs. 6.4 c-d). Similar intriguing effects have recently been reported by Mena-Osteritz et al. describing a selective imaging of MOs of macrocyclic oligothiophene-diacetylenes physisorbed on HOPG.[250,251]

To evaluate how important the anion-covered surface is for the arrangement of the squares, preliminary experiments were performed on HOPG: A series of molecular squares in different solvents (1 and 4 in H_2O; 2, 5, and 6 in CH_2Cl_2) have been deposited by solution casting on HOPG. All measurements show one-dimensional striped patterns, which could result from a selforganization that is probably unstable under the scanning tip (even with soft tunneling parameters) or from stacking of the molecules dominated by intermolecular interactions. The best high-resolution images were obtained with square 5 (Fig. 6.8).[66] This is clearly pointing to the absence of a strong template effect and the presence of inter-adsorbate interactions ruling the 2D phase behavior on HOPG.

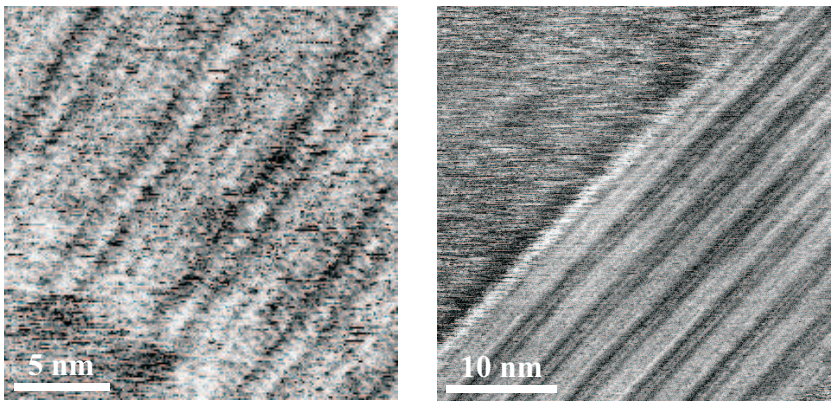

Figure 6.8: Inter-adsorbate interactions of square 5 ruling the 2D phase behavior on HOPG.[66]

6.1.6 Second-Order Template Effect – Cyclophanes on Top of the Chloride Adlayer

A second, slightly modified, approach towards the formation of cavitand structures at electrode surfaces is the adsorption of *Stoddart's* Cyclobis(paraquat-p-phenylene) from the aqueous phase (see 6.1.4). Again a chloride pre-covered Cu(100) surface serves as template. The pure supporting electrolyte is exchanged by an aqueous solution of the cavitands (50 mM in 10 mM HCl) under potential control. Again, copper steps can be observed on a mesoscopic length scale which are oriented parallel to substrate directions which again is a strong hint for an intact c(2 × 2) chloride layer. Molecularly resolved STM images exhibit again that the cyclophanes are lying flatly on the electrode surface with their cavities pointing towards the solution (Fig.6.9).

Clearly visible is the lateral order with only minor defects, which leads to large and well ordered domains. As the cyclophanes are rectangular, the fourfold symmetry is reduced. And indeed, two domains are observed, which are almost perpendicular (α = 85±5 °), leading to a twofold symmetry (rectangular unit cell $|\overrightarrow{a}|$ = 2.1± 0.1 nm $|\overrightarrow{b}|$ = 0.9 ± 0.1 nm). Although the [4,4']-bipyridines are quite close to each other, which means that their positive charges have to be compensated by the chloride adlayer, a commensurate superstructure is formed (Fig. 6.10).

Another interesting feature of these STM-experiments reveals, when the bias voltage is increased and the tunneling current is reduced. This leads to a smaller interaction and a larger distance between sample and tip. Over the first adsorbate layer more complexes become visible. Densely packed rows of cyclophanes can be found. However, a second complete monolayer is not observed. The distance between these two layers corresponds well with the height of the first monolayer, indicating that the second layer is again lying flat on top of the flat lying cyclophanes of the first layer.

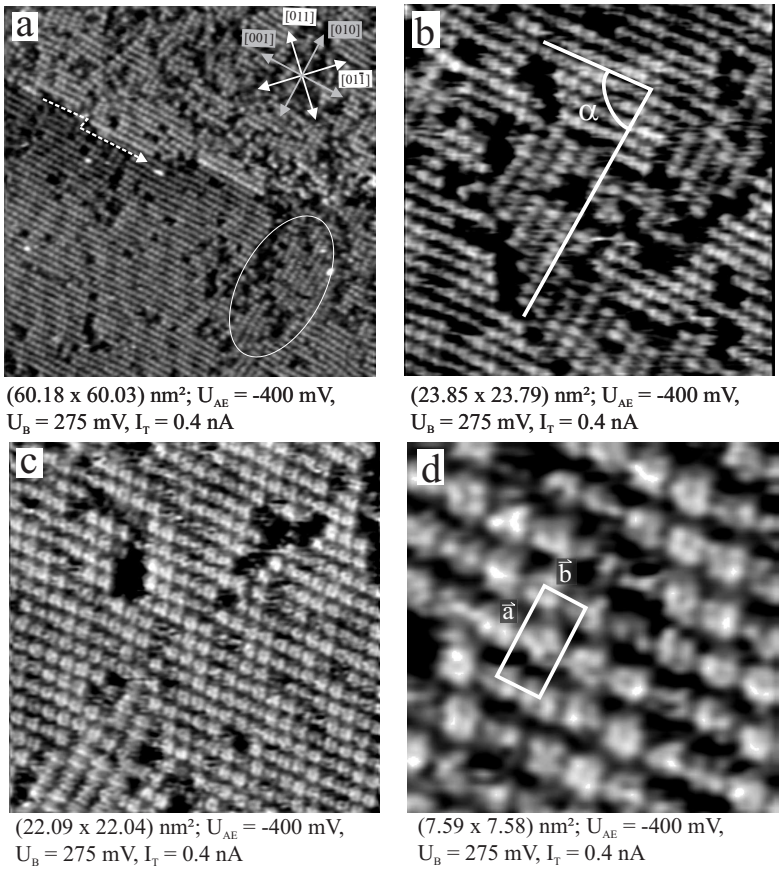

Figure 6.9: Cyclobis(paraquat-p-phenylene) on top of Cu (100).[139]

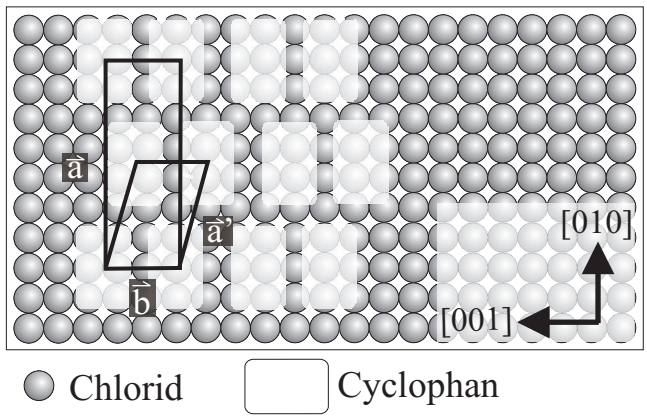

Figure 6.10: Model of Cyclobis(paraquat-p-phenylene) on top of Cu (100).[139]

6.1.7 Outlook

The stage is now set to attempt the insertion of guest molecules into the cavities of the squares and directly observe the guests within the host at electrified solid/liquid interfaces by means of high-resolution scanning probe techniques.

In the case of *Stoddart's* Cyclobis(paraquat-p-phenylene), electron rich guests like phenols or benzene compounds with more than one hydroxy group offer appropriate binding energies in water. Future measurements should focus on the inclusion of guest molecules into the cavitand structures similar as recently reported by Pan et al. who succeeded in imaging host-guest complexes at the solid/liquid interface.[252]

Longer and more flexible bis-pyridines lead to an equilibrium between squares and triangles[249d]. Another interesting study would be to find, which species can be deposited on surfaces with threefold symmetries.

6.2 Gravimetric Detection of Ethene by QMB[†]

6.2.1 Introduction

Ethene is of both biogenic[214] and anthropogenic[215] origin, and thus almost ubiquitous. As a phytohormone, it induces the process of ripening, stimulates epinasty, and indicates exposure of plants to stress.[216] Furthermore, monitoring of ethene is pivotal for air-quality management in cities because it is a volatile organic compound (VOC) which is known to have a strong photochemical ozone creating potential (POCP).[217] Furthermore, ca. 100 million tons of ethene were consumed in industrial processes in 2003 indicating its major role for modern economy.[218]

Therefore, an inexpensive and robust real-time method for quantitative monitoring its content in analyte gases represents a highly interesting target for analytical chemistry. At present, several analytical methods exist for a continuous quantitative survey of ethene, among them laser photoacoustic techniques with

[†]The results of this section were obtained in collaboration with Dr. Boris Graewe in the working group of Prof. Dr. J. Bargon and Dr. Jan Haubrich. Parts of these results are published in reference.[213] The compounds in this section are numbered **QMB** for **Q**uarz **M**icro **B**alances.

an extremely low detection limit in the ppt range[216] or optical methods which operate at concentrations down to 30 ppb.[219] These methods often suffer from costly equipment and require sophisticated procedures. For example, laser photoacoustic devices are quite sensitive to the flow rates which consequently need to be precisely controlled. FT-IR spectroscopy is a standard method for the detection of ethene,[220] but suffers severely from its cross-sensitivity to water, an omnipresent analyte.

In principle, mass-sensitive detection based on quartz microbalances (QMB) provides an inexpensive and robust method to detect volatile compounds.[221] A QMB utilizes the piezoelectric effect of quartz plates coated with a sensor-active layer. Upon binding of the analyte, the resulting mass increase lowers the resonance frequency (see chapter 4.4.2). A combination of sensor arrays (see Fig. 4.7) with different coatings and pattern recognition software also provides the necessary selectivity to distinguish different analyte molecules in mixtures so that cross-sensitivity problems can be solved.[222]

However, two problems hamper the gravimetric detection of ethene: (i) its low molecular weight, which directly affects the sensor response and (ii) the fact that the double bond is the only functional group, which can be utilized for binding the analyte to the sensor-active layers.[223] Correspondingly, all attempts with either commercial polymer-coated QMB's or home-made analogues coated with typical organic receptor molecules did not yield any detectable signal, when ethene was present in the gas stream.

6.2.2 Experimental Setup

For the experiments discussed here, 167 μm thick 10 MHz quartz plates with one gold electrode on each side were electrospray-coated[153] with a 0.084 μm (=5 kHz frequency shift) or 0.168 μm (=10 kHz frequency shift) or 0.252 μm (=15 kHz frequency shift) thick layer of the metallo supramolecular macrocycles[26,61,63,66] and metal complexes shown in Scheme 6.2.

Palladium and platinum complexes are excellent candidates for the detection of ethene, because they represent stable 16 electron complexes that may offer a binding site to the ethene. At the same time, the binding energy of the analyte

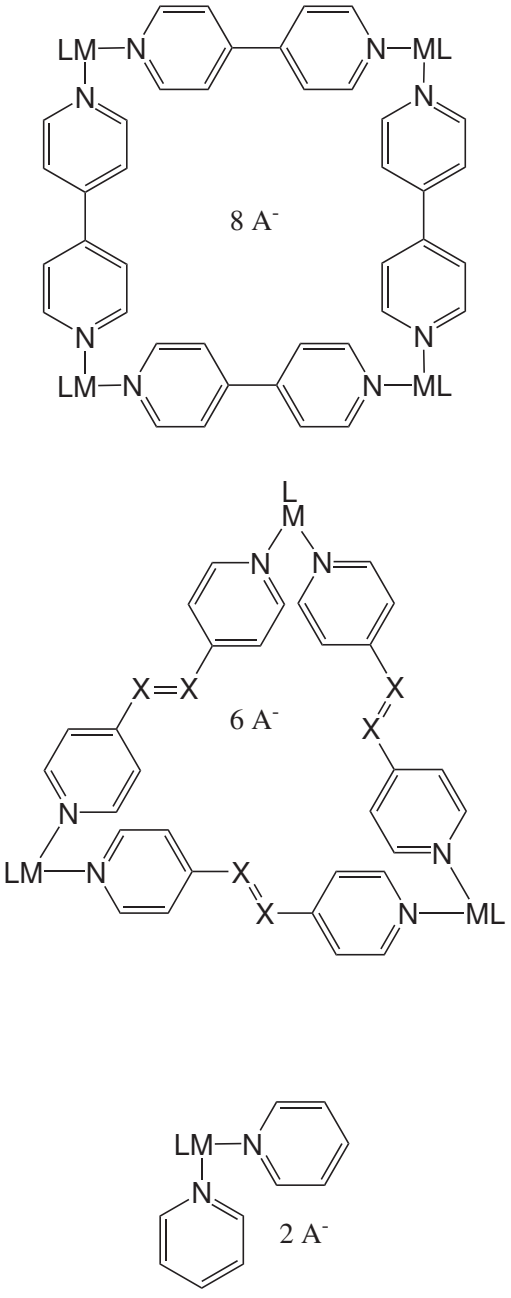

[QMB1] M = Pd, L= (dppp), A = OTf^-
[QMB2] M = Pt, L= (dppp), A = OTf^-
[QMB3] M = Pd, L= (en), A = NO_3^-
[QMB4] M = Pt, L= (en), A = NO_3^-

[QMB5] M = Pd, L= (dppp), X = CH, A = OTf^-
[QMB6] M = Pd, L= (dppp), X = N, A = OTf^-
[QMB7] M = Pt, L= (dppp), X = CH, A = OTf^-
[QMB8] M = Pt, L= (dppp), X = N, A = OTf^-
[QMB9] M = Pd, L= (en), X = CH, A = NO_3^-
[QMB10] M = Pd, L= (en), X = N, A = NO_3^-
[QMB11] M = Pt, L= (en), X = CH, A = NO_3^-
[QMB12] M = Pt, L= (en), X = N, A = NO_3^-

[QMB13] M = Pd, L= (dppp), A = OTf^-
[QMB14] M = Pt, L= (dppp), A = OTf^-
[QMB15] M = Pd, L= (en), A = NO_3^-
[QMB16] M = Pt, L= (en), A = NO_3^-

Scheme 6.2: Materials **QMB1** - **QMB16** for coating the QMB sensors. In solution, self-assembled supramolecular triangles[224] **QMB5** to **QMB12** are in equilibrium[225] with the corresponding squares.

is expected to be quite low due to the preference of these metals to form square planar complexes with 16 valence electrons.[226] From the low binding energies, one may expect binding to be reversible —a necessary prerequisite for a real-time sensor. Twelve sensors were transferred at a time into a temperature controlled measuring chamber and exposed to a 200 ml/min flow of dry nitrogen containing a defined concentration of ethene in the range of 0-1000 ppm by volume.

6.2.3 Results and Discussion

In contrast to all purely organic and macromolecular substances tested, all metal complexes give rise to a detectable frequency shift when ethene is present. This indicates that binding occurs at the metal centers. Nevertheless, compounds with larger cavities give rise to a higher sensor response. In particular **QMB9** and **QMB12** are excellent ethene sensor-active layers. Tentatively, we attribute the higher sensor responses of the macrocyclic compounds to the presence of cavities in the sensor-active layer, which may provide the necessary space for binding of ethene and the required conformational flexibility at the metal centers. In addition, electronic effects at the metal centers depending on the presence of bis-1,3-diphenylphosphinopropane (dppp) versus ethylene diamine (en) ligands are expected to play a role. In the following, we focus on the best sensor-active compound observed so far, i.e. **QMB12**. For this substance, measurements were performed with variable layer thicknesses and at different temperatures. With increasing temperatures T, the sensor response decreases. The increase in sensor response with increasing layer thickness provides evidence for volume sorption of ethene and clearly rules out exclusive binding on the surface.

Thus, calculating binding energies on a basis of Langmuir isotherms would usually not applicable. On the other hand, using a Brunauer-Emmet-Teller isotherm neither is appropriate because it does not allow us to describe a saturation situation like the one observed in our cases. The solution to this problem is a model taking into account surface adsorption with a very small equilibrium constant (i.e. predominantly on the side of desorbed ethene molecules) combined with a rather high diffusion rate of ethene within the coating. Both assumptions perfectly fit into the physico-chemical behavior one would expect from ethene regarding ad-

sorption on and diffusion into coatings: ethene hardly adheres to any kind of organic coating material, but once it finds an appropriate site to dock onto (here the metal centers) it quickly diffuses into the volume due to great mobility which it owes to weak binding. For all coatings under study the ratio of bound ethene (derived from the QMB's frequency shift) to metal centers never exceeds 1 indicating the presence of a single binding site on each metal atom. This result is not only in line with expectation, but also corroborates our DFT calculations described below. On the basis of these arguments a standard Langmuir isotherm (Eq. 6.1) together with Arrhenius' equation (Eq. 6.2) may be used to derive the binding energy of the analyte from a plot of ln$b$ versus $1/T$ in the present case (S and S_0 are the observed and maximum frequency shifts, b is the curvature factor of the isotherm, and c the analyte concentration).[227] With this approach, we determine a quite low binding energy of ethene of ca. -1 kJ/mol.

$$S = S_0 \frac{bc}{(1+bc)} \tag{6.1}$$

$$b(T) = \frac{k_A}{k_D} \;\; \alpha \;\; \exp \frac{E_B}{k_b T} \tag{6.2}$$

For comparison with the experimental binding energy, resolution-of-the-identity[228] density-functional-theory (RI-DFT) calculations were performed with "Turbomole 5"[229](Becke-Perdew functional[230] with TZVPP basis sets and effective core potential (ECP for Pt, 60 core electrons). In order to reduce the computational cost, only a truncated model complex, **QMB16**, was used. The calculated local minimum of 7.6 kJ/mol obtained for the most favorable adsorbed complex using TZVPP basis sets and a pseudopotential for Pt (ECP-60)[231] indicates a slightly metastable binding state. Within the DFT error bar, the binding energy obtained here is still close to the very weak interaction determined experimentally. The deviation is mainly ascribed to the truncated model and to the limited size of the basis set, as evidenced by a significantly unfavorable local minimum of 24.2 kJ/mol obtained with the smaller SVP basis sets. Several other binding possibilities have been considered, among them ligand exchanges, which replace one of the ethylene diamine or a pyridine ligand by ethylene. They are all significantly less favorable in energy. In the most favorable structure, ethene is bound in the

plane of a distorted trigonal-bipyramid formed around the metal center with Pt-C distances of 2.12 Å and a C-C bond length of 1.44 Å. The Pt-N2 bond length of pyridine in plane is elongated to 2.29 Å as compared to the model complex before ethene binding (2.05 Å). Also, the Pt-N3 distance to the ethylene diamine ligand increases from 2.09 to 2.36 Å upon ethene binding.

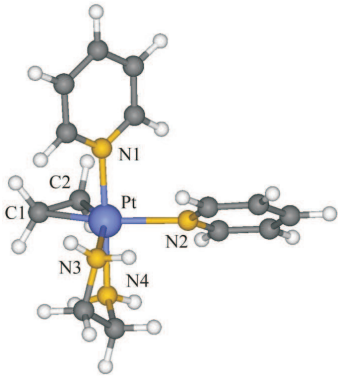

Figure 6.11: Ball and stick model of the ethene-**QMB16**-complex. The distorted trigonal-bipyramidal structure is clearly visible.

With **QMB12**, the extrapolation of the linearly fitted part of the Langmuir isotherm yields a lower detection limit for ethene of 3 ppm. In the range between 5 and 100 ppm, the sensor response correlates linearly with analyte concentration (Fig. 6.12). At higher ethene concentrations, i.e. 100-600 ppm, the concentration/sensor response correlation can be fitted with a second order polynomial (Fig. 6.12). Consequently, a calibration of the sensor is easily possible and a quantitative determination of the ethene concentration is feasible between 3 and 600 ppm, a highly attractive range for many practical applications which is not easily covered by other methods. Above 600 ppm, the sensor approaches saturation, which indicates binding of ethene at specific sites in the sensor-active layer.

Upon a change of the ethene concentration, the sorption equilibrium is reached within minutes. Thus, the sensor responds quickly and is suitable for real time measurements. To get a more detailed insight into the kinetics of ethene diffusion into the sensor-active layer, a simulation on the basis of a model combining Langmuir surface absorption and volume diffusion was performed.[153,230] Experimental and simulated sensor responses for two different layer thicknesses were compared.

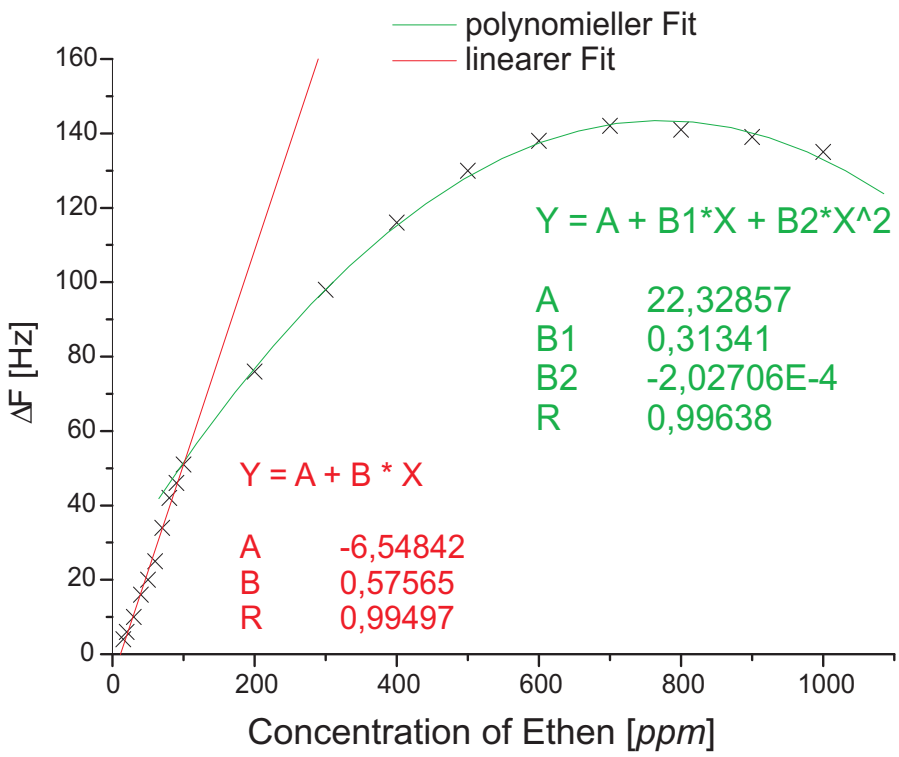

Figure 6.12: Linearly fitted Langmuir isotherm of the "ethene concentration : sensor response"-correlation for **QMB12** in the range of 3-100 ppm. Langmuir isotherm fitted to a second order polynomial in the ethene concentration range of 100-1000 ppm.

Both simulations have been carried out with the same set of parameters.[232] Only the maximum uptake of ethene, which directly correlates to the layer thickness, had to be altered in order to receive good fits in both cases. According to these simulations, ethene diffusion through a layer of **QMB12** is characterized by a diffusion coefficient of $2.3 \cdot 10^{-10} m^2 s^{-1}$ which on the minute time scale of the experiment nicely agrees with layer thicknesses in the upper nanometer range.[233]

Interestingly substance **QMB12** is not only the most sensitive of all tested coatings towards ethene but it also shows the lowest cross sensitivities towards other analytes like cyclohexanone, nitromethane or toluene. The strongest cross sensitivity with a frequency shift of 95 Hz at 1000 ppm was measured for nitromethane. Substitution isomers of ethene (tetrachloroethylene, trichloroethylene, cis and trans-dichloroethylene and 2,3-dimethyl-2-butene) at a concentration of 1000 ppm all produce a frequency shift of less than 30 Hz (best: tetrachloroethylene, 28 Hz, worst: 2,3-dimethyl-2-butene, 8 Hz). Thus, one can say that also the selectivity of **QMB12** towards the almost completely unfunctionalized substance ethylene is amazingly high.

6.2.4 Summary and Conclusion

For the first time, a real-time gravimetric detection of trace amounts of ethene in the range of 5–600 ppm could be realized using metallo-supramolecular macrocycles as sensor-active layers that bear Pd and Pt centers. The thermodynamic analysis, theoretical calculations, simulations, and control experiments with purely organic control compounds all corroborate ethene binding at the metal centers rather than inside the cavities formed by the macrocycles. Interestingly, this interaction does not only occur on the surface, but uses the whole volume of the sensor active layer. Since an inexpensive platform for an array of six differently coated QMB sensors has already been developed for the detection of other volatile analytes,[234] the transfer of these results into commercial applications should be easily possible. Nevertheless, cross-sensitivities with other volatile compounds have to be taken into account. Preliminary results indicate that these issues can be resolved. Particularly helpful in this respect is the fact that ethene did not give any sensor response with organic and macromolecular coatings. Such coatings

however respond to the presence of many other analytes, particularly water, from which ethene needs to be distinguished.

6.3 Mass Spectrometric Investigation of Oligothiophene-Based Macrocycles, Catenates and Catenanes[‡]

6.3.1 Introduction

Oligo- and polythiophenes are organic semiconductors that have important applications in organic electronics.[255] Thus, α-conjugated oligothiophenes have become one of the most investigated classes of compounds for studying structure–property relationships in organic electronic materials of a defined structure over the past two decades.[256] In this context, a protocol for the synthesis of α-conjugated oligothiophene macrocycles was recently published.[257] Besides their unexpected properties due to their cyclic structure,[258] they represent a model of an ultimate, defect-free conjugated oligothiophene chain. In the past few years, several attempts have been made towards the realization of individually addressable, switchable devices based on interlocked macrocyclic structures.[259] Catenanes have been intensively investigated and several synthetic approaches towards these compounds utilizing highly efficient templating strategies[101] have been developed in the past few decades.

In this respect, it was the goal to prepare new conjugated supramolecular topologies based on oligothiophene macrocycles that combine their electronic material benefits and the properties of a defined supramolecular architecture. Nevertheless, threading of an oligothiophene chain through a conjugated macrocycle and the subsequent preparation of intertwined conjugated catenanes represents a yet unsolved major synthetic challenge. The design of interlocked π-conjugated

[‡]The results of this section were obtained in collaboration with Dr. M. Ammann, Dr. M. Wilde, Dr. G. Götz and Dr. E. Mena-Osteritz in the working group of Prof. Dr. P. Bäuerle (University of Ulm) and are published in references.[253,254] The compounds in this section are numbered **OTC** for **O**ligo**T**hiophen-Based **C**atenanes.

macrocycles by an efficient strategy calls for the use of specific template binding sites that do not interrupt the molecule's entire π-conjugation. Therefore, among all the available template methods, the well-known [1,10]phenanthroline-based catenane synthesis originally introduced by Sauvage and coworkers[260] appeared to be the most suitable approach and is the basis for the synthesis of the first conjugated catenates.

6.3.2 Compounds Under Investigation

The following seven compounds, platinum macrocycle **OTC1**, bis-platinum copper catenate **OTC4**, deplatinated copper catenate **OTC5** and open chain copper adduct **OTC6**, with three thiophene units per ring respectively as well as platinum macrocycle **OTC2**, macrocycle **OTC3** and catenane **OTC7**, with four thiophene units, (see Scheme 6.3) were prepared by Dr. M. Ammann and Dr. M. Wilde in the group of Prof. Dr. P. Bäuerle. Their synthesis and characterization by NMR are described in detail in the references.[253,254]

6.3.3 Structural Proof of the Macrocycles, Catenates and Catenanes by MS

The synthesis of catenanes is still a considerable challenge, as is the identification of their intertwined topology. If no crystal structure is available, NMR experiments may provide some evidence. They often reveal up-field chemical shifts for the signals of those parts of a macrocycle that are inserted into the cavity of the other.[100,261] However, this is not necessarily the case for all catenanes because this effect is often caused by the anisotropy of aromatic rings incorporated in the two macrocycles of the catenane. Mass spectrometry represents a complementary method of investigation.[262] In addition to the analytical characterization with respect to the exact mass, charge state and isotope patterns, MS allows gas-phase experiments to be carried out in which molecules can be studied under environment-free conditions. Tandem mass spectrometric (MS/MS) experiments such as collision-induced dissociation (CID) provide an insight into a molecule's reactivity and often indirectly into its structural features such as

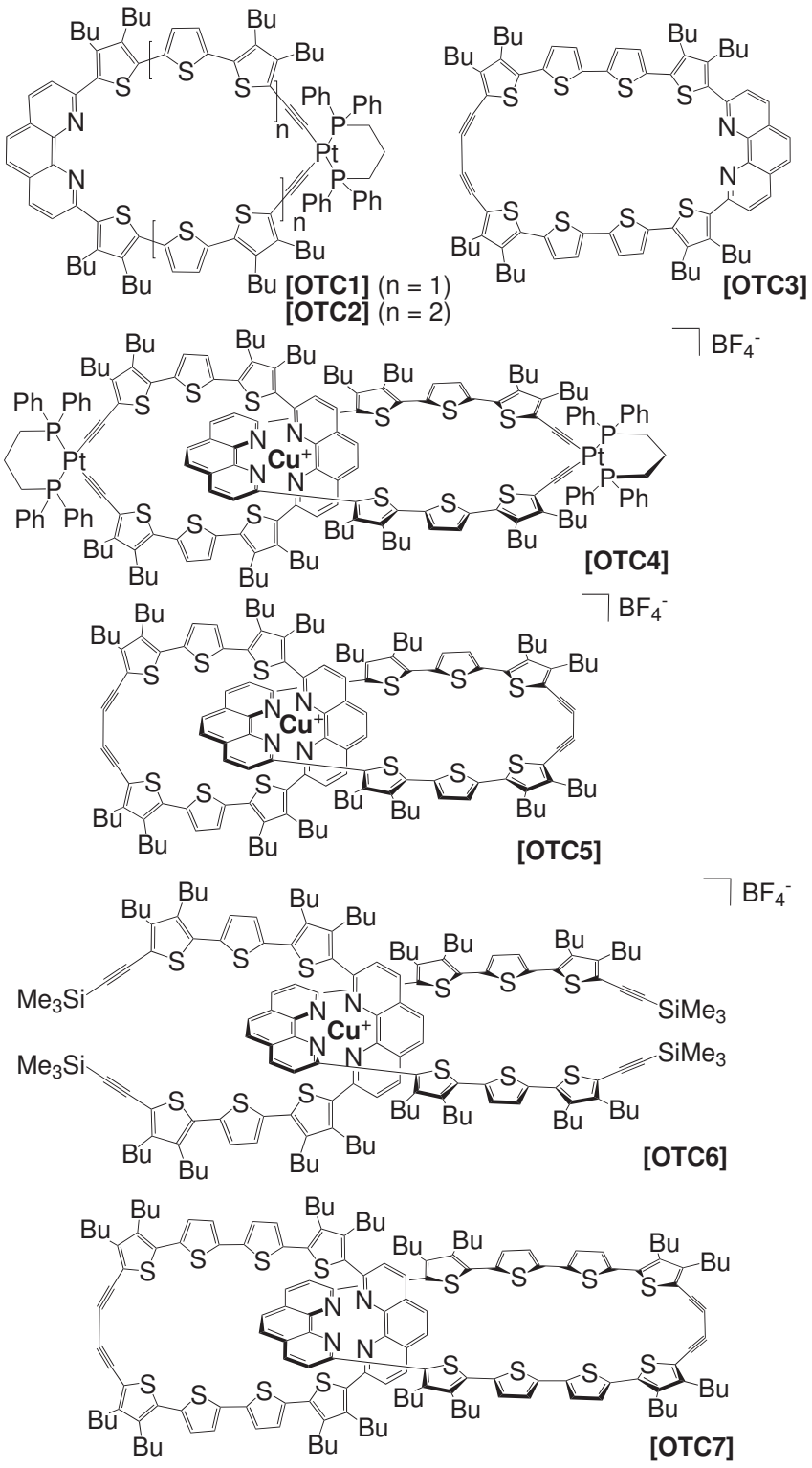

Scheme 6.3: Oligothiophene-Based Macrocycles, Catenates and Catenanes **OTC1** - **OTC7**.

guest encapsulation[125,263] and intertwined topologies.[126,127] Consequently, tandem electrospray-ionization Fourier-transform ion-cyclotron-resonance (ESI-FT-ICR) mass spectrometry provides an insight into the structures of the compounds under study here and their reactivity in the gas phase (for an introduction see 4.2.3).

Macrocycles **OTC1** and **OTC2** can be charged by two different methods. Spraying them from methanol solutions leads to the protonated species with signals at m/z = 1775.57815 Da $[M+H]^+$ for **OTC1** (Δm = 15 ppm) and m/z = 2328.78884 Da $[M+H]^+$ for **OTC2** (Δm = 8 ppm), respectively. Spraying these compounds from a nonacidic solvent gives rise to small contributions of radical cations which points to the ease of one-electron oxidation of the fully conjugated macrocycles. These radical cations could almost be completely suppressed in favor of the protonated compounds when trifluoroacetic acid is added to the solution. On the other hand, adding a small amount of $[Cu(CH_3CN)_4]BF_4$ to acetonitrile solutions of **OTC1** and **OTC2** leads to the corresponding copper adduct peaks which appear at m/z = 1837.3 Da $[M+Cu]^+$ for **OTC1** and at m/z = 2391.7 Da $[M+Cu]^+$ for **OTC2**.

Catenates **OTC4** and **OTC5** are easily ionized by the loss of the counteranion. Electrospray ionization from acetonitrile solutions results in a peak at m/z = 3612.85458 Da [**OTC4** – BF_4]$^+$ (Δm = 3 ppm) for catenate **OTC4** and a peak at m/z = 2398.91162 Da [**OTC5** – BF_4]$^+$ (Δm = 8 ppm) for catenate **OTC5** (see Figure 6.14 a) and b).

Methanol solutions (again with 0.5% CF_3CO_2H) of **OTC3** and **OTC7** generate ions corresponding to [**OTC3**+H]$^+$ and [**OTC7**+H]$^+$ at the expected m/z values of 1331.4693 Da (Δm = 5 ppm) and 2661.9399 Da (Δm = 8 ppm), respectively (see Figure 6.14 c).

Not only the exact masses of these seven compounds, but also the isotope patterns agree excellently within the error margins with those calculated on the basis of natural abundances, thus confirming the elemental compositions (see Figure 6.13 insets).

While the ESI mass spectrum of **OTC5** proves the presence of a pure sample and does not show any decomposition products, two major fragments are

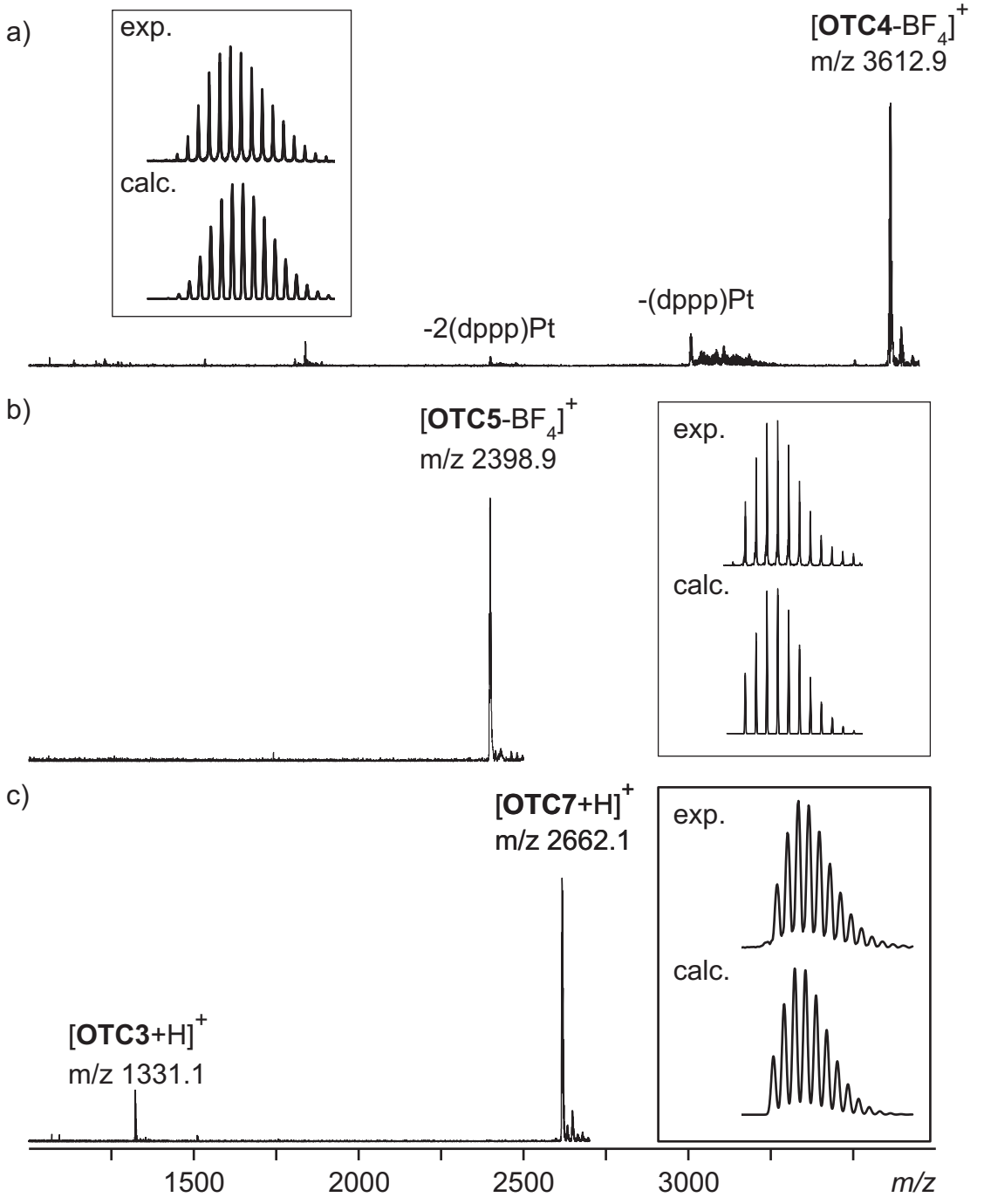

Figure 6.13: ESI-FT-ICR mass spectra of a) **OTC4**, b) **OTC5** and c) **OTC7** (ca. $30 \cdot 10^{-6}$M solutions in acetonitrile a) and b) or methanol c)); Insets: isotope patterns (experimental and calculated on the basis of natural isotope abundances).

observed in the spectrum of **OTC4** whose relative and absolute intensities vary with the spray conditions. One signal is observed at m/z = 3005.8 Da, which is more prominent than the second one at m/z = 2398.6 Da under soft ionization conditions, but still small relative to the parent-ion base peak. The second signal, which has the same mass as catenate **OTC5**, increases in intensity with harsher ionization conditions at the expense of both the parent ion and the first signal at m/z = 3005.9 Da. The fact that the relative intensities vary with ionization conditions indicates that both are fragments of the parent catenate [**OTC4** – BF_4]$^+$ rather than impurities in the sample. We have therefore attributed these signals to consecutive losses of two neutral [(dppp)Pt] moieties (Δm = 607 Da) formed during the ionization process or subsequently in the gas phase. To confirm this, mass-selected [**OTC4** – BF_4]$^+$ is subjected to a tandem MS experiment in which it is collisionally activated with argon as the collision gas in the FT-ICR cell (CID). Again, the two major fragments are observed at m/z = 3005.9 Da (Δm = 607 Da) and m/z = 2398.9 Da (Δm = 1214 Da = 2×607 Da) (see Figure 6.14 a). As these masses correspond to the loss of two [(dppp)Pt] units, it is suggested that two consecutive reductive eliminations of [(dppp)Pt] lead to the formation of catenate **OTC5** from catenate **OTC4** in the gas phase. After the reductive eliminations, two fully conjugated, catenated macrocycles are obtained. Further support for this structural assignment comes from three additional experiments.

- When the collision energy is increased in the CID experiment with bis-platinum copper catenate [**OTC4** – BF_4]$^+$, a series of fragmentations of the *n*-butyl side-chains is observed from the [**OTC4** – BF_4 – 2 (dppp)Pt]$^+$ ion following the two-fold reductive elimination [i.e., –30 Da (C_2H_6), –42 Da (C_3H_6), –44 Da (C_3H_8), –58 Da (C_4H_{10})], etc. relative to the fully deplatinated ion peak at m/z = 2398.9 Da. Instead, the loss of one of the ligands of the copper ion almost vanishes within the noise.

- Under the same collision conditions, catenate **OTC5** shows the same series of fragmentations of the *n*-butyl side-chains (see Figure 6.14 b). Owing to the completely conjugated nature of the intertwined macrocycles, all bonds within the macrocycle are difficult to cleave. In addition, simple bond cleavage within the macrocycle backbone alone would not give rise to fragmen-

tation because both halves are still connected through coordination to the CuI ion. Consequently, the cleavage of C–C single bonds in the *n*-butyl side-chains represents the lowest energy processes.

- As a control experiment, intermediate **OTC6**, a copper-bridged dimer, is subjected to a CID experiment. Since it is an open-chain analogue of **OTC5**, it can either give fragments of the *n*-butyl chains or decompose with the loss of one of the ligands from the central copper ion. The monoisotopic ions of **OTC6** are isolated (m/z = 2687.1 Da) and upon collisional activation the only fragment observed is m/z = 1375.1 Da, which corresponds to the loss of one neutral ligand (see Figure 6.14 c). As no further fragments between the parent ion and the daughter ion are observed, the weakest bonds are now the two dative N–Cu bonds. Because the structure is not mechanically bound, one ligand can easily be removed. This is in marked contrast to the fragmentation of [**OTC5** – BF_4]$^+$ and [**OTC4** – BF_4 – 2 (dppp)Pt]$^+$, in which ligand loss would require an additional bond cleavage within the fully conjugated macrocycles to permit the loss of one ligand from the copper ion.

These three observations provide definitive and independent evidence (i) for the catenated structure of both **OTC4** and **OTC5** and (ii) for the feasibility of the reductive elimination processes leading to ring-closure in the gas phase, when the ions are collisionally activated, which basically means that their internal energy is increased. Since no oxidant is present in the high vacuum of the mass spectrometer, ring-closure occurs without oxidation of the [(dppp)Pt] moieties.

As the mass as well as the elemental composition of catenane **OTC7** is the same like two individual macrocycles **OTC3** and a two times larger macrocycle, high resolution mass spectrometry can not be used to distinguish these three possible compounds. But as the reactivity of the three compounds in the gas phase might be different, MS-MS investigations might be able to distinguish these three substances. Mass-selected 2262.1 Da, the mass of the protonated three substances, is subjected to collision-induced dissociation. The only fragment stemming from cleavage of a covalent bond within the macrocycle backbone corresponds to loss of one complete wheel. As in case of catenate **OTC5**, a series of alkyl chain losses from the *n*-butyl groups on the thiophene rings originating from both the

parent catenane and the macrocycle are also found (see Figure 6.14 d). Macrocycle **OTC3** shows the same series of alkyl side-chain fragmentations in an analogous MS-MS experiment. This fragmentation pattern is not in line with a weak, proton-bridged, complex of two non-intertwined wheels, because the extensive losses of alkyl groups cannot compete with dissociation of such a weak complex into two separate macrocycles. Neither does the fragmentation pattern support a single, large macrocycle with the elemental composition of the catenane, since the only backbone fragment (excluding the losses of alkyl groups) is the loss of one wheel. This behavior is typical of catenanes, in which only one covalent bond within a macrocycle backbone needs to be broken, while a single macrocycle would require the cleavage of two covalent bonds and thus should lead to a number of different fragments. The only remaining topology is consequently that of a catenane.

An overview of the four collisionally induced dissociations (CID) can be found in Figure 6.15.

6.3.4 Properties of the Catenane

The geometrical structure and preferred conformation in solution of catenane **OTC7** and macrocycle **OTC3** are investigated by detailed analysis of ^{1}H NMR and 2D-NMR spectra in combination with semi-empirical calculations. One set of signals in the ^{1}H NMR spectra of macrocycle **OTC3**, a down-field shift of the β protons on the "inner" thiophene rings and a up-field shift of the closest phenanthroline protons (H3, H3') relative to those of the open chained precursor, point to a symmetric over-all conformation of the macrocycle and to a distortion of the "inner" thiophene rings. This proposal agrees well with calculations which gave a symmetrical minimum energy conformation in which the "inner" thiophene rings are rotated by 95–100°, thus leading to a puckering of the phenanthroline unit by 27° from coplanarity (see 6.16). According to calculations, a fully coplanar conformation of macrocycle **OTC3** could be achieved by an *anti* arrangement of one "inner" thiophene ring, thus leading to a nonsymmetric structure.

Additionally, STM experiments on monolayers of macrocycle **OTC3** adsorbed on graphite display the symmetrical structure of the conjugated macrocycle **OTC3** (see Figure 6.17). The same trends are found in the ^{1}H NMR spectra of catenane

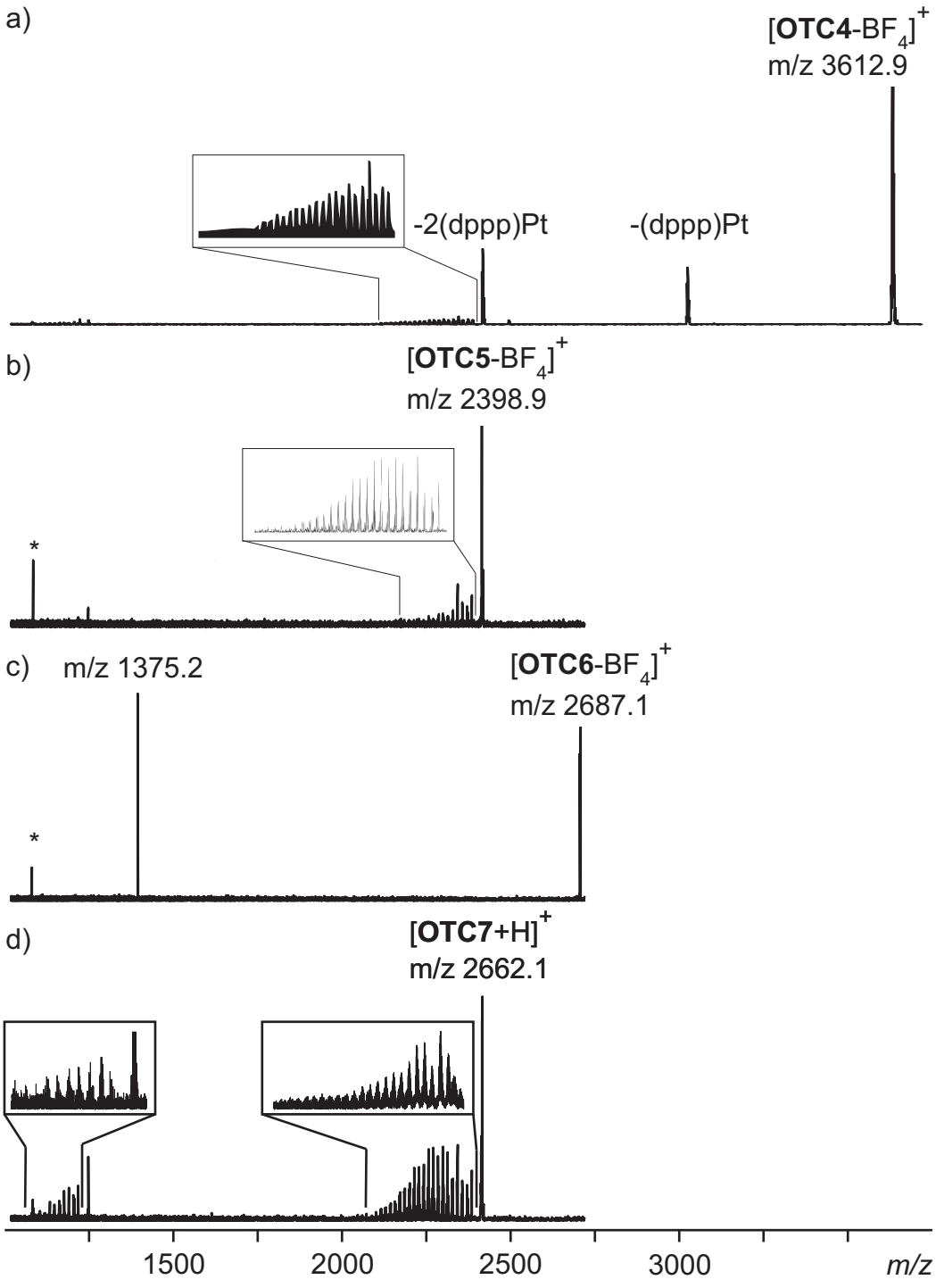

Figure 6.14: Tandem mass spectra (CID) of a) **OTC4**, b) **OTC5**, c) **OTC6** and d) **OTC7**; Insets: fragmentations from bond cleavages of the *n*-butyl chains; * radio peak.

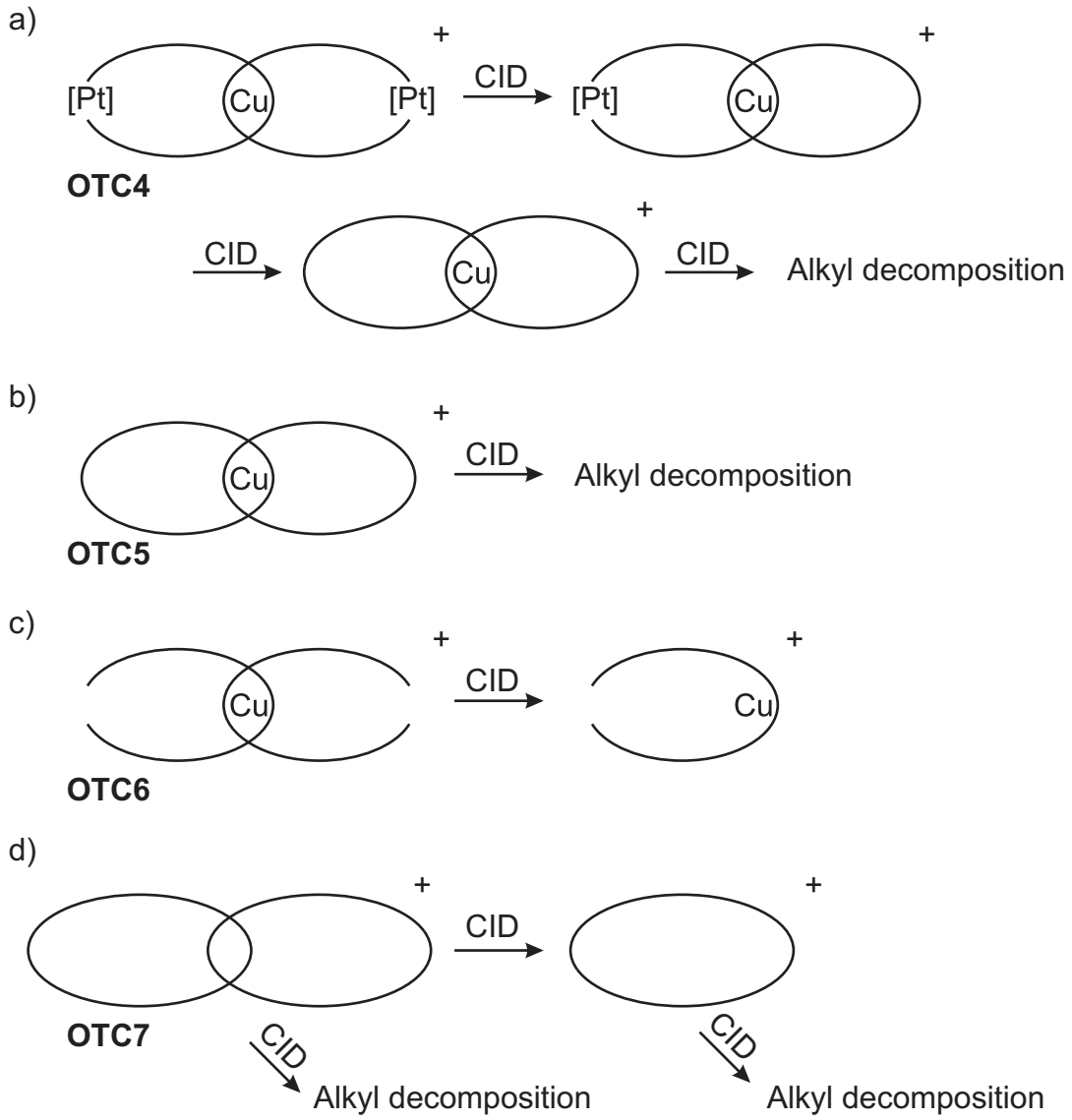

Figure 6.15: Illustration of the collisionally induced dissociations (CID) of a) **OTC4**, b) **OTC5**, c) **OTC6** and d) **OTC7**.

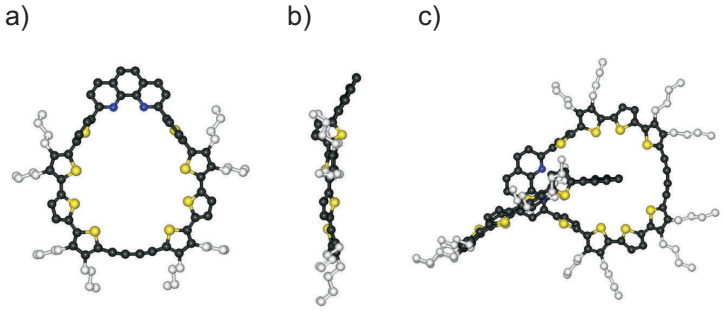

Figure 6.16: Calculated minimum energy conformation of macrocycle **OTC3** (a) top view, b) side view) and c) catenane **OTC7**.

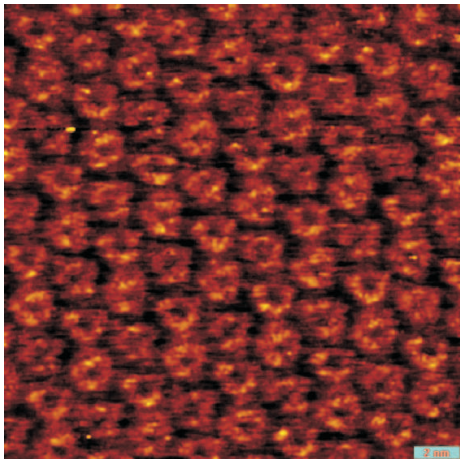

Figure 6.17: STM image of a monolayer of macrocycle **OTC3** at the solid (highly ordered pyrolytic graphite; HOPG)/liquid (1,2,4-trichlorobenzene) interface.

OTC7, and temperature-dependent measurements showed that the dynamic motion of the two interlocked macrocycles, which is frequently found for conventional catenanes,[264] is hindered up to 100°C. Calculations predict a stable minimum energy conformation of catenane **OTC7** consisting of two puckered, but intertwined symmetric macrocycles of **OTC3**.

Catenane **OTC7** is a unique molecular system in which the conjugated macrocycles are mechanically kept in proximity and may influence each other electronically "through space". Investigation of the optical and redox properties of **OTC7** compared to those of macrocycle **OTC3** provides clear evidence for a mu-

tual interaction between its two rings. The absorption spectra of both compounds showed a broad band arising from the $\pi - \pi^*$ transition of the conjugated system, with a maximum at nearly the same position and a tailing at lower energy, which is typical for cyclothiophenes[258] (see Figure 6.18). However, the molar extinction coefficient is doubled for catenane **OTC7**, thus indicating an additive contribution of both rings in the intertwined system. If both spectra are normalized (same concentration of rings), a difference spectrum shows additional bands for catenane **OTC7** from which the band at lower energy (λ=530 nm) indicates an inter-ring charge-transfer (CT) transition. This finding is compatible with the conformation discussed above in which the (oligo)thiophene donor units in one ring are in proximity to the phenanthroline acceptor unit of the other ring. The decrease in the fluorescence quantum yield of catenane **OTC7** (ϕ = 2%) relative to that of macrocycle **OTC3** (ϕ = 6%) is also consistent with a quenching arising from an "intermolecular" charge-transfer interaction in catenane **OTC7**.

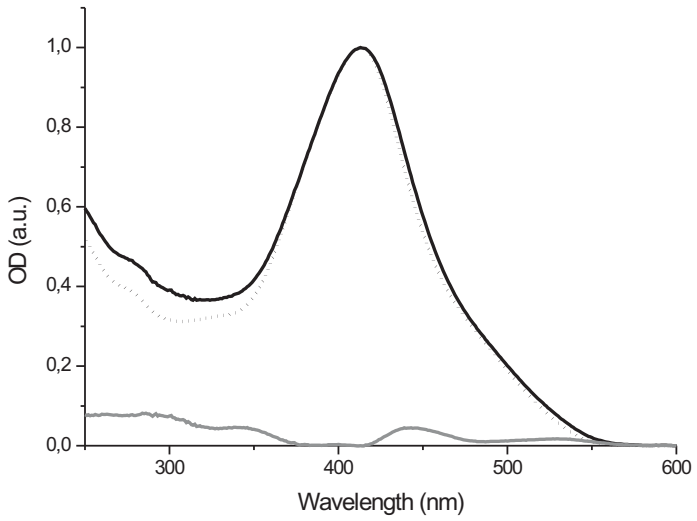

Figure 6.18: Normalized absorption spectra of catenane **OTC7** (solid black line) in comparison to that of macrocycle **OTC3** (dotted line) in dichloromethane and a difference spectrum comparing the two compounds (gray line).

Cyclic voltammetry studies show the remarkably different redox properties of

OTC7 and **OTC3** (see 6.19). The important electrophores in our systems are the four thiophene units which typically are oxidized reversibly to radical cations and dications by successive one-electron transfers. The corresponding potentials at which these processes occur generally depend on electronic influences in the vicinity of the electrophore. In this respect, macrocycle **OTC3** shows first and second one-electron oxidation at potentials slightly negative of those of open-chained precursor, which correspond to the formation of stable radical cations. Further oxidation leads to tri- and tetracationic macrocycles at potentials which are more positive than those of the precursor. All oxidation processes (of the four thiophene units) of intertwined catenane **OTC7** are in general shifted to positive potentials because of the proximity of the electron withdrawing phenanthroline unit. This effect is also due to inter-ring, through-space, donor–acceptor interactions, and strongly corroborates the symmetrical and puckered conformation discussed above.

6.3.5 Summary

In conclusion, a unique "π-conjugated catenane" is prepared consisting of intertwined oligothiophene–phenanthroline macrocycles as a novel topological structure in the field of conjugated oligomers and polymers by a double metal template strategy. The interesting optical and redox properties found are in line with the structural and conformational analysis, which gave clear evidence that the two macrocycles in catenane **OTC7** influence each other by through-space donor–acceptor interactions.

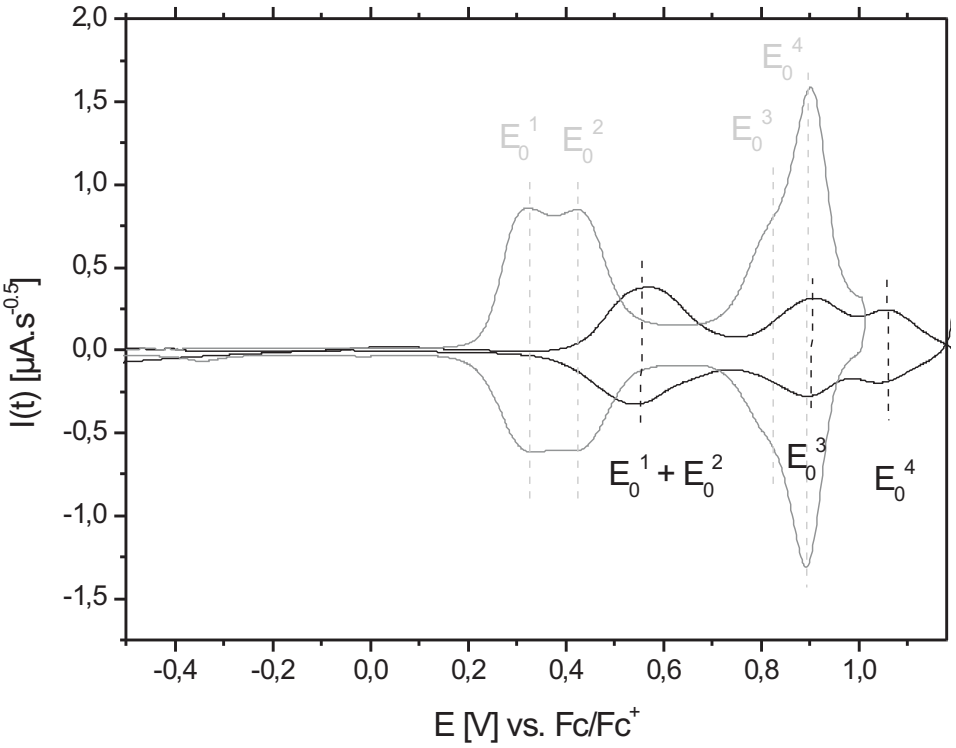

Figure 6.19: Deconvoluted cyclic voltammogram of catenane **OTC7** (black line) in comparison to that of macrocycle **OTC3** (gray line) (**OTC7**: 2.5×10^{-4}M, **OTC3**: 5.0×10^{-4}M, in CH_2Cl_2/0.1M $(C_4H_9)_4NPF_6$ at 295 K, v=100 mVs^{-1}, potentials versus the ferrocene/ferrocenium (Fc/Fc+) couple.

Chapter 7

Summary and Outlook

7.1 Summary

The aims of this thesis are divided into seven sections. Hence, the summary adopts this structuring.

1. **A Supramolecular Construction Kit of Functional Self-Assembled Metallo Supramolecular Squares**

   SAMS have proven themselves to be interesting materials for several application within the Collaborative Research Initiative 624 at the University of Bonn.

   (a) For the first time, a real-time gravimetric detection of trace amounts of ethene in the range between 5 and 600 ppm could be realized using SAMS as sensor-active layers. In particular **QMB9** and **QMB12** are excellent ethene sensor-active layers.

   (b) Furthermore, SAMS and related compounds (like *Stoddart's* Cyclobis-(paraquat-p-phenylene)) have been successfully adsorbed and monitored by means of EC-STM using a second order template effect. High-resolution images were recorded from the cyclophanes lying flatly on the electrode surface with their cavities pointing towards the solution. In some cases, high lateral ordering with only minor defects, in other cases, stacking of further assemblies on top of the first monolayer were

observed. Useful information (size, reactivity towards chloride) was extracted.

(c) In addition to literature known SAMS, a convergent synthetic strategy towards functionalized [4,4']-bipyridines was developed: Key steps of the reaction sequence are (i) a modified reductive coupling of several alkyl-pyridines (picolines and lutidines), (ii) conversion of two methyl groups into carboxylic acids (oxidation or deprotonation followed by quenching with carbon dioxide) and (iii) standard peptide coupling reactions (acid chlorides or PYBOP).

(d) As an unexpected by-product of the synthetic effort, an alternative route towards dihydro-[3,8]-phenanthrolines was found. This roughly developed route is neither short nor cheap, but affords unusually substituted [3,8]-phenanthrolines.

2. **Self-Assembled Defect Free Dendrimers**

With the above mentioned reaction sequence self-assembled dendrimers of the third generation were synthesized with molecular masses of more than 15000 Da, which allowed valuable inside into their self-assembly reactions like the effect of the metal complex (Pd vs. Pt) or the solvent of choice. Visualization of films of these dendrimers using atomic force microscopy (AFM) provided information on their molecular dimensions as well as their multi-layer formation. The results of this study were not described in this thesis but can be found in the references.[195]

3. **Chiral Self-Assembled Supramolecular Squares**

Two sorts of chiral SAMS were developed:

(a) SAMS from alanine-decorated bipyridines showed an outstanding heterochiral self-sorting.[268] The absolute configuration of one final assembly was determined on the basis of crystal structure analysis.

(b) SAMS from axially chiral [4,4']-bipyridines. This completely new class of compounds was obtained by an elegant reaction sequences either flexible (with CH_2-Spacer) or stiff (without any spacer). Three different

racemic mixtures were separated into their enantiomers by means of chiral HPLC. Enantiopure ligands show a notably selective self-assembly in marked contrast to their racemic mixtures.

4. **Isomeric Structures in Self-Assembly**

   560 independent isomers could be identified. [4,4']-Bipyridines, substituted with small and achiral residues, showed overlapping peaks in the ^{1}H NMR spectra indicating mixture formation. Dendron substituted [4,4']-bipyridines allowed valuable inside into their self-assembly reactions. In case of the sterically demanding axially chiral ligands, the amount of possible isomers could be narrowed down to two isomers, which could however not been safely assigned. In the solid-phase structures of alanine-decorated SAMS, only one isomer was found exclusively. NMR analysis gave clear evidence that only this isomer is formed in solution, too. These results, give a first insight, which factors govern the outcome of self-assembly.

5. **Unidirectional Self-Assembled Supramolecular Squares**

   The synthesis of the desired ligand for unidirectional SAMS was successfully carried out. Unfortunately, all attempts to grow single crystals of the final assembly failed, so that an incontestable evidence for unidirectionality could not be given.

6. **Mass Spectrometric Investigations of *Fujita*-Squares** have proven to be far more difficult than the corresponding *Stang*-square measurements. However, ionization (and complete desolvation) was accomplished by exchanging the anion (PF_6^- instead of NO_3^-) and the solvent (nitromethane). First insight into interesting dissociation pathways was obtained. As these results are only preliminary, further investigation are advisable to get more profound insight.

7. **Mass Spectrometric Investigation of Oligothiophene-Based Macrocycles, Catenates and Catenanes by ESI-FTICRMS**

   A unique "π-conjugated catenane" was prepared by the working group of Prof. Bäuerle (Ulm) consisting of intertwined oligothiophene–phenanthroline

macrocycles. The interesting optical and redox properties found were in line with the structural and conformational analysis, which gave clear evidence that the two macrocycles in the catenane influence each other by through-space donor–acceptor interactions. Structural proof for this catenation came from MSMS measurements, in which further evidences were found for the complete conjugation. Moreover, MSMS studies of platinated precursors macrocycles and catenates showed an unexpected reactivity in the gas phase: Reductive eliminations at the platinum centers were observed in the gas phase, yielding fully conjugated macrocycles.

In conclusion, the aims of this thesis were exceeded. Results of this study were incorporated in twelve accepted publications as well as six poster contributions. Nevertheless, science will never answer all possible question. Thus, an of course incomplete list of impulses might be found in the next sub chapter.

7.2 Outlook

Hantzsch [4,4']-Bipyridine Reaction

The Hantzsch dihydropyridine/pyridine reaction sequence allows the preparation of dihydropyridine derivatives by condensation of an aldehyde with two equivalents of a β-ketoester in the presence of ammonia. Subsequent oxidation gives pyridine-3,5-dicarboxylates, which may be decarboxylated to yield the corresponding pyridines. As seen in Scheme 7.1, the aldehyde component can be isonicotinaldehyde, yielding [4,4']-bipyridines.[265] Thus, this sequence might be an ideal opportunity to obtain sterically demanding [4,4']-bipyridines with further functional groups like amides.

Enantioselective Deprotonation of Tetramethyl-[4,4']-bipyridine

Axially-pro-chiral 2,2',6,6'-tetramethyl-biphenyl can be twofold deprotonated with *n*-butyllithium. An enantioselective dilithiation in the presence of the chiral auxiliary (-)-spartein, followed by quenching with gaseous carbon dioxide, yields (+)-2,2'-(6,6'-dimethyl-biphenyl-2,2'-diyl)diacetic acid in moderate stereoselectivity (40%ee).[266] The absolute configuration of the chiral diacid is thereby still unknown. As the methyl protons of 3,5,3',5'-tetramethyl-[4,4']-bipyridine **24** are

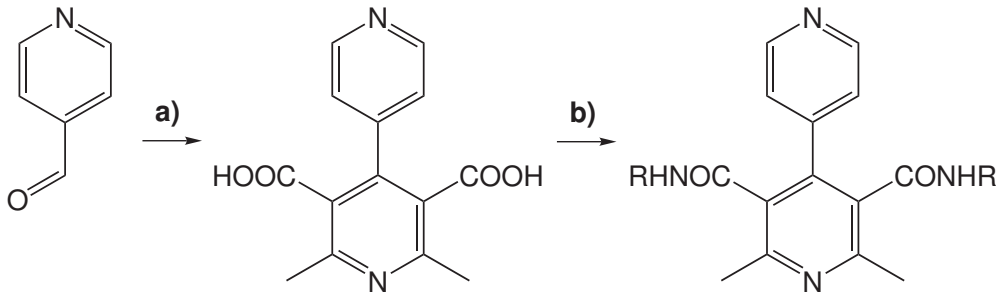

Scheme 7.1: a) Hantzsch [4,4']-bipyridine reaction; b) standard amide coupling conditions.

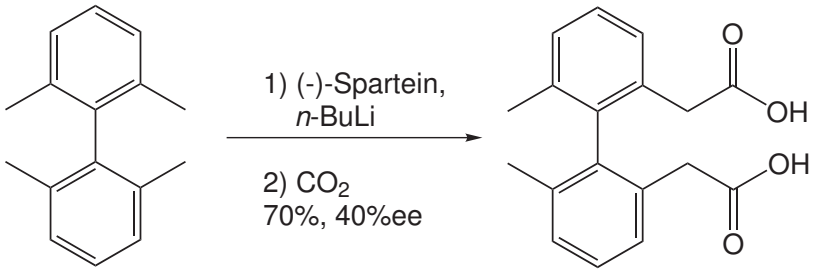

Scheme 7.2: Enantioselective deprotonation of 2,2',6,6'-tetramethyl-biphenyl with (-)-spartein in 70% with 40%ee.

less acidic than those of 2,2',6,6'-tetramethyl-biphenyl, (-)-spartein might however not be strong enough for twofold deprotonation. Nevertheless, these results demonstrate nicely that enantioselective dilithiation might be a promising route towards axially chiral diacid **56**.

Chiral Separation by Crystallization

As the solubility of chiral diacids **52** and **56** is poor in organic solvents, separation into enantiomers with chiral HPLC seems not to be operable. A promising alternative might hence be the use of chiral ion exchange resins[267] (water as mobile phase).

On the other hand, some racemic compounds are known to crystallize as 1:1 mixtures of enantiopure crystals. More efficient is the chiral crystallization with the use of resolving agents to form diastereomeric salts, which is a widely used technique for resolving chiral compounds. The racemic mixtures of chiral diacids **52** and **56** might thus be resolved by crystallization with chiral amines like brucine or sparteine. However, the approach to resolve chiral compounds by this method

is still conducted mainly on a trial-and-error basis.

When larger amounts of enantiopure diacids will become available, these chiral bipyridines will offer a versatile platform for further functionalization through ester or amide bond formation or the reduction of the acids to the corresponding aldehydes and alcohols.

Labeled Enantiomers in Square Formation

The results from chapter 5.3.3.1 and 5.3.3.2 show that the outcome of self-assembly is completely different, when either racemic mixtures of axial chiral ligands are used or enantiopure ligands. NMR Spectroscopy seems not to be feasible to study these complex product mixtures. Mass spectrometric investigations of mass-labeled enantiomers might however be the method of choice. **(*aR*)-88** dif-

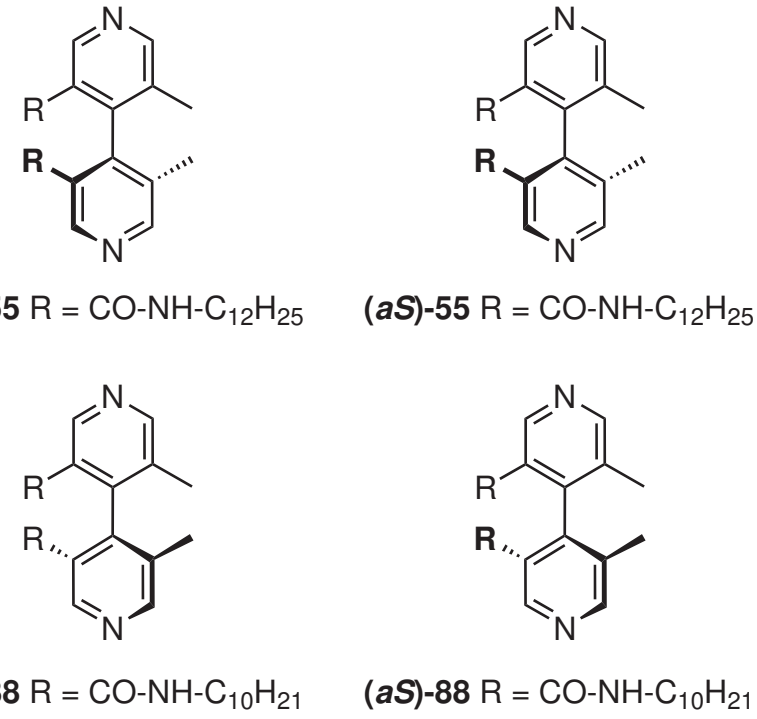

Scheme 7.3: Axial chiral [4,4']-bipyridine-derivatives **55** and **88**.

fers from **(*aR*)-55** (see Scheme 7.3) only by the length of its alkyl chains ($C_{10}H_{21}$ and $C_{12}H_{25}$). This should however not have any significant impact on their self-assembly reactions. 1:1:2 mixtures of **(*aR*)-55**:**(*aR*)-88**:[a] should hence show a statistical ligand-distribution within the squares' peaks:

(1:4:6:4:1 = $\mathbf{55}_4\mathbf{88}_0$:$\mathbf{55}_3\mathbf{88}_1$:$\mathbf{55}_2\mathbf{88}_2$:$\mathbf{55}_1\mathbf{88}_3$:$\mathbf{55}_0\mathbf{88}_4$, all (aR)).
Even though the palladium squares show broad isotope patterns, this distribution should be easily observable be MS, as the peaks are separated by 56 Da. 1:1:2 mixtures of **(*aR*)-55**:**(*aS*)-88**:**[a]** should however show a significant deviance from the statistical distribution. These results would nicely put the finishing touch to the previously discussed results.

Amino Acid Decorated [4,4']-Bipyridines

Alanine decorated [4,4']-bipyridines have been used palmy in self-assembly reactions. Thereby, the amino acid substituents avoid sterical congestion with dppp's phenyl groups. Due to the modular approach, larger amino acids can easily be attached to the [4,4']-bipyridine-system. These larger residues might however increase the sterical congestion, hence, hamper or alter the outcome of the self-assembly reactions. When smaller blocking ligands instead of dppp are designed, even small peptide-chains might be attached to self-assembled supramolecular squares.

Chapter 8

Experimental Part

8.1 List of Abbreviations

br	broad signal	CID	Collision Induced Decay
CSI	Cold Spray Ionization	Cq	quaternary carbon atom
d	doublet	DMF	N,N-dimethylformamide
DMSO	dimethylsulfoxide	EtOAc	ethyl acetate
EI	Electron Ionization	ESI	ElectroSpray Ionization
FAB	Fast Atom Bombardment	FT	Fourier-Transformation
ICR	Ion Cyclotron Resonance	IRMPD	IR Multi Photon Dissociation
J	coupling constant [Hz]	m	multiplet
$M^{\cdot+}$	molecular radical cation	MALDI	Matrix Assisted Laser
MeOH	methanol		Desorption Ionization
quart	quartet	MHz	megahertz
R_f	retention factor	quin	quintet
t	triplet	s	singlet

8.2 General Techniques

- The routine NMR spectra were recorded on a Bruker Avance 300 (^{1}H: 300 MHz, ^{13}C: 76 MHz) and a Bruker AM 400 (^{1}H: 400 MHz, ^{13}C: 101 MHz). All

NMR spectra are recorded at 298 K, unless otherwise stated.

- Variable temperature measurements were performed on a Bruker DRX 500 (^{1}H: 500 MHz, ^{13}C:125 MHz, ^{19}F: 470 MHz, and ^{31}P: 202 MHz).

- 2D-NMR measurements (HH-COSY, HMQC, HMBC) were recorded on a Bruker AM 500 (^{1}H: 500 MHz, ^{13}C: 126 MHz).

- All ^{1}H chemical shifts are reported in ppm relative to residual non-deuterated solvent signals as the internal standard: [D_6]-acetone (2.05 ppm), [D_3]-acetonitrile (1.94 ppm), [D_1]-chloroform (7.27 ppm), D_2O (4.80 ppm), [D_7]-dimethylformamide (2.75 ppm), [D_6]-dimethylsulfoxide (2.50 ppm), and [D_4]-methanol (3.31 ppm). ^{13}C chemical shifts are given in ppm relative to the carbon resonance of the deuterated NMR solvent: [D_6]-acetone (29.92 ppm), [D_3]-acetonitrile (1.39 ppm), [D_1]-chloroform (77.23 ppm), [D_7]-di-methyl formamide (29.76 ppm), [D_6]-dimethylsulfoxide (39.51 ppm), and [D_4]-methanol (49.15 ppm). ^{31}P chemical shifts are provided in ppm relative to external 86% H_3PO_4 (0.00 ppm). ^{19}F chemical shifts are reported relative to external $CFCl_3$ (0.00 ppm).

- GC/MS measurements were performed with two Hewlett-Packard instruments (Palo Alto, USA): GC HP 5890 Series II (Crosslinked Methyl Silicon column, 0.2μm core) and MS HP 5989A both at 70 eV.

- EI(HighRes) spectra were measured on a Thermo Finnigan instrument (Bremen, Germany): MAT 95 XL (sector mass spectrometer).

- High-resolution ESI mass spectra and MS/MS spectra were recorded on a Bruker (Bremen, Germany) Apex IV FT-ICR mass spectrometer (7 T-Magnet, Apollo electrospray ion source). For a detailed description see chapter 4.2.4.

- **Chiral HPLC**: The semi-preparative enantiomer separations of the racemic 4,4'-bipyridine derivatives **54**, **55** and **58** were carried out with an Agilent 1100 Series HPLC system (Waldbronn, Germany), consisting of a quaternary gradient pump, a solvent degasser, a multiple wavelength UV-detector,

an autosampler, and a column thermostat. Fraction collection was achieved via time-controlled by an Agilent 1200 Series 12 position/13 port-selection valve integrate downstream at the UV detector unit. System operation and data processing were performed using HP ChemStation software, installed on a personal computer. The enantiomer separations were carried out with a analytical column (250 x 4.6 mm core), packed with a chiral stationary phase based on tris-(3,5-dimethylphenyl)cellulose, covalently immobilized to macroporous 10 μm spherical silica gel.[184] The employed mobile phase was a mixture of n-heptane/2-propanol (15:1, v/v). The flow rate was 1 mL/min, and the column temperature was kept at 25±1°C. Peaks were monitored by UV detection at multiple wavelengths (230, 254, 270, 360 nm). Samples were injected as filtered solutions in chloroform (50 mg/ml), and injection volumes were typically 30 to 80 μL, corresponding to a specific sample load of 1.5 to 4.0 mg racemic 4,4'-bipyridine derivative per run. Due to the extreme peak tailing of the analytes, even at low sample loads, "safe" fraction collection was firstly programmed to collect the front region of the first eluting enantiomer, to pool the middle section to a mixed fraction, and collect the rear section of the second eluting enantiomer. To improve yields, the mixed fractions were reprocessed after evaporation of the solvents. The first and third fractions were evaporated under reduced pressure at a bath temperature < 40°C to avoid thermally-induced racemization. The respective enantiomerically enriched bi-pyridines were obtained as colorless solids, generally with ee $> 92\%$.

- **CD**: CD-Spectra were recorded with a Jasco J-810 Spektrophotometer (Jasco Corp., Tokyo, Japan). Cell: 1 mm and 10 mm (Hellma, Müllheim, Germany); solvent: methanol (spectrophotometric grade, 99.9%, Sigma).

- **Melting Points**: Melting points were measured with an homebuilt instrument (Elektronikwerkstätten Chemie Uni Bonn, Germany) and are uncorrected.

- **CHN Elemental Analysis**: The elemental compositions were determined with a Vario EL (Heraeus, Hanau, Germany).

- **Thin Layer Chromatography**: Merk's (Darmstadt, Germany) precoated thin layer chromatography plates were used (60 F254).

- **Column Chromatography**: Stationary phase: Merk's (Darmstadt, Germany) silica gel (0.063-0.200μm); mobile phase as stated in the experimental section (pre-distilled, solvent grade).

- **Commercially available starting materials**: Starting materials were purchased from the following suppliers and were used without further purifications: Acros Organics, Aldrich, Fluka, Lancaster, Merck, and Riedel De Haen.

- **Solvents**: All solvents were distilled prior to use.[269]

8.3 Synthesis of Organic Precursors

4-Chloro-3-nitro-pyridine 16[270]

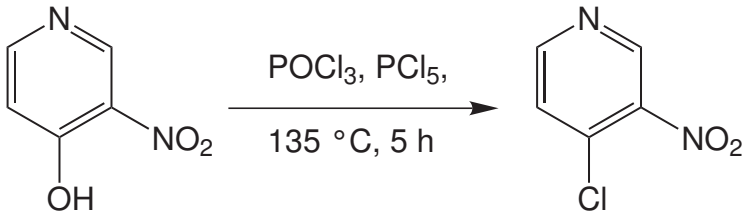

Procedure modified from *Reich et al.*[270] In 17 ml phosphorylchloride, 1.7 g phosphorpentachloride and 1.000 g (140.1 g/mol, 7.1 mmol) 3-nitro-pyridin-4-ol **15** are heated at 135 °C for 5 hours. The volatile compounds were removed *in vacuo* and the residue is poured in 100 ml of ice. The aqueous phase is brought to pH = 8 with solid sodium carbonate and extracted with diethylether (3 times 25 ml). The combined organic phases are dried over magnesium sulphate and the diethylether is removed *in vacuo*. The crude product can be used without further purification. Yield of the crude product: 0.996 g, 6.3 mmol, 88%. Analytical clean 4-chloro-3-nitro-pyridine **16** can be obtained by distillation (90°C at 2 mbar).

Mol. Weight: 158.6 g/mol ($C_5H_3ClN_2O_2$).

MS (GC-MS): (R_t= min): m/z (%): 158 ($M^{\cdot+}$,87), 112 ($[M-NO_2]^+$, 100), 85 ($[M-NO_2-HCN]^+$, 90).

Melting Point: 154 °C (154-155 °C[271]).

3,3'-Dinitro-[4,4']-bipyridine 17[169]

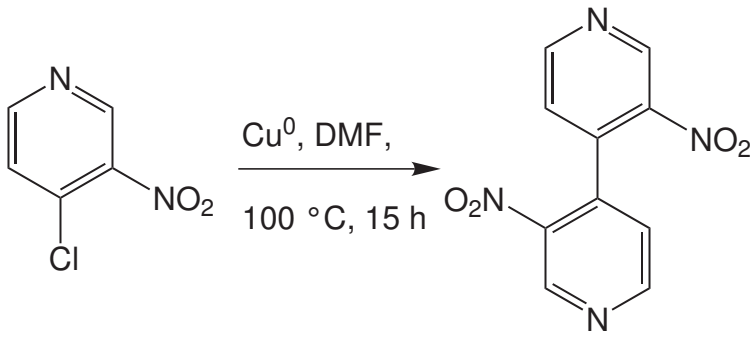

Procedure modified from *Kanoktanaporn et al.*[169] (Valuable discussion with T. Weilandt is gratefully acknowledged). In 7 ml of dry dimethylformamide, 4-chloro-3-nitro-pyridine **16** (2.04 g, 158.6 g/mol, 12.9 mmol) and copper powder (2.00 g, 63.6 g/mol, 31.50 mmol) were suspended and heated under argon for 15 hours at 100°C. 40 ml aqueous ammonia solution are added and the aqueous phase is extracted with diethylether until the extract is colorless. The combined organic phases are washed with water (20 ml) and dried over magnesium sulphate. All volatile compounds are removed *in vacuo* (GCMS-analysis). Yield: (0.767 g, 3.1 mmol, 48%).

Mol. Weight: 246.2 g/mol ($C_{10}H_6N_4O_4$).

MS (GC-MS): (R_t= 8.67 min): m/z (%): 216 ($[M-NO]^+$, 5),
200 ($[M-NO_2]^+$, 100),
170 ($[M-NO_2-NO]^{\cdot+}$, 10),
144 ($[M-NO_2-NO-C_2H_2]^{\cdot+}$, 30),
117 ($[M-NO_2-NO-C_2H_2-HCN]^{\cdot+}$, 35),
90 ($[M-NO_2-NO-C_2H_2-HCN-HCN]^{\cdot+}$, 40).

Melting Point: 129 °C (127-128 °C[169]).

[4,4']-Bipyridinyl-3,3'-diamine 18[169,272]

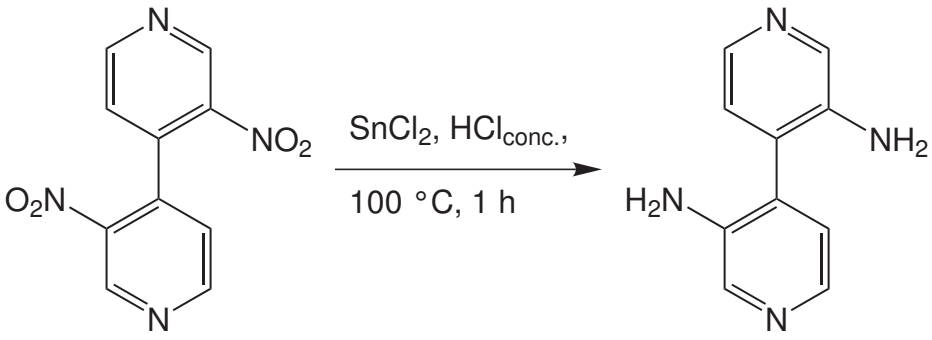

Procedure modified from *Kanoktanaporn et al.*:[169]
In 14 ml hydrochloric acid, 0.695 g (246.2 g/mol, 2.8 mmol) 3,3'-dinitro-[4,4']-bipyridine **17** and 5.101 g (22.6 mmol) tin dichloride dihydrate were suspended and heated at 100 °C for 1 hour. The precipitate is filtered of and resolved in water The aqueous phase is brought to pH = 8 and stored at 4 °C over night. White crystals are filtered off and dried roughly. Yield 0.563 g (77%).

Mol. Weight: 186.2 g/mol ($C_{10}H_{10}N_4$).

MS (GC-MS): (R_t= min): m/z (%): 186 ($M^{\cdot+}$, 100), 185 ($[M-H]^+$, 18), 170 ($[M-NH_2]^+$, 10), 169 ($[M-NH_3]^{\cdot+}$, 10), 159 ($[M-HCN]^{\cdot+}$, 6), 158 ($[M-H-HCN]^+$, 7).

Melting Point: > 250 °C (276-277 °C[169]).

3,3'-Dimethyl-[4,4']-bipyridine 20[170]

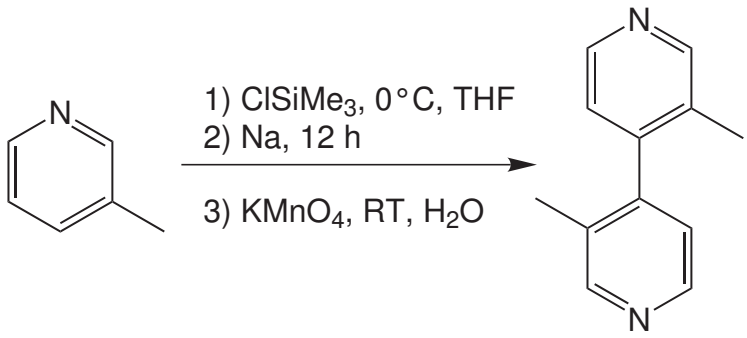

Procedure modified from *Rebek et al.*:[170] In dry diethylether, (instead of tetrahydrofuran) 3-methyl pyridine **19** (18.5 ml, 0.95 g/ml, 17.6 g, 93.1 g/mol, 189 mmol), chlorotrimethylsilane (1 eq.) and sodium (1.05 eq., small portions) were added at 0°C. The suspension was stirred for 24 hour and dried roughly. The residue is extracted with hot toluene several times until the extract is colorless. The toluene is removed and the residue is dried roughly, again. An acetone-water-mixture and solid potassium permanganate is added under stirring until the characteristic color remains. Stirring is continued for further 30 min., the solid is filtered off, washed with a warm acetone-water-mixture and the acetone is removed from the filtrate. The aqueous phase is extracted with chloroform several times until the extract is colorless. After drying over sodium sulfate and removing of the solvent, the crude product was purified by flash chromatography. Yield: 8.35 g, 90.7 mmol, 48 % (instead of 40 %[170]).

R_f-Value: 0.52 (5:1)=(ethylacetate:methanol).

Mol. Weight: 184.1 g/mol ($C_{12}H_{12}N_2$).

^{1}**H-NMR**: (400 MHz, Chloroform-d_1) δ (ppm): 8.55 (d, $^4J_{HH} = 0.6$ Hz, 2 H, H-2 and H-2'), 8.50 (dd, $^3J_{HH} = 5.0$ Hz, $^4J_{HH} = 0{,}6$ Hz, 2 H, H-6 and H-6'), 7.00 (d, $^3J_{HH} = 5.1$ Hz, 2 H, H-5 and H-5'), 2.25 (s, 6 H, H_{CH_3}).

^{13}C-NMR: (100 MHz, Chloroform-d_1) δ (ppm): 151.6, 147.8, 146.7, 130.8, 123.2, 16.8.

File Name(s): 2002, 51x4a073.

MS (GC-MS): (R_t= 6.167 min): m/z (%): 184 ($M^{\cdot+}$, 100), 183 ($[M\text{-}H]^+$, 71), 169 ($[M\text{-}CH_3]^+$, 35), 168 ($[M\text{-}CH_3\text{-}H]^+$, 23), 157 ($[M\text{-}HCN^{\cdot+}$, 14), 156 ($[M\text{-}H\text{-}HCN]^+$, 18), 142 ($[M\text{-}CH_3\text{-}HCN]^+$, 28), 128 ($[M\text{-}CH_3\text{-}HCN\text{-}CH_2]^+$, 9).

Melting Point: 124°C.

3,3'-Diethyl-[4,4']-bipyridine 22

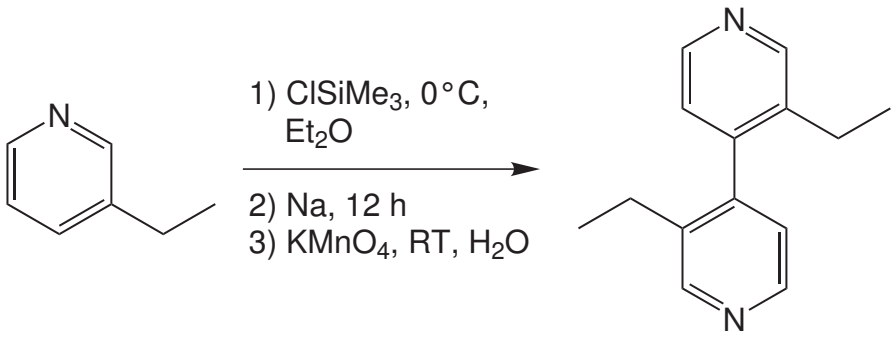

Procedure modified from *Rebek et al.*:[170] In dry diethylether, 3-ethyl-pyridine **21** (1.05 ml, 0.95 g/ml, 1.00 g, 107.2 g/mol, 9.3 mmol), chlorotrimethylsilane (1 eq.) and sodium (1.1 eq., small portions) were added at 0°C. The suspension was stirred over night and dried roughly. The residue is extracted with hot toluene several times until the extract is colorless. The toluene is removed and the residue is dried roughly, again. An acetone-water-mixture and solid potassium permanganate is added under stirring until the characteristic color remains. Stirring is continued for further 30 min., the solid is filtered off, washed with a warm acetone-water-mixture and the acetone is removed from the filtrate. The aqueous phase is extracted with chloroform (3 times 10 ml). After drying over sodium sulfate and removing of the solvent, the crude product was purified by flash chromatography (Yield: 194 mg, 0.9 mmol, 19 %).

R_f-Value: 0.40 (ethylacetate).

Mol. Weight: 212.2 g/mol ($C_{14}H_{16}N_2$).

^{1}H-NMR: (400 MHz, Chloroform-d_1) δ (ppm):8.59 (s, 2 H, H-2 and H-2'), 8.49 (d, $^3J_{HH}$ = 5.0 Hz, 2 H, H-6 and H-6'), 7.00 (d, $^3J_{HH}$ = 5.0 Hz, 2 H, H-5 and H-5'), 2.45 (m, 2 H, CH_2), 2.35 (m, 2 H, CH_2), 1.06 (t, $^3J_{HH}$ = 7.6 Hz, 6 H, CH_3).

^{13}**C-NMR**:	(100 MHz, Chloroform-d_1) δ (ppm): 150.6, 147.2, 145.9, 136.5, 123.4, 23.8, 15.1.
File Name(s):	2004, 44x4a105.
MS (GC-MS):	(R_t= 9.2 min): m/z (%): 212 ([M]$^{\cdot+}$, 100), 197 ([M-CH_3, 29), 183 ([M-C_2H_5, 46), 168 ([M-C_2H_5-CH_3 42), 156 ([M-C_2H_4-C_2H_4 13), 154 ([M-C_2H_5-C_2H_5 13).
MS (EI):	Exact mass: 212.1313 Da calc. for: $C_{14}H_{16}N_2$ 212.1311 Da (1 ppm).

3,5,3',5'-Tetramethyl-[4,4']-bipyridine 24

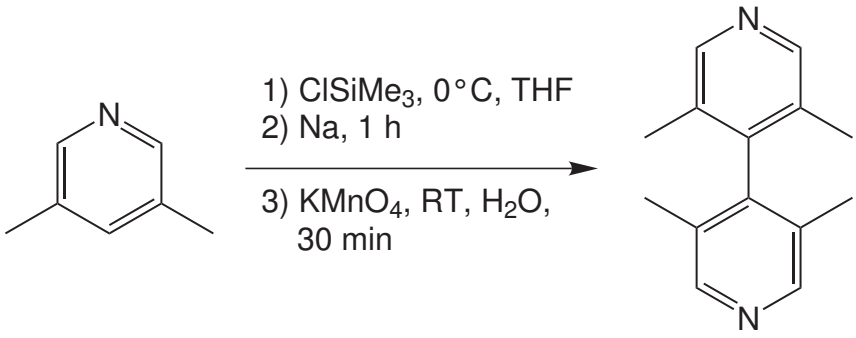

Procedure according to *Rebek et al.*[170] for 3,3'-dimethyl-[4,4']-bipyridine **20**. In diethylether, 3,5-dimethyl pyridine **23** (23.7 ml, 0.94 g/ml, 22.3 mg, 107.2 g/mol, 208.0 mmol), chlorotrimethylsilane (1 eq.) and sodium (1.05 eq., powder) were added at 0 °C. The suspension was stirred over night and dried roughly. The residue is extracted with hot toluene several times until the extract is colorless. The toluene is removed and the residue is dried roughly, again. An acetone-water-mixture and solid potassium permanganate is added under stirring until the characteristic color remains. Stirring is continued for further 30 min., the solid is filtered off, washed with a warm acetone-water-mixture and the acetone is removed from the filtrate. The aqueous phase is extracted with chloroform several times until the extract is colorless. After drying over sodium sulfate and removing of the solvent, the crude product was purified by flash chromatography. Yield: 10.1 g (47.8 mmol, 23 %)

R_f-Value: 0.57 (5:1)=(ethylacetate:methanol).

Mol. Weight: 212.3 g/mol ($C_{21}H_{25}N_3$).

^{1}H-NMR: (400 MHz, Chloroform-d_1) δ (ppm): 8.40 (s, 4 H, H-2, H-6, H-2' and H-6'), 1.90 (s, 12 H, H_{CH_3}).

^{13}C-NMR: (100 MHz, Chloroform-d_1) δ (ppm): 149.0, 145.0, 129.6, 16.3.

File Name(s): 2004, 15x4a017.

MS (GC-MS): (R_t= 6.879 min): m/z (%): 212 ($M^{\cdot+}$, 98), 197 ([M-CH_3]$^+$, 100), 182 ([M-CH_3-CH_3]$^{\cdot+}$, 34), 170 ([M-CH_3-HCN]$^+$, 18), 154 ([M-H-CH_3-CH_3-HCN]$^+$, 16), 128 ([M-CH_3-CH_3-HCN-HCN]$^+$, 11).

MS (EI): Exact mass: 212.1318 Da calc. for: $C_{14}H_{16}N_2$ 212.1313 Da (2.4 ppm).

Melting Point: 126 °C.

3,5-Dimethyl-4-trimethylsilanyl-pyridine 25

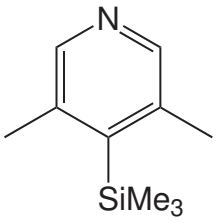

Byproduct in variable yields of 3,5,3',5'-tetramethyl-[4,4']-bipyridine **24**.

R_f-Value: 0.73 (ethylacetate).

Mol. Weight: 179.3 g/mol ($C_{10}H_{17}NSi$).

^{1}H-NMR: (300 MHz, Chloroform-d_1) δ (ppm): 8.13 (s, 2 H, H-2 and H-6), 2.36 (s, 6 H, H_{CH_3}), 0.39 (s, 9 H, $H_{Si(CH_3)_3}$).

^{13}C-NMR: (75 MHz, Chloroform-d_1) δ (ppm): 148.3, 146.3, 137.8, 21.3, 2.7.

File Name(s): 2005, 51x3a040.

MS (GC-MS): (R_t= 4.5 min): m/z (%): 179 ($M^{\cdot+}$, 64), 164 ([M-CH_3]$^+$, 80), 73 ([$Si(CH_3)_3$]$^+$, 100).

MS (EI): Exact mass: 179.1131 Da calc. for: $C_{10}H_{17}NSi$ 179.1130 Da (1 ppm).

Melting Point: liquid.

2,6,2',6'-Tetramethyl-[4,4']-bipyridine 27[273]

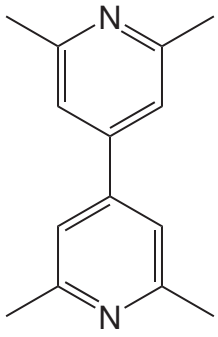

Sodium (2.91 g, 23 g/mol, 126.6 mmol, dispersion in toluene) and 2,6-dimethyl pyridine **26** (14.7 ml, 0.923 g/ml, 13.5 g, 107 g/mol, 126.6 mmol) were stirred in 100 ml diethylether inside an ultrasonic bath for 24 hours. Isopropanol (50 ml, to remove excess of sodium), and after 1 hour water (100 ml) are added. The pH-Value was adjusted to pH = 7 with dilute hydrochloric acid. Solid potassium permanganate is added under stirring until the characteristic color remains. Stirring is continued for further 30 min, the solid is filtered off, washed with a warm acetone-water-mixture and the acetone is removed from the filtrate. The aqueous phase is extracted with chloroform several times until the extract is colorless. After drying over sodium sulfate and removing of the solvent, the crude product was purified by column chromatography. Yield: 0.9 g (4.2 mmol, 7 %).

R_f-Value: 0.70 (28:1)=(dichloromethane:methanol).

Mol. Weight: 212.3 g/mol ($C_{14}H_{16}N_2$).

^{1}H-NMR: (400 MHz, Chloroform-d_1) δ (ppm): 7.16 (s, 4H, H-2, H-2', H-6 and H-6'), 2.59 (s, 12H, H_{CH_3}).

^{13}C-NMR: (100 MHz, Chloroform-d_1) δ (ppm): 158.6, 146.9, 118.2, 24.6.

File Name(s): 2005, 10x4b050.

MS (GC-MS): (R_t= 7.5 min): m/z (%): 212 ($M^{\cdot+}$, 100), 197 $[M-CH_3]^+$, 6), 51 ($[C_4H_3]^+$, 7).

5,6-Dihydro-[3,8]phenanthroline 30

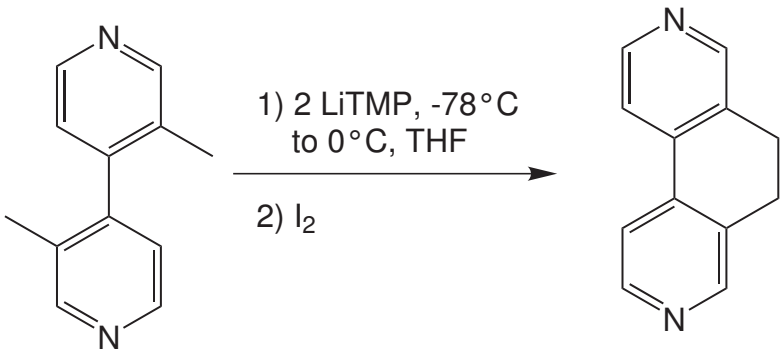

In 2 ml of dry THF 2.3 eq. 2,2,6,6-tetramethyl-piperidine were reacted with 2.3 eq. *n*-butyllithium (1.6 M solution in pentane) at -78 °C. After 30 min. at this temperature, 1 eq. of 3,3'-dimethyl-[4,4']-bipyridine **20** (505 mg, 2.7 mmol) was added in 1 ml of dry THF. The reaction mixture was allowed to warm to 0 °C and stirred for 2 h. The temperature was lowered to -78 °C again, 2.3 eq. of iodide in 2 ml of dry THF were added and the reaction mixture was stirred over night while it was allowed to warm to room temperature. Water (5 ml) was added and the aqueous layer was extracted with dichloromethane. The combined organic phases were dried over sodium sulfate and after removing of the solvents, the crude product was purified by flash chromatography (420 mg, 2.3 mmol, 85%).

R_f-Value: 0.25 (5:1)=(ethylacetate:methanol).

Mol. Weight: 182.1 g/mol ($C_{12}H_{10}N_2$).

^{1}H-NMR: (400 MHz, Chloroform-d_1) δ (ppm): 8.60 (d, $^3J_{HH}$ = 5 Hz, 2 H, H-6 and H-6'), 8.56 (s, 2 H, H-2 and H-2'), 7.61 (d, $^3J_{HH}$ = 5 Hz, 2 H, H-5 and H-5'), 2.94 (s, 4 H, $H_{ethylene}$).

^{13}C-NMR: (100 MHz, Chloroform-d_1) δ (ppm): 149.8, 149.1, 139.1, 132.2, 117.8, 24.8.

File Name(s): 2005, 39x4b004.

MS (GC-MS): (R_t= 7.922 min): m/z (%): 182 ($M^{\cdot+}$, 100), 181 ($[M-H]^+$, 95), 167 ($[M-CH_3)]^+$, 18), 154 ($[M-H-HCN]^+$, 27).

Melting Point: 127 °C.

[3,8]-phenanthroline 31

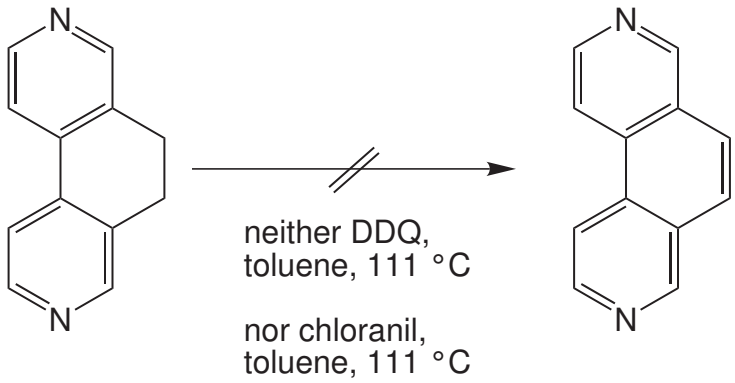

Small amounts of 5,6-dihydro-[3,8]phenanthroline **30** (typically 10 mg) were heated in toluene with two equivalents of oxidants chloranil or DDQ under reflux. After continuous heating (111 °C) for seven days, GCMS and TLC analysis showed in both cases no conversion of the starting material and the reactions were stopped. In the first case 95 % of the starting material could be recovered after flash chromatography, in the second case 85 %.

[4,4']-Bipyridinyl-3,3'-dicarboxylic acid 36[170]

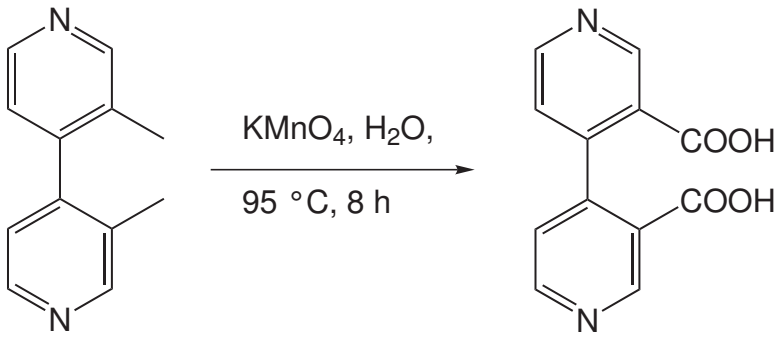

Procedure according to *Rebek et al.*[170] Yield (58 %, Lit.: 61 %). After filtration of the product, all volatile compounds of the filtrate are removed *in vacuo*. The resulting residue is recrystallized from methanol, to yield another 15 % of crude [4,4']-bipyridinyl-3,3'-dicarboxylic acid **36**.

Mol. Weight: 244.2 g/mol ($C_{12}H_8N_2O_4$).

Melting Point: > 250°C (Lit.: > 250°C[170]).

[4,4']-Bipyridinyl-3,3'-dicarboxamide 37

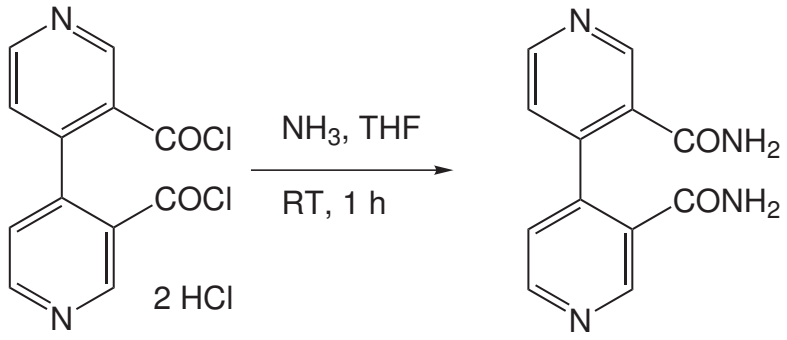

In 15 ml tetrahydrofuran, [4,4']-bipyridinyl-3,3'-dicarbonyl dichloride dihydrochloride (260 mg, 354.0 g/mol, 0.73 mmol) is suspended and gaseous ammonia is led through the suspension for 5 min. The suspension is stirred for 1 hour and all volatile compounds are removed *in vacuo*. The resulting residue is resolved in water and stored at 0 °C for 48 hours. White crystals are filtered off and dried roughly. Yield (160 mg, 0.66 mmol, 90%).

Mol. Weight: 242.2 g/mol ($C_{12}H_{10}N_4O_2$).

^{1}H-NMR: (400 MHz, dimethylsulfoxide-d_6) δ (ppm): 8.76 (s, 2H, H-2 and H-2'), 8.66 (d, $^3J_{HH} = 5$ Hz, 2H, H-6 and H-6'), 8.05 (b, 2H, H_{amid}), 7.55 (b, 2H, H_{amid}), 7.19 (d, $^3J_{HH} = 5$ Hz, 2H, H-5 and H-5').

^{13}C-NMR: (100 MHz, dimethylsulfoxide-d_6) δ (ppm): 168.4, 150.7, 148.4, 145.1, 131.4, 123.8.

File Name(s): 2005, 19xab031.

MS (ESI): sprayed from water: 243.1 Da $[M+H]^+$
Exact mass: 243.0893 Da calc. for $[M+H]^+$: $C_{12}H_{11}N_4O_2^+$ 243.0877 Da (7 ppm).

[4,4']-Bipyridinyl-3,3'-dicarboxylic acid bis-methylamide 38

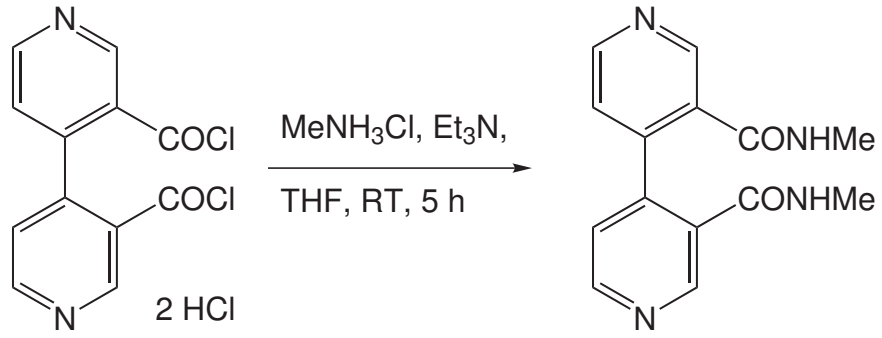

In 15 ml tetrahydrofuran, [4,4']-bipyridinyl-3,3'-dicarbonyl dichloride dihydrochloride (250 mg, 354.0 g/mol, 0.71 mmol) and methylammonium chloride (3 eq., 2.12 mmol, 66.5 g/mol, 138 mg) are suspended and 1 ml triethylamine is added. The suspension is stirred for 5 hours and all volatile compounds are removed *in vacuo*. The resulting residue is resolved in dichloromethane and washed with a dilute aqueous sodium carbonate solution. All volatile compounds are removed *in vacuo*. The resulting residue is purified by column chromatography. Yield (145 mg, 0.53 mmol, 76%).

R_f-Value: 0.20 (9:1)=(dichloromethane:methanol).

Mol. Weight: 270.3 g/mol ($C_{14}H_{14}N_4O_2$).

^{1}**H-NMR**: (400 MHz, methanol-d_4) δ (ppm): 8.61 (s, 2H, H-2, H-2'), 8.50 (d, $^3J_{HH}$ = 5 Hz, 2H, H-6, H-6'), 8.31 (b, 2H, H_{amide}), 7.02 (d, $^3J_{HH}$ = 5 Hz, 2H, H-6, H-6'), 2.60 (s, 6H, H_{CH_3}).

^{13}**C-NMR**: (100 MHz, methanol-d_4) δ (ppm): 167.9, 150.5, 148.0, 145.4, 131.3, 123.6, 26.4.

File Name(s): 2004, 27x4a109.

MS (EI): Exact mass: 270.1110 Da calc. for $M^{\cdot+}$ $C_{14}H_{14}N_4O_2$: 270.1110 Da (0 ppm) .

[4,4']-Bipyridinyl-3,3'-dicarboxylic acid bis-pentylamide 39

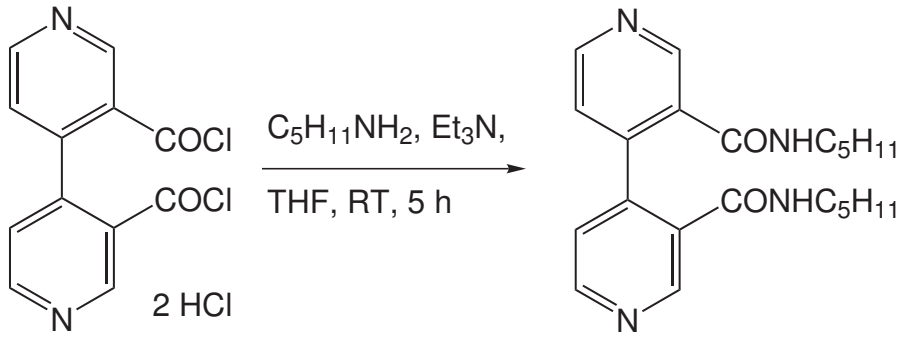

[4,4']-Bipyridinyl-3,3'-dicarbonyl dichloride dihydrochloride (734 mg, 354.0 g/mol, 2.1 mmol) and pentane-1-amine (3 eq., 6.2 mmol, 87.2 g/mol, 542 mg, 0.75 g/ml, 0.72 ml) are suspended in 15 ml tetrahydrofuran and 1 ml triethylamine is added. The suspension is stirred for 5 hours and all volatile compounds are removed *in vacuo*. The resulting residue is resolved in dichloromethane and washed with a dilute aqueous sodium carbonate solution. All volatile compounds are removed *in vacuo*. The resulting residue is purified by column chromatography. Yield (145 mg, 0.53 mmol, 66%).

R_f-Value: 0.27 (9:1)=(dichloromethane:methanol).

Mol. Weight: 382.5 g/mol ($C_{22}H_{30}N_4O_2$).

^{1}H-NMR: (400 MHz, Chloroform-d_1) δ (ppm): 8.73 (s, 2H, H-2 and H-2'), 8.59 (d, $^3J_{HH}$ = 5 Hz, 2H, H-5 and H-5'), 7.94 (s, 2H, H_{amide}), 7.03 (d, $^3J_{HH}$ = 5 Hz, 2H, H-6 and H-6'), 3.15 (t, $^3J_{HH}$ = 5 Hz, 4H, $H_{CO-CH_2-C_4H_9}$), 1.26 (m, 12H, $H_{CH_2-C_3H_6-CH_3}$), 0.83 (t, $^3J_{HH}$ = 5 Hz, 6H, $H_{C_4H_8-CH_3}$).

^{13}C-NMR: (100 MHz, Chloroform-d_1) δ (ppm): 167.2, 150.8, 148.5, 145.2, 131.9, 123.2, 40.2, 29.3, 29.2, 22.6, 14.1.

File Name(s): 2003, 09x4a048.

MS (GC-MS): (R_t= 12.9 min): m/z (%): 382 ($M^{\cdot+}$, 23), 354 ($[M-C_2H_4]^{\cdot+}$, 20), 326 ($[M-C_2H_4-C_2H_4]^{\cdot+}$, 23), 296 ($[M-C_5H_{12}N]^+$, 43), 268 ($[M-CONHC_5H_{11}]^+$, 100).

[4,4']-Bipyridinyl-3,3'-dicarboxylic acid bis-benzylamide 40

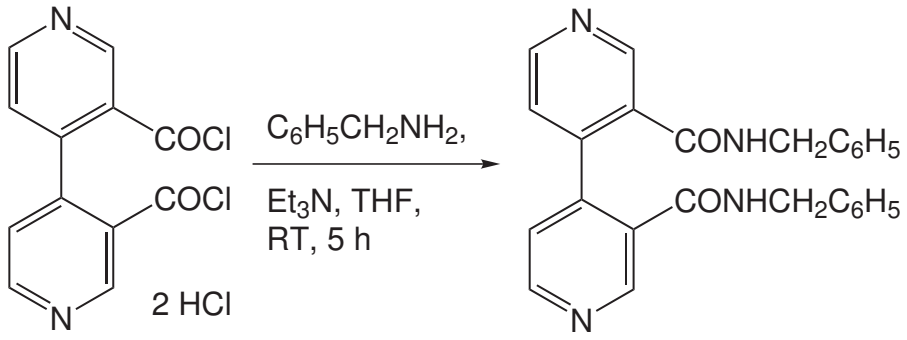

In 15 ml tetrahydrofuran, [4,4']-bipyridinyl-3,3'-dicarbonyl dichloride dihydrochloride (150 mg, 354.0 g/mol, 0.42 mmol), benzylamine (3 equivalents, 1.27 mmol, 107.2 g/mol, 136 mg, 0.98 g/ml, 0.14 ml), and 1 ml triethylamine are suspended. The suspension is stirred for 5 hours and all volatile compounds are removed *in vacuo*. The resulting residue is resolved in dichloromethane and washed with a dilute aqueous sodium carbonate solution. All volatile compounds are removed *in vacuo*. The resulting residue is purified by column chromatography. Yield (130 mg, 0.31 mmol, 74%).

R_f-Value: 0.40 (9:1)=(dichloromethane:methanol).

Mol. Weight: 422.5 g/mol ($C_{26}H_{22}N_4O_2$).

^{1}H-NMR: (400 MHz, Chloroform-d_1) δ (ppm): 8.75 (s, 2H, H-2 and H-2'), 8.59 (d, $^3J_{HH}$ = 5 Hz, 2H, H-6 and H-6'), 7.50 (t, $^3J_{HH}$ =5 Hz, 2H, H_{amide}), 7.23-7.26 (m, 6H, H-6, H-6' and $H_{C_6H_5}$), 7.02-6.96 (m, 6H, $H_{C_6H_5}$), 4.37 (b, 4 H, H_{CH_2}).

^{13}C-NMR: (100 MHz, Chloroform-d_1) δ (ppm): 166.4, 150.4, 147.7, 144.9, 137.3, 131.0, 128.8, 127.7, 127.6, 123.0, 43.9.

File Name(s): 2004, 26x4a055 and 26x4a065.

MS (ESI): sprayed from methanol: 423.2 Da $[M+H]^+$
Exact mass: 423.1816 Da calc. for $[M+H]^+$: $C_{26}H_{23}N_4O_2^+$ 423.1818 Da (+0.5 ppm).

(*S*,*S*)-2-[3'-(1-Methoxycarbonyl-ethylcarbamoyl)-[4,4']-bipyridinyl--3-carbonyl]-amino-propionic acid methyl ester 41

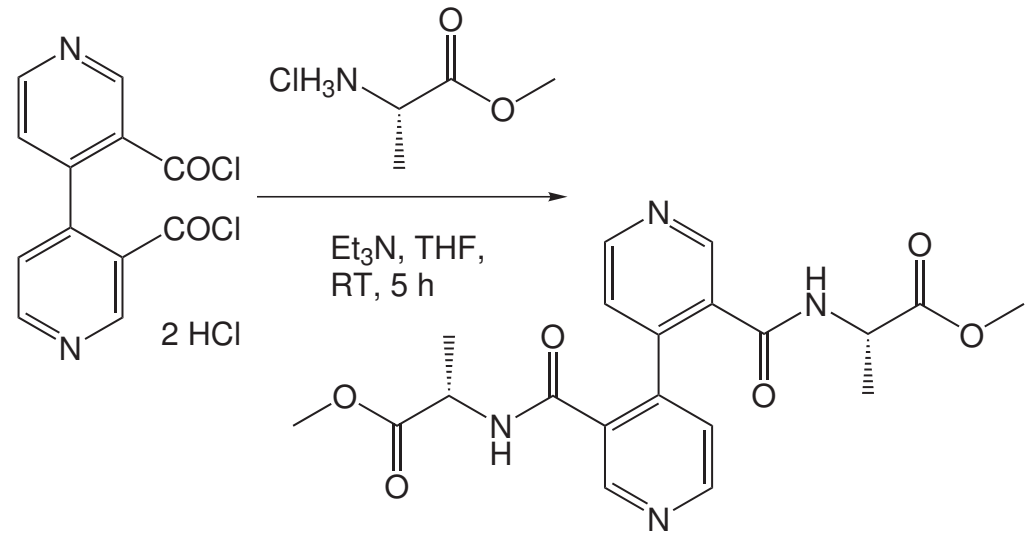

In 15 ml tetrahydrofuran, [4,4']-bipyridinyl-3,3'-dicarbonyl dichloride dihydrochloride (470 mg, 354.0 g/mol, 1.3 mmol) and (S)-methyl-2-amino-propanoic acid methyl ester (3 eq., 4.0 mmol, 139.6 g/mol, 556 mg), and triethylamine (8 eq., 10.6 mmol, 101.2 g/mol, 0.73 g/ml, 1.5 ml) are suspended. The suspension is stirred for 5 hours and all volatile compounds are removed *in vacuo*. The resulting residue is resolved in dichloromethane and washed with a dilute aqueous sodium carbonate solution. All volatile compounds are removed *in vacuo*. The residue is purified by column chromatography. Yield (242 mg, 0.58 mmol, 44%).

R_f-Value: (9:1)=(dichloromethane:methanol).

Mol. Weight: 414.4 g/mol ($C_{20}H_{22}N_4O_6$).

^{1}H-NMR: (400 MHz, Chloroform-d_1) δ (ppm): 8.80 (s, 2H, H-2 and H-2'), 8.67 (d, $^3J_{HH}$ = 4 Hz, 2H, H-6 and H-6'), 7.92 (s, 2H, H_{amide}), 7.16 (d, $^3J_{HH}$ = 4 Hz, 2H, H-5 and H-5'), 4.53 (q, $^3J_{HH}$ = 7 Hz, 2H, H_{CH-CH_3}), 3.63 (s, 6H, H_{COOCH_3}), 1.31 (d, $^3J_{HH}$ = 7 Hz, 6H, H_{CH-CH_3}).

^{13}C-NMR: (100 MHz, Chloroform-d_1) δ (ppm): 174.0, 166.7, 150.7, 147.9, 144.3, 131.1, 123.7, 52.7, 48.5, 17.8.

File Name(s): 2004, 10x4a059.

MS (EI): High resolution: 414.1537 Da calc. for $C_{20}H_{22}N_4O_6$ 414.1539 Da (0.5 ppm).

3'-Methyl-[4,4']-bipyridinyl-3-carboxylic acidmethylamide 44

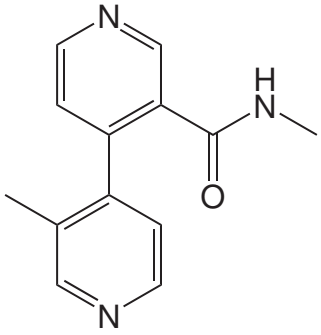

Byproduct of [4,4']-bipyridinyl-3,3'-dicarboxylic acid bis-methylamide **38**.

R_f-Value: 0.27 (17:1)=(dichloromethane:methanol).

Mol. Weight: 227.1 g/mol ($C_{13}H_{13}N_3O$).

^{1}H-NMR: (400 MHz, Chloroform-d_1) δ (ppm): 8.92 (s, 1H, H-2), 8.71 (d, $^3J_{HH}$ =5 Hz, 1H, H-6), 8.52 (s, 1H, H-2'), 8.48 (d, $^3J_{HH}$ =5 Hz, 1H, H-6'), 7.13 (d, $^3J_{HH}$ =5 Hz, 1H, H-5), 7.07 (d, $^3J_{HH}$ =5 Hz, 1H, H-5'), 2.76 (d, $^3J_{HH}$ =5 Hz, 3H, H_{NHCH_3}), 2.12 (s, 3H, H_{CH_3}).

File Name(s): 2005, 14x4b005.

MS (GC-MS): (R_t= 7.944 min): m/z (%): 227 ($M^{\cdot+}$, 12), 212 ($[M-CH_3]^+$, 13), 197 ($[M-NHCH_3]^+$, 100), 169 ($[M-CONHCH_3]^+$, 15), 141 ($[M-CONHCH_3-HCN]^+$, 9).

MS (ESI): sprayed from methanol: 305.1 Da $[M+Cl]^-$
Exact mass: 305.0782 Da
calc. for $[M+Cl]^-$: $C_{14}H_{14}N_4O_2Cl_1^-$ 305.0811 Da (-9 ppm).

1,10-Dimethyl-5,6-dihydro-[3,8]phenanthroline 49

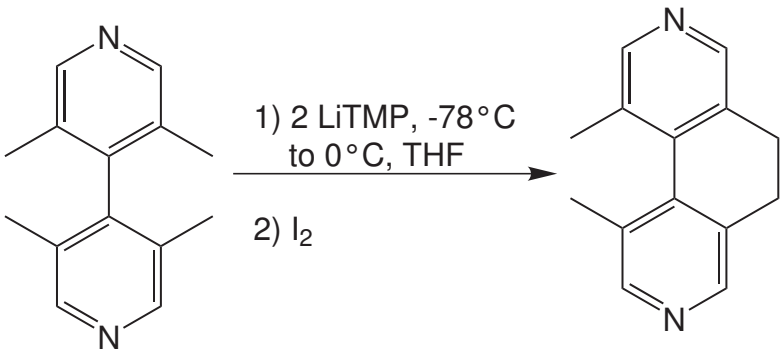

In 2 ml of dry tetrahydrofuran 2.3 eq. 2,2,6,6-tetramethyl-piperidine were reacted with 2.3 eq. *n*-butyllithium (1.6 mol l^{-1} solution in pentane) at -78°C. After 30 minutes at this temperature, 1 eq. of 3,5,3',5'-tetramethyl-[4,4']-bipyridine **24** (50 mg, 0.24 mmol) was added in 1 ml of dry tetrahydrofuran. The reaction mixture was allowed to warm to 0°C and stirred for 2 hours. The temperature was lowered to -78°C, 2.3 eq. iodide in 2 ml of dry tetrahydrofuran were added and the reaction mixture was stirred over night while it was allowed to warm to room temperature. Water (5 ml) was added and the aqueous layer was extracted with dichloromethane. After drying over sodium sulfate and removing of the solvents, the crude product was purified by flash chromatography (Yield 10 mg, 0.05 mmol, 20%).

R_f-Value: 0.50 (5:1)=(ethylacetate:methanol).

Mol. Weight: 210.1 g/mol ($C_{14}H_{14}N_2$).

^{1}H-NMR: (400 MHz, Chloroform-d_1) δ (ppm): 8.47 (s, 2 H, H-4, H-7), 8.38 (s, 2 H, H-2, H-9), 2.85 (d, $^2J_{HH}$ = 10.1 Hz, 2 H, H-5, H-6), 2.50 (d, $^2J_{HH}$ = 10.1 Hz, 2 H, H-5, H-6), 2.27 (s, 6 H, H_{CH_3}).

^{13}C-NMR: (100 MHz, Chloroform-d_1) δ (ppm): 151.1, 145.2, 139.5, 135.4, 130.0, 26.9, 18.2.

File Name(s): 2005, 40x4a008.

MS (GC-MS): (R_t= 8.692 min): m/z (%): 210 ($M^{\cdot+}$, 100), 209 ($[M-H]^+$, 28), 195 ($[M-CH_3]^+$, 88), 181 ($[M-CH_3-CH_2]^+$, 12), 168 ($[M-CH_3-HCN]^+$, 20).

MS (EI): Exact mass: 210.1151 Da calc. for $M^{\cdot+}$ $C_{14}H_{14}N_2$: 210.1156 Da (-2,4 ppm).

Melting Point: not measured.

N,N'-Didodecyl-5,5'-dimethyl-[4,4']-bipyridine-3,3'-dicarboxamide 55

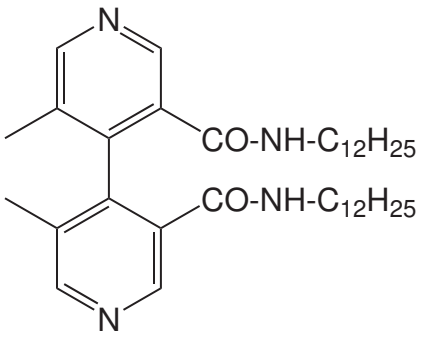

1) 3,5,3',5'-Tetramethyl-[4,4']-bipyridine **24** (1.00 g, 212.3 g/mol, 4.71 mmol) and potassium permanganate (4 eq., 18.8 mmol, 158.0 g/mol, 2.98 g) are stirred in 100 ml of water at 100°C for twelve hours. The precipitate is filtered of and washed rigorously with water. The aqueous phase is neutralized with hydrochloric acid, the water is removed *in vacuo* and the residue is dried roughly. The obtained mixture of acids is not separated. 2) The residue is suspended in thionyl chloride (25 ml) and stirred at 78 °C for eight hours. All volatile compounds are removed *in vacuo*. Again, the obtained mixture of acid chlorides is not separated. 3) This residue, dodecylamine (2 eq., 9.42 mmol, 185.3 g/mol, 1.75 g) and triethylamine (5 ml, excess) are suspended in 15 ml of dry dimethylsulfoxide and stirred for two days. All volatile compounds are removed *in vacuo* and the crude product is purified by column chromatography. Yield: 457 mg, 0.75 mmol, 16% among other byproducts and over three steps.

R_f-Value: 0.22 (ee:methanol)=(15:1).

Mol. Weight: 606.5 g/mol ($C_{38}H_{62}N_4O_2$).

^{1}**H-NMR**: (400 MHz, Chloroform-d_1) δ (ppm): 8.6 (s, 2H, H-2 and H-2' or H-6 and H-6'), 8.53 (s, 2H, H-2 and H-2' or H-6 and H-6'), 7.63 (t, $^3J_{HH}$ = 5.7 Hz, 2H, H$_a$*mide*), 3.21 (m, 2H, NH$-CH_2-CH_2$), 3.10 (m, 2H, NH$-CH_2-CH_2$), 1.90 (s, 6H, CH_3), 1.23 (b, 40H, $CH_2-(CH_2)_{10}-CH_3$), 0.86 (t, $^3J_{HH}$ = 6.8 Hz, 6H, $(CH_2)_{11}-CH_3$).

^{13}**C-NMR**:	(100 MHz, Chloroform-d_1) δ (ppm): 167.5, 152.5, 145.8, 142.5, 131.6, 130.4, 40.0, 32.0, 29.8, 29.7, 29.7, 29.7, 29.6, 29.5, 29.3, 26.9, 22.8, 16.8, 14.2.
File Name(s):	2006, 13x4a111.
MS (ESI):	($50 * 10^{-6}$ M, MeOH): 607.5 Da ($[M+H]^+$), 1214.0 Da ($[M_2+H]^+$), 1842.5 Da ($[M_3+Na]^+$). High-Resolution: 607.4931 Da (calc. for $[M+H]^+$ $C_{38}H_{63}N_4O_2^+$: 607.4946 Da, -2.5 ppm)

2,2'-(5,5'-Dimethyl-[4,4']-bipyridine-3,3'-diyl)diacetic acid 56

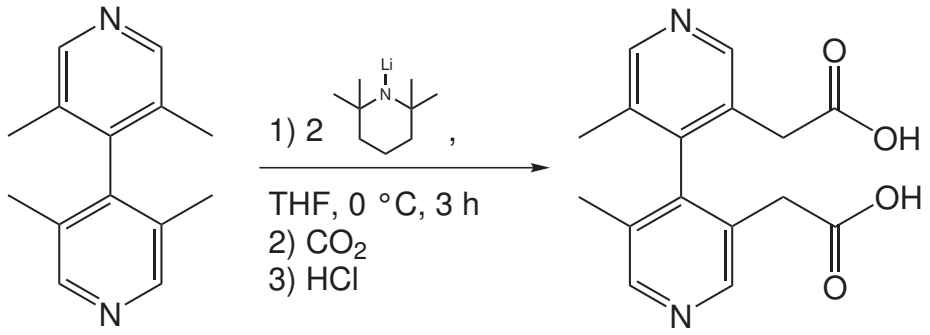

In 10 ml tetrahydrofuran, 2,2,6,6-tetramethyl-piperidine (0.8 ml, 0.83 g/ml, 664 mg, 141.25 g/mol, 4.70 mmol) are cooled down to -78°C, under argon. *t*-Butyllithium (2.5 mol l^{-1} solution in pentane, 1.9 ml, 4.70 mmol, 1 eq.) is added. The mixture is stirred for 30 min at this temperature, allowed to warm to 0°C, and cooled to -78°C again. 3,5,3',5'-Tetramethyl-[4,4']-bipyridine **24** (250 mg, 212 g/mol, 1.17 mmol, 0.25 eq.) in 5 ml tetrahydrofuran is added and the resulting mixture is stirred for 3 hours at 0°C. At this temperature, gaseous carbon dioxide is introduced until the mixture is colorless. Water (10 ml) is added, the aqueous phase is extracted with dichloromethane, neutralized with hydrochloric acid and all volatile compounds are removed *in vacuo*. Yield after column chromatography: (157 mg, 0.52 mmol, 45 %).

R_f-Value: 0.14 (2:1)=(dichloromethane:methanol).

Mol. Weight: 300.3 g/mol ($C_{16}H_{16}N_2O_4$).

^{1}**H-NMR**: (400 MHz, Water-d_2) δ (ppm): 8.43 (b, 4H, H-2, H-2', H-6, and H-6'), 3.26 (d, $^2J_{HH}$ =15 Hz, 2H, H_{CH_2}), 3.02 (d, $^2J_{HH}$ =15 Hz, 2H, H_{CH_2}), 1.94 (s, 6H, H_{CH_3}).

^{13}**C-NMR**: (100 MHz, Water-d_2) δ (ppm): 179.8, 149.6, 149.2, 148.6, 135.5, 133.9, 41.6, 18.3.

File Name(s): 2005, 46x4a066.

MS (ESI): Exact mass: 299.1005 Da calc. for [M−H^+] $C_{16}H_{15}N_2O_4^-$: 299.1037 Da (-11 ppm).

2,2'-(5,5'-Dimethyl-[4,4']-bipyridine-3,3'-diyl)bis(methylacetamide) 57

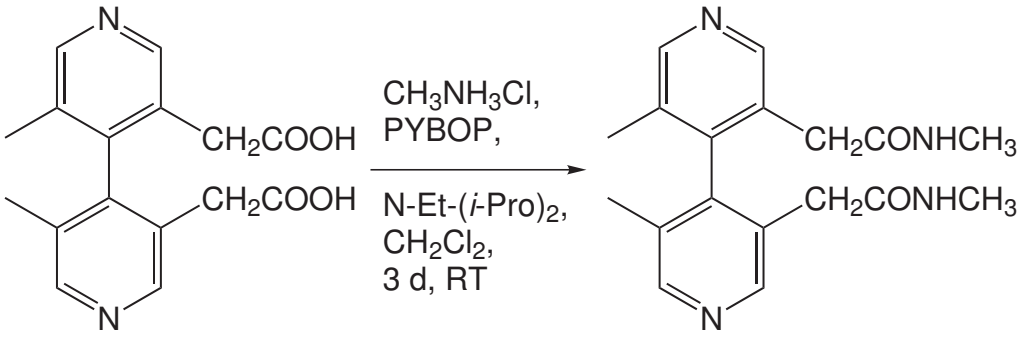

Under argon, 9 mg of 2,2'-(5,5'-dimethyl-[4,4']-bipyridine-3,3'-diyl)diacetic acid **56**, 29 mg benzotriazole-1-yl-oxy-tris-pyrrolidino-phosphonium hexafluorophos phate (PYBOP) (2 eq.), 23 mg methylammonium chloride (12 eq.) and 0.1 ml of ethyldiisopropylamine (12 eq.) were suspended in 15 ml of dry dichloromethane and stirred for three days (low solubility of starting material). The dichloromethane is removed in vacuo and the crude product is purified by column chromatography (Yield: 0.004 g, 0.01 mmol, 41%). The obtained racemic mixture of axial chiral **57** was submitted to chiral HPLC separation. Due to peak tailoring, the enantiomers could however not be separated.

R_f-Value: 0.40 (CH_2Cl_2:MeOH)=(25:1).

Mol. Weight: 326.4 g/mol ($C_{18}H_{22}N_4O_2$).

^{1}H-NMR: (400 MHz, Chloroform-d_1) δ (ppm): 8.57 (s, 2H, H-2 and H-2'or H-6 and H-6'), 8.48 (s, 2H, H-2 and H-2'or H-6 and H-6'), 6.44 (b, 2H, H_{amide}), 3.30 (d, $^2J_{HH}$ = 15 Hz, 2 H, CH_2), 3.16 (d, CH_2 = 15 Hz, 2 H, CH_2), 2.68 (d, CH_3 = 5 Hz, 3 H, $NHCH_3$), 1.93 (s, 6H, CH_3).

File Name(s): 2006, 08x4a116.06.

MS (GC-MS): (R_t= 13.9 min): m/z (%): 326 ($M^{\cdot+}$, 100), 295 ([M-NH_2CH_3]$^+$, 33), 254 ([M-$CH_2CONHCH_3$]$^+$, 60), 223 ([M-$CH_2CONHCH_3$-NH_2CH_3]$^+$, 60), 195 ([M-$CH_2CONHCH_3$-$HCONHCH_3$]$^+$, 83), 58 ([$CONHCH_3$]$^+$, 87).

2,2'-(5,5'-Dimethyl-[4,4']-bipyridine-3,3'-diyl)bis(dodecylacetamide) 58

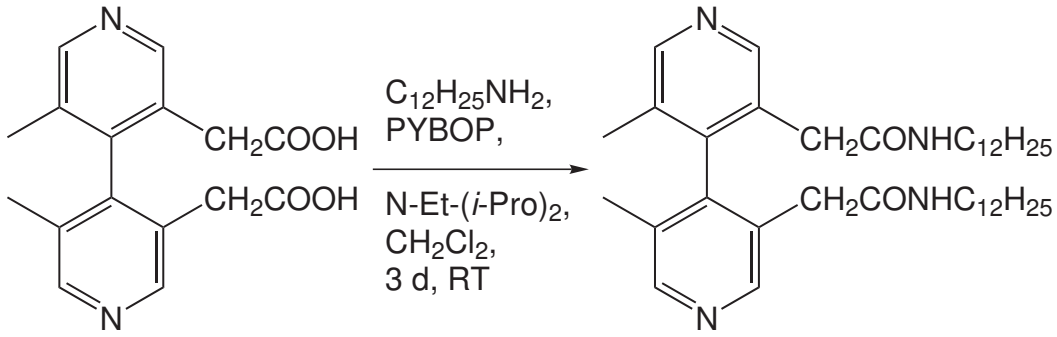

Under argon, 102 mg of 2,2'-(5,5'-dimethyl-[4,4']-bipyridine-3,3'-diyl)diacetic acid **56**, 356 mg benzotriazole-1-yl-oxy-tris-pyrrolidino-phosphonium hexafluorophosphate (PYBOP) (2 eq.), 127 mg dodecylamine (2 eq.) and 1.2 ml of ethyldiisopropylamine (12 eq.) were suspended in 15 ml of dry dimethylsulfoxide and stirred for two days (low solubility of starting material). The dimethylsulfoxide is removed in vacuo and the crude product is purified by column chromatography (Yield: 71 mg, 0.11 mmol, 33%).

R_f-Value: 0.24 (ethylacetate:MeOH)=(15:1).

Mol. Weight: 635.0 g/mol ($C_{40}H_{66}N_4O_2$).

^{1}**H-NMR**: (400 MHz, Acetone-d_6) δ (ppm): 8.49 (s, 2H, H-2 and H-2'or H-6 and H-6'), 8.41 (s, 2H, H-2 and H-2'or H-6 and H-6'), 7.30 (b, 2H, H_{amide}), 3.24 (d, $^2J_{HH}$ = 15 Hz, 2 H, CH_2), 3.15 (d, $^2J_{HH}$ = 15 Hz, 2 H, CH_2), 3.07 (m, 4 H, CH_2), 1.90 (s, CH_3, 6 H), 1.28 (m, 40 H, $(CH_2)_{10}$), 0.88 (t, $^3J_{HH}$ = 7 Hz, CH_3, 6 H).

^{13}**C-NMR**: (100 MHz, Acetone-d_6) δ (ppm): 170.1, 150.1, 150.0, 144.9, 131.2, 130.0, 40.1, 39.9, 38.3, 32.7, 30.6, 30.4, 30.4, 30.3, 30.2, 27.7, 23.3, 16.7, 14.4.

File Name(s): 2007, 34x4a029.07 and 34x3a008.07.

MS (ESI): Exact mass: 635.5207 Da calc. for $[M^+H^+]$ $C_{40}H_{67}N_4O_2^+$: 635.5259 Da (-8 ppm).

4-Iodo-3,5-dimethyl-pyridine 59

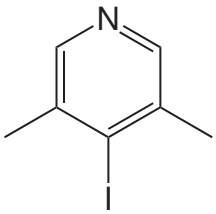

3,5-Dimethyl-4-trimethylsilanyl-pyridine **25** (250 mg, 1.39 mmol) is dissolved in iodmonochloride (0.25 ml) at 0°C and stirred in the dark for 2 days first at 0°C than at room temperature. 25 mg of ice is added and the mixture is allowed to come to room temperature. After the mixture is cooled down to 0°C again, solid sodium thiosulfate is added until the mixture is colorless. The aqueous phase is extracted three times with 10 ml of dichloromethane. The combined organic phases were dried over sodium sulfate. After removal of the solvent and chromatographic workup 4-iodo-3,5-dimethyl-pyridine **59** is obtained as a white solid (Yield: 256.5 mg, 1.10 mmol, 79%). The free base is unstable even in the solid phase and at low temperatures. Within two days in the freezer the white crystals decompose.

R_f-Value: 0.36 (1:1) = (dichloromethane:ethylacetate).

Mol. Weight: 233.0 g/mol ($C_7H_{10}NI$).

^{1}H-NMR: (400 MHz, Chloroform-d_1) δ (ppm): 8.12 (s, 2 H, H-2 and H-6), 2.40 (s, 6 H, H_{CH_3}).

^{13}C-NMR: (100 MHz, Chloroform-d_1) δ (ppm): 146.6, 137.8, 119.6, 26.0.

File Name(s): 2005, 51x4b020.

MS (GC-MS): (R_t= 4.1 min): m/z (%): 233 ($M^{\cdot+}$, 100), 127 (I^+, 16), 106 ($[M\text{-}I]^+$, 46), 77 ($C_5H_3N^+$, 92), 51 ($C_4H_3^+$, 31).

MS (EI): Exact mass: 232.9699 Da calc. for: $C_7H_{10}NI$ 232.9702 Da (-1 ppm).

Melting Point: > 80°C decomposition.

2,6-Dimethyl-[4,4']-bipyridine 81[185]

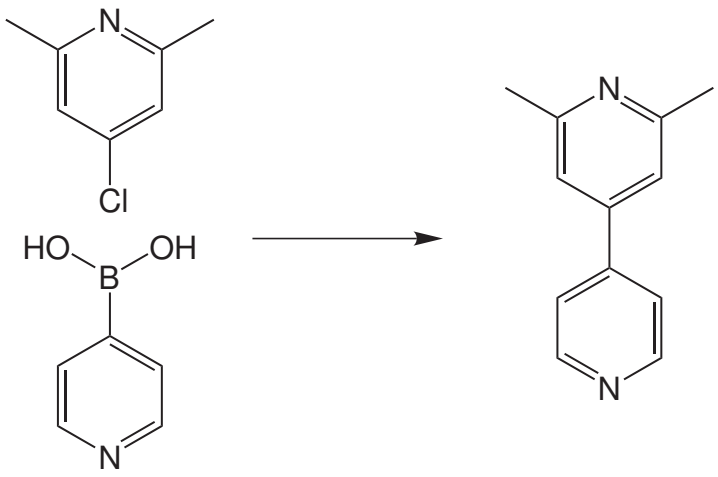

In 8 ml 1,4-dioxane, 4-chloro-2,6-dimethyl-pyridine **83** (862 mg, 141.6 g/mol, 6.1 mmol), 4-pyridinyl boronic acid (797 mg, 122.9 g/mol, 6.5 mmol, 1.07 eq.), bis(tri-*tert*-butylphosphine)palladium(0) (90 mg, 511.1 g/mol, 0.2 mmol, 0.03 eq.) and cesium carbonate (2420 mg, 325.8 g/mol, 7.4 mmol, 1.2 eq.) were suspended and heated for 4 hours at 80°C. All volatile compounds were removed *in vacuo* and the mixture was purified by column chromatography: 217 mg, 1.2 mmol, 19%.

R_f-Value: 0.36 (9:1)=(ethylacetate:methanol).

Mol. Weight: 184.3 g/mol ($C_{12}H_{12}N_2$).

^{1}**H-NMR**: (300 MHz, Chloroform-d_1) δ (ppm): 8.64 (AA'XX', J_{HH} = 5 Hz, 2H, H-2' and H-6'), 7.43 (AA'XX', J_{HH} = 5 Hz, 2H, H-3' and H-5'), 7.13 (s, 2H, H-3 and H5), 2.54 (s, 6H, H_{CH_3}.

^{13}**C-NMR**: (75 MHz, Chloroform-d_1) δ (ppm): 158.7, 150.6, 146.3, 146.1, 121.5, 118.2, 24.5.

File Name(s): 2006, 01x3a060.

MS (GC-MS): (R_t= min): m/z (%): 184 ($M^{\cdot+}$, 100), 168 ($[M-CH_4]^{\cdot+}$, 13), 169 ($[M-CH_3]^+$, 10), 156 ($[M-C_2H_4]^{\cdot+}$, 8), 142 ($[M-CH_3-HCN]^+$, 12), 115 ($[M-CH_3-HCN-HCN]^+$, 15).

MS (EI): High resolution: 184.1001 Da calc. for $C_{12}H_{12}N_2$ 184.1001 Da (0 ppm).

4-Chloro-2,6-dimethyl-pyridine 83[186]

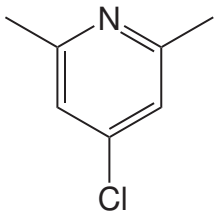

Modified from *Evans et al.*:.[186] In 10 ml hydrochloric acid, 2,6-dimethyl-pyridin-N-oxide **82** (5.0 g, 123.2 g/mol, 40.6 mmol) was solved and stirred for 30 min. All volatile compounds were removed *in vacuo*. The resulting residue is resolved in 15 ml phosphorylchloride at 0 °C and the mixture is stirred at 105 °C over night and poured into 50 ml of ice containing solid sodium carbonate. The aqueous phase is extracted with chloroform, the combined organic phases are dried over magnesium sulphate and all volatile compounds were removed *in vacuo*. The crude product mixture was distilled to yield 3.1 g of 4-chloro-2,6-dimethyl-pyridine **83** (21.6 mmol, 53 %) and 0.8 g of 2-chloromethyl-6-methyl-pyridine.

Mol. Weight: 141.6 g/mol (C_7H_8ClN).

^{1}H-NMR: (400 MHz, Chloroform-d_1) δ (ppm): 6.93 (s, 2H, H-3 and H-5), 2.46 (s, 6H, H_{CH_3}).

^{13}C-NMR: (100 MHz, Chloroform-d_1) δ (ppm): 159.2, 144.1, 120.4, 24.3.

File Name(s): 2005, 30x4a086.

MS (GC-MS): (R_t= 1.629 min): m/z (%): 141 ($M^{\cdot+}$, 100), 106 ($[M-Cl]^+$, 21), 79 ($[M-Cl-HCN]^+$, 13), 63 ($[M-Cl-HCN-CH_4]^+$, 20).

Melting Point: liquid.

4-Bromo-2,6-dimethyl-pyridine 86 [279]

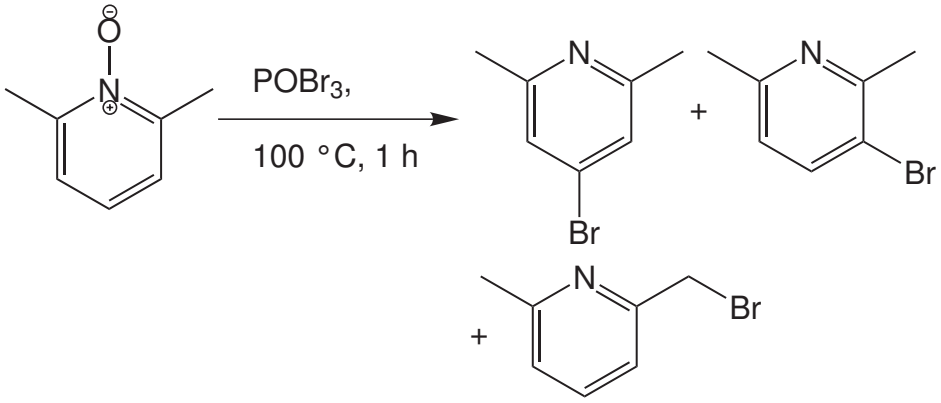

2,6-Dimethyl-pyridin-N-oxide hydrobromide 0.5 g (204.1 g/mol, 2.4 mmol) and phosphorylbromid (5.0 g, MP = 55 °C) are heated at 100 °C for 1 hour. The suspension is cooled down and poured into 100 ml of ice containing solid sodium carbonate. The aqueous phase is extracted with chloroform. The combined organic phases are dried over magnesium sulphate and all volatile compounds are removed *in vacuo*. GCMS-analysis showed three peaks with the desired mass and isotopic distribution (185 Da, one bromid). One isomer was removed synthetically (refluxing in triethylamine). The remaining two isomers can neither be separated by column chromatography nor distillation.

Mol. Weight: 186.1 g/mol (C_7H_8BrN).

MS (GC-MS): **A)** (R_t= 4.593 min): m/z (%): 185 ($M^{\cdot+}$, 90), 106 ($[M-Br]^+$, 75), 79 ($[M-Br-HCN]^+$, 52), 65 ($[M-Br-HCN-CH_2]^+$, 100), 51 ($[C_4H_3]^+$, 24),
B) (R_t= 4.880 min): m/z (%): 185 ($M^{\cdot+}$, 100), 106 ($[M-Br]^+$, 91), 79 ($[M-Br-HCN]^+$, 82), 63 ($[M-Br-HCN-CH_4]^+$, 71), 51 ($[C_4H_3]^+$, 36),
C) (R_t= 6.566 min): m/z (%): 185 ($M^{\cdot+}$, 10), 106 ($[M-Br]^+$, 100), 79 ($[M-Br-HCN]^+$, 59), 63 ($[M-Br-HCN-CH_4]^+$, 18), 51 ($[C_4H_3]^+$, 12).

8.4 Synthesis of Metal-Precursors

8.4.1 Stang's (dppp)M(OTf)$_2$ (M = Pd and Pt)

According to well-known literature procedures,[188] chelation of $PdCl_2$ and $PtCl_2$ with 1,3-bis(diphenylphosphino)-propane (dppp) by standard procedures results in complexes (dppp)$PdCl_2$ and (dppp)$PtCl_2$, respectively. Interaction of these metal dichlorides with AgOTf gives, after workup, the related triflate complexes, (dppp)Pd(OTf)$_2$ and (dppp)Pt(OTf)$_2$.[61]

8.4.2 Fujita's (en)M(NO$_3$)$_2$ (M = Pd and Pt)

Likewise according to well-known literature procedures, reaction of K_2PdCl_6 and K_2PtCl_6 with ethylenediamine (en) by standard procedures results in complexes (en)$PdCl_2$[189] and (en)$PtCl_2$,[190] respectively. Interaction of these metal dichlorides with $AgNO_3$ gives, after workup, the related nitrate complexes, (en)Pd$(NO_3)_2$[26] and (en)Pt$(NO_3)_2$.[29] In early publications by *Fujita et al.*, these complexes were used *in situ*, while in recent publications, they are precipitated and dried roughly. For mass spectrometric measurements, (en)Pd$(PF_6)_2$[27] is prepared from (en)$PdCl_2$ and $AgPF_6$.

8.5 Synthesis of Self-Assembled Supramolecular Squares

General procedure for square formation: Equimolar amounts of organic ligand (in case of axially chiral ligands only one enantiomer) and metal precursor complexes (dppp)M(OTf)$_2$ with M = Pd(II) **[a]** or Pt(II) **[b]** are mixed in acetone (MS, $4{\cdot}10^{-4}$ mol l^{-1}) or [D_6]-acetone (NMR, $9{\cdot}10^{-3}$ mol l^{-1}) and stirred for 24 hours before measurement, to avoid kinetically controlled product formation. For CD-spectroscopy, the acetone is removed in vacuo, and the resulting residues are dissolved in methanol. Note that ^{195}Pt (natural abundance 34%) is the only NMR active Pt-isotope. Thus, phosphorous atoms in platinum squares are split in one singlet (^{190}Pt - ^{194}Pt and ^{196}Pt - ^{198}Pt, 66%) and one typically broadened doublet

(^{195}Pt, 34%) at the same chemical shift. In the cases of axially chiral ligands, a characterization by ^{13}C NMR could not be carried out due to the small amounts of enantiopure ligands obtained from the HPLC separation. Racemic mixtures of the ligands cannot be used instead, because they unavoidably form mixed assemblies with new signals not present in the NMR spectra of the assemblies obtained from enantiopure ligands. ^{13}C NMR spectra of platinum squares **DSG0b - DSG3b** were not recorded, due to broadened peaks even at higher temperatures. All SAMS have melting points higher than 250°C, the instrument's limit. Mass spectrometric investigations of **DSG3a** and **DSG3b** failed, as even the +3 charge-state is out of the instrument's limit.

DSG0a

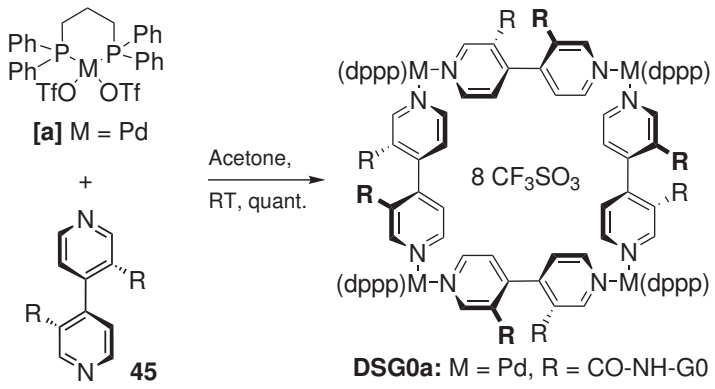

Mol. Weight: 4952.5 g/mol ($C_{220}H_{192}F_{24}N_{16}O_{32}P_8Pd_4S_8$).

^{1}**H-NMR**: (400 MHz, [D_7]-dimethylformamide) δ (ppm): 9.12 (b, 8H, H_{amide}), 8.82 (s, 8H, $H_{pyridine}$), 8.74 (d, 8H, $3J_{HH}$ = 4.93 Hz, $H_{pyridine}$), 7.89 (m, 32H, H_{dppp}), 7.71 (m, 16H, H_{dppp}), 7.60 (m, 32H, H_{dppp}), 7.25 (m, 32H, H_{phenyl}), 7.04 (m, 16H, H_{phenyl} + $H_{pyridine}$), 4.38 (d, 16H, $3J_{HH}$ = 5.94 Hz, $H_{benzylic}$), 3.18 (m, 16H, H_{dppp}), 2.12 (m, 8H, H_{dppp}).

^{13}**C-NMR**: (100 MHz, [D_7]-dimethylformamide) δ (ppm): 166.1, 151.3, 149.0, 139.1, 134.0 (b, C_{dppp}), 133.3, 130.2, 130.1, 128.9, 127.5, 127.5, 125.8 (d, J_{PC}= 58.3 Hz), 124.8 (b, C_{dppp}), 123.6, 120.4, 43.5, 22.3 (d, J_{PC}= 43.1 Hz), 18.6.

^{19}**F-NMR**: (376 MHz, [D_7]-dimethylformamide) δ (ppm): -78.95.

^{31}**P-NMR**: (162 MHz, [D_7]-dimethylformamide) δ (ppm): 18.9.

MS (ESI): m/z = 2329.4 Da $[M\text{-}2OTf]^{2+}$.

DSG0b

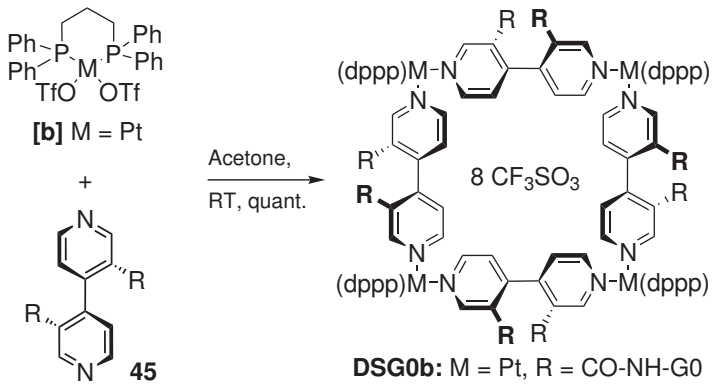

Mol. Weight: 5308.8 g/mol ($C_{220}H_{192}F_{24}N_{16}O_{32}P_8Pt_4S_8$).

^{1}H-NMR: (400 MHz, [D_7]-dimethylformamide) δ (ppm): 8.82 (b, 24H, $H_{amide} + H_{pyridine}$), 7.87 (m, 32H, H_{dppp}), 7.54 (m, 56H, $H_{dppp} + H_{phenyl}$), 7.24 (m, 40H, $H_{phenyl} + H_{pyridine}$), 4.33 (m, 16H, $H_{benzylic}$), 3.21 (m, 16H, H_{dppp}), 2.31 (m, 8H, H_{dppp}).

^{13}C-NMR: (100 MHz, [D_7]-dimethylformamide) δ (ppm): 167.0, 149.3, 148.3, 139.0, 133.8, 133.0, 129.9, 129.8, 128.7, 127.3, 127.2, 124.8, 123.4, 120.2, 116.9, 43.3, 21.9, 18.4.

^{19}F-NMR: (376 MHz, [D_7]-dimethylformamide) δ (ppm):-78.37.

^{31}P-NMR: (202 MHz, [D_7]-dimethylformamide, 373 K) δ (ppm): -9.79 $^1J_{Pt195,P} = 3116$ Hz.

MS (ESI): m/z = 2506.4 Da [M-2OTf]$^{2+}$, 1621.6 Da [M-3OTf]$^{3+}$, 1179.2 Da [M-4OTf]$^{4+}$ 913.2 Da [M-5OTf]$^{5+}$.

DSG1a

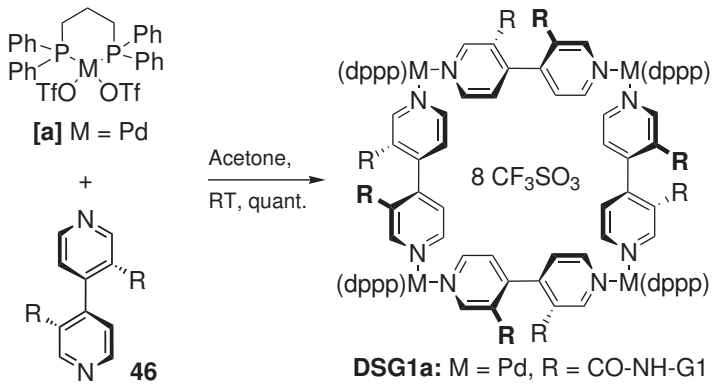

Mol. Weight: 6649.2 g/mol ($C_{332}H_{288}F_{24}N_{16}O_{48}P_8Pd_4S_8$).

^{1}**H-NMR**: (400 MHz, [D_7]-dimethylformamide) δ (ppm): 9.05 (b, 8H, H_{amide}), 8.85 (s, 8H, $H_{pyridine}$), 8.68 (d, 8H, $3J_{HH} = 4.08$ Hz, $H_{pyridine}$), 7.89 (m, 32H, H_{dppp}), 7.69 (m, 16H, H_{dppp}), 7.58 (m, 32H, H_{dppp}), 7.51 (m, 32H, H_{phenyl}), 7.44 (m, 32H, H_{phenyl}), 7.36 (m, 16H, H_{phenyl}), 7.25 (d, 8H, $3J_{HH} = 5.16$ Hz, $H_{pyridine}$), 6.63 (t, 8H, $^4J_{HH} = 2.22$ Hz, $H_{aromatic}$), 6.49 (d, 16H, $^4J_{HH} = 1.88$ Hz, $H_{aromatic}$), 5.09 (s, 32H, $H_{benzylic}$), 4.33 (d, 16H, $3J_{HH} = 5.80$ Hz, $H_{benzylic}$), 3.18 (m, 16H, H_{dppp}), 2.26 (m, 8H, H_{dppp}).

^{13}**C-NMR**: (100 MHz, [D_7]-dimethylformamide) δ (ppm): 165.7, 160.4, 151.2, 148.7, 141.3, 137.7, 133.7, 133.0, 129.9, 129.8, 128.8, 128.2, 128.1, 125.6 (d, J_{PC}= 59.3 Hz), 124.9, 123.4, 120.2, 106.9, 100.4, 70.0, 43.4, 22.1 (d, J_{PC}= 42.9 Hz), 18.4.

^{19}**F-NMR**: (376 MHz, [D_7]-dimethylformamide) δ (ppm): -78.15.

^{31}**P-NMR**: (162 MHz, [D_7]-dimethylformamide) δ (ppm): 18.90.

MS (ESI): m/z = 3177.3 Da $[M\text{-}2OTf]^{2+}$, 2069.5 Da $[M\text{-}2OTf]^{2+}$.

DSG1b

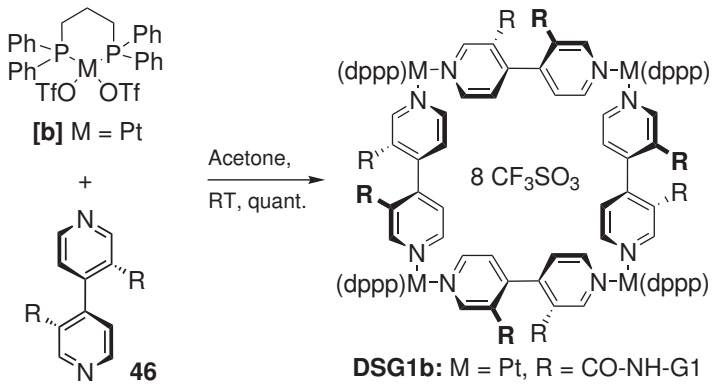

Mol. Weight: 7005.4 g/mol ($C_{332}H_{288}F_{24}N_{16}O_{48}P_8Pt_4S_8$).

^{1}H-NMR: (400 MHz, [D_7]-dimethylformamide) δ (ppm): 8.83 (b, 8H, $H_{pyridine}$), 8.64 (b, 16H, $H_{pyridine}$ + H_{amide}), 7.86 (b, 32H, H_{dppp}), 7.62 (b, 16H, H_{dppp}), 7.54 (b, 32H, H_{dppp}), 7.45 (b, 32H, H_{phenyl}), 7.38 (b, 32H, H_{phenyl}), 7.32 (b, 16H, H_{phenyl}), 7.18 (b, 8H, $H_{pyridine}$), 6.62 (b, 8H, $H_{aromatic}$), 6.50 (b, 16H, $H_{aromatic}$), 5.09 (b, 32H, $H_{benzylic}$), 4.28 (b, 16H, $H_{benzylic}$), 3.19 (b, 16H, H_{dppp}), 2.31 (b, 8H, H_{dppp}) .

^{19}F-NMR: (376 MHz, [D_7]-dimethylformamide) δ (ppm): -79.03.

^{31}P-NMR: (202 MHz, [D_7]-dimethylformamide, 373 K) δ (ppm): -9.76 $^1J_{Pt195,P} = 3286$ Hz.

MS (ESI): m/z = 3355.1 Da [M-2OTf]$^{2+}$, 2187.6 Da [M-3OTf]$^{3+}$.

DSG2a

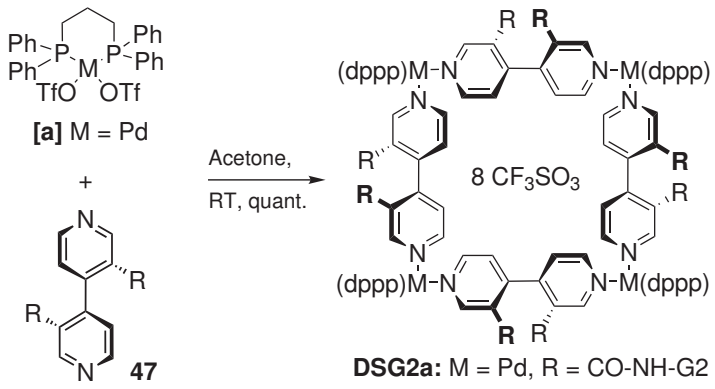

Mol. Weight: 10042.5 g/mol ($C_{556}H_{480}F_{24}N_{16}O_{80}P_8Pd_4S_8$).

^{1}**H-NMR**: (400 MHz, [D_7]-dimethylformamide) δ (ppm): 9.06 (b, 8H, H_{amide}), 8.85 (b, 8H, $H_{pyridine}$), 8.68 (d, 8H, $3J_{HH}$=4.68 Hz, $H_{pyridine}$), 7.89 (m, 32H, H_{dppp}), 7.69 (m, 16H, H_{dppp}), 7.58 (m, 32H, H_{dppp}), 7.49 (m, 64H, H_{phenyl}), 7.40 (m, 64H, H_{phenyl}), 7.36 (m, 32H, H_{phenyl}), 7.24 (d, 8H, $3J_{HH}$=5.05 Hz, $H_{pyridine}$), 6.82 (d, 32H, $^4J_{HH}$ =2.15 Hz, $H_{aromatic}$), 6.71 (t, 16H, $^4J_{HH}$ =2.21 Hz, $H_{aromatic}$), 6.63 (t, 8H, $^4J_{HH}$ =1.96, $H_{aromatic}$), 6.48 (d, 16H, $^4J_{HH}$ =1.77, $H_{aromatic}$), 5.14 (s, 64H, $H_{benzylic}$, 5.04 (s, 32H, $H_{benzylic}$, 4.33 (d, 16H, $3J_{HH}$=5.68 Hz, $H_{benzylic}$), 3.16 (m, 16H, H_{dppp}), 2.25 (m, 8H, H_{dppp}).

^{13}**C-NMR**: (100 MHz, [D_7]-dimethylformamide) δ (ppm): 166.6, 160.5, 160.3, 151.0, 148.6, 141.4, 140.2, 137.7, 133.8 (b, C_{dppp}), 133.1, 129.9, 128.8, 128.3, 128.2, 128.1, 125.5 (d, J_{PC}=56.9 Hz), 123.4, 120.2, 107.0, 106.9, 101.5, 100.6, 70.1, 69.9, 43.5, 22.1 (d, J_{PC}=43.5 Hz), 18.6.

^{19}**F-NMR**: (376 MHz, [D_7]-dimethylformamide) δ (ppm): -79.11.

^{31}**P-NMR**: (162 MHz, [D_7]-dimethylformamide) δ (ppm): 19.02.

MS (ESI): m/z=4876.7 Da $[M\text{-}2OTf]^{2+}$, 3200.9 Da $[M\text{-}2OTf]^{2+}$.

DSG2b

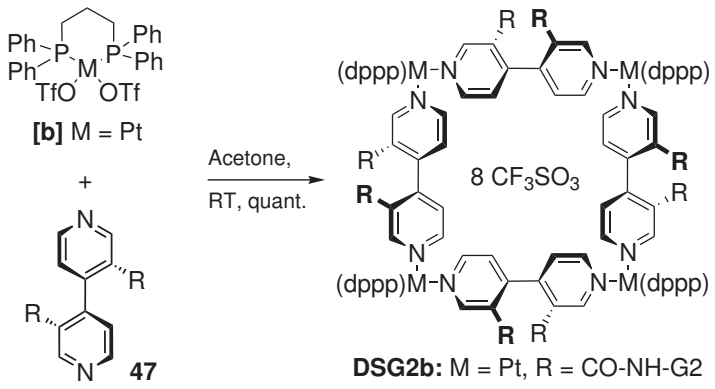

Mol. Weight: 10398.8 g/mol ($C_{556}H_{480}F_{24}N_{16}O_{80}P_8Pt_4S_8$).

^{1}H-NMR: (400 MHz, [D_7]-dimethylformamide) δ (ppm): 8.83 (b, 8H, $H_{pyridine}$), 8.62 (b, 16H, $H_{pyridine}$ + H_{amide}), 7.85 (b, 32H, H_{dppp}), 7.54 (b, 48H, H_{dppp} +H_{dppp}), 7.44 (b, 64H, H_{phenyl}), 7.36 (b, 64H, H_{phenyl}), 7.30 (b, 32H, H_{phenyl}), 7,16 (b, 8H, $H_{pyridine}$), 6.78 (s, 32H, $H_{aromatic}$), 6.70 (s, 16H, $H_{aromatic}$), 6.62 (s, 8H, $H_{aromatic}$), 6.49 (m, 16H, $H_{aromatic}$), 5.12 (s, 64H, $H_{benzylic}$), 5.03 (s, 32H, $H_{benzylic}$), 4.29 (s, 16H, $H_{benzylic}$), 3.16 (s, 16H, H_{dppp}), 2.29 (m, 8H, H_{dppp}).

^{19}F-NMR: (376 MHz, [D_7]-dimethylformamide) δ (ppm): -78.87.

^{31}P-NMR: (202 MHz, [D_7]-dimethylformamide, 373 K) δ (ppm): -8.32 $^1J_{Pt195,P}$ = 3237 Hz.

MS (ESI): m/z = 5053.9 Da [M-2OTf]$^{2+}$, 3318.8 Da [M-3OTf]$^{3+}$.

DSG3a

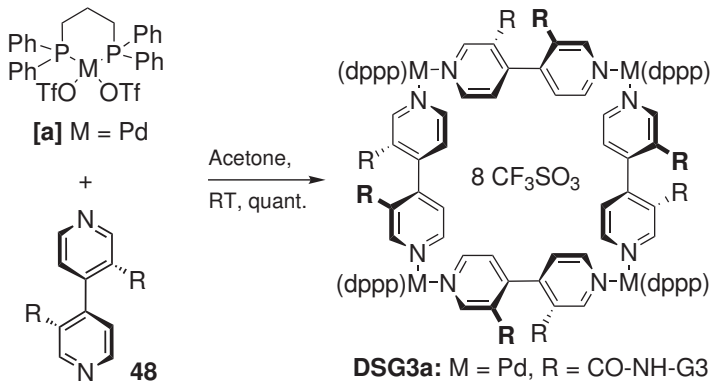

Mol. Weight: 17573.5 g/mol ($C_{1052}H_{904}F_{24}N_{16}O_{152}P_8Pd_4S_8$).

^{1}H-NMR: (400 MHz, [D_7]-dimethylformamide) δ (ppm): 9.01 (b, 8H, H_{amide}), 8.70 (s, 8H, $H_{pyridine}$), 8.56 (d, 8H, $3J_{HH}$=4.44 Hz, $H_{pyridine}$), 7.75 (m, 32H, H_{dppp}), 7.60 (m, 16H, H_{dppp}), 7.50 (m, 32H, H_{dppp}), 7.37-7.24 (m, 320H, H_{phenyl}), 7.08 (d, 8H, $3J_{HH}$=5.04 Hz, $H_{pyridine}$), 6.66 (m, 96H, $H_{aromatic}$), 6.58 (m, 48H, $H_{aromatic}$), 6.51 (b, 8H, $H_{aromatic}$), 6.34 (b, 16H, $H_{aromatic}$), 5.00 (b, 128H, $H_{benzylic}$), 4.95 (b, 64H, $H_{benzylic}$, 4.89 (b, 32H, $H_{benzylic}$, 4.18 (s, 16H, ($H_{benzylic}$), 2.88 (m, 16H, H_{dppp}), 1.92 (m, 8H, H_{dppp}).

^{13}C-NMR: (100 MHz, [D_7]-dimethylformamide) δ (ppm): 161.9, 159.5, 159.5, 159.4, 148.3, 148.0, 140.7, 139.3, 136.8, 136.5, 133.3, 132.6, 129.2, 128.3, 127.7, 127.6, 125.9, 106.5, 106.2, 101.1, 73.5, 69.3, 69.1, 47.9, 24.9, 17.7.

^{19}F-NMR: (376 MHz, [D_7]-dimethylformamide) δ (ppm): -78.13.

^{31}P-NMR: (162 MHz, [D_7]-dimethylformamide) δ (ppm): 19.98.

MS (ESI): m/z=4876.7 Da $[M\text{-}2OTf]^{2+}$, 3200.9 Da $[M\text{-}2OTf]^{2+}$.

DSG3b

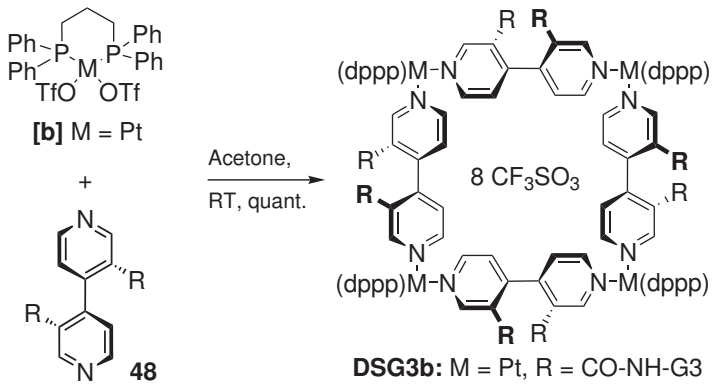

Mol. Weight: 17929.7 g/mol ($C_{1052}H_{904}F_{24}N_{16}O_{152}P_8Pt_4S_8$).

^{1}**H-NMR**: (400 MHz, [D_7]-dimethylformamide) δ (ppm): 8.81 (b, 8H, $H_{pyridine}$), 8.56 (b, 16H, $H_{pyridine}$ + H_{amide}), 7.85 (b, 32H, H_{dppp}), 7.65 (b, 16H, H_{dppp}), 7.56 (b, 32H, H_{dppp}), 7.43-7.28 (b, 320H, H_{phenyl}), 7.11 (m, 8H, $H_{pyridine}$), 6.86 -6.52 (m, 168H, $H_{aromatic}$), 5.10 (b, 128H, $H_{benzylic}$), 5.06 (b, 64H, $H_{benzylic}$), 5.00 (b, 32H, $H_{benzylic}$), 4.29 (b, 16H, $H_{benzylic}$), 3.14 (m, 16H, H_{dppp}), 2.28 (m, 8H, H_{dppp}).

^{19}**F-NMR**: (376 MHz, [D_7]-dimethylformamide) δ (ppm): -78.16.

^{31}**P-NMR**: (202 MHz, [D_7]-dimethylformamide, 373 K) δ (ppm): -9.19 $^1J_{Pt195,P} = 3237$ Hz.

AS1a

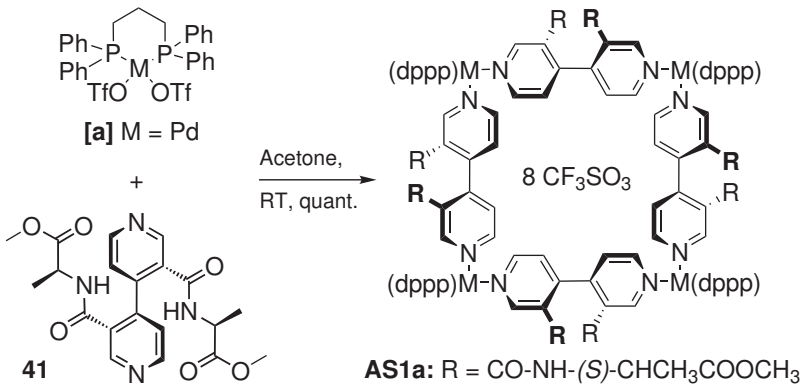

Mol. Weight: 4920.4 g/mol ($C_{196}H_{192}F_{24}N_{16}O_{48}P_8Pd_4S_8$).

^{1}H-NMR: (500 MHz, [D_6]-acetone) δ (ppm): 9.44 (d, $^3J_{HH}$ = 4 Hz, 4H, $H2_{out}$), 9.20 (d, $^3J_{HH}$ = 4 Hz, 4H, $H2_{in}$), 8.54 (d, $^3J_{HH}$ = 2 Hz, 4H, $H6_{in}$), 8.41 (d, $^3J_{HH}$ = 2 Hz, 4H, $H6_{out}$), 8.40 (m, 16H, H_{dppp}), 7.34 (m, 80H, H_{amides}, H_{dppp}, H_{dppp}, $H5_{in}$, $H5_{out}$), 4.08 (dq, $^3J_{HH}$ = 7 Hz and 6 Hz, 4H, H_{CH}), 3.99 (dq, $^3J_{HH}$ = 7 Hz and 6 Hz, 4H, H_{CH}), 3.54 (s, 12H, H_{OCH3}), 3.41 (br, 8H, H_{dppp}), 3.24 (s, 12H, H_{OCH3}), 3.09 (br, 8H, H_{dppp}), 1.46 (d, $^3J_{HH}$ = 7 Hz, 24H, H_{CH3}), 1.28 (m, 8H, H_{dppp}).

^{13}C-NMR: (125 MHz, [D_6]-acetone) δ (ppm): 172.6 (CO), 171.5 (CO), 162.6 (CO), 162.1 (CO), 150.6 (C2), 150.4 (C2), 149.3 (C6), 148.8 (C6), 147.4 (C4), 145.2 (C4), 135.4, 135.3, 134.6, 133.4, 133.3, 133.3, 132.6, 132.4, 130.7, 130.6, 130.4, 130.4, 130.2, 130.2, 129.7, 129.6, 129.6, 128.6, 128.6 (C3), 127.9 (C3), 125.3, 125.2, 124.8, 124.7, 124.5, 124.2, 123.9, 123.7, 122.3 (C5), 119.8 (C5), 51.6 (OCH3), 51.4 (OCH3), 49.8 (CH), 49.6 (CH), 28.8, 22.4, 22.1, 17.2, 16.5, 16.3, 15.6 (CH3), 15.3 (CH3).

^{31}P-NMR: (202 MHz, [D_6]-acetone) δ (ppm): 6.2 (d, $^2J_{PP}$ =31 Hz, 4P), 4.4 (d, $^2J_{PP}$ =31 Hz, 4P).

File Name(s): 41x4b005.07 and 44m5m002.07.

MS (ESI): m/z = 2313.3 Da $[M\text{-}2OTf]^{2+}$.

AS1b

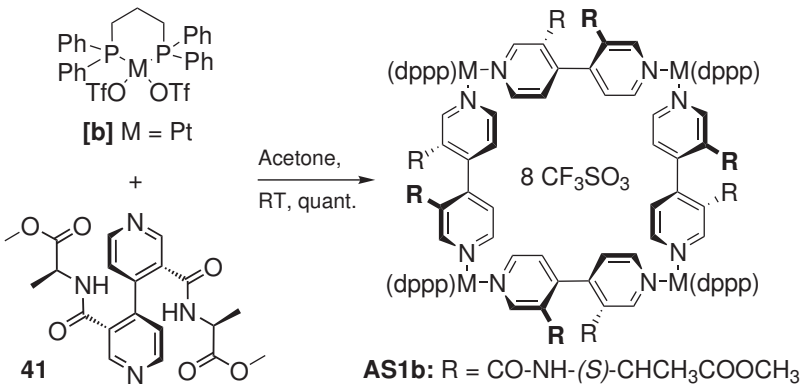

Mol. Weight: 5276.7 g/mol ($C_{196}H_{192}F_{24}N_{16}O_{48}P_8Pt_4S_8$).

^{1}H-NMR: (500 MHz, [D_6]-acetone) δ (ppm): 9.43 (dd, $^3J_{HH}$ = 6 Hz and 2 Hz, 4H, $H2_{out}$), 9.21 (dd, $^3J_{HH}$ = 6 Hz and 2 Hz, 4H, $H2_{in}$), 8.63 (d, $^3J_{HH}$ = 3 Hz, 4H, $H6_{in}$), 8.57 (d, $^3J_{HH}$ = 3 Hz, 4H, $H6_{out}$), 8.40 (m, 16H, H_{dppp}), 7.40 (m, 80H, H_{amides}, H_{dppp}, $H5_{in}$, $H5_{out}$), 4.09(dq, $^3J_{HH}$ = 7 Hz and 6 Hz, 4H, H_{CH}), 3.96 (dq, $^3J_{HH}$ = 7 Hz and 6 Hz, 4H, H_{CH}) , 3.50 (br, 20H, H_{OCH3} and H_{dppp}), 3.26 (br, 20H, H_{OCH3} and H_{dppp}), 1.47 (d, $^3J_{HH}$ = 7 Hz, 24H, H_{CH3}), 1.29 (m, 8H, H_{dppp}).

^{13}C-NMR: (125 MHz, [D_6]-acetone) δ (ppm): 172.4 (CO), 171.3 (CO), 162.4 (CO), 161.9 (CO), 150.4 (C2), 150.3 (C2), 149.1 (C6), 148.6 (C6), 147.2 (C4), 145.0 (C4), 135.2, 134.4, 133.2, 133.1, 132.4, 132.2, 130.5, 130.4, 130.3, 130.2, 130.1, 130.0, 129.6, 129.5, 129.4, 128.4 (C3), 127.7 (C3), 125.1, 125.0, 124.6, 124.5, 124.3, 124.0, 123.8, 123.5, 122.1 (C5), 119.6 (C5), 51.4 (OCH3), 51.3 (OCH3), 49.6 (CH), 49.4 (CH), 22.1, 21.9, 17.0, 15.5 (CH3), 15.1(CH3).

^{31}P-NMR: (202 MHz, [D_6]-acetone) δ (ppm): -12.7 (d, $^2J_{PP}$ = 30 Hz, 4P), -13.7 (d, $^2J_{PP}$ = 30 Hz, 4P), $^1J_{Pt195,P}$ = 3057 Hz.

File Name(s): 41x4b006.07 and 44m5m001.07.

MS (ESI): m/z = 1611.0 Da $[M\text{-}3OTf]^{3+}$ and 2490.5 Da $[M\text{-}2OTf]^{2+}$.

CS1a

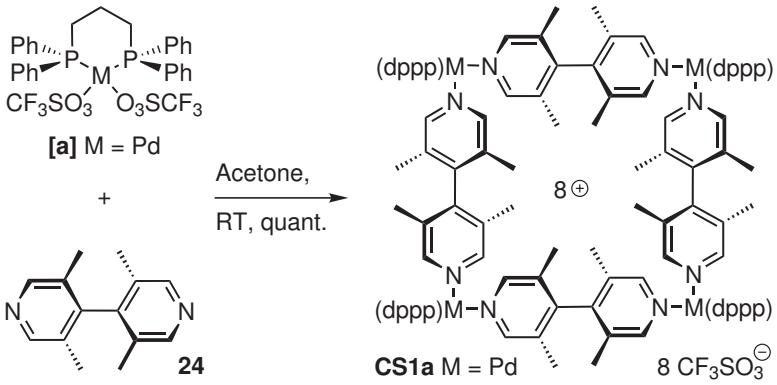

Mol. Weight: 4112.4 g/mol ($C_{172}H_{168}F_{24}N_8O_{24}P_8Pd_4S_8$).

^{1}H-NMR: (400 MHz, [D_6]-acetone) δ (ppm): 8.83 (s, 8H, $H_{Py(out)}$), 8.43 (s, 8H, $H_{Py(in)}$), 7.60 (m, 80H, H_{dppp}), 3.33 (br, 16H, H_{dppp}), 2.41 (br, 8H, H_{dppp}), 1.49 (s, 24H, $H_{CH3(out)}$), 1.22 (s, 24H, $H_{CH3(in)}$).

^{31}P-NMR: (162 MHz, [D_6]-acetone) δ (ppm): 9.65 (s, 8P).

File Name(s): 37x4a028.07 and 37x4a042.07 for [D_7]-dimethylformamide.

MS (ESI): m/z = 1223.2 Da $[M\text{-}3OTf]^{3+}$.

CS1b

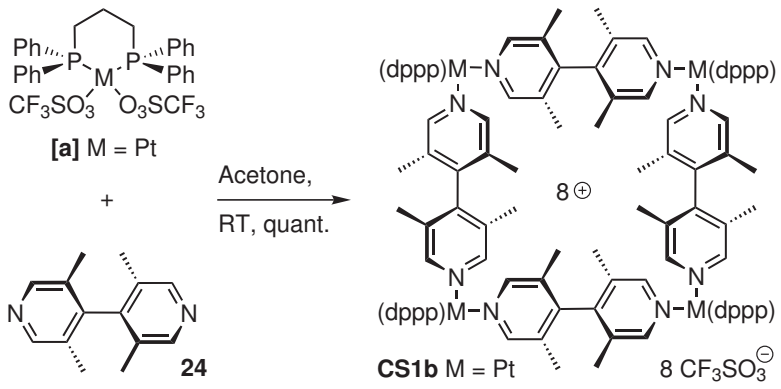

Mol. Weight:	4468.6 g/mol ($C_{172}H_{168}F_{24}N_8O_{24}P_8Pt_4S_8$).
^{1}**H-NMR**:	(400 MHz, [D_6]-acetone) δ (ppm): 8.46 (s, 8H, $H_{Py(out)}$), 8.36 (s, 8H, $H_{Py(in)}$), 7.28 (m, 80H, H_{dppp}), 2.81 (br, 16H, H_{dppp}), 1.97 (br, 8H, H_{dppp}), 1.42 (s, 24H, $H_{CH3(out)}$), 0.95 (s, 24H, $H_{CH3(in)}$).
^{31}**P-NMR**:	(162 MHz, [D_6]-acetone) δ (ppm): -12.26 (s, 8P); $^1J_{Pt195,P}$ = 3050 Hz.
MS (ESI):	m/z = 1341.3 Da $[M\text{-}3OTf]^{3+}$.

CS2a

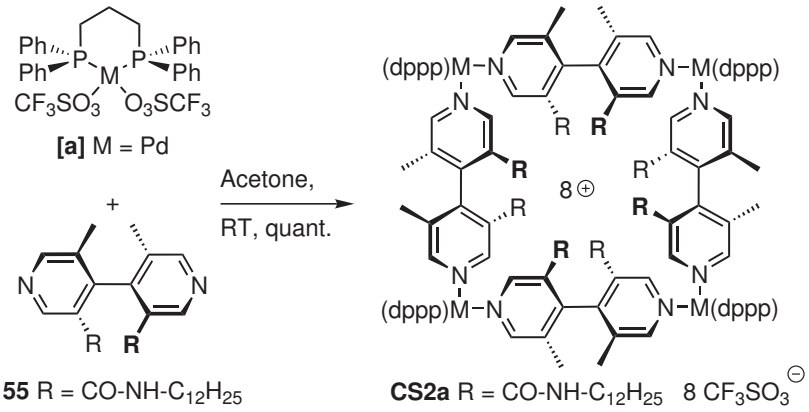

Mol. Weight:	5689.8 g/mol ($C_{268}H_{352}F_{24}N_{16}O_{32}P_8Pd_4S_8$).
^{1}**H-NMR**:	(400 MHz, [D$_6$]-acetone) δ (ppm): 8.00 (m, 104H, H_{py}, H_{amide} and H_{dppp}), 3.20 (m, 32H, $H_{NH-CH2-C11H23}$ and H_{dppp}), 1.20 (m, 216H, H_{CH3}, $H_{NH-CH2-C11H23}$ and H_{dppp}).
^{31}**P-NMR**:	(162 MHz, [D$_6$]-acetone) δ (ppm): 10.61 (d, $^2J_{PP} = 33.6$ Hz, 2P), 10.17 (d, $^2J_{PP} = 32.0$ Hz, 2P), 8.73 (d, $^2J_{PP} = 31.3$ Hz, 2P), 8.02 (d, $^2J_{PP} = 33.6$ Hz, 2P).
File Name(s):	35x4a116.07.
MS (ESI):	m/z = 2699.0 Da $[M\text{-}2OTf]^{2+}$.

CS2b

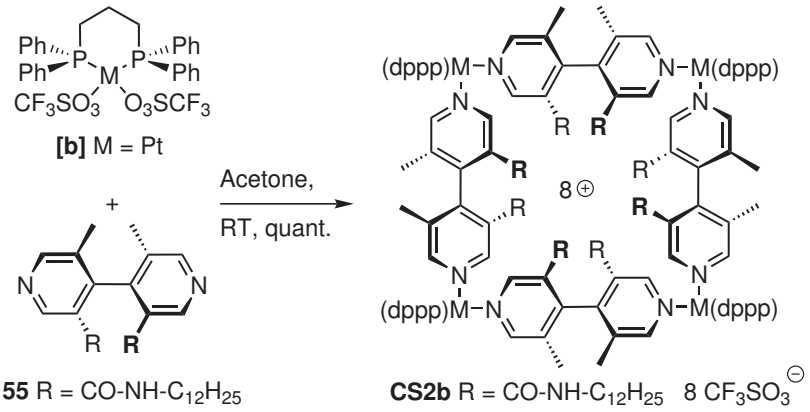

Mol. Weight: 6046.0 g/mol ($C_{268}H_{352}F_{24}N_{16}O_{32}P_8Pt_4S_8$).

^{1}H-NMR: (400 MHz, [D_6]-acetone) δ (ppm): 8.00 (m, 104H, H_{py}, H_{amide} and H_{dppp}), 3.20 (m, 32H, $H_{NH-CH2-C11H23}$ and H_{dppp}), 1.20 (m, 216H, H_{CH3}, $H_{NH-CH2-C11H23}$ and H_{dppp}).

^{31}P-NMR: (162 MHz, [D_6]-acetone) δ (ppm): -12.26 (d, $^2J_{PP}$ = 31.3 Hz, 4P), -14.01 (d, $^2J_{PP}$ = 30.5 Hz, 2P), -14.87 (d, $^2J_{PP}$ = 31.3 Hz, 2P), $^1J_{Pt195,P}$ = ca. 3050 Hz, in all three cases.

File Name(s): 35x4a118.07.

MS (ESI): m/z = 2876.2 Da $[M\text{-}2OTf]^{2+}$.

CS3a

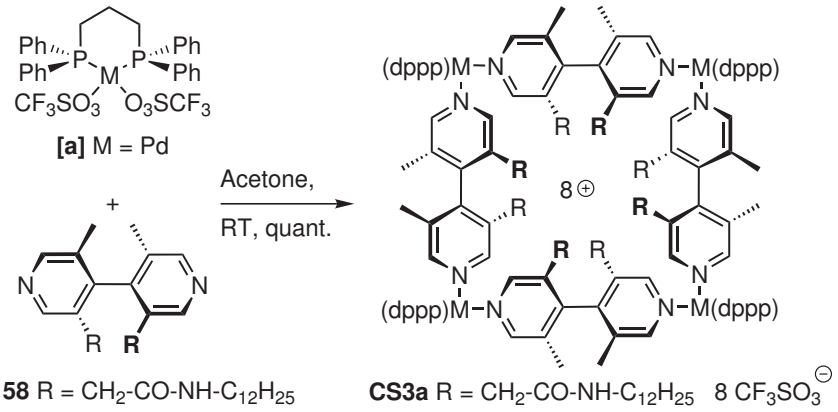

Mol. Weight: 5801.9 g/mol ($C_{276}H_{368}F_{24}N_{16}O_{32}P_8Pd_4S_8$).

^{1}H-NMR: (400 MHz, [D_7]-dimethylformamide) δ (ppm): 8.62 (br, 8H, H-2 and H-2'or H-6 and H-6'), 8.33 (br, 8H, H-2 and H-2'or H-6 and H-6'), 7.78 (br, 32H, H_{dppp}), 7.49 (br, 16H, H_{dppp}), 7.41 (br, 32H, H_{dppp}), 3.18 (br, 48 H, H_{CH2} , H_{CH2} and H_{dppp}), 2.19 (br, 8H, H_{dppp}), 1.56 (br, 24H; H_{CH3}), 1.14 (br, 160H, $H_{(CH2)10}$), 0.76 (t, 3JHH = 7 Hz, 24H, H_{CH3}).

^{31}P-NMR: (162 MHz, [D_7]-dimethylformamide) δ (ppm): 16.81 (br, 4P), 10.05 (br, 4P).

File Name(s): 35x4b034.07.

MS (ESI): m/z = 1787.1 Da $[M\text{-}3OTf]^{3+}$.

CS3b

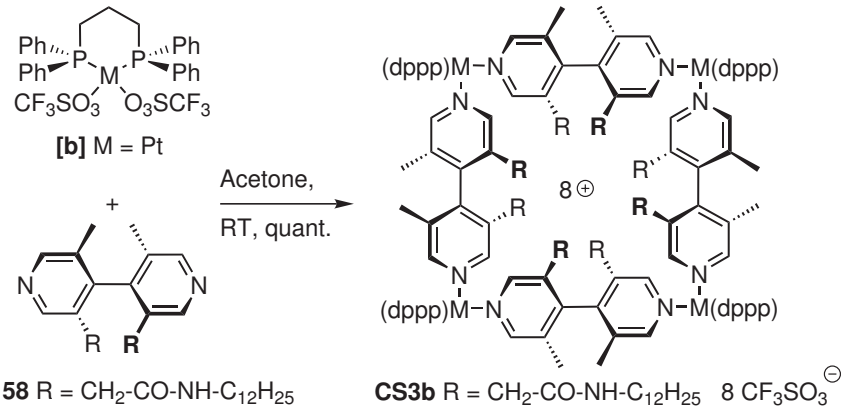

Mol. Weight: 6158.2 g/mol ($C_{276}H_{368}F_{24}N_{16}O_{32}P_8Pt_4S_8$).

^{1}H-NMR: (400 MHz, [D_7]-dimethylformamide) δ (ppm): 8.60 (br, 16H, H-2, H-2', H-6 and H-6'), 7.51 (br, 80H, H_{dppp}), 3.10 (br, 48 H, H_{CH2} , H_{CH2} and H_{dppp}), 2.12 (br, 8H, H_{dppp}), 1.29 (br, 24H; H_{CH3}), 1.13 (br, 160H, $H_{(CH2)10}$), 0.76 (br, 24H, H_{CH3}).

^{31}P-NMR: (162 MHz, [D_7]-dimethylformamide) δ (ppm): -9.36 (br, 2P), -11.70 (br, 6P), $^1J_{Pt195,P}$ ca. 3100 Hz, in both cases.

File Name(s): 35x4a120.07.

MS (ESI): m/z = 1905.4 Da [M-3OTf]$^{3+}$.

8.6 Data of Crystal Structures

The following single-crystal X-ray diffraction studies were carried out by Dr. Martin Nieger on Nonius Kappa-CCD diffractometers at 123 K using $Mo_{K\alpha}$ radiation ($\alpha = 0.71073$Å). Direct methods (SHELXS-97[280]) were used for structure solution; full-matrix least squares on F^2 (SHELXL-97[281]) for refinement. No absorption corrections were applied, and H atoms were refined using a riding model. Compounds **22**, **24**, **27**, and **30** were measured in Bonn, whereas **41**, **42**, and **AS1b** were measured in Helsinki.

8.6.1 3,3'-Diethyl-[4,4']-bipyridine 22

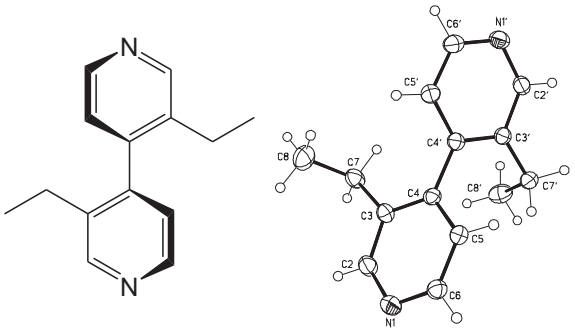

Figure 8.1: 3,3'-Diethyl-[4,4']-bipyridine **22**

Identification code	cas011
Empirical formula	$C_{14}H_{16}N_2$
Formula weight	212.29
Temperature	123(2) K
Wavelength	0.71073Å
Crystal system, space group	Triclinic, P-1 (No.2)
Unit cell dimensions	a = 7.4320(3)Å alpha = 99.171(2) deg.
	b = 9.3120(4)Å beta = 109.708(2) deg.
	c = 10.4064(5)Å gamma = 112.462(2) deg.
Volume	591.18(4) $Å^3$
Z, Calculated density	2, 1.193 Mg/m^3
Absorption coefficient	0.071 mm^{-1}
F(000)	228
Crystal size	0.50 x 0.40 x 0.10 mm
Diffractometer	Nonius KappaCCD
Theta range for data collection	3.06 to 25.03 deg.
Limiting indices	$-7 \leq h \leq 8$, $-11 \leq k \leq 11$, $-12 \leq l \leq 10$
Reflections collected / unique	4729 / 2081 [R(int) = 0.0278]
Completeness to theta = 25.03	99.5 %
Absorption correction	None
Refinement method	Full-matrix least-squares on F^2
Data / restraints / parameters	2081 / 0 / 145
Goodness-of-fit on F^2	1.000
Final R indices [I>2sigma(I)]	R1 = 0.0369, wR2 = 0.0910
R indices (all data)	R1 = 0.0494, wR2 = 0.0965
Largest diff. peak and hole	0.137 and -0.184 e.$Å^{-3}$

Table 8.1: Crystal data and structure refinement for 3,3'-diethyl-[4,4']-bipyridine **22**.

	x	y	z	U(eq)
N(1)	7218(2)	4463(1)	3578(1)	28(1)
C(2)	5454(2)	4088(1)	2387(1)	26(1)
C(3)	4294(2)	4973(1)	2187(1)	22(1)
C(4)	5069(2)	6403(1)	3331(1)	20(1)
C(5)	6890(2)	6803(1)	4585(1)	21(1)
C(6)	7888(2)	5816(1)	4665(1)	24(1)
C(7)	2286(2)	4334(1)	791(1)	28(1)
C(8)	368(2)	2885(2)	746(2)	38(1)
N(1')	2033(2)	9550(1)	3129(1)	26(1)
C(2')	3983(2)	10035(1)	3144(1)	23(1)
C(3')	5050(2)	9087(1)	3170(1)	20(1)
C(4')	4022(2)	7501(1)	3231(1)	19(1)
C(5')	1990(2)	6983(1)	3220(1)	23(1)
C(6')	1066(2)	8019(1)	3155(1)	25(1)
C(7')	7159(2)	9757(1)	3052(1)	26(1)
C(8')	6821(2)	9067(2)	1506(2)	34(1)

Table 8.2: Atomic coordinates (x 10^4) and equivalent isotropic displacement parameters (Å^2 x 10^3) for 3,3'-diethyl-[4,4']-bipyridine **22**. U(eq) is defined as one third of the trace of the orthogonalized Uij tensor.

♯1	-x+1	-y+2	-z+1

Table 8.3: Symmetry transformations used to generate equivalent atoms.

8.6.2 3,5,3',5'-Tetramethyl-[4,4']-bipyridine 24

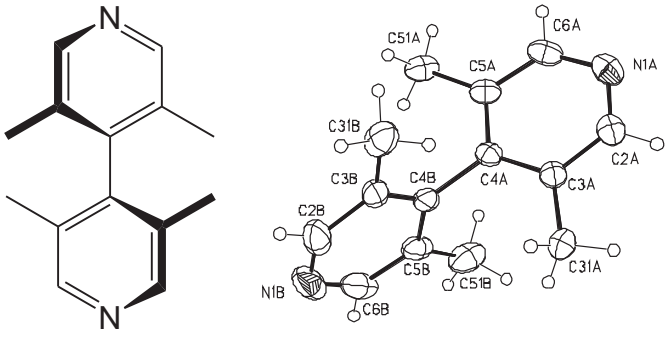

Figure 8.2: 3,5,3',5'-Tetramethyl-[4,4']-bipyridine **24**

Identification code	cas005
Empirical formula	$C_{14}H_{16}N_2$
Formula weight	212.29
Temperature	123(2) K
Wavelength	0.71073Å
Crystal system, space group	Monoclinic, C2/c (No.15)
Unit cell dimensions	a = 28.3010(5)Å alpha = 90 deg.
	b = 11.4661(2)Å beta = 99.471(2) deg.
	c = 14.8096(3)Å gamma = 90 deg.
Volume	4740.24(15) $Å^3$
Z, Calculated density	16, 1.190 Mg/m^3
Absorption coefficient	0.071 mm^{-1}
F(000)	1824
Crystal size	0.25 x 0.20 x 0.10 mm
Diffractometer	Nonius KappaCCD
Theta range for data collection	2.92 to 25.03 deg.
Limiting indices	-33≤h≤28, -11≤k≤13, -17≤l≤17
Reflections collected / unique	11694 / 4187 [R(int) = 0.0287]
Completeness to theta = 25.03	99.7 %
Absorption correction	None
Refinement method	Full-matrix least-squares on F^2
Data / restraints / parameters	4187 / 0 / 297
Goodness-of-fit on F^2	0.961
Final R indices [I>2sigma(I)]	R1 = 0.0381, wR2 = 0.0917
R indices (all data)	R1 = 0.0584, wR2 = 0.0984
Largest diff. peak and hole	0.157 and -0.185 e.$Å^{-3}$

Table 8.4: Crystal data and structure refinement for 3,5,3',5'-tetramethyl-[4,4']-bipyridine **24**.

	x	y	z	U(eq)
N(1)	800(1)	515(1)	6733(1)	31(1)
C(2)	631(1)	1521(1)	7010(1)	28(1)
C(3)	894(1)	2302(1)	7609(1)	24(1)
C(31)	667(1)	3404(1)	7878(1)	34(1)
C(4)	1373(1)	2027(1)	7943(1)	22(1)
C(5)	1564(1)	995(1)	7653(1)	23(1)
C(51)	2081(1)	674(1)	7940(1)	31(1)
C(6)	1259(1)	280(1)	7063(1)	29(1)
N(1')	2237(1)	4384(1)	9792(1)	32(1)
C(2')	2170(1)	4532(1)	8883(1)	29(1)
C(3')	1901(1)	3795(1)	8251(1)	23(1)
C(31')	1857(1)	4018(1)	7241(1)	31(1)
C(4')	1676(1)	2843(1)	8586(1)	21(1)
C(5')	1732(1)	2671(1)	9538(1)	25(1)
C(51')	1495(1)	1680(1)	9949(1)	37(1)
C(6')	2018(1)	3459(1)	10088(1)	29(1)
N(1A)	5100(1)	2291(1)	4859(1)	37(1)
C(2A)	5012(1)	3210(1)	5356(1)	32(1)
C(3A)	4612(1)	3326(1)	5786(1)	27(1)
C(31A)	4547(1)	4411(1)	6318(1)	35(1)
C(4A)	4284(1)	2409(1)	5700(1)	25(1)
C(5A)	4360(1)	1434(1)	5174(1)	29(1)
C(51A)	4021(1)	419(1)	5045(1)	37(1)

Table 8.5: To be continued on next page.

	x	y	z	U(eq)
C(6A)	4773(1)	1441(1)	4774(1)	35(1)
N(1B)	3048(1)	2482(1)	7052(1)	59(1)
C(2B)	3029(1)	2865(2)	6196(1)	49(1)
C(3B)	3414(1)	2871(1)	5721(1)	34(1)
C(31B)	3353(1)	3326(2)	4758(1)	43(1)
C(4B)	3854(1)	2453(1)	6173(1)	29(1)
C(5B)	3889(1)	2060(1)	7077(1)	37(1)
C(51B)	4353(1)	1639(2)	7617(1)	50(1)
C(6B)	3474(1)	2094(2)	7464(1)	51(1)

Table 8.6: Atomic coordinates (x 10^4) and equivalent isotropic displacement parameters (Å^2 x 10^3) for 3,5,3',5'-tetramethyl-[4,4']-bipyridine **24**. U(eq) is defined as one third of the trace of the orthogonalized Uij tensor.

8.6.3 2,6,2',6'-Tetramethyl-[4,4']-bipyridine 27

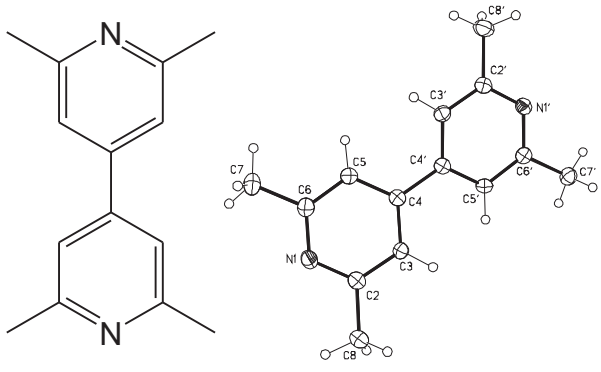

Figure 8.3: 3,5,3',5'-Tetramethyl-[4,4']-bipyridine **24**

Identification code	cas012
Empirical formula	$C_{14}H_{16}N_2$
Formula weight	212.29
Temperature	123(2) K
Wavelength	0.71073Å
Crystal system, space group	Tetragonal, I4(1)/a (No.88)
Unit cell dimensions	a = 21.8717(7)Å alpha = 90 deg.
	b = 21.8717(7)Å beta = 90 deg.
	c = 9.9277(3)Å gamma = 90 deg.
Volume	4749.1(3) $Å^3$
Z, Calculated density	16, 1.188 Mg/m^3
Absorption coefficient	0.071 mm^{-1}
F(000)	1824
Crystal size	0.40 x 0.20 x 0.20 mm
Diffractometer	Nonius KappaCCD
Theta range for data collection	2.92 to 25.03 deg.
Limiting indices	-26≤h≤17, -25≤k≤26, -11≤l≤8
Reflections collected / unique	9821 / 2092 [R(int) = 0.0296]
Completeness to theta = 25.03	99.7 %
Absorption correction	None
Refinement method	Full-matrix least-squares on F^2
Data / restraints / parameters	2092 / 0 / 149
Goodness-of-fit on F^2	1.067
Final R indices [I>2sigma(I)]	R1 = 0.0411, wR2 = 0.1132
R indices (all data)	R1 = 0.0508, wR2 = 0.1180
Largest diff. peak and hole	0.261 and -0.206 $e.Å^{-3}$

Table 8.7: Crystal data and structure refinement for 2,6,2',6'-tetramethyl-[4,4']-bipyridine **27**.

	x	y	z	U(eq)
N(1)	3693(1)	3719(1)	4212(1)	22(1)
C(2)	3327(1)	3809(1)	5280(1)	20(1)
C(3)	2890(1)	3385(1)	5678(1)	17(1)
C(4)	2811(1)	2846(1)	4953(1)	18(1)
C(5)	3191(1)	2758(1)	3844(2)	21(1)
C(6)	3628(1)	3195(1)	3512(2)	23(1)
C(7)	4061(1)	3099(1)	2360(2)	33(1)
C(8)	3427(1)	4390(1)	6050(2)	29(1)
N(1')	1466(1)	1496(1)	6025(1)	20(1)
C(2')	1950(1)	1357(1)	5234(1)	20(1)
C(3')	2398(1)	1778(1)	4903(1)	19(1)
C(4')	2346(1)	2382(1)	5342(1)	17(1)
C(5')	1842(1)	2526(1)	6140(1)	18(1)
C(6')	1423(1)	2074(1)	6487(1)	19(1)
C(7')	903(1)	2205(1)	7434(2)	24(1)
C(8')	1973(1)	713(1)	4710(2)	30(1)

Table 8.8: Atomic coordinates (x 10^4) and equivalent isotropic displacement parameters (Å^2 x 10^3) for 2,6,2',6'-tetramethyl-[4,4']-bipyridine **27**. U(eq) is defined as one third of the trace of the orthogonalized Uij tensor.

♯1	-x+1/2	-y+1/2	-z+3/2

Table 8.9: Symmetry transformations used to generate equivalent atoms.

8.6.4 5,6-Dihydro-[3,8]phenanthroline 30

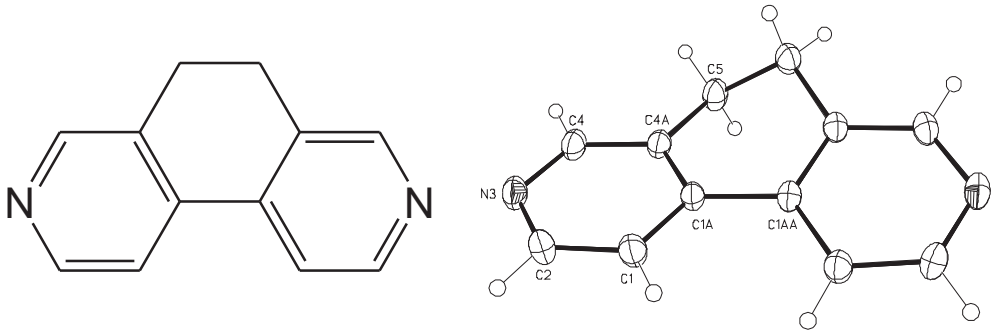

Figure 8.4: 5,6-Dihydro-[3,8]phenanthroline **30**

Identification code	cas002
Empirical formula	$C_{12}H_{10}N_2$
Formula weight	182.22
Temperature	123(2) K
Wavelength	0.71073Å
Crystal system, space group	Monoclinic, C2/c (No.15)
Unit cell dimensions	a = 13.1952(3)Å alpha = 90 deg.
	b = 7.5665(2)Å beta = 117.392(1) deg.
	c = 9.8732(3)Å gamma = 90 deg.
Volume	875.23(4) $Å^3$
Z, Calculated density	4, 1.383 Mg/m^3
Absorption coefficient	0.084 mm^{-1}
F(000)	384
Crystal size	0.30 x 0.25 x 0.20 mm
Diffractometer	Nonius KappaCCD
Theta range for data collection	3.21 to 27.45 deg.
Limiting indices	-17≤h≤17, -9≤k≤9, -12≤l≤12
Reflections collected / unique	8549 / 987 [R(int) = 0.0360]
Completeness to theta = 27.45	98.7%
Absorption correction	None
Refinement method	Full-matrix least-squares on F^2
Data / restraints / parameters	987 / 0 / 64
Goodness-of-fit on F^2	1.096
Final R indices [I>2sigma(I)]	R1 = 0.0406, wR2 = 0.1125
R indices (all data)	R1 = 0.0440, wR2 = 0.1149
Largest diff. peak and hole	0.259 and -0.178 e.$Å^{-3}$

Table 8.10: Crystal data and structure refinement for 5,6-dihydro-[3,8]phenanthroline **30**.

	x	y	z	U(eq)
C(1A)	4568(1)	5727(1)	6686(1)	19(1)
C(1)	4006(1)	4207(1)	5912(1)	24(1)
C(2)	3221(1)	4316(1)	4379(1)	26(1)
N(3)	2939(1)	5834(1)	3589(1)	25(1)
C(4)	3470(1)	7294(2)	4355(1)	23(1)
C(4A)	4293(1)	7324(1)	5880(1)	20(1)
C(5)	4893(1)	8997(1)	6668(1)	25(1)

Table 8.11: Atomic coordinates (x 10^4) and equivalent isotropic displacement parameters (Å^2 x 10^3) for 5,6-dihydro-[3,8]phenanthroline **30**. U(eq) is defined as one third of the trace of the orthogonalized Uij tensor.

ǂ1 -x+1 y -z+3/2

Table 8.12: Symmetry transformations used to generate equivalent atoms.

8.6.5 N,N',N",5'-Tetramethyl-[4,4']-bipyridine -3,3',5-tricarboxamide

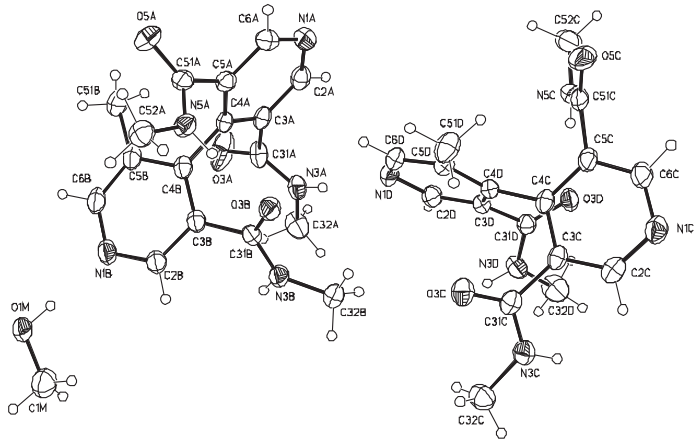

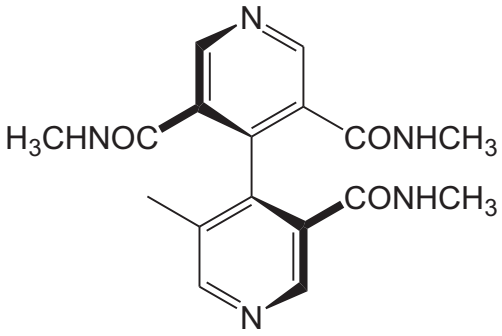

Figure 8.5: 3,5,3',5'-Tetramethyl-[4,4']-bipyridine **24**

Identification code	cas008c
Empirical formula	$C_{17}H_{19}N_5O_3$ - 0.5 MeOH
Formula weight	357.39
Temperature	123(2) K
Wavelength	0.71073Å
Crystal system, space group	Monoclinic, P2(1)/c (No.14)
Unit cell dimensions	a = 16.1602(4)Å alpha = 90 deg.
	b = 14.6920(3)Å beta = 107.408(1) deg.
	c = 16.1009(3)Å gamma = 90 deg.
Volume	3647.68(14) $Å^3$
Z, Calculated density	8, 1.302 Mg/m^3
Absorption coefficient	0.093 mm^{-1}
F(000)	1512
Crystal size	0.30 x 0.20 x 0.10 mm
Diffractometer	Nonius KappaCCD
Theta range for data collection	2.93 to 25.03 deg.
Limiting indices	$-17\leq h\leq 19$, $-15\leq k\leq 17$, $-18\leq l\leq 19$
Reflections collected / unique	23215 / 6431 [R(int) = 0.0393]
Completeness to theta = 25.03	99.8 %
Absorption correction	None
Refinement method	Full-matrix least-squares on F^2
Data / restraints / parameters	6431 / 7 / 499
Goodness-of-fit on F^2	0.990
Final R indices [I>2sigma(I)]	R1 = 0.0404, wR2 = 0.1003
R indices (all data)	R1 = 0.0656, wR2 = 0.1087
Largest diff. peak and hole	0.297 and -0.248 e.$Å^{-3}$

Table 8.13: Crystal data and structure refinement for N,N',N",5'-tetramethyl-[4,4']-bipyridine-3,3',5-tricarboxamide.

	x	y	z	U(eq)
N(1A)	992(1)	5852(1)	3455(1)	33(1)
C(2A)	766(1)	5902(1)	4190(1)	31(1)
C(3A)	1126(1)	6508(1)	4862(1)	26(1)
C(31A)	789(1)	6577(1)	5635(1)	33(1)
O(3A)	403(1)	7261(1)	5743(1)	67(1)
N(3A)	952(1)	5866(1)	6165(1)	31(1)
H(3A)	1235(11)	5407(11)	6031(11)	37
C(32A)	730(1)	5846(2)	6977(1)	44(1)
C(4A)	1794(1)	7079(1)	4793(1)	24(1)
C(5A)	2029(1)	7047(1)	4028(1)	25(1)
C(51A)	2720(1)	7652(1)	3880(1)	26(1)
O(5A)	2531(1)	8225(1)	3288(1)	37(1)
N(5A)	3514(1)	7510(1)	4405(1)	28(1)
H(5A)	3555(12)	7086(11)	4822(10)	34
C(52A)	4256(1)	8057(1)	4371(1)	33(1)
C(6A)	1604(1)	6432(1)	3384(1)	32(1)
N(1B)	2972(1)	8883(1)	6911(1)	36(1)
C(2B)	3227(1)	8020(1)	6924(1)	31(1)
C(3B)	2877(1)	7407(1)	6252(1)	26(1)
C(31B)	3234(1)	6455(1)	6298(1)	26(1)
O(3B)	3508(1)	6161(1)	5709(1)	30(1)
N(3B)	3246(1)	5984(1)	7008(1)	29(1)
H(3B)	3024(12)	6247(12)	7389(11)	35
C(32B)	3577(1)	5056(1)	7163(1)	37(1)
C(4B)	2221(1)	7713(1)	5525(1)	26(1)
C(5B)	1933(1)	8613(1)	5506(1)	31(1)
C(51B)	1198(1)	8976(1)	4765(1)	41(1)
C(6B)	2337(1)	9160(1)	6212(1)	35(1)

Table 8.14: To be continued on next page.

	x	y	z	U(eq)
N(1C)	3927(1)	144(1)	5434(1)	36(1)
C(2C)	4137(1)	731(1)	6097(1)	33(1)
C(3C)	3725(1)	1560(1)	6114(1)	26(1)
C(31C)	4086(1)	2236(1)	6827(1)	28(1)
O(3C)	4231(1)	3024(1)	6646(1)	40(1)
N(3C)	4265(1)	1938(1)	7644(1)	35(1)
H(3C)	4159(13)	1375(11)	7766(12)	41
C(32C)	4618(1)	2549(1)	8374(1)	40(1)
C(4C)	3013(1)	1785(1)	5400(1)	25(1)
C(5C)	2786(1)	1180(1)	4699(1)	29(1)
C(51C)	2044(1)	1344(1)	3891(1)	32(1)
O(5C)	2183(1)	1420(1)	3177(1)	47(1)
N(5C)	1269(1)	1368(1)	4002(1)	36(1)
H(5C)	1228(13)	1316(14)	4522(10)	44
C(52C)	476(1)	1442(2)	3280(1)	49(1)
C(6C)	3271(1)	388(1)	4747(1)	34(1)
N(1D)	1673(1)	4276(1)	5559(1)	32(1)
C(2D)	1530(1)	3514(1)	5945(1)	30(1)
C(3D)	1922(1)	2688(1)	5893(1)	23(1)
C(31D)	1668(1)	1859(1)	6292(1)	26(1)
O(3D)	1432(1)	1160(1)	5854(1)	31(1)
N(3D)	1696(1)	1926(1)	7123(1)	35(1)
H(3D)	1873(13)	2419(11)	7411(12)	42
C(32D)	1455(2)	1163(2)	7583(1)	51(1)
C(4D)	2515(1)	2645(1)	5415(1)	24(1)
C(5D)	2672(1)	3435(1)	4998(1)	28(1)
C(51D)	3325(1)	3453(1)	4507(1)	41(1)

Table 8.15: To be continued on next page.

	x	y	z	U(eq)
C(6D)	2231(1)	4218(1)	5094(1)	31(1)
O(1M)	3896(1)	10153(1)	8099(1)	46(1)
H(1M)	3611(14)	9736(14)	7738(13)	70
C(1M)	4488(1)	9697(1)	8807(1)	47(1)

Table 8.16: Atomic coordinates (x 10^4) and equivalent isotropic displacement parameters (Å^2 x 10^3) for N,N',N",5'-tetramethyl-[4,4']-bipyridine-3,3',5-tricarboxamide. U(eq) is defined as one third of the trace of the orthogonalized Uij tensor.

♯1	x	-y+3/2	z+1/2
♯2	x	y-1	z
♯3	x	-y+1/2	z+1/2
♯4	-x	y-1/2	-z+1/2
♯5	-x	-y+1	-z+1
♯6	-x+1	y+1/2	-z+3/2
♯7	x	y+1	z
♯8	x	-y+3/2	z-1/2

Table 8.17: Symmetry transformations used to generate equivalent atoms.

8.6.6 *S,S*)-2-[3'-(1-methoxycarbonyl-ethylcarbamoyl)-[4,4']-bipyridinyl-[4]-3-carbonyl]-amino-propionic acid methyl ester 41

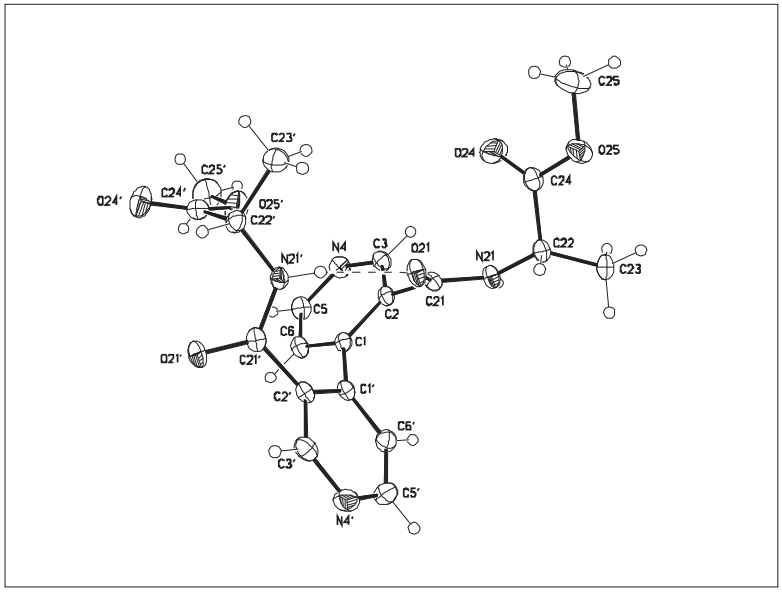

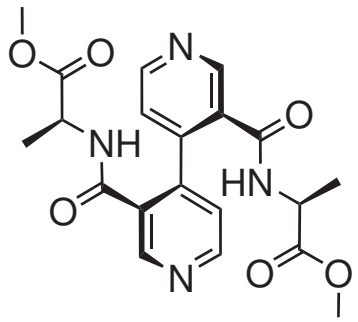

(S,S,aS)-**41**

Figure 8.6: (*S,S*)-2-[3'-(1-Methoxycarbonyl-ethylcarbamoyl)-[4,4']-bipyridinyl-[4]-3-carbonyl]-amino-propionic acid methyl ester **41**

Identification code	cas015hy
Empirical formula	$C_{20}H_{22}N_4O_6$
Formula weight	414.42
Temperature	123(2) K
Wavelength	0.71073Å
Crystal system, space group	Orthorhombic, P2(1)2(1)2(1) (No.19)
Unit cell dimensions	a = 8.732(1)Å alpha = 90 deg.
	b = 11.123(1)Å beta = 90 deg.
	c = 21.076(2)Å gamma = 90 deg.
Volume	2047.0(4) $Å^3$
Z, Calculated density	4, 1.345 Mg/m^3
Absorption coefficient	0.101 mm^{-1}
F(000)	872
Crystal size	0.35 x 0.25 x 0.20 mm
Theta range for data collection	5.02 to 27.48 deg.
Limiting indices	$-11 \leq h \leq 11$, $-14 \leq k \leq 14$, $-27 \leq l \leq 27$
Reflections collected / unique	29007 / 4671 [R(int) = 0.0674]
Completeness to theta = 27.48	99.1 %
Absorption correction	None
Refinement method	Full-matrix least-squares on F^2
Data / restraints / parameters	4671 / 2 / 279
Goodness-of-fit on F^2	1.088
Final R indices [I>2sigma(I)]	R1 = 0.0414, wR2 = 0.0944
R indices (all data)	R1 = 0.0507, wR2 = 0.0991
Absolute structure parameter	-0.7(9), cannot be determined reliabl.
Largest diff. peak and hole	0.254 and -0.243 e.$Å^{-3}$

Table 8.18: Crystal data and structure refinement for **41**.

	x	y	z	U(eq)
C(1)	7065(2)	5632(2)	4314(1)	14(1)
C(2)	8199(2)	5960(2)	3883(1)	15(1)
C(3)	8971(2)	7044(2)	3977(1)	19(1)
N(4)	8663(2)	7797(1)	4456(1)	21(1)
C(5)	7567(2)	7471(2)	4858(1)	20(1)
C(6)	6753(2)	6402(2)	4816(1)	19(1)
C(21)	8454(2)	5249(2)	3291(1)	16(1)
O(21)	7349(1)	4986(1)	2951(1)	21(1)
N(21)	9892(2)	4938(1)	3155(1)	18(1)
H(21)	10630(20)	5143(19)	3413(9)	21
C(22)	10278(2)	4440(2)	2539(1)	17(1)
C(23)	11847(2)	3839(2)	2551(1)	21(1)
C(24)	10224(2)	5434(2)	2043(1)	20(1)
O(24)	10000(2)	6475(1)	2153(1)	39(1)
O(25)	10490(2)	4991(1)	1470(1)	26(1)
C(25)	10289(3)	5801(2)	950(1)	39(1)
C(1')	6267(2)	4443(2)	4288(1)	16(1)
C(2')	4765(2)	4295(2)	4080(1)	16(1)
C(3')	4083(2)	3168(2)	4151(1)	21(1)
N(4')	4774(2)	2213(1)	4400(1)	25(1)
C(5')	6212(2)	2369(2)	4591(1)	26(1)
C(6')	6997(2)	3448(2)	4548(1)	22(1)
C(21')	3804(2)	5271(2)	3793(1)	16(1)
O(21')	2471(1)	5422(1)	3979(1)	20(1)
N(21')	4445(2)	5899(1)	3329(1)	17(1)
H(21')	5379(19)	5732(18)	3193(9)	20
C(22')	3624(2)	6882(2)	3019(1)	19(1)
C(23')	4303(2)	7125(2)	2367(1)	27(1)

Table 8.19: To be continued on next page.

	x	y	z	U(eq)
C(24')	3628(2)	8012(2)	3423(1)	21(1)
O(24')	2499(2)	8574(1)	3549(1)	34(1)
O(25')	5040(2)	8297(1)	3606(1)	33(1)
C(25')	5160(3)	9398(2)	3972(1)	40(1)

Table 8.20: Atomic coordinates (x 10^4) and equivalent isotropic displacement parameters ($Å^2$ x 10^3) for **41**. U(eq) is defined as one third of the trace of the orthogonalized Uij tensor.

D-H...A	d(D-H)	d(H...A)	d(D...A)	∢ (DHA)
N(21)-H(21)...O(21')♯1	0.871(15)	2.030(16)	2.8956(19)	173(2)
N(21')-H(21')...O(21)	0.884(15)	1.977(16)	2.8454(19)	167.0(19)
C(5)-H(5)...O(21')♯2	0.95	2.47	3.392(2)	163.3
C(6)-H(6)...N(4)♯3	0.95	2.49	3.230(2)	135.0
C(6')-H(6')...N(4')♯4	0.95	2.57	3.366(3)	141.2
C(23)-H(23A)...O(24)♯5	0.98	2.52	3.147(2)	121.8

Table 8.21: Hydrogen bonds for **41** [Åand deg.].

♯1	x+1	y	z
♯2	x+1/2	-y+3/2	-z+1
♯3	x-1/2	-y+3/2	-z+1
♯4	x+1/2	-y+1/2	-z+1
♯5	-x+2	y-1/2	-z+1/2

Table 8.22: Symmetry transformations used to generate equivalent atoms.

8.6.7 *R,R*)-2-[3'-(1-methoxycarbonyl-ethylcarbamoyl)-[4,4']-bipyridinyl-[4]-3-carbonyl]-amino-propionic acid methyl ester 42

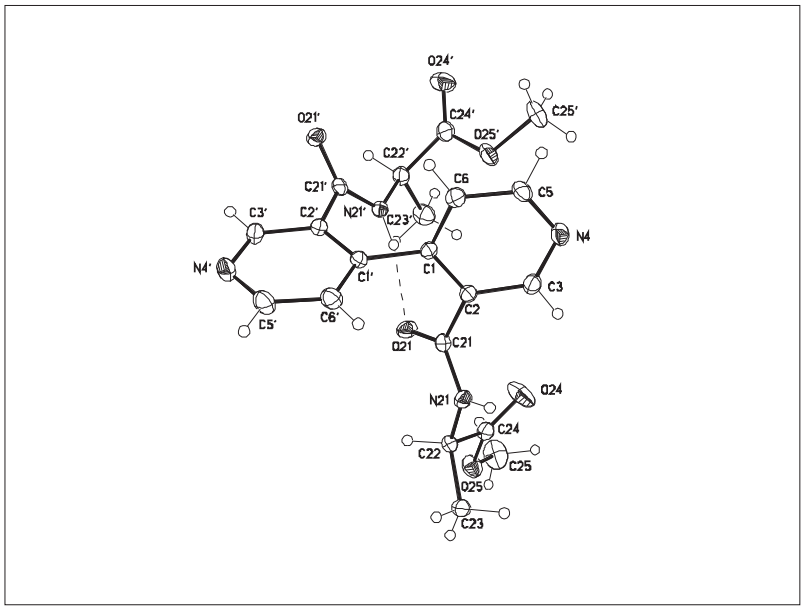

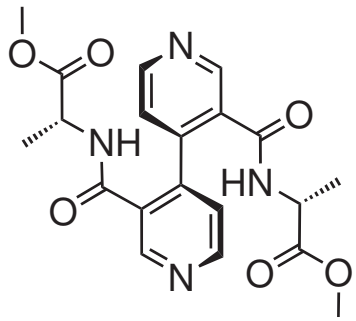

(R,R,aR)-**42**

Figure 8.7: (*R*,*R*)-2-[3'-(1-Methoxycarbonyl-ethylcarbamoyl)-[4,4']-bipyridinyl-[4]-3-carbonyl]-amino-propionic acid methyl ester **42**

Identification code	cas014hy
Empirical formula	$C_{20}H_{22}N_4O_6$
Formula weight	414.42
Temperature	123(2) K
Wavelength	0.71073Å
Crystal system, space group	Orthorhombic, P 212121
Unit cell dimensions	a = 8.709(1)Å alpha = 90 deg.
	b = 11.104(1)Å beta = 90 deg.
	c = 21.032(3)Å gamma = 90 deg.
Volume	2033.9(4) $Å^3$
Z, Calculated density	4, 1.353 Mg/m^3
Absorption coefficient	0.102 mm^{-1}
F(000)	872
Crystal size	0.50 x 0.30 x 0.15 mm
Theta range for data collection	5.03 to 27.47 deg.
Limiting indices	$-11 \leq h \leq 11$, $-14 \leq k \leq 14$, $-27 \leq l \leq 27$
Reflections collected / unique	33705 / 4640 [R(int) = 0.0449]
Completeness to theta = 27.47	98.8 %
Absorption correction	None
Refinement method	Full-matrix least-squares on F^2
Data / restraints / parameters	4640 / 2 / 279
Goodness-of-fit on F^2	1.053
Final R indices [I>2sigma(I)]	R1 = 0.0298, wR2 = 0.0731
R indices (all data)	R1 = 0.0325, wR2 = 0.0752
Absolute structure parameter	-0.1(7), cannot be determined reliabl.
Largest diff. peak and hole	0.261 and -0.185 $e.Å^{-3}$

Table 8.23: Crystal data and structure refinement for **41**.

	x	y	z	U(eq)
C(1)	2939(1)	4368(1)	686(1)	15(1)
C(2)	1800(1)	4034(1)	1118(1)	16(1)
C(3)	1028(1)	2958(1)	1023(1)	20(1)
N(4)	1337(1)	2204(1)	545(1)	22(1)
C(5)	2434(2)	2530(1)	141(1)	22(1)
C(6)	3248(1)	3596(1)	186(1)	20(1)
C(21)	1551(1)	4750(1)	1710(1)	17(1)
O(21)	2654(1)	5010(1)	2050(1)	22(1)
N(21)	110(1)	5059(1)	1846(1)	18(1)
H(21)	-610(17)	4847(14)	1589(7)	21
C(22)	-274(1)	5556(1)	2462(1)	18(1)
C(23)	-1846(1)	6161(1)	2449(1)	21(1)
C(24)	-224(2)	4563(1)	2957(1)	21(1)
O(24)	-9(2)	3523(1)	2848(1)	40(1)
O(25)	-490(1)	5008(1)	3531(1)	27(1)
C(25)	-296(2)	4198(2)	4051(1)	41(1)
C(1')	3735(1)	5554(1)	712(1)	17(1)
C(2')	5243(1)	5702(1)	921(1)	17(1)
C(3')	5922(2)	6825(1)	849(1)	23(1)
N(4')	5236(2)	7780(1)	601(1)	27(1)
C(5')	3788(2)	7626(1)	409(1)	27(1)
C(6')	3007(2)	6548(1)	455(1)	23(1)
C(21')	6200(1)	4726(1)	1206(1)	17(1)
O(21')	7531(1)	4571(1)	1022(1)	21(1)
N(21')	5554(1)	4093(1)	1672(1)	18(1)
H(21')	4648(16)	4277(14)	1799(7)	21
C(22')	6373(2)	3113(1)	1982(1)	20(1)
C(23')	5697(2)	2870(1)	2633(1)	28(1)

Table 8.24: To be continued on next page.

	x	y	z	U(eq)
C(24')	6371(2)	1984(1)	1576(1)	23(1)
O(24')	7498(1)	1421(1)	1452(1)	35(1)
O(25')	4960(1)	1699(1)	1394(1)	34(1)
C(25')	4838(2)	601(1)	1028(1)	41(1)

Table 8.25: Atomic coordinates (x 10^4) and equivalent isotropic displacement parameters (Å^2 x 10^3) for (*R*,*R*)-2-[3'-(1-methoxycarbonyl-ethylcarbamoyl)-[4,4']-bipyridinyl-[4]-3-carbonyl]-amino-propionic acid methyl ester **42**. U(eq) is defined as one third of the trace of the orthogonalized Uij tensor.

D-H...A	d(D-H)	d(H...A)	d(D...A)	∢ (DHA)
N(21)-H(21)...O(21')♯1	0.860(13)	2.034(14)	2.8882(14)	171.7(15)
N(21')-H(21')...O(21)	0.858(13)	1.990(13)	2.8376(14)	169.5(15)
C(5)-H(5)...O(21')♯2	0.95	2.46	3.3806(15)	163.4
C(6)-H(6)...N(4)♯3	0.95	2.48	3.2222(17)	135.2
C(6')-H(6')...N(4')♯4	0.95	2.57	3.3632(18)	140.6
C(23)-H(23A)...O(24)♯5	0.98	2.51	3.1434(18)	121.8

Table 8.26: Hydrogen bonds for (*R*,*R*)-2-[3'-(1-methoxycarbonyl-ethylcarbamoyl)-[4,4']-bipyridinyl-[4]-3-carbonyl]-amino-propionic acid methyl ester **42** [Åand deg.].

♯1	x-1	y	z
♯2	x-1/2	-y+1/2	-z
♯3	x+1/2	-y+1/2	-z
♯4	x-1/2	-y+3/2	-z
♯5	-x	y+1/2	-z+1/2

Table 8.27: Symmetry transformations used to generate equivalent atoms.

8.6.8 Supramolecular Square AS1b

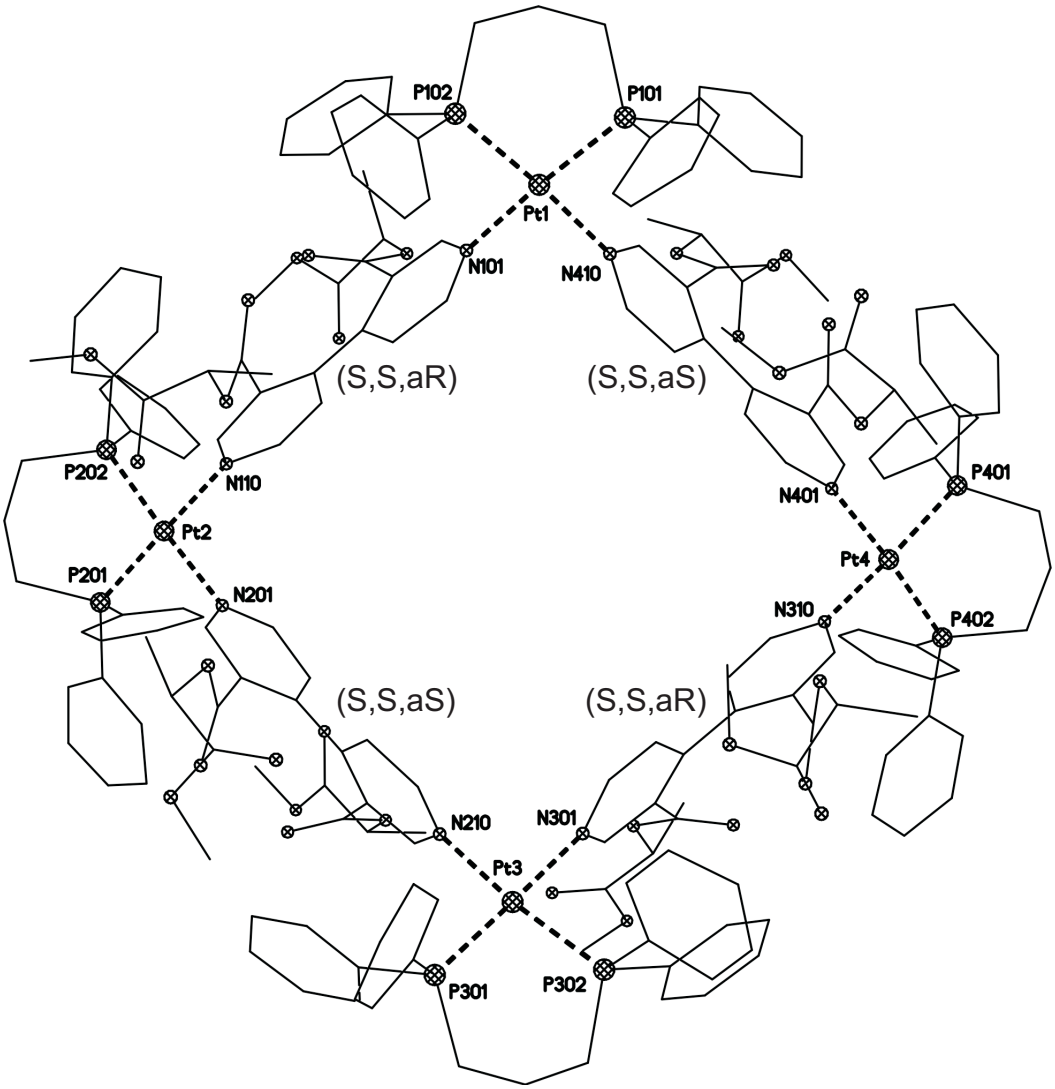

Figure 8.8: **AS1b**

Identification code	cas013hy
Empirical formula	$C_{217}H_{234}F_{24}N_{16}O_{55}P_8Pt_4S_8$
Formula weight	5686.80
Temperature	123 K
Wavelength	0.71073 Å
Crystal system, space group	Monoclinic, P2(1) (No.4)
Unit cell dimensions	a = 14.955(1) Åα = 90°.
	b = 27.472(1) Åβ = 100.57°.
	c = 31.536(3) Åγ = 90°.
Volume	12736.5 Å^3
Z, Calculated density	2, 1.483 Mg/m^3
Absorption coefficient	2.398 mm-1
F(000)	5728
Crystal size	0.60 x 0.50 x 0.40 mm
Theta range for data collection	5.02 to 25.03 deg.
Limiting indices	-17<=h<=17, -32<=k<=32, -36<=l<=37
Reflections collected / unique	113953 / 42874 [R(int) = 0.0273]
Completeness to theta = 25.03	98.5%
Absorption correction	Semi-empirical from equivalents
Max. and min. transmission	0.4305 and 0.3258
Refinement method	Full-matrix least-squares on F^2
Data / restraints / parameters	42874 / 3078 / 1433
Goodness-of-fit on F2	1.070
Final R indices [I>2sigma(I)]	R1 = 0.0758, wR2 = 0.1915
R indices (all data)	R1 = 0.0900, wR2 = 0.2047
Absolute structure parameter	0.062(8)
Largest diff. peak and hole	2.811 and -1.549 e.Å^{-3}

Table 8.28: Crystal data and structure refinement for **AS1b**.

	x	y	z	U(eq)
Pt(1)	7791(1)	4080(1)	5507(1)	26(1)
P(101)	8377(3)	3486(2)	5144(1)	33(1)
P(102)	8369(3)	4691(2)	5159(2)	35(1)
N(101)	7226(8)	4598(4)	5872(4)	30(3)
C(102)	6420(10)	4800(5)	5726(5)	31(3)
C(103)	6079(6)	5169(4)	5932(4)	24(3)
C(104)	6584(9)	5362(5)	6340(5)	26(3)
C(105)	7406(11)	5105(6)	6490(6)	38(4)
C(106)	7714(11)	4717(6)	6245(6)	42(4)
C(107)	6307(9)	5720(5)	6600(5)	26(3)
C(108)	5428(11)	5693(6)	6717(6)	42(4)
C(109)	5176(10)	6012(5)	6981(5)	31(3)
N(110)	5749(8)	6384(5)	7170(4)	31(3)
C(111)	6534(10)	6409(6)	7077(5)	34(3)
C(112)	6847(7)	6086(5)	6790(4)	31(3)
C(113)	5193(6)	5410(3)	5746(5)	33(3)
O(113)	5131(7)	5847(3)	5713(4)	44(3)
N(113)	4516(6)	5113(3)	5608(4)	40(2)
C(114)	3625(8)	5326(5)	5418(4)	53(3)
C(115)	3612(14)	5507(8)	4957(4)	82(5)
C(116)	3320(11)	5684(5)	5702(4)	58(3)
O(116)	3429(11)	5658(6)	6091(4)	83(4)
O(117)	2835(9)	6045(4)	5485(4)	70(3)
C(117)	2505(17)	6416(7)	5770(7)	91(6)
C(118)	7752(7)	6184(7)	6672(4)	51(3)
O(118)	7869(8)	6144(5)	6305(3)	55(3)
N(118)	8431(8)	6245(6)	6995(4)	85(4)
C(119)	9344(10)	6323(7)	6893(7)	120(5)

Table 8.29: To be continued on next page.

	x	y	z	U(eq)
C(120)	9903(17)	5852(9)	6949(12)	154(9)
C(121)	9808(16)	6734(8)	7127(7)	150(5)
O(121)	10040(20)	6745(9)	7515(7)	198(9)
O(122)	9788(18)	7113(7)	6862(8)	171(6)
C(122)	10580(30)	7455(12)	6987(14)	198(10)
C(123)	8551(11)	3654(6)	4603(6)	41(4)
C(124)	9124(9)	4122(7)	4591(4)	43(3)
C(125)	8568(11)	4573(6)	4627(5)	39(4)
C(126)	7656(10)	2953(6)	5080(5)	33(3)
C(127)	6911(12)	2941(7)	4741(6)	47(4)
C(128)	6326(12)	2553(6)	4693(6)	44(4)
C(129)	6536(13)	2165(7)	4982(6)	54(5)
C(130)	7234(13)	2178(7)	5330(6)	52(4)
C(131)	7805(12)	2558(7)	5374(6)	46(4)
C(132)	9491(11)	3312(6)	5406(6)	43(4)
C(133)	9991(12)	2991(7)	5220(6)	55(4)
C(134)	10868(14)	2872(8)	5434(7)	68(5)
C(135)	11264(15)	3048(8)	5804(7)	71(5)
C(136)	10842(19)	3435(10)	5979(9)	94(7)
C(137)	9932(14)	3555(8)	5800(6)	65(5)
C(138)	7619(11)	5199(6)	5081(6)	39(4)
C(139)	6852(11)	5201(6)	4743(6)	38(4)
C(140)	6245(14)	5565(8)	4699(7)	58(5)
C(141)	6345(13)	5987(7)	4971(6)	52(4)
C(142)	7095(13)	5989(8)	5296(7)	56(5)
C(143)	7729(12)	5606(7)	5359(6)	46(4)
C(144)	9438(11)	4919(6)	5456(6)	44(4)
C(145)	9768(13)	4814(7)	5855(6)	57(4)

Table 8.30: To be continued on next page.

	x	y	z	U(eq)
C(146)	10567(15)	4956(8)	6067(7)	74(6)
C(147)	11048(19)	5299(10)	5885(9)	91(7)
C(148)	10691(18)	5471(10)	5478(9)	90(7)
C(149)	9871(18)	5307(9)	5266(9)	86(7)
Pt(2)	5282(1)	6872(1)	7596(1)	30(1)
P(201)	4769(3)	7383(2)	8060(2)	35(1)
P(202)	4789(3)	7373(2)	7031(2)	40(1)
N(201)	5812(7)	6374(4)	8110(3)	23(2)
C(202)	6670(10)	6442(5)	8305(5)	34(3)
C(203)	7053(8)	6144(6)	8640(4)	38(3)
C(204)	6545(9)	5757(5)	8748(4)	26(3)
C(205)	5676(10)	5695(5)	8558(5)	34(3)
C(206)	5323(10)	6008(5)	8213(5)	31(3)
C(207)	6969(9)	5385(5)	9087(5)	33(3)
C(208)	7774(11)	5175(6)	9036(5)	42(4)
C(209)	8149(11)	4784(6)	9333(5)	40(4)
N(210)	7685(8)	4624(5)	9613(4)	34(3)
C(211)	6900(10)	4822(5)	9659(5)	35(3)
C(212)	6509(7)	5199(5)	9399(5)	35(3)
C(213)	7989(9)	6255(9)	8875(4)	81(4)
O(213)	8155(9)	6354(6)	9254(4)	78(4)
N(213)	8637(9)	6297(8)	8648(5)	105(4)
C(214)	9515(11)	6491(7)	8888(6)	124(5)
C(215)	10123(16)	6640(12)	8567(8)	146(9)
C(216)	9974(16)	6157(7)	9219(6)	123(5)
O(216)	9778(14)	5733(6)	9258(6)	121(6)
O(217)	10506(13)	6408(6)	9531(6)	126(5)
C(217)	10950(20)	6099(10)	9902(7)	123(8)

Table 8.31: To be continued on next page.

	x	y	z	U(eq)
C(218)	5631(7)	5406(4)	9484(5)	38(3)
O(218)	5576(7)	5829(3)	9584(4)	54(3)
N(218)	4959(6)	5103(4)	9462(4)	46(3)
C(219)	4051(7)	5269(4)	9521(4)	58(3)
C(220)	3409(11)	4827(6)	9495(8)	88(6)
C(221)	3658(9)	5635(5)	9202(4)	55(3)
O(221)	3751(8)	5650(4)	8830(3)	55(3)
O(222)	3033(8)	5886(4)	9362(3)	63(3)
C(222)	2543(13)	6251(6)	9050(6)	72(5)
C(223)	4889(11)	8029(6)	7946(5)	43(4)
C(224)	4395(12)	8184(7)	7509(6)	50(4)
C(225)	4871(13)	8018(7)	7133(6)	55(5)
C(226)	5398(10)	7298(5)	8599(4)	34(3)
C(227)	5087(13)	7008(7)	8885(6)	57(4)
C(228)	5592(14)	6919(8)	9300(7)	68(5)
C(229)	6468(16)	7145(9)	9350(8)	77(6)
C(230)	6773(19)	7429(10)	9096(8)	91(7)
C(231)	6225(16)	7487(8)	8707(8)	74(6)
C(232)	3557(10)	7297(5)	8070(5)	33(3)
C(233)	3192(12)	6839(8)	7988(6)	58(5)
C(234)	2259(12)	6733(6)	7990(6)	48(4)
C(235)	1737(13)	7144(7)	8071(6)	56(4)
C(236)	2153(14)	7572(7)	8182(6)	61(5)
C(237)	3038(14)	7660(8)	8173(7)	61(5)
C(238)	5479(10)	7296(5)	6604(5)	33(3)
C(239)	5163(10)	6984(6)	6262(5)	35(3)
C(240)	5687(11)	6932(7)	5953(6)	46(4)

Table 8.32: To be continued on next page.

	x	y	z	U(eq)
C(241)	6503(13)	7177(7)	5990(6)	49(4)
C(242)	6794(16)	7480(9)	6347(8)	68(6)
C(243)	6291(12)	7533(7)	6656(6)	48(4)
C(244)	3635(13)	7274(7)	6801(6)	50(4)
C(245)	3211(15)	6874(9)	6944(8)	73(6)
C(246)	2213(16)	6817(9)	6762(8)	75(6)
C(247)	1830(20)	7131(10)	6483(9)	93(8)
C(248)	2300(20)	7513(13)	6296(12)	106(10)
C(249)	3189(13)	7566(7)	6485(6)	52(4)
Pt(3)	8265(1)	4070(1)	10035(1)	36(1)
P(301)	8985(3)	4595(2)	10518(1)	51(1)
P(302)	8803(3)	3397(2)	10441(2)	52(1)
N(301)	7590(8)	3583(4)	9570(4)	30(3)
C(302)	6745(9)	3415(5)	9597(5)	32(3)
C(303)	6330(7)	3047(5)	9318(5)	38(3)
C(304)	6786(9)	2857(5)	9009(5)	33(3)
C(305)	7595(11)	3077(6)	8970(5)	45(4)
C(306)	7985(11)	3410(6)	9236(5)	39(3)
C(307)	6372(12)	2478(6)	8697(6)	48(4)
C(308)	5513(10)	2532(5)	8449(5)	36(3)
C(309)	5134(11)	2198(6)	8144(5)	37(3)
N(310)	5621(8)	1809(5)	8048(4)	36(3)
C(311)	6479(12)	1760(7)	8295(6)	51(4)
C(312)	6914(9)	2071(6)	8603(5)	40(4)
C(313)	5435(8)	2856(4)	9387(6)	60(4)
O(313)	5278(9)	2426(4)	9409(5)	70(3)
N(313)	4826(8)	3185(5)	9429(6)	75(3)
C(314)	4012(10)	3013(6)	9590(6)	98(4)

Table 8.33: To be continued on next page.

	x	y	z	U(eq)
C(315)	3358(14)	2776(9)	9215(7)	103(7)
C(316)	3639(15)	3374(7)	9840(8)	115(4)
O(316)	3869(16)	3797(6)	9886(8)	157(7)
O(317)	3015(13)	3187(6)	10047(6)	125(5)
C(317)	2590(20)	3567(9)	10287(10)	127(8)
C(318)	7866(11)	1951(13)	8827(6)	133(7)
O(318)	8079(12)	1998(8)	9213(5)	123(6)
N(318)	8490(11)	1942(11)	8588(6)	156(6)
C(319)	9457(12)	1855(9)	8775(8)	180(7)
C(320)	9660(20)	1309(9)	8837(12)	173(10)
C(321)	9791(19)	2130(10)	9170(9)	207(7)
O(321)	10350(20)	1970(12)	9469(9)	239(10)
O(322)	9830(20)	2602(9)	9057(11)	222(8)
C(322)	9800(40)	2639(16)	8579(12)	246(12)
C(323)	9172(12)	4395(6)	11077(6)	53(4)
C(324)	9674(12)	3921(6)	11167(6)	58(4)
C(325)	9106(12)	3488(7)	11022(6)	55(4)
C(326)	8352(10)	5157(5)	10487(5)	40(3)
C(327)	7586(14)	5164(8)	10702(7)	64(5)
C(328)	7076(18)	5601(9)	10648(8)	85(7)
C(329)	7286(16)	5996(9)	10405(7)	78(6)
C(330)	8024(17)	5953(10)	10188(8)	86(7)
C(331)	8547(13)	5531(7)	10243(6)	60(4)
C(332)	10114(10)	4722(5)	10438(5)	40(3)
C(333)	10434(13)	4561(7)	10077(6)	58(4)
C(334)	11283(15)	4710(8)	10005(7)	74(6)
C(335)	11915(18)	4901(9)	10357(8)	86(7)

Table 8.34: To be continued on next page.

	x	y	z	U(eq)
C(336)	11622(16)	5064(8)	10693(8)	80(6)
C(337)	10702(13)	4976(7)	10741(6)	61(4)
C(338)	7957(11)	2916(6)	10396(5)	47(4)
C(339)	7281(15)	2953(8)	10605(7)	68(5)
C(340)	6610(15)	2623(8)	10565(7)	69(5)
C(341)	6581(15)	2234(8)	10291(7)	74(5)
C(342)	7239(14)	2190(8)	10065(7)	68(5)
C(343)	7949(15)	2516(8)	10121(7)	67(5)
C(344)	9777(12)	3103(6)	10261(6)	56(4)
C(345)	10096(14)	3278(8)	9924(6)	65(5)
C(346)	10790(20)	3009(11)	9736(10)	104(8)
C(347)	11170(30)	2541(14)	9928(12)	132(11)
C(348)	10820(20)	2420(12)	10305(10)	114(9)
C(349)	10127(16)	2662(9)	10483(8)	83(6)
Pt(4)	5132(1)	1318(1)	7587(1)	34(1)
P(401)	4701(3)	792(2)	7043(2)	40(1)
P(402)	4562(3)	848(2)	8061(2)	44(1)
N(401)	5610(7)	1796(4)	7167(4)	26(2)
C(402)	6449(11)	1745(6)	7075(6)	40(4)
C(403)	6813(8)	2038(6)	6790(5)	38(4)
C(404)	6209(10)	2439(6)	6583(5)	37(4)
C(405)	5386(9)	2469(5)	6679(5)	30(3)
C(406)	5046(11)	2131(6)	6963(5)	36(3)
C(407)	6584(10)	2827(6)	6310(5)	34(3)
C(408)	7402(11)	3053(6)	6482(6)	40(4)
C(409)	7694(10)	3414(6)	6251(5)	34(3)

Table 8.35: To be continued on next page.

	x	y	z	U(eq)
N(410)	7244(8)	3550(4)	5861(4)	29(3)
C(411)	6433(9)	3333(5)	5712(5)	27(3)
C(412)	6084(7)	2960(5)	5932(5)	32(3)
C(413)	7731(9)	1943(8)	6684(5)	73(4)
O(413)	7867(9)	1960(6)	6318(4)	71(4)
N(413)	8338(9)	1721(7)	6971(5)	95(4)
C(414)	9171(11)	1537(6)	6832(7)	123(5)
C(415)	9774(17)	1262(11)	7201(9)	148(9)
C(416)	9672(17)	1914(7)	6648(9)	143(5)
O(416)	10121(17)	1838(8)	6372(7)	158(7)
O(417)	9483(18)	2353(7)	6786(8)	156(6)
C(417)	9860(30)	2770(8)	6566(13)	175(10)
C(418)	5222(6)	2729(3)	5702(4)	30(3)
O(418)	5168(7)	2292(3)	5665(3)	40(2)
N(418)	4566(6)	3026(3)	5544(4)	35(2)
C(419)	3696(7)	2824(4)	5313(4)	51(3)
C(420)	3040(10)	3242(5)	5146(6)	66(4)
C(421)	3304(11)	2477(5)	5581(4)	61(3)
O(421)	3381(9)	2493(4)	5968(3)	60(3)
O(422)	2853(9)	2125(4)	5339(4)	71(3)
C(422)	2444(16)	1759(7)	5600(7)	84(6)
C(423)	4779(12)	159(7)	7201(6)	48(4)
C(424)	4258(14)	11(8)	7541(7)	58(5)
C(425)	4694(12)	207(6)	7997(6)	50(4)
C(426)	5347(11)	840(6)	6638(5)	39(4)
C(427)	5120(12)	1140(7)	6274(6)	47(4)
C(428)	5706(11)	1220(7)	5980(6)	45(4)
C(429)	6515(19)	989(10)	6022(9)	85(7)

Table 8.36: To be continued on next page.

	x	y	z	U(eq)
C(430)	6767(19)	663(10)	6363(9)	82(7)
C(431)	6227(18)	601(10)	6681(9)	81(7)
C(432)	3550(12)	906(7)	6766(6)	44(4)
C(433)	3138(17)	554(10)	6443(9)	80(7)
C(434)	2227(16)	686(9)	6277(8)	70(6)
C(435)	1737(14)	1039(7)	6362(7)	62(5)
C(436)	2175(14)	1355(9)	6676(7)	67(5)
C(437)	3054(12)	1275(7)	6883(6)	53(4)
C(438)	5091(10)	956(5)	8617(5)	40(3)
C(439)	4718(12)	1251(6)	8878(5)	50(4)
C(440)	5156(13)	1360(7)	9300(6)	61(4)
C(441)	5985(12)	1156(6)	9454(6)	54(4)
C(442)	6394(17)	836(9)	9208(8)	79(6)
C(443)	5939(15)	745(8)	8781(7)	70(5)
C(444)	3379(11)	983(6)	8057(5)	46(4)
C(445)	3013(14)	1425(8)	7939(7)	65(5)
C(446)	2140(20)	1542(12)	7937(10)	103(9)
C(447)	1560(17)	1198(9)	8079(8)	78(6)
C(448)	1909(18)	760(10)	8209(8)	86(7)
C(449)	2847(15)	599(9)	8189(7)	69(6)
S(1)	4793(3)	4064(2)	6349(1)	57(1)
O(11)	4683(6)	4063(5)	5887(2)	58(2)
O(12)	5227(8)	4489(4)	6549(4)	76(3)
O(13)	5037(9)	3606(4)	6548(5)	91(4)
C(1)	3632(6)	4147(4)	6425(3)	83(4)
F(11)	3572(8)	4136(6)	6836(3)	116(4)
F(12)	3322(9)	4571(4)	6268(5)	123(4)
F(13)	3065(8)	3820(5)	6236(5)	126(4)

Table 8.37: To be continued on next page.

	x	y	z	U(eq)
S(2)	6344(3)	4072(2)	3653(1)	59(1)
O(21)	5566(6)	4112(6)	3312(3)	81(3)
O(22)	6544(9)	4490(4)	3922(4)	78(4)
O(23)	6380(9)	3617(4)	3877(4)	72(3)
C(2)	7278(6)	4044(4)	3369(3)	64(3)
F(21)	7199(8)	3683(5)	3092(4)	87(3)
F(22)	8068(6)	3981(5)	3626(3)	94(3)
F(23)	7382(9)	4445(5)	3155(4)	102(4)
S(3)	2883(3)	9096(2)	8283(1)	64(1)
O(31)	2953(9)	9546(4)	8522(4)	85(4)
O(32)	3621(6)	9016(6)	8062(4)	91(4)
O(33)	2602(9)	8687(4)	8506(4)	79(4)
C(3)	1935(6)	9203(4)	7857(3)	85(4)
F(31)	2060(9)	9577(4)	7617(4)	103(4)
F(32)	1772(10)	8824(4)	7601(4)	122(4)
F(33)	1186(7)	9292(5)	8005(4)	114(4)
S(4)	7733(3)	558(2)	7939(1)	57(1)
O(41)	7783(11)	1019(4)	7727(5)	103(4)
O(42)	6990(7)	261(5)	7740(5)	91(4)
O(43)	7913(10)	591(6)	8396(2)	105(4)
C(4)	8713(6)	249(4)	7814(4)	82(4)
F(41)	8822(10)	-187(4)	7982(5)	121(4)
F(42)	9477(7)	485(5)	7944(5)	120(4)
F(43)	8662(10)	184(6)	7399(4)	128(4)
S(5)	5330(3)	4143(2)	8654(1)	72(1)
O(51)	5217(7)	4159(5)	9095(2)	64(3)
O(52)	5849(9)	4535(5)	8523(5)	104(4)
O(53)	5555(10)	3675(4)	8505(5)	95(4)

Table 8.38: To be continued on next page.

	x	y	z	U(eq)
C(5)	4200(6)	4257(4)	8365(3)	96(4)
F(51)	4146(10)	4228(6)	7948(3)	138(5)
F(52)	3602(8)	3949(5)	8461(5)	139(5)
F(53)	3927(10)	4696(4)	8442(5)	136(5)
S(6)	7843(4)	7653(2)	7696(2)	103(2)
O(61)	7093(8)	7930(6)	7779(6)	118(5)
O(62)	7798(12)	7137(3)	7720(6)	119(5)
O(63)	8214(11)	7820(6)	7324(4)	122(5)
C(6)	8752(7)	7808(5)	8128(4)	114(5)
F(61)	8502(11)	7677(6)	8487(4)	135(5)
F(62)	8931(11)	8275(4)	8132(5)	136(5)
F(63)	9514(8)	7586(6)	8096(5)	142(5)
S(7)	9584(6)	3966(4)	7052(3)	170(4)
O(71)	9504(11)	4085(9)	6608(4)	135(4)
O(72)	9079(12)	4271(7)	7296(6)	186(5)
O(73)	9535(14)	3455(5)	7145(7)	183(5)
C(7)	10746(8)	4105(6)	7267(5)	212(18)
F(71)	10962(12)	3967(8)	7672(5)	199(5)
F(72)	11294(10)	3882(7)	7052(6)	187(5)
F(73)	10890(12)	4573(5)	7242(7)	187(5)
S(8)	-38(6)	3937(4)	8736(4)	159(4)
O(81)	-108(11)	4117(8)	9152(4)	130(4)
O(82)	-392(13)	4249(7)	8380(6)	181(5)
O(83)	-315(13)	3436(5)	8666(7)	183(5)
C(8)	1152(8)	3897(5)	8727(5)	140(13)
F(81)	1324(13)	3504(6)	8517(7)	198(5)
F(82)	1652(11)	3858(8)	9110(5)	187(5)
F(83)	1462(12)	4258(6)	8523(7)	194(5)

Table 8.39: To be continued on next page.

	x	y	z	U(eq)
O(11L)	5536(8)	4053(6)	4912(3)	76(3)
C(11L)	4972(7)	4029(6)	4582(4)	64(4)
C(12L)	4640(15)	3548(7)	4402(7)	83(6)
C(13L)	4590(16)	4471(7)	4342(7)	93(6)
O(21L)	6084(8)	4116(7)	10325(4)	79(3)
C(21L)	5542(8)	4174(5)	10566(4)	63(4)
C(22L)	5228(16)	3750(7)	10796(7)	94(6)
C(23L)	5169(18)	4662(7)	10644(8)	110(7)
O(31L)	3439(9)	5790(5)	7494(4)	63(3)
C(31L)	2857(10)	5476(5)	7451(5)	80(6)
C(32L)	2550(20)	5232(10)	7026(7)	132(9)
C(33L)	2423(15)	5320(8)	7820(7)	89(6)
O(41L)	3329(11)	2382(6)	7414(5)	80(4)
C(41L)	2871(12)	2748(7)	7336(6)	111(8)
C(42L)	2400(20)	2867(12)	6891(8)	143(9)
C(43L)	2750(20)	3102(10)	7684(9)	147(9)
O(51L)	6231(14)	9140(11)	8085(6)	162(7)
C(51L)	6689(14)	9178(7)	8450(7)	127(8)
C(52L)	7643(15)	8995(14)	8551(9)	144(9)
C(53L)	6330(20)	9405(11)	8807(8)	128(8)
O(61L)	7302(11)	2601(6)	7713(6)	102(5)
C(61L)	7144(12)	3037(6)	7718(4)	94(6)
C(62L)	6214(13)	3234(8)	7580(8)	92(6)
C(63L)	7890(16)	3396(8)	7865(10)	126(8)
O(71L)	6707(19)	5438(10)	7692(9)	171(9)

Table 8.40: To be continued on next page.

	x	y	z	U(eq)
C(71L)	6510(19)	5009(11)	7640(7)	174(12)
C(72L)	5550(20)	4841(15)	7552(16)	196(12)
C(73L)	7230(30)	4632(12)	7663(17)	208(12)

Table 8.41: Atomic coordinates (x 10^4) and equivalent isotropic displacement parameters (Å^2 x 10^3) for **AS1b**. U(eq) is defined as one third of the trace of the orthogonalized Uij tensor.

D-H...A	d(D-H)	d(H...A)	d(D...A)	∢ (DHA)
N(113)-H(113)...O(11)	0.88	2.16	3.011(17)	161.3
N(218)-H(218)...O(51)	0.88	2.05	2.895(16)	161.4
N(313)-H(313)...O(51)	0.88	2.11	2.971(18)	166.2
N(413)-H(413)...O(41)	0.88	2.57	3.289(19)	139.9
N(418)-H(418)...O(11)	0.88	2.21	3.042(17)	158.3

Table 8.42: Atomic coordinates (x 10^4) and equivalent isotropic displacement parameters (Å^2 x 10^3) for **AS1b**. U(eq) is defined as one third of the trace of the orthogonalized Uij tensor.

	0/4	1/3	2/2	3/1	4/0	aR/aS
0/8	1	1	2	1	1	
1/7	1	4	6	4	1	
2/6	6	16	26	16	6	
3/5	7	28	42	28	7	
4/4	12	36	56	36	12	
5/3	7	28	42	28	7	
6/2	6	16	26	16	6	
7/1	1	4	6	4	1	
8/0	1	1	2	1	1	
Out/In						= 560

Table 8.43: Number of isomers for the combination of the two types of isomerism: Rows: ligands' absolute configuration; Columns: Amount of substituents pointing inside or outside the cavity. As the table is symmetrical only the 15 highlighted entries have to be considered. The number of isomers sums up to 560.

8.7 Symmetry Considerations – 560 Isomers

The combination of two types of isomers (aR/aS isomerism and In/Out-isomerism) lead to a multitude of different isomeric structures.

For example, only one isomer exists in which a) all substituents are pointing inside the cavity and b) all ligands are aS. When the absolute configuration of one ligand is changed to aR, another isomer is obtained. When the absolute configuration of two ligands is changed to aR, two further isomers are obtained (two adjacent or two opposite ligands). Analogously, only one isomer exists, in which three out of four, and all four ligands are exchanged, respectively. These results are summarized in the first row of Table 8.7. The same considerations hold true for the last row, in which all substituents are pointing outside. Please note one very important aspect: Due to the "symmetry" of the table, only the 15 highlighted entries need to be considered.

In the following, the entries of the first column are discussed. Again starting from the very first isomer (all aS and all in), one substituent is turned outwards

to obtain another isomer. If a second is turned outwards (see figure 8.9 a), seven isomers (one of the eight positions is already occupied) can be obtained, on the first glance. Two of them can be superimposed by rotation. Thus, only six individual isomers are listed in table 8.7. Seven isomers are obtained for three X outside (see figure 8.9 b), and twelve isomers for four X outside (see c). In a next step, the second column is described in more detail: If the absolute configuration of one of the four ligands is changed, four mathematical unequal isomers are obtained (see figure 8.9 d). These four are chemically equal as long as all ligands are either pointing inside or outside, respectively (see remarks for the first column of table 8.7). Analogously, six isomers exist if the absolute configuration of two ligands is changed to aR (see figure 8.9 e). These two types of isomers are now combined in a final step: Again, isomers, which can be super imposed by rotation, are grayed out in the following two figures (8.10 and 8.11). The remaining isomers are counted and listed in table 8.7. Three important aspects should be noted: a) as non of the column-isomers of Figures 8.10 and 8.11 can be rotated into an isomer of a different column, one only has to check for identical isomers in each column independently, which makes the situation much more comfortable. b) The substituents are either above or below the plane spanned by the four metal atoms. To distinguish whether an X is above or below in all given isomers, the absolute configuration of the ligand has to be taken into account. Or in other words, the actual position of a substituent (above/below the square's plane) is determined by the absolute configuration (aR/aS) of the ligand. c) Off course, some of the listed isomers are enantiomers for achiral X. As X may contain chiral information (see below), these isomers are separated here. Mirroring of two isomers would lead to superposition in some cases, too. However, aR-ligands would thereby be transferred into aS-ligands as well.

Figure 8.9: Number of isomers when a) two, b) three, or c) four substituents (X) are turned outwards. Isomers, which can be superimposed by rotation into other isomers, are grayed out (see arrow). The remaining Substituents, which are pointing inside the square's cavity, are omitted for clarity. Number of isomers when the absolute configuration of d) one or e) two ligands is changed to aS.

Figure 8.10: Combination of a) two X out and 3aS/1aR yielding 16 isomers, b) two X out and 2aS/2aR: 26 isomers, c) three X out and 3aS/1aR yielding 28 isomers and d) three X out and 2aS/2aR: 42 isomers.

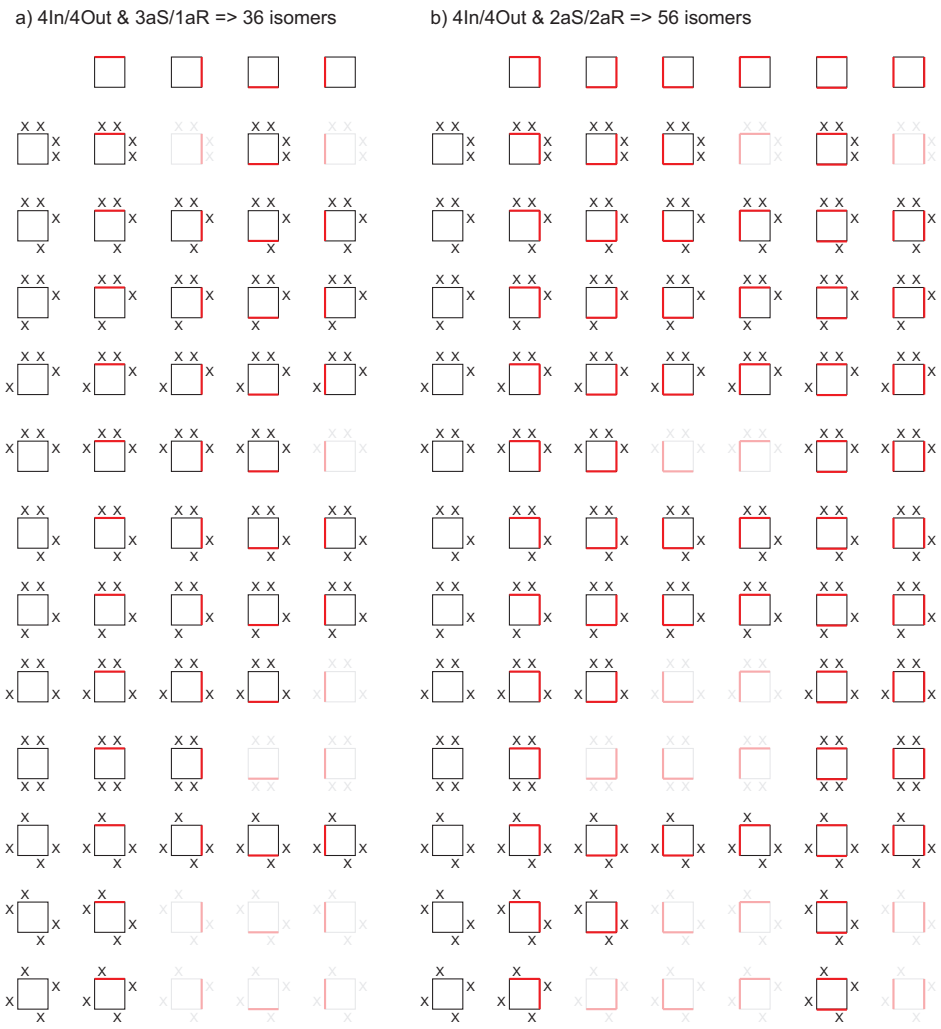

Figure 8.11: Combination of a) four X out and 3aS/1aR yielding 36 isomers and b) four X out and 2aS/2aR: 56 isomers.

Bibliography

[1] a) E. Fischer, *Ber. Dtsch. Chem. Ges.* **1890**, *23*, 799-805; b) E. Fischer, *Ber. Dt. Chem. Ges.* **1894**, *27*, 2985-2993.

[2] a) J.-M. Lehn, *Supramolecular Chemistry: Concepts and Perspectives* VCH, Weinheim, **1995**; b) J.-M. Lehn, *Science* **2002**, *295*, 2400-2403; c) A. Lützen, *Chemkon* **2007**, *14*, 123-130.

[3] D. E. Koshland *Proc. Natl. Acad. Sci.* **1958**, *44*, 98-104.

[4] R. Boyer, *Concepts in Biochemistry*, 2nd Edition, John Wiley & Sons, Inc., New York, **2002**, 137-138.

[5] A. Vasella, G. J. Davies, M. Bohm, *Curr. Opin. Chem. Biol.* **2002**, *6*, 619-629.

[6] B. Alberts, A. Johnson, J. Lewis, *Molecular Biology of the Cell*, 2. Edition, Garland, New York, **1989**, 84-85.

[7] a) Self-Assembly at all scales: G. M. Whitesides, B. Grzybowski, *Science* **2002**, *295*, 2418-2421; b) early examples: C. T. Seto, G. M. Whitesides, *J. Am. Chem. Soc.* **1990**, *112*, 6409-6411; c) U. Koert, M. M. Harding, J.-M. Lehn, *Nature*, **1990**, *346*, 339-342; d) D. Philip, J. F. Stoddart, *Synlett* **1991**, 445-458; e) C. T. Seto, G. M. Whitesides, *J. Am. Chem. Soc.* **1991**, *113*, 712-6411.

[8] a) Self-Assembly in Nanochemistry: G. M. Whitesides, J. P. Mathias, C. T. Seto, *Science* **1991**, *254*, 1312-1319;

[9] J. S. Manka, D. S. Lawrence, *J. Am. Chem. Soc.* **1990**, *112*, 2440-2441.

[10] G. Prakash, E. T. Kool, *J. Chem. Soc. Chem. Commun.* **1991**, 1161-1163.

[11] Initial experiments by John Zeleny in 1917: a) J. Zeleny, *Phys. Rev.* **1930**, *36*, 35-43; b) J. B. Fenn, M. Mann, C. K. Meng, S. F. Wong, C. M. Whitehouse, *Science* **1989**, *246*, 64-71; c) J. B. Fenn, M. Mann, C. K. Meng, S. F. Wong, C. M. Whitehouse, *Mass Spec. Rev.* **1990**, *9*, 37-70.

[12] a) W. M. Stanley, *Phytopathology* **1934**, *24*, 1269-1289; b) W. M. Stanley, *Am. J. Botany* **1937**, *24*, 59-68.

[13] B. Bothner, G. Siuzdak, *Chem. Bio. Chem.* **2004**, *5*, 258-260.

[14] J. C. Kendrew, G. Bodo, H. M. Dintzis, R. G. Parrish, H. Wyckoff, D. C. Phillips, *Nature* **1958**, *181*, 662-666.

[15] F. A. L. Anet, A. J. R. Bourn, *J. Am. Chem. Soc.* **1965**, *87*, 5250-5251; K. Wüthrich, *J. Biol. Chem.* **1990**, *265*, 22059-22062.

[16] For an early review, see: a) C. L. Perrin, T. J. Dwyer, *Chem. Rev.* **1990**, *90*, 935-967; for application in (bio)-chemistry see: b) J. Lu, D. Ma, J. Hu, W. Tang, D. Zhub, *J. Chem. Soc., Dalton Trans.* **1998**, 2267-2273; c) B. J. Wik, M. Lersch, A. Krivokapic, M. Tilset, *J. Am. Chem. Soc.* **2006**, *128*, 2682-2696; for an application in supramolecular chemistry see: d) S. L. Craig, S. Lin, J. Chen, J. Rebek, Jr. *J. Am. Chem. Soc.* **2002**, *124*, 8780-8781.

[17] a) K. Wüthrich, *NMR of Proteins and Nucleic Acids*, Wiley-VCH, Weinheim, **1986**; b) H. Friebolin, *Basic One-Dimensional and Two-Dimensional NMR Spectroscopy*, 3. Edition, Wiley-VCH, Weinheim, **2004**; c) G. S. Rule, T. K. Hitchens, *Fundamentals of Protein NMR Spectroscopy*, Springer, Berlin, Heidelberg, **2006**.

[18] a) C. A. Schalley, A. Lützen, M. Albrecht, *Chem. Eur. J.* **2004**, *10*, 1072-1080.

[19] a) M. Karas, D. Bachmann, F. Hillenkamp, *Anal. Chem.* **1985**, *57*, 2935-2939; b) K. Tanaka, H. Waki, Y. Ido, S. Akita, Y. Yoshida, T. Yoshida, *Rapid Commun. Mass Spectrom.* **1988**, *2*, 151-153.

[20] a) P. Arpino, *Mass Spectrom. Rev.* **1989**, *8*, 35-55; b) P. Arpino, *Mass Spectrom. Rev.* **1992**, *11*, 3-40; c) K. B. Tomer, M. A. Moseley, L. J. Deterding, C. E. Parker, *Mass Spectrom. Rev.* **1994**, *13*, 431-457.

[21] R. P. Feynman, *Sat. Rev.* **1960**, *43*, 45-47.

[22] a) E. Buhleier, W. Wehner, F. Vögtle, *Synthesis* **1978**, 155-158; b) D. A. Tomalia, H. Baker, J. R. Dewald, M. Hall, G. Kallos, S. Martin, J. Roeck, J. Ryder, P. Smith, *Polymer J.* **1985**, *17*, 117-132.

[23] a) S. C. Zimmerman, L. J. Lawless, *Top. Curr. Chem.* **2001**, *217*, 95-120; b) H.-J. van Manen, F. C. J. M. van Veggel, D. N. Reinhoudt, *Top. Curr. Chem.* **2001**, *217*, 121-162; c) J. M. J. Fréchet, *Proc. Nat. Acad. Sci. U.S.A.* **2002**, *99*, 4782-4787; d) V. Persec, M. Glodde, T. K. Bera, Y. Miura, I. Shiyanoskaya, K. D. Singer, V. S. K. Balagurusamy, P.

A. Heiney, I. Schnell, A. Rapp, H.-W. Spiess, S. D. Hudson, H. Duan, *Nature* **2002**, *419*, 384-387; e) T. Yamaguchi, T. Kimura, H. Matsuda, T. Aida, *Angew. Chem.* **2004**, *116*, 6510-6515; *Angew. Chem. Int. Ed.* **2004**, *43*, 6350-6355; f) A. E. Kaifer, D. Sobransingh, J. Grindstaff, K. Moon, *Angew. Chem.* **2004**, *116*, 5612-5615; *Angew. Chem. Int. Ed.* **2004**, *43*, 5496-5499; g) A. Franz, W. Bauer, A. Hirsch, *Angew. Chem.* **2005**, *117*, 1588-1592; *Angew. Chem. Int. Ed.* **2005**, *44*, 1564-1567; h) H. Tokuhisa, M. Kanesato, *Langmuir* **2005**, *21*, 9728-9732; i) F. Würthner, V. Stepanenko, A. Sautter, *Angew. Chem.* **2006**, *118*, 1973-1976; *Angew. Chem. Int. Ed.* **2006**, *45*, 1939-1942; j) H.-B. Yang, N. Das, F. Huang, A. M. Hawkridge, D. C. Muddiman, P. J. Stang, *J. Am. Chem. Soc.* **2006**, *128*, 10014-10015.

[24] Hydrogen bonding: a) G. A. Jeffrey, *An Introduction to Hydrogen Bonding*, Oxford University Press, Oxford **1997**; cation-π interactions: b) J. C. Ma, D. A. Dougherty, *Chem. Rev.* **1997**, *97*, 1303-1324; c) C. A. Hunter, J. K. M. Sanders, *J. Am. Chem. Soc.* **1990**, *112*, 5525-5534; Forces between multipoles: d) R. Paulini, K. Müller, F. Diederich, *Angew. Chem.* **2005**, *117*, 1820-1839; *Angew. Chem. Int. Ed.* **2005**, *44*, 1788-1805; Interactions between nitrogen and halogen atoms: e) P. Auffinger, F. A. Hays, E. Westhof, P. S. Ho, *Proc. Natl. Acad. Sci. USA* **2004**, *101*, 16789-16794; dihydrogen bridges: f) R. H. Crabtree, P. E. M. Siegbahn, O. Eisenstein, A. L. Rheingold, T. F. Koetzle, *Acc. Chem. Res.* **1996**, *29*, 348-354; Hydrophobic effect: g) P. L. Privalov, S. J. Gill, *Adv. Protein Chem.* **1988**, *39*, 191-234; h) K. P. Murphy, P. L. Privalov, S. J. Gill, *Science* **1990**, *247*, 559-561; i) K. A. Dill, *Science* **1990**, *250*, 297-298; j) P. L. Privalov, S. J. Gill, K. P. Murphy, *Science* **1990**, *250*, 298-299; k) J. Herzfield, *Science* **1991**, *253*, 88.

[25] a) G. M.Whitesides, E. E. Simanek, J. P. Mathias, C. T. Seto, D. N. Chin, M. Mammen, D. M. Gordon, *Acc. Chem. Res.* **1995**, *28*, 37-44; b) G. M. Whitesides, M. Boncheva, *Proc. Nat. Acad. Sci. U.S.A.* **2002**, *99*, 4769-4774.

[26] M. Fujita, J. Yazaki, K. Ogura, *J. Am. Chem. Soc.* **1990**, *112*, 5645-5647.

[27] S. Sakamoto, M. Fujita, K. Kim, K. Yamaguchi, *Tetrahedron* **2000**, *56*, 955-964.

[28] M. Aoyagi, K. Biradha, M. Fujita, *Bull. Chem. Soc. Jpn.* **1999**, *72*, 2603-2606.

[29] a) M. Fujita, J. Yazaki, K. Ogura, *Tetrahedron Lett.* **1991**, *32*, 5589-5592; b) M. Fujita, J. Yazaki, K. Ogura, *Chem. Lett.* **1991**, *6*, 1031-1032.

[30] M. Fujita, M. Aoyagi, F. Ibukuro, K. Ogura, K. Yamaguchi, *J. Am. Chem. Soc.* **1998**, *120*, 611-612.

[31] A. Hori, T. Sawada, K.-I. Yamashita, M. Fujita, *Angew. Chem.* **2005**, *117*, 4974-4977; *Angew. Chem. Int. Ed.* **2005**, *44*, 4896-4899.

[32] M. Fujita, F. Ibukuro, H. Hagihara, K. Ogura, *Nature* **1994**, *367*, 720-723.

[33] K. Umemoto, H. Tsukui, T. Kusukawa, K. Biradha, M. Fujita, *Angew. Chem.* **2001**, *113*, 2690-2692; *Angew. Chem. Int. Ed.* **2001**, *40*, 2620-2622.

[34] M. Fujita, S.-Y. Yu, T. Kusukawa, H. Funaki, K. Ogura, K. Yamaguchi, *Angew. Chem.* **1998**, *110*, 2192-2196; *Angew. Chem. Int. Ed.* **1998**, *37*, 2082-2085.

[35] F. Ibukuro, T. Kusukawa, M. Fujita. *J. Am. Chem. Soc.* **1998**, *120*, 8561-8562.

[36] M. Tominaga, K. Suzuki, M. Kawano, T. Kusukawa, T. Ozeki, S. Sakamoto, K. Yamaguchi, M. Fujita, *Angew. Chem.* **2004**, *116*, 5739-5743; *Angew. Chem. Int. Ed.* **2004**, *43*, 5621-5625.

[37] M. Hong, Y. Zhao, W. Su, R. Cao, M. Fujita, Z. Zhou, A. S. C. Chan, *J. Am. Chem. Soc.* **2000**, *122*, 4819-4820.

[38] Y. Yamanoi, Y. Sakamoto, T. Kusukawa, M. Fujita, S. Sakamoto, K. Yamaguchi, *J. Am. Chem. Soc.* **2001**, *123*, 980-981.

[39] N. Fujita, K. Biradha, M. Fujita, S. Sakamoto, K. Yamaguchi, *Angew. Chem.* **2001**, *113*, 1768-1771; *Angew. Chem. Int. Ed.* **2001**, *40*, 1718-1721.

[40] a) M. Aoyagi, K. Biradha, M. Fujita, *J. Am. Chem. Soc.* **1999**, *121*, 7457-7458; b) S. Tashiro, M. Tominaga, T. Kusukawa, M. Kawano, S. Sakamoto, K. Yamaguchi, M. Fujita, *Angew. Chem.* **2003**, *115*, 3389-3392; *Angew. Chem. Int. Ed.* **2003**, *42*, 3267-3270.

[41] M. Fujita, J. Yazaki, K. Ogura, *Tetrahedron Lett.* **1991**, *32*, 5589-5592.

[42] a) T. Kusukawa, M. Fujita, *Angew. Chem.* **1998**, *110*, 3327-3329; *Angew. Chem. Int. Ed.* **1998**, *37*, 3142-3144; b) T. Kusukawa, M. Fujita, *J. Am. Chem. Soc.* **2002**, *124*, 13576-13582.

[43] K. Ono, M. Yoshizawa, T. Kato, K. Watanabe, M. Fujita, *Angew. Chem.* **2007**, *119*, 1835 -1838; *Angew. Chem. Int. Ed.* **2007**, *46*, 1803-1806.

[44] M. Yoshizawa, J. Nakagawa, K. Kumazawa, M. Nagao, M. Kawano, T. Ozeki, M. Fujita, *Angew. Chem.* **2005**, *117*, 1844-1847; *Angew. Chem. Int. Ed.* **2005**, *44*, 1810-1813.

[45] a) M. Yoshizawa, T. Kusukawa, M. Fujita, K. Yamaguchi, *J. Am. Chem. Soc.* **2000**, *122*, 6311-6312; b) M. Yoshizawa, T. Kusukawa, M. Fujita, S. Sakamoto, K. Yamaguchi, *J. Am. Chem. Soc.* **2001**, *123*, 10454-10459.

[46] J.-P. Bourgeois, M. Fujita, M. Kawano, S. Sakamoto, K. Yamaguchi, *J. Am. Chem. Soc.* **2003**, *125*, 9260-9261.

[47] K. Nakabayashi, M. Kawano, M. Fujita, *Angew. Chem.* **2005**, *117*, 5456-5459; *Angew. Chem. Int. Ed.* **2005**, *44*, 5322-5325.

[48] a) S. Tashiro, M. Tominaga, Y. Yamaguchi, K. Kato, M. Fujita, *Angew. Chem.* **2006**, *118*, 247-250; *Angew. Chem. Int. Ed.* **2006**, *45*, 241-244; b) S. Tashiro, M. Kobayashi, M. Fujita, *J. Am. Chem. Soc.* **2006**, *128*, 9280-9281.

[49] M. Yoshizawa, Y. Takeyama, T. Kusukawa, M. Fujita, *Angew. Chem.* **2002**, *114*, 1403-1405; *Angew. Chem. Int. Ed.* **2002**, *41*, 1347-1349.

[50] M. Yoshizawa, T. Kusukawa, M. Kawano, T. Ohhara, I. Tanaka, K. Kurihara, N. Niimura, M. Fujita, *J. Am. Chem. Soc.* **2005**, *127*, 2798-2799.

[51] T. Kusukawa, M. Fujita, *J. Am. Chem. Soc.* **1999**, *121*, 1397-1398.

[52] M. Fujita, S. Nagao, K. Ogura, *J. Am. Chem. Soc.* **1995**, *117*, 1649-1650.

[53] S. Hiraoka, M. Fujita, *J. Am. Chem. Soc.* **1999**, *121*, 10239-10240.

[54] K. Umemoto, K. Yamaguchi, M. Fujita, *J. Am. Chem. Soc.* **2000**, *122*, 7150-7151.

[55] a) B. Hasenknopf, J.-M. Lehn, G. Baum, B. O. Kneisel, D. Fenske, *Angew. Chem.* **1996**, *108*, 1987-1990; *Angew. Chem. Int. Ed.* **1996**, *35*, 1838-1840; b) B. Hasenknopf, J.-M. Lehn, N. Boumediene, A. Dupont-Gervais, A. V. Dorsserlaer, B. O. Kneisel, D. Fenske, *J. Am. Chem. Soc.* **1997**, *119*, 10956-10962; c) J. M. Rivera, T. Martin, J. Rebek, Jr., *J. Am. Chem. Soc.* **1998**, *120*, 819-820; d) F. Hof, C. Nuckolls, J. Rebek, Jr., *J. Am. Chem. Soc.* **2000**, *122*, 4251-4252.

[56] K. Suzuki, M. Kawano, M. Fujita, *Angew. Chem.* **2007**, *119*, 2877-2880; *Angew. Chem. Int. Ed.* **2007**, *46*, 2819-2822.

[57] A. Hori, K.-I. Yamashita, M. Fujita, *Angew. Chem.* **2004**, *116*, 5126-5129; *Angew. Chem. Int. Ed.* **2004**, *43*, 5016-5019.

[58] T. M. Fyles, C. C. Tong, *New J. Chem.* **2007**, *2*, 296-304.

[59] T. M. Fyles, *Chem. Soc. Rev.* **2007**, *36*, 335-347.

[60] T. M. Fyles, C. C. Tong, *New J. Chem.* **2007**, *5*, 655-661.

[61] a) P. J. Stang, D. H. Cao, *J. Am. Chem. Soc.* **1994**, *116*, 4981-4982; b) P. J. Stang, D. H. Cao, S. Saito, A. M. Arif, *J. Am. Chem. Soc.* **1995**, *117*, 6273-6283.

[62] J. A. Whiteford, E. M. Rachlin, P. J. Stang, *Angew. Chem.* **1996**, *108*, 2643-2648; *Angew. Chem. Int. Ed.* **1996**, *35*, 2524-2529.

[63] C. A. Schalley, T. Müller, P. Linnartz, M. Witt, M. Schäfer, A. Lützen, *Chem. Eur. J.* **2002**, *8*, 3538-3551.

[64] M. Engeser, A. Rang, M. Ferrer, A. Gutiérrez, H. T. Baytekin, C. A. Schalley, *Int. J. Mass Spec.* **2006**, *255*, 185-194.

[65] T. Weilandt, R. W. Troff, H. Saxell, K. Rissanen, C. A. Schalley, *Inorg. Chem.* **2008**, *47*, 7588-7598.

[66] C. Safarowsky, L. Merz, A. Rang, P. Broekmann, B. A. Herrmann, C.A Schalley, *Angew. Chem.* **2004**, *116*, 1311-1314; *Angew. Chem. Int. Ed.* **2004**, *43*, 1291-1294.

[67] M. Schweiger, S. R. Seidel, A. M. Arif, P. J. Stang, *Angew. Chem.* **2001**, *113*, 3575-3577; *Angew. Chem. Int. Ed.* **2001**, *40*, 3467-3469.

[68] Y. K. Kryschenko, S. R. Seidel, A. M. Arif, P. J. Stang, *J. Am. Chem. Soc.* **2003**, *125*, 5193-5198.

[69] C. J. Kuehl, S. D. Huang, P. J. Stang, *J. Am. Chem. Soc.* **2001**, *123*, 9634-9641.

[70] J. A. Whiteford, C. V. Lu, P. J. Stang, *J. Am. Chem. Soc.* **1997**, *119*, 2524-2533.

[71] B. Olenyuk, S. Leininger, P. J. Stang, *Chem. Rev.* **2000**, *100*, 853-907.

[72] P. S. Mukherjee, N. Das, P. J. Stang, *J. Org. Chem.* **2004**, *69*, 3526-3529.

[73] S. Leininger, J. Fan, M. Schmitz, P. J. Stang, *Proc. Nat. Acad. Sci. U.S.A.* **2000**, *97*, 1380-1384.

[74] B. Olenyuk, M. D. Levin, J. A. Whiteford, J. E. Shield, P. J. Stang, *J. Am. Chem. Soc.* **1999**, *121*, 10434-10435.

[75] B. Olenyuk, J. A. Whiteford, A. Fechtenkötter, P. J. Stang, *Nature* **1999**, *398*, 796-799.

[76] T. Yamamoto, A. M. Arif, P. J. Stang, *J. Am. Chem. Soc.* **2003**, *125*, 12309-12317.

[77] S. R. Seidel, P. J. Stang, *Acc. Chem. Res.* **2002**, *35*, 972-983.

[78] P. J. Stang, D. H. Cao, K. Chen, G. M. Gray, D. C. Muddiman, R. D. Smith, *J. Am. Chem. Soc.* **1997**, *119*, 5163-5168.

[79] M. A. Mateos-Timoneda, M. Crego-Calama, D. N. Reinhoudt, *Chem. Soc. Rev.* **2004**, *33*, 363-372.

[80] J. M. Rivera, T. Martin, J. Rebek, Jr., *Science* **1998**, *279*, 1021-1023.

[81] C. Nuckolls, F. Hof, T. Martin, J. Rebek, Jr., *J. Am. Chem. Soc.* **1999**, *121*, 10281-10285.

[82] a) D. Whang, J. Heo, C.-A. Kim, K. Kim, *Chem. Commun.* **1997**, 2361-2362; b) S. Sailaja, M.V. Rajasekharan, *Inorg. Chem.* **2000**, *39*, 4586-4590; c) A. Erxleben, *Inorg. Chem.* **2001**, *40*, 412-414; d) A. Erxleben, *Inorg. Chem.* **2001**, *40*, 2928-2931. e) M. Kondo, M. Miyazawa, Y. Irie, R. Shinagawa, T. Horiba, A. Nakamura, T. Naito, K. Maeda, S. Utsuno, F. Uchida, *Chem. Commun.* **2002**, 2156-2157; f) D. Fiedler, D. H. Leung, R. G. Bergman, K. N. Raymond, *J. Am. Chem. Soc.* **2004**, *126*, 3674-3675.

[83] a) P. Baret, D. Gaude, G. Gellon, J.-L. Pierre, *New J. Chem.* **1997**, *21*, 1255-1257; b) O. Mamula, F. J. Monlien, A. Porquet, G. Hopfgartner, A. E. Merbach, A. von Zelewsky, *Chem. Eur. J.* **2001**, *7*, 2533-2539.

[84] O. Mamula, M. Lama, H. Stoeckli-Evans, S. Shova, *Angew. Chem.* **2006**, *118*, 5062-5066; *Angew. Chem. Int. Ed.* **2006**, *45*, 4940-4944.

[85] A. P. H. J. Schenning, P. Jonkheijm, E. Peeters, E. W. Meijer, *J. Am. Chem. Soc.* **2001**, *123*, 409-416.

[86] L. J. Prins, J. Huskens, F. de Jong, P. Timmerman, D. N. Reinhoudt, *Nature* **1999**, *398*, 498-502.

[87] M. Albrecht, *Angew. Chem.* **2005**, *117*, 6606-6609; *Angew. Chem. Int. Ed.* **2005**, *44*, 6448-6451; and references herein.

[88] R. Prabaharan, N. C. Fletcher, M. Nieuwenhuyzen, *J. Chem. Soc., Dalton Trans.* **2002**, 602-608.

[89] S. Fernandez-Lopez, H.-S. Kim, E. C. Choi, M. Delgado, J. R. Granja, A. Khasarov, K. Kraehenbuehl, G. Long, D. A. Weinberger, K. M. Wilcoxen, M. R. Ghadiri, *Nature* **2001**, *412*, 452-455.

[90] M. A. Masood, E. J. Enemark, T. D. P. Stack, *Angew. Chem.* **1998**, *110*, 973-977; *Angew. Chem. Int. Ed.* **1998**, *37*, 928-932.

[91] B. M. Trost, *Science* **1991**, *254*, 1471-1477.

[92] A. Hori, A. Akasaka, K. Biradha, S. Sakamoto, K. Yamaguchi, M. Fujita *Angew. Chem.* **2002**, *114*, 3403-3406; *Angew. Chem. Int. Ed.* **2002**, *41*, 3269-3272.

[93] B. Olenyuk, J. A. Whiteford, P. J. Stang, *J. Am. Chem. Soc.* **1996**, *118*, 8221-8230.

[94] P. J. Stang, B. Olenyuk, *Angew. Chem.* **1996**, 108, 798-802; *Angew. Chem. Int. Ed.* **1996**, *35*, 732-736.

[95] C. Müller, J. A. Whiteford, P. J. Stang, *J. Am. Chem. Soc.* **1998**, *120*, 9827-9837.

[96] O. Safarowsky, B. Windisch, A. Mohry, F. Vögtle, *J. Prakt. Chem.* **2000**, *342*, 437-444.

[97] a) E. Wassermann, *J. Am. Chem. Soc.* **1960**, *82*, 4433-4434; b) G. Schill, *Catenanes, Rotaxanes and Knots*, Academic Press, New York, **1971**; c) D. B. Amabilino, J. F.; Stoddart, *Chem. Rev.* **1995**, *95*, 2725-2828; d) J.-P. Sauvage, C. O. Dietrich-Buchecker, *Molecular Catenanes, Rotaxanes and Knots*, Wiley-VCH, Weinheim, **1999**.

[98] G. A. Breault, C. A. Hunter, P. C. Mayers, *Tetrahedron* **1999**, *55*, 5265-5293.

[99] F. Vögtle, T. Dünnwald, T. Schmidt, *Acc. Chem. Res.* **1996**, *29*, 451-460.

[100] T. Felder, C. A. Schalley, *Angew. Chem.* **2003**, *115*, 2360-2363; *Angew. Chem. Int. Ed.* **2003**, *42*, 2258-2260.

[101] For general reviews on template effects, see: a) D. H. Busch, N. A. Stephensen, *Coord. Chem. Rev.* **1990**, *100*, 119-154; b) R. Cacciapaglia, L. Mandolini, *Chem. Soc. Rev.* **1993**, *22*, 221-231; c) S. Anderson, H. L. Anderson, J. K. M. Sanders, *Acc. Chem. Res.* **1993**, *26*, 469-475; d) *Templated Organic Synthesis*, (Eds.: F. Diederich, P. J. Stang), Wiley-VCH, Weinheim, **2000**; e) T. J. Hubin, D. H. Busch, *Coord. Chem. Rev.* **2000**, *200*, 5-52; f) M. Kogej, P. Ghosh, C. A. Schalley, in *Strategies and Tactics in Organic Synthesis*, Vol. 4 (Ed.: M. Harmata), Elsevier, Amsterdam, **2004**, 171-210; For selected examples on template effects, see: g) F. Vögtle, S. Meier, R. Hoss, *Angew. Chem.* **1992**, *104*, 1628-1631; *Angew. Chem. Int. Ed.* **1992**, *31*, 1619-1622; h) S. A. Nepogodiev, J. F. Stoddart, *Chem. Rev.* **1998**, *98*, 1959-1976; i) F. M. Raymo, J. F. Stoddart, *Chem. Rev.* **1999**, *99*, 1043-1063. j) C. A. Schalley, G. Silva, C. F. Nising, P. Linnartz, *Helv. Chim. Acta* **2002**, *85*, 1578-1596; k) P. Ghosh, O. Mermagen, C. A. Schalley, *Chem. Commun.* **2002**, 2628-2629.

[102] a) C. Hamers, F. M. Raymo, J. F. Stoddart, *Eur. J. Org. Chem.* **1998**, *10*, 2109-2117; b) J. L. Weidmann, J. M. Kern, J. P. Sauvage, D. Muscat, S. Mullins, W. Kohler, C. Rosenauer, H. J. Rader, K. Martin, Y. Geerts, *Chem. Eur. J.* **1999**, *5*, 1841-1851.

[103] C. P. Collier, G. Mattersteig, E. W. Wong, Y. Luo, K. Beverly, J. Sampaio, F. M. Raymo, J. F. Stoddart, J. R. Heath, *Science* **2000**, *289*, 1172-1175.

[104] a) J.-P. Sauvage, *Acc. Chem. Res.* **1998**, *31*, 611-619; b) C. A. Schalley, K. Beizai, F. Vögtle, *Acc. Chem. Res.* **2001**, *34*, 465-476; c) V. Balzani, M. Venturi, A. Credi, *Molecular Devices and Machines*, Wiley-VCH, Weinheim, **2002**; d) D. Pijper, R. A. van Delden, A. Meetsma, B. L. Feringa, *J. Am. Chem. Soc.* **2005**, *127*, 17612-17613; e) M. K. J. Ter Wiel, R. A. Van Delden, A. Meetsma, B. L. Feringa, *J. Am. Chem. Soc.* **2005**, *127*, 14208-14222.

[105] a) M. S.Deleuze, D. A. Leigh, F. Zerbetto, *J. Am. Chem. Soc.* **1999**, *121*, 2364-2379; b) D. A. Leigh, A. Troisi, F. Zerbetto, *Chem. Eur. J.* **2002**, *7*, 1450-1454.

[106] J.-C. Chambron, C. O. Dietrich-Buchecker, J.-P. Sauvage, *Top. Curr. Chem.* **1993**, *165*, 131-162.

[107] Y. Cohen, L. Avram, L. Frish, *Angew. Chem.* **2005**, *117*, 524-560; *Angew. Chem. Int. Ed.* **2005**, *44*, 520-554; and references therein.

[108] a) M. B. Comisarow, A. G. Marshall, *Chem. Phys. Lett.* **1974**, *25*, 282-283; b) M. B. Comisarow, A. G. Marshall, *Chem. Phys. Lett.* **1974**, *26*, 489-490; c) M. B. Comisarow, A. G. Marshall, *Can. J. Chem.* **1974**, *52*, 1997-1999.

[109] See standard textbooks in physics, e.g. P. A. Tipler, G. Mosca, D. Pelte, *Physik*, Spektrum Akademischer Verlag, **2006**.

[110] A. G. Marshall, C. L. Hendrickson, G. S. Jackson, *Mass Spec. Rev.* **1998**, *17*, 1-35.

[111] M. Dole, L. L. Mach, R. L. Hines, R. C. Mobley, R. C. Ferguson, M. B. Alice, *J. Chem. Phys.* **1968**, *49*, 2240-2249.

[112] J. B. Fenn, *Angew. Chem.* **2003**, *115*, 3999-4024; *Angew. Chem. Int. Ed.* **2003**, *42*, 3871-3894.

[113] G. I. Taylor, *Proc. R. Soc. London Ser. A* **1964**, *280*, 383-397.

[114] J. W. Strutt (Lord Rayleigh), *Philos. Mag.* **1882**, *14*, 184-186.

[115] K. Yamaguchi, *J. Mass Spectrom.* **2003**, *38*, 473-490.

[116] L. Sleno, D. A. Volmer, *J. Mass Spectrom.* **2004**, *39*, 1091-1112.

[117] R. B. Cody, R. C. Burnier, B. S. Freiser, *Anal. Chem.* **1982**, *54*, 96-101.

[118] R. A. Zubarev, N. L. Kelleher, F. W. McLafferty, *J. Am. Chem. Soc.* **1998**, *120*, 3265-3266.

[119] W. D. Bowers, S.-S. Delbert, R. L. Hunter, R. T. McIver, Jr., *J. Am. Chem. Soc.* **1984**, *106*, 7288-7289.

[120] a) D. P. Little, J. P. Speir, M. W. Senko, P. B. O'Connor, F. W. McLafferty, *Anal. Chem.* **1994**, *66*, 2809-2815; b) D. M. Peiris, M. A. Cheeseman, R. Ramanathan, J. E. Eyler, *J. Phys. Chem.* **1993**, *97*, 7839-7843; c) R. L. Woodlin, D. S. Bomse, J. L. Beauchamp, *J. Am. Chem. Soc.* **1978**, *100*, 3248-3250.

[121] R. C. Dunbar, T. B. McMahon, *Science* **1998**, *279*, 194-197.

[122] J. W. Gauthier, T. R. Trautman, D. B. Jacobson, *Anal. Chim. Acta* **1991**, *246*, 211-222.

[123] J. Laskin, J. H. Futrell, *Mass Spectrom. Rev.* **2003**, *22*, 158-181.

[124] T. Felder, C. A. Schalley, H. Fakhrnabavi, O. Lukin, *Chem. Eur. J.* **2005**, *11*, 5625-5636.

[125] a) C. A. Schalley, *Int. J. Mass Spectrom.* **2000**, *194*, 11-39; b) C. B. Lebrilla, *Acc. Chem. Res.* **2001**, *34*, 653-661; c) C. A. Schalley, *Mass Spectrom. Rev.* **2001**, *20*, 253-309. d) B. M. O'Leary, T. Szabo, N. Svenstrup, C. A. Schalley, A. Lützen, M. Schäfer, J. Rebek Jr., *J. Am. Chem. Soc.* **2001**, *123*, 11519-11533; e) H. Mansikkamäki, M. Nissinen, C. A. Schalley, K. Rissanen, *New J. Chem.* **2003**, *27*, 88-97; f) S. S. Zhu, H. Staats, K. Brandhorst, J. Grunenberg, F. Gruppi, E. Dalcanale, A. Lützen, K. Rissanen, C. A. Schalley, *Angew. Chem.* **2008**, *120*, 800-804; *Angew. Chem. Int. Ed.* **2008**, *47*, 788-792.

[126] C. A. Schalley, J. Hoernschemeyer, X. Lia, G. Silva, P. Weis, *Int. J. Mass Spec.* **2003**, *228*, 373-388.

[127] C. A. Schalley, P. Ghosh, M. Engeser, *Int. J. Mass Spec.* **2004**, *232*, 249-258.

[128] a) T. Wyttenbach, M. T. Bowers, in "Topics in Current Chemistry – Modern Mass Spectrometry", Springer, Berlin **2003**, 207-232; b) S. C. Henderson, S. J. Valentine, A. E. Counterman, D. E. Clemmer, *Anal. Chem.* **1999**, *71*, 291-301; c) C. S. Hoaglund, S. J. Valentine, C. R. Sporleder, J. P. Reilly, D. E. Clemmer, *Anal. Chem.* **1998**, *70*, 2236-2242; d) G. F. Verbeck, B. T. Ruotolo, H. A. Sawyer, K. J. Gillig, D. H. Russell, *J. Biomol. Tech.* **2002**, *13*, 56-61.

[129] a) D. Schröder, H. Schwarz, S. Shaik, in "Structure and Bonding", Springer, Berlin, **2000**, 91-123; b) E. Uggerud, in "Topics in Current Chemistry – Modern Mass Spectrometry", Springer, Berlin **2003**, 3-36; c) D. A. Plattner, in "Topics in Current Chemistry – Modern Mass Spectrometry", Springer, Berlin **2003**, 153-203.

[130] a) P. Chen, *Angew. Chem.* **2003**, *115*, 2938-2954; *Angew. Chem. Int. Ed.* **2003**, *42*, 2832-2847; b) R. Dietiker, P. Chen, *Angew. Chem.* **2004**, *116*, 5629-5632; *Angew. Chem. Int. Ed.* **2004**, *43*, 5513-5516; c) D. K. Böhme, H. Schwarz, *Angew. Chem.* **2005**, *117*, 2388-2406; *Angew. Chem. Int. Ed.* **2005**, *44*, 2336-2354.

[131] a) M. T. Rodgers, K. M. Ervin, P. B. Armentrout, *J. Chem. Phys.* **1997**, *106*, 4499-4508; b) P. B. Armentrout, in "Topics in Current Chemistry – Modern Mass Spectrometry", Springer, Berlin **2003**, 233-262.

[132] S. Narancic, A. Bach, P. Chen, *J. Phys. Chem. A*. **2007**, 111, 7006-7013.

[133] U. Mazurek, M. Engeser, C. Lifshitz, *Int. J. Mass Spectrom.* **2006**, *249*, 473-476.

[134] Original publications: a) G. Binning, H. Rohrer, *Helv. Phys. Acta* **1982**, *55*, 726-735; b) G. Binnig, H. Rohrer, C. Gerber, E. Weibel, *Phys. Rev. Lett.* **1982**, *49*, 57-61; c) G. Binning, H. Rohrer, *Surf. Sci.* **1983**, *126*, 236-244.

[135] Reviews a) G. Binnig, H. Rohrer, *IBM J. Res. Develop.* **1986**, *30*, 355-369; b) G. Binnig, H. Rohrer, *Reviews of Modern Physics* **1987**, *59*, 615-625; c) J. E. Griffith, G. E. Kochanski, *Annu. Rev. Mater. Sci.* **1990**, *20*, 219-244; d) T. Sakurai, *Progr. Surf. Sci.* **1990**, *33*, 3-89; e) L. E. C. van de Leemput, H. van Kempen, *Rep. Prog. Phys.* **1992**, *55*, 1165-1240.

[136] E. Stoll, A. Baratoff, A. Selloni, P. Carnevali, *J. Phys. C* **1984**, *17*, 3073-3086.

[137] J. Golovchenko, *Science* **1986**, *232*, 48-53.

[138] G. Binning, H. Rohrer, *IBM J. Res. Develop.* **2000**, *44*, 279-293.

[139] C. Zörlein, *PhD Thesis*, *"Supramolekulare Architekturen an fest/flüssig-Grenzflächen"*, Rheinische Friedrich-Wilhelms-Universität Bonn, **2005**.

[140] a) S. De Feyter, A. Gesquière, M. M. Abdel-Mottaleb, P. C. M. Grim, F. C. De Schryver, C. Meiners, M. Sieffert, S. Valiyaveetil, K. Müllen, *Acc. Chem. Res.* **2000**, *33*, 520-531; b) J. Michl, T. F. Magnery, *Proc. Nat. Acad. Sci. U.S.A.* **2002**, *99*, 4788-4792; c) S. De Feyter, F. C. De Schryver, *Chem. Soc. Rev.* **2003**, *32*, 139-150.

[141] First measurements in an electrochemical environment were reported by Sonnenfeld and Hansma in 1996: R. Sonnenfeld, P. K. Hansma, *Science* **1996**, *232*, 211.

[142] T. Dretschkow, T. Wandlowski, "*Solid-Liquid Interfaces*", Springer, Heidelberg, **2003**.

[143] M. Wilms, M. Kruft, G. Bermes, K. Wandelt, *Rev. Sci. Instr.* **1999**, *70*, 3641-3650.

[144] a) A. A. Gewirth, B. K. Niece, *Chem. Rev.* **1997**, *97*, 1129-1162; b) P. A. Christensen, *Chem. Soc. Rev.* **1992**, 197-208.

[145] A. Shkurankov, F. Endres, W. Freyland, *Rev. Sci. Instr.* **2002**, *73*, 102-107.

[146] J. Curie, P. Curie, *Bulletin de la Société Minéralogique de France* **1880**, *3*, 90-93.

[147] W. Göpel, *Technisches Messen* **1995**, *625*, 183-185.

[148] G. Sauerbrey, *Z. Phys.* **1959**, *155*, 206-222.

[149] F. L. Dickert, A. Haunschild, *Adv. Mater.* **1993**, *5*, 887-895.

[150] J. Bargon, B. Graewe, T. Jonischkeit, K. Woelk, *Chem. uns. Zeit* **2003**, *37*, 212-213.

[151] K. Cammann, U. Lemke, A. Rohen, J. Sander, H. Wilken, B. Winter, *Angew. Chem.* **1991**, *103*, 519-541; *Angew. Chem. Int. Ed.* **1991**, *30*, 516-539.

[152] W. H. King, Jr., *Anal. Chem.* **1964**, *36*, 1735-1739.

[153] U. Schramm, *PhD Thesis*, *"Entwicklung von Prototypen zur Ammoniaküberwachung in feuchter Luft für den Einsatz innerhalb eines Multigassensors"*, Rheinische Friedrich-Wilhelms-Universität Bonn, **1999**.

[154] M. Albrecht, M. Schlupp, J. Bargon, G. van Koten, *Chem. Commun.* **2001**, 1874-1875.

[155] C. Heil, G. R. Windscheif, S. Braschohs, J. Flörke, F. Gläser, M. Lopez, J. Müller-Albrecht, U. Schramm, J. Bargon, F. Vögtle, *Sens. Actuators B* **1999**, *61*, 51-58.

[156] F. L. Dickert, U. Geiger, K. Weber, *Fresenius J. Anal. Chem.* **1999**, *364*, 128-132.

[157] F. L. Dickert, A. Haunschild, M. Reif, W.-E. Bulst, *Adv. Mater.* **1993**, *5*, 277-279.

[158] D. B. Mitzi, L. L. Kosbar, C. E. Murray, M. Copel, A. Afzail, *Nature* **2004**, *428*, 299-303.

[159] L. Wächter, *PhD Thesis*, *"Elektrospraybeschichtung von mikrogravimetrichen Sensoren - Beschichtungsvarianten für leitfähige und nicht-leitfähige Oberflächen"*, Rheinische Friedrich-Wilhelms-Universität Bonn, **2003**.

[160] P. J. Steel, *Acc. Chem. Res.* **2005**, *38*, 243-250.

[161] a) P. Lloyd-Williams, E. Giralt, *Chem. Soc. Rev.* **2001**, *30*, 145-157; b) G. Bringmann, A. J. Price Mortimer, P. A. Keller, M. J. Gresser, J. Garner, M. Breuning, *Angew. Chem.* **2005**, *117*, 5518-5563; *Angew. Chem. Int. Ed.* **2005**, *44*, 5384-5427.

[162] a) U. Kiehne, A. Lützen, *Org. Lett.* **2007**, *9*, 5333-5336; b) U. Kiehne, T. Bruhn, G. Schnakenburg, R. Fröhlich, G. Bringmann, A. Lützen, *Chem. Eur. J.* **2008**, *14*, 4246-4255.

[163] K. P. C. Vollhardt, N. E. Schore, *Organische Chemie*, 3. Auflage, Wiley-VCH, Weinheim, **2000**, 1257.

[164] K. P. C. Vollhardt, N. E. Schore, *Organische Chemie*, 3. Auflage, Wiley-VCH, Weinheim, **2000**, 1258.

[165] K. Thomas, D. Jerchel, *Angew. Chem.* **1958**, *70*, 719-737.

[166] G. Panke, T. Schwalbe, W. Stirner, S. Taghavi-Moghadam, G. Wille, *Synthesis* **2003**, *18*, 2827-2830.

[167] L. C. Craig, *J. Am. Chem. Soc.* **1933**, *55*, 2854-2857.

[168] a) J. M. Bakke, *Pure Appl. Chem.* **2003**, *75*, 1403-1415; b) K. Thomas, D. Jerchel, *Angew. Chem.* **1958**, *70*, 719-37.

[169] S. Kanoktanaporn, J. A. H. MacBride, *J. Chem. Soc., Perkin Trans. 1* **1978**, *10*, 1126-1131.

[170] J. Rebek, Jr., T. Costello, R. Wattley, *J. Am. Chem. Soc.* **1985**, *107*, 7487-7493.

[171] T. Weilandt, *Diploma Thesis*, "*Hierarchische Selbstorganisation funktionalisierter supramolekularer Quadrate*", Rheinische Friedrich-Wilhelms-Universität Bonn, **2004**.

[172] R. C. Larock, *Comprehensive Organic Transformations*, 2. Edition, Wiley-VCH, Weinheim, **1999**.

[173] R. R. Fraser, T. S. Mansour, S. Savard, *J. Org. Chem.* **1985**, *50*, 3232-3234.

[174] D. M. Hodgson, M. J. Fleming, S. J. Stanway, *J. Am. Chem. Soc.* **2004**, *126*, 12250-12251.

[175] P. D. Beer, Z. Chen, A. Grieve, J. Haggitt, *J. Chem. Soc., Chem. Commun.* **1994**, *20*, 2413-2414.

[176] E. Mann, A. Montero, M. A. Maestro, B. Herradon, *Helvet. Chim. Acta* **2002**, *85*, 3624-3638.

[177] a) C. J. Hawker, J. M. J. Fréchet, *J. Am. Chem. Soc.* **1990**, *112*, 7638-7647; b) C. J. Hawker, J. M. J. Fréchet, *J. Chem. Soc., Chem. Commun.* **1990**, 1010-1013.

[178] a) F. Vögtle, M. Plevoets, G. Nachtsheim, U. Wörsdörfer, *J. Prakt. Chem.* **1998**, *340*, 112-121; b) M. Luostarinen, T. Partanen, C. A. Schalley, K. Rissanen, *Synthesis* **2004**, 255-262.

[179] J. Coste, D. Le-Nguyen, B. Castro, *Tetrahedron Lett.* **1990**, *31*, 205-208.

[180] R. C. Brian, G. W. Driver, R. F. Homer, R. L. Jones, GB 813531 (1958).

[181] a) C. M. Palm, D. Tsiourvas, *Angew. Chem.* **1995**, *107*, 1839-1855; *Angew. Chem. Int. Ed.* **1995**, *34*, 1696-1711; b) C. Meiners, S. Valiyaveettil, V. Enkelmann, K. Müllen, *J. Mater. Chem.* **1997**, *7*, 2367-2374.

[182] a) P. R. Ashton, T. T. Goodnow, A. E. Kaifer, M. V. Reddington, A. M. Z. Slawin, N. Spencer, J. F. Stoddart, C. Vicent, D. J. Williams, *Angew. Chem.* **1989**, *101*, 1404-1408; *Angew. Chem. lnt. Ed.* **1989**, *28*, 1396; b) R. V. Slone, J. T. Hupp, C. L. Stern, T. E. Albrecht-Schmitt, *Inorg. Chem.* **1996**, *35*, 4096-4097; c) D. C. Caskey, R. K. Shoemaker, J. Michl, *Org. Lett.* **2004**, *6*, 2093-2096.

[183] a) 4,4'-Biquinoline: P. Carsky, S. Huenig, I. Stemmler, D. Scheutzow, *Liebigs Ann. Chem.* **1980**, 291-304. Substituted 4,4'-Biquinolines: b) S. Kanoktanaporn, J. A. H. MacBride, *J. Chem. Soc., Perkin Trans. 1* **1978**, *10*, 1126-1131; c) M. Slany, P. J. Stang, *Synthesis* **1996**, *8*, 1019-1028.

[184] a) E. Francotte, *J. Chromatogr. A* **2001**, *906*, 379-397; b) E. Francotte, WO 9749733 (1997); c) E. Francotte, T. Zhang, WO 9704011 (1997).

[185] R. F. Homer, *J. Chem. Soc.* **1958**, 1574-1577.

[186] a) R. F. Evans, H. C. Brown, *J. Org. Chem.* **1962**, *27*, 1329-1336; b) B. Singh, G. Y. Lesher, P. O. Pennock, *J. Heterocyclic Chem.* **1990**, *27*, 1841-1842.

[187] S. D. Walker, T. E. Barder, J. R. Martinelli, S. L. Buchwald, *Angew. Chem.* **2004**, *116*, 1907-1912; *Angew. Chem. Int. Ed.* **2004**, *43*, 1871-1876.

[188] T. G. Appleton, M. A. Bennett, I. B. Tomkins, *J. Chem. Soc., Dalton Trans.* **1976**, 439-446.

[189] a) H. D. K. Drew, F. W. Pinkard, G. H. Preston, W. Wardlaw, *J. Chem. Soc.* **1932**, 1895-1909; b) D. P. Asanin, S. Rajkovic, D. Molnar-Gabor, M. I. Djuran, *Monatsh. Chem.* **2004**, *135*, 1445-1453.

[190] Y. Kidani, K. Inagaki, *J. Med. Chem.* **1978**, *21*, 1315-1318.

[191] a) R. V. Slone, D. I. Yoon, R. M. Calhoun, J. T. Hupp, *J. Am. Chem. Soc.* **1995**, *117*, 11813-11814; b) R. V. Slone, J. T. Hupp, C. L. Stern, T. E. Albrecht-Schmitt, *Inorg. Chem.* **1996**, *35*, 4096-4097.

[192] The augmented MM2 force field as implemented in the CACHE 5.0 program package for Windows was used for the calculation (Fujitsu Ltd., Krakow, Poland, **2001**).

[193] T. W. Kim, M. S. Lah, J.-I. Hong, *Chem. Commun.* **2001**, 743-745.

[194] a) X. Chi, A. J. Guerin, R. A. Haycock, C. A. Hunter, L. D. Sarson, *J. Chem. Soc., Chem. Commun.* **1995**, 2567-2569; b) G. Ercolani, *J. Phys. Chem. B* **1998**, *102*, 5699-5703.

[195] H. T. Baytekin, M. Sahre, A. Rang, M. Engeser, A. Schulz, C. A. Schalley, *Small* **2008**, DOI: 10.1002/smll.200800135.

[196] C. A. Schalley, B. Baytekin, H. T. Baytekin, M. Engeser, T. Felder, A. Rang, *J. Phys. Org. Chem.* **2006**, *19*, 479-490.

[197] Overview on dendrimers: G. R. Newkome, C. N. Moorefield, F. Vögtle, *Dendrimers and Dendrons. Concepts, Syntheses, Applications* Wiley-VCH, Weinheim **2001**; J. M. J. Fréchet, D. A. Tomalia, *Dendrimers and other dendritic polymers* Wiley, New York **2001**.

[198] M. Fujita, F. Ibukuro, K. Yamaguchi, K. Ogura, *J. Am. Chem. Soc.* **1995**, *117*, 4175-4176.

[199] Examples for dynamic ligand exchange: a) S. Hiraoka, M. Shiro, M. Shionoya, *J. Am. Chem. Soc.* **2004**, *126*, 1214-1218; b) F. Dumitru, E. Petit, A. van der Lee, M. Barboiu, *Eur. J. Inorg. Chem.* **2005**, 4225-4262; c) S. J. Park, D. M. Shin, S. Sakamoto, K. Yamaguchi, Y. K. Chun, M. S. Lah, J.-I. Hong, *Chem. Eur. J.* **2005**, *11*, 235-241; d) M. Albrecht, S. Mirtschin, M. De. Groot, I. Janser, J. Runsink, G. Raabe, M. Kogej, C. A. Schalley, R. Fröhlich, *J. Am. Chem. Soc.* **2005**, *127*, 10371-10387.

[200] A. Rang, M. Nieger, M. Engeser, A. Lützen, C. A. Schalley, *Chem. Commun.* **2008**, 4789-4791.

[201] a) R. Krämer, J.-M. Lehn, A. Marquis-Rigault, *Proc. Natl. Acad. Sci. USA* **1993**, *90*, 5394-5398; b) D. L. Caulder, K. N. Raymond, *Angew. Chem.* **1997**, *109*, 1508-1510; *Angew. Chem. Int. Ed.* **1997**, *36*, 1440-1442; c) M. Albrecht, M. Schneider, H. Röttele, *Angew. Chem.* **1999**, *111*, 512-515; *Angew. Chem. Int. Ed.* **1999**, *38*, 557-559; d) T. J. Burchell, R. J. Puddephatt, *Inorg. Chem.* **2006**, *45*, 650-659; e) M. Albrecht, R. Fröhlich, *Bull. Chem. Soc. Jpn.* **2007**, *80*, 797-808; f) U. Kiehne, T. Weilandt, A. Lützen, *Org. Lett.* **2007**, *9*, 1283-1286; g) U. Kiehne, T. Weilandt, A. Lützen, *Eur. J. Org. Chem.* **2008**, 2056-2064.

[202] a) M. Kitamura, S. Okada, S. Suga, R. Noyori, *J. Am. Chem. Soc.* **1989**, *111*, 4028-4036; b) B. Hasenknopf, J.-M. Lehn, G. Baum, D. Fenske, *Proc. Natl. Acad. Sci. USA* **1996**, *93*, 1397-1400; c) R. Wang, M. Hong, D. Yuan, Y. Sun, L. Xu, J. Luo, R. Cao, A. S. C. Chan, *Eur. J. Inorg. Chem.* **2004**, 37-43.

[203] a) S. J. Lee, W. Lin, *J. Am. Chem. Soc.* **2002**, *124*, 4554-4555; b) S. J. Lee, C. R. Luman, F. N. Castellano, W. Lin, *Chem. Commun.* **2003**, 2124-2125.

[204] A. Rang, M. Engeser, N. M. Maier, M. Nieger, W. Lindner, C. A. Schalley, *Chem. Eur. J.* **2008**, *14*, 3855-3859.

[205] Reviews on chiral assemblies: a) F. R. Keene, *Chem. Soc. Rev.* **1998**, *27*, 185-193; b) B. J. Holliday, C. A. Mirkin, *Angew. Chem.* **2001**, *113*, 2076-2097; *Angew. Chem. Int. Ed.* **2001**, *40*, 2022-2043; c) S. G. Telfer, R. Kuroda, *Coord. Chem. Rev.* **2003**, *242*, 33-46; d) O. Mamula, A. von Zelewsky, *Coord. Chem. Rev.* **2003**, *242*, 87-95.

[206] K. S. Jeong, S. Y. Kim, U.-S. Shin, M. Kogej, N. T. M. Hai, P. Broekmann, N. Jeong, B. Kirchner, M. Reiher, C. A. Schalley, *J. Am. Chem. Soc.* **2005**, *127*, 17672-17685.

[207] C. A. Stanier, S. J. Alderman, T. D. W. Claridge, H. L. Anderson *Angew. Chem.* **2002**, *114*, 1847-1850; *Angew. Chem. Int. Ed.* **2002**, *41*, 1769-1772.

[208] C. Yamamoto, Y. Okamoto, T. Schmidt, R. Jäger, F. Vögtle, *J. Am. Chem. Soc.* **1997**, *119*, 10547-10548.

[209] a) T. Oshikiri, Y. Takashima, H. Yamaguchi, A. Harada, *J. Am. Chem. Soc.* **2005**, **127**, 12186-12187; b) I. Tomatsu, A. Hashidzume, A. Harada, *Angew. Chem.* **2006**, *118*, 4721-4724; *Angew. Chem. Int. Ed.* **2006**, *45*, 4605-4608; c) L. Trembleau, J. Rebek, Jr., *Science* **2003**, *301*, 1219-1220; d) T. Amaya, J Rebek, Jr., *J. Am. Chem. Soc.* **2004**, *126*, 6216-6217.

[210] S. R. Nam, H.-J. Kim, S. Sakamoto, K. Yamaguchi, J.-I. Hong, *Tetrahedron Lett.* **2004**, 45, 1339-1342.

[211] F. Würthner, C.-C. You, C. R. Saha-Möller, *Chem. Soc. Rev.* **2004**, *33*, 133-146.

[212] M. Ferrer, A. Gutiérrez, M. Mounir, O. Rossell, E. Ruiz, A. Rang, M. Engeser, *Inorg. Chem.* **2007**, *46*, 3395-3406.

[213] B. Graewe, A. Rang, C. A. Schalley, J. Haubrich, J. Bargon, *Sens. Actuators B* **2006**, *119*, 302-307.

[214] J. Kesselmeier, M. Staudt, *J. Atmos. Chem.* **1999**, *33*, 23-88.

[215] K. Mannschreck, K. Bächmann, I. Barnes, K. H. Becker, T. Heil, R. Kurtenbach, M. Memmesheimer, V. Mohnen, A. Obermeier, D. Poppe, R. Steinbrecher, T. Schmitz, A. Volz-Thomas, F. Zabel *J. Atmos. Chem.* **2002**, *42*, 281-286.

[216] L. Taiz, E. Zeiger, "*Physiologie der Pflanzen*", Spektrum Akademischer Verlag, Heidelberg, **1999**, 649.

[217] Österreichische Akademie der Wissenschaften—Kommission für Reinhaltung der Luft, GZ. 01 1800/4-I/7/94, Wien, **1996**.

[218] H. Zimmermann, R. Walzl, "Ullmann's Encyclopedia of Industrial Chemistry, electronic release" Wiley-VCH, Weinheim, **2001**.

[219] J. Janata, M. Josowicz, D. M. DeVaney, *Chemical Sensors, Anal. Chem.* **1994**, *66*, 207R-228R.

[220] O. Pogodina, V. Pustogov, F. De Melas, C. Haberhauer-Troyer, E. Rosenberg, H. Puxbaum, A. Inberg, N. Croitoru, B. Mizaikoff, *Anal. Chem.* **2004**, *76*, 464-468.

[221] a) T. Hamacher, J. Niessa, P. Schulze-Lammers, B. Diekmann, P. Boeker, *Sens. Actuators B* **2003**, *95*, 39-45; b) U. Schramm, D. Meinhold, S. Winter, C. Heil, J. Müller-Albrecht, L. Wächter, H. Hoff, C. E. O. Roesky, T. Rechenbach, P. Boeker, P. Schulze- Lammers, E. Weber, J. Bargon, *Sens. Actuators B* **2000**, *67*, 219-226.

[222] A. Basilevsky "Statistical Factor Analysis and Related Methods", Wiley, New York, **1994**.

[223] For the only examples for a gravimetric detection of alkenes, see: a) E. T. Zellers, G.-Z. Zhang *Anal. Chem.* **1992**, *64*, 1277-1284; b) E. T. Zellers, G.-Z. Zhang *Anal. Chem.* **1993**, *65*, 1340-1349.

[224] For examples of triangles, see: a) M. Fujita, M. Aoyagi, K. Ogura, *Inorg. Chim. Acta* **1996**, *246*, 53-57; b) R.-D. Schnebeck, L. Randaccio, E. Zangrando, B. Lippert, *Angew. Chem.* **1998**, *110*, 128-130; *Angew. Chem. Int. Ed.* **1998**, *37*, 119-121; c) R.-D. Schnebeck, E. Freisinger, B. Lippert, *Chem. Commun.* **1999**, 675-676; d) S.-W. Lai, M. C.-W. Chan, S.-M. Peng, C.-M. Che, *Angew. Chem.* **1999**, *111*, 708-710; *Angew. Chem. Int. Ed.* **1999**, *38*, 669-671; e) T. Habereder, M. Warchhold, H. Nöth, K. Severin, *Angew. Chem.* **1999**, *111*, 3422-3425; *Angew. Chem. Int. Ed.* **1999**, *38*, 3225-3228; f) S.-S. Sun, A. J. Lees, *Inorg. Chem.* **1999**, *38*, 4181-4182; g) S.-S. Sun, A. J. Lees, *J. Am. Chem. Soc.* **2000**, *122*, 8956-8967; h) R.-D. Schnebeck, E. Friesinger, F. Glahé, B. Lippert, *J. Am. Chem. Soc.* **2000**, *122*, 1381-1390.

[225] For square-triangle equilibria, see: a) S. B. Lee, S. Hwang, D. S. Chung, H. Yun, J.-I. Hong, *Tetrahedron Lett.* **1998**, *39*, 873-876; b) R.-D. Schnebeck, E. Freisinger, B. Lippert, *Eur. J. Org. Chem.* **2000**, 1193-1200; c) A. Sautter, D. G. Schmid, G. Jung, F. Würthner, *J. Am. Chem. Soc.* **2001**, *123*, 5424-5430.

[226] C. Elschenbroich, *Organometallchemie*, 4. Auflage, (Eds.: C. Elschenbroich, F. Hensel, H. Hopf), Teubner, Stuttgart, **2003**, 256-261.

[227] See standard textbooks in physical chemistry, e.g. P. W. Atkins, *Physical Chemistry*, 3. ed., Oxford University Press, **1986**.

[228] K. Eichkorn, O. Treutler, H. Öhm, M. Häser, R. Ahlrichs, *Chem. Phys. Lett.* **1995**, *240*, 283-289.

[229] R. Ahlrichs, M. Bär, M. Häser, H. Horn, C. Kölmel, *Chem. Phys. Lett.* **1989**, *162*, 165-169.

[230] a) A. D. Becke, *Phys. Rev. A* **1988**, *38*, 3098-3100; b) S. H. Vosko, L. Wilk, M. Nusair, *Can. J. Phys.* **1980**, *58*, 1200-1211; c) J. P. Perdew, *Phys. Rev. B* **1986**, *33*, 8822-8824.

[231] D. Andrae, U. Haeussermann, M. Dolg, H. Stoll, H. Preuss, *Theor. Chim. Acta*, **1990**, *77*, 123-141.

[232] P. Boeker, O. Wallenfang, G. Horner, *Sens. Actuators, B, Chem.* **2002**, *83*, 202-208.

[233] B. Graewe, PhD thesis, "*Metallo-Supramolekulare Substanzen als sensoraktive Schichten für die Mikroschwingquarzwaage*", Universität Bonn, **2004**.

[234] Five Technologies GmbH, Frauenstr. 22, 80469 München.

[235] C. Safarowsky, A. Rang, C. A. Schalley, K. Wandelt, P. Broekmann, *Electrochim. Acta* **2005**, *50*, 4257-4268.

[236] F. Vögtle, "*Supramolecular Chemistry*", Wiley and Sons, Chichester, **1991**.

[237] J.-M. Lehn, "*Supramolecular Chemistry*", VCH, Weinheim, **1995**.

[238] V. Balzani, A. Credi, F. M. Raymo, J. F. Stoddart, *Angew. Chem.* **2000**, *112*, 3484-3530; *Angew. Chem. Int. Ed.* **2000**, *39*, 3348-3391.

[239] J.-M. Lehn, *Angew. Chem.* **1988**, *100*, 91-116; *Angew. Chem. Int. Ed.* **1988**, *27*, 89-112.

[240] S. De Feyter, F. C. De Schryver, *Chem. Soc. Rev.* **2003**, *32*, 139-150.

[241] O. M. Magnussen, *Chem. Rev.* **2002**, *102*, 679-725.

[242] a) S. Yoshimoto, K. Suto, K. Itaya, N. Kobayashi, *Chem. Commun.* **2003**, 2174-2175; b) S. Griessl, M. Lackinger, M. Edelwirth, M. Hietschold, W. M. Heckl, *Single Mol.* **2002**, *3*, 25-31.

[243] P. L. Anelli, P. R. Ashton, R. Ballardini, V. Balzani, M. Delgado, M. T. Gandolfi, T. T. Goodnow, A. E. Kaifer, D. Philp, M. Pietraszkiewicz, L. Prodi, M. V. Reddington, A. M. Z. Slawin, N. Spencer, J. F. Stoddart, C. Vicent, D. J. Williams, *J. Am. Chem. Soc.* **1992**, *114*, 193-218.

[244] W. Geuder, A. Suchy, *Tetrahedron* **1986**, *42*, 1665-1677.

[245] D. B. Amabilino, P. R. Ashton, C. L. Brown, E. Cordova, L. A. Godinez, T. T. Goodnow, A. E. Kaifer, S. P. Newton, M. Pietraszkiewicz, D. Philp, F. M. Raymo, A. S. Reder, M. T. Rutland, A. M. Z. Slawin, N. Spencer, J. F. Stoddart, D. J. Williams, *J. Am. Chem. Soc.* **1995**, *117*, 1271-1293.

[246] S. Chia, J. Cao, J. F. Stoddart, J. I. Zink, *Angew. Chem.* **2001**, *113*, 2513-2517; *Angew. Chem. Int. Ed.* **2001**, *40*, 2447-2451.

[247] a) D. W. Suggs, A. J. Bard, *J. Phys. Chem.* **1995**, *99*, 8349-8355; b) M. R. Vogt, A. Lachenwitzer, O. M. Magnussen, R. J. Behm, *Surf. Sci.* **1998**, *399*, 49-69; c) O. M. Magnussen, M. R. Vogt, *Phys. Rev. Lett.* **2000**, *85*, 357-360; d) O. M. Magnussen, L. Zitzler, B. Gleich, M. R. Vogt, R. J. Behm, *Electrochem. Acta* **2001**, *46*, 3725-3733.

[248] M. T. M. Koper, *J. Electroanal. Chem.* **1998**, *450*, 189-201.

[249] For reviews, see: a) D. L. Caulder, K. N. Raymond, *Acc. Chem. Res.* **1999**, *32*, 975-982; b) B. J. Holliday, C. A. Mirkin, *Angew. Chem.* **2001**, *113*, 2076-2098; *Angew. Chem. Int. Ed.* **2001**, *40*, 2022-2042; c) M. Fujita, K. Umemoto, M. Yoshizawa, N. Fujita, T. Kusukawa, K. Biradha, *Chem. Commun.* **2001**, 509-518.

[250] E. Mena-Osteritz, P. Bäuerle, *Adv. Mater.* **2001**, *13*, 243-246.

[251] E. Mena-Osteritz, *Adv. Mater.* **2002**, *14*, 609-616.

[252] G. B. Pan, J. M. Liu, H. M. Zhang, L. J. Wan, Q. Y. Zheng, C. L. Bai, *Angew. Chem.* **2003**, *115*, 2853-2857; *Angew. Chem. Int. Ed.* **2003**, *42*, 2747-2751.

[253] M. Ammann, A. Rang, C. A. Schalley, P. Bäuerle, *Eur. J. Org. Chem.* **2006**, *8*, 1940-1948.

[254] P. Bäuerle, M. Ammann, M. Wilde, G. Götz, E. Mena-Osteritz, A. Rang, C. A. Schalley, *Angew. Chem.* **2007**, *119*, 367-372; *Angew. Chem. Int. Ed.* **2007**, *46*, 363-368.

[255] *Handbook of Oligo- and Polythiophenes* (Ed.: D. Fichou), Wiley-VCh, Weinheim, **1999**.

[256] P. Bäuerle, *Oligothiophenes in Electronic Materials: The Oligomeric Approach* (Eds.: K. Müllen, G. Wegner), Wiley- VCH, Weinheim, 1998.

[257] a) J. Krömer, I. Rios-Carreras, G. Fuhrmann, C. Musch, M. Wunderlin, T. Debaerdemaeker, E. Mena-Osteritz, P. Bäuerle, *Angew. Chem.* **2000**, *112*, 3623-3628; *Angew. Chem. Int. Ed.* **2000**, *39*, 3481-3486; b) G. Fuhrmann, J. Krömer, P. Bäuerle, *Synth. Met.* **2001**, *119*, 125-126; c) G. Fuhrmann, T. Debaerdemaeker, P. Bäuerle, *Chem. Commun.* **2003**, 948-949.

[258] M. Bednarz, P. Reineker, E. Mena-Osteritz, P. Bäuerle, *J. Lumin.* **2004**, *110*, 225-231.

[259] a) V. Balzani, A. Credi, F. M. Raymo, J. F. Stoddart, *Angew. Chem. 2000*, *112*, 3484-3530; *Angew. Chem. Int. Ed.* **2000**, *39*, 3348-3391; b) A. R. Pease, J. O. Jeppesen, J. F. Stoddart, Y. Luo, C. P. Collier, J. R. Heath, *Acc. Chem. Res.* **2001**, *34*, 433-444.

[260] a) C. O. Dietrich-Buchecker, J.-P. Sauvage, J. P. Kintzinger, *Tetrahedron Lett.* **1983**, *24*, 5095-5098; b) C. O. Dietrich-Buchecker, J.-P. Sauvage, *Chem. Rev.* **1987**, *87*, 795-810; c) J.-P. Sauvage, *Acc. Chem. Res.* **1990**, *23*, 319-327.

[261] a) P. Linnartz, S. Bitter, C. A. Schalley, *Eur. J. Org. Chem.* **2003**, 4819-4829; b) P. Linnartz, C. A. Schalley, *Supramol. Chem.* **2004**, *16*, 263-267.

[262] a) M. Vincenti, *J. Mass Spectrom.* **1995**, *30*, 925-939; b) M. Przybylski, M. O. Glocker, *Angew. Chem.* **1996**, *108*, 878-899; *Angew. Chem. Int. Ed.* **1996**, *35*, 807-826; c) J. S. Brodbelt, *Int. J. Mass Spectrom.* **2000**, *200*, 57-69; d) C. A. Schalley, *Int. J. Mass Spectrom.* **2000**, *194*, 11-39; e) C. A. Schalley, *Mass Spectrom. Rev.* **2001**, *20*, 253-309; f) C. B. Lebrilla, *Acc. Chem. Res.* **2001**, *34*, 653-661.

[263] a) C. A. Schalley, R. K. Castellano, M. S. Brody, D. M. Rudkevich, G. Siuzdak, J. Rebek, Jr, *J. Am. Chem. Soc.* **1999**, *121*, 4568-4579; b) C. A. Schalley, T. Martín, U. Obst, J. Rebek Jr, *J. Am. Chem. Soc.* **1999**, *121*, 2133-2138; c) R. Zadmard, M. Junkers, T. Schrader, T. Grawe, A. Kraft, *J. Org. Chem.* **2003**, *68*, 6511-6521; d) R. Zadmard, T. Schrader, U. Linne, *Chem. Eur. J.* **2004**, *10*, 4233-4239; e) I. Müller, D. Möller, C. A. Schalley, *Angew. Chem.* **2005**, *117*, 485-488; *Angew. Chem. Int. Ed.* **2005**, *44*, 480-484.

[264] A. R. Pease, J. O. Jeppesen, J. F. Stoddart, Y. Luo, C. P. Collier, J. R. Heath, *Acc. Chem. Res.* **2001**, *34*, 433-444.

[265] W. Treibs, J. Beger, *Liebigs Ann. Chem.* **1962**, *652*, 192-203.

[266] L. M. Engelhardt, W.-P. Leung, C. L. Raston, G. Salem, P. Twiss, A. H. White, *J. Chem. Soc. Dalton Trans.* **1988**, 2403-2409.

[267] W. Lindner, M. Lämmerhofer, WO068397 (2003).

[268] a) A. Wu, L. Isaacs, *J. Am. Chem. Soc.* **2003**, *125*, 4831-4835; b) P. Mukhopadhyay, P. Y. Zavalij, L. Isaacs *J. Am. Chem. Soc.* **2006**, *128*, 14093-14102.

[269] D. D. Perrin, W. L. F. Armarego, D. R. Perrin, *Purification of Laboratory Chemicals*, Pergamon Press, Oxford, **1982**.

[270] M. F. Reich, P. F. Fabio, V. J. Lee, N. A. Kuck, R. T. Testa, *J. Med. Chem.* **1989**, *32*, 2474-2485.

[271] H. Yamanaka, T. Araki, T. Sakamoto, *Chem. Pharm. Bull.* **1988**, *36*, 2244-2247.

[272] L. Kaczmarek, A. Becalski, P. Nantka-Namirski, *Pol. J. Chem.* **1980**, *54*, 1585-1590.

[273] M. Yoshizawa, M. Nagao, K. Kumazawa, M. Fujita, *J. Organomet. Chem.* **2005**, *690*, 5383-5388.

[274] T. Sakamoto, S. Kaneda, S. Nishimura, H. Yamanaka, *Chem. Pharm. Bull.* **1985**, *33*, 565-571.

[275] a) C. S. Swindell, R. H. Duffy, *Heterocycles* **1986**, *24*, 3373-3377; b) Z.-Q. Wu, X.-K. Jiang, Z.-T. Li, *Tetrahedron Lett.* **2005**, *46*, 8067-8070.

[276] M. Makosza, M. Sypniewski, *Tetrahedron* **1994**, *50*, 4913-4920.

[277] M. Freifelder, G. R. Stone, *J. Org. Chem.* **1961**, *26*, 3805-3808.

[278] A. A. Pletnev, Q. Tian, R. C. Larock, *J. Org. Chem.* **2002**, *67*, 9276-9287.

[279] T. Sakamoto, M. Shiraiwa, Y. Kondo, H. Yamanaka, *Synthesis* **1983**, *4*, 312-314.

[280] G.M. Sheldrick, *Acta Cryst.* **1990**, A46, 467-473.

[281] G.M. Sheldrick, Univ. Göttingen 1997.

Der Lebenslauf und die Danksagung wurden in dieser Online Ausgabe gelöscht.

Publications

1. A. R. Far, Y. L. Cho, A. Rang, J. Rebek, Jr, *Tetrahedron* **2002**, 741-755.
2. C. Safarowsky, L. Merz, A. Rang, P. Broekmann, B. A. Herrmann, C. A. Schalley, *Angew. Chem.* **2004**, *116*, 1311-1314; *Angew. Chem. Int. Ed.* **2004**, *43*, 1291-1294.
3. A. Rang, C. A. Schalley, "Catenanes and Other Interlocked Molecules" in *Encyclopedia of Supramolecular Chemistry*, (Eds.: J. L. Atwood, J. W. Steed), Dekker, New York **2004**, 206-213.
4. C. Safarowsky, A. Rang, C. A. Schalley, K. Wandelt, P. Broekmann, *Electrochim. Acta*, **2005**, *50*, 4257-4268.
5. B. Graewe, A. Rang, C. A. Schalley, J. Haubrich, J. Bargon, *Sens. Act. B. Chem.* **2006**, *119*, 302-307.
6. M. Engeser, A. Rang, M. Ferrer, A. Gutiérrez, H. T. Baytekin, C. A. Schalley, *Int. J. Mass Spec.* **2006**, *255*, 185-194.
7. M. Ammann, A. Rang, C. A. Schalley, P. Bäuerle, *Eur. J. Org. Chem.* **2006**, *8*, 1940-1948.
8. C. A. Schalley, B. Baytekin, H. T. Baytekin, M. Engeser, T. Felder, A. Rang, *J. Phys. Org. Chem.* **2006**, *19*, 479-490.
9. P. Bäuerle, M. Ammann, M. Wilde, G. Götz, E. Mena-Osteritz, A. Rang, C. A. Schalley, *Angew. Chem.* **2007**, *119*, 367-372; *Angew. Chem. Int. Ed.* **2007**, *46*, 363-368.
10. M. Ferrer, A. Gutiérrez, M. Mounir, O. Rossell, E. Ruiz, A. Rang, M. Engeser, *Inorg. Chem.* **2007**, *46*, 3395-3406.
11. A. Rang, M. Engeser, N. M. Maier, M. Nieger, W. Lindner, C. A. Schalley, *Chem. Eur. J.* **2008**, *14*, 3855-3859.
12. H. T. Baytekin, M. Sahre, A. Rang, M. Engeser, A. Schulz, C. A. Schalley, *Small* **2008**, DOI: 10.1002/smll.200800135.
13. A. Rang, M. Nieger, M. Engeser, A. Lützen, C. A. Schalley, *Chem. Commun.* **2008**, 4789-4791.

Poster Contributions

1. A. Rang, H. Mansikkamäki, C. A. Schalley, "A Toolbox of Substituted Molecular Squares for Molecular Recognition", GDCh-Jahrestagung 2003 in München.

2. A. Rang, C. Safarowsky, P. Broekmann, C. A. Schalley, "EC-STM-Investigations of Molecular Squares", GDCh-Jahrestagung 2003 in München.

3. A. Rang, T. Weilandt, T. Baytekin, C. A. Schalley, "Modified Metallo-Supramolecular Squares", SFB-242-Symposium 2004 in Münster.

4. B. Graewe, A. Rang, C. A. Schalley, J. Bargon, "Bestimmung der Templat-Substrat-Wechselwirkung mit Hilfe von Massenschwingern in der Gasphase", SFB-624-Begutachtung 2005 in Bonn Bad-Godesberg.

5. A. Rang, T. Baytekin, M. Engeser, C. A. Schalley, "Dynamic Combinatorial Libraries of Self-Assembled Metallo-Supramolecular Dendrimers", GDCh-Jahrestagung 2005 in Düsseldorf.

6. A. Rang, M. Engeser, N. Maier, W. Lindner, C. A. Schalley, "Axially Chiral Ligands in Self-Assembled Metallo-Supramolecular Squares", GDCh-Wissenschaftsforum 2007 in Ulm.

Declaration

Hiermit versichere ich an Eides statt, dass diese Dissertation von mir persönlich, selbständig und ohne jede unerlaubte Hilfe angefertigt wurde. Aus fremden Quellen entnommene Gedanken und Daten sind als solche kenntlich gemacht. Die Daten, die im Rahmen einer Kooperation gewonnen wurden, sind ausnahmslos gekennzeichnet. Die vorliegende Arbeit wurde an keiner anderen Hochschule als Dissertation eingereicht. Ich habe früher noch keinen Promotionsversuch unternommen. Teile der Arbeit sind auszugsweise veröffentlicht worden; dies ist zu Beginn des jeweiligen Kapitels angegeben.